A computational journey from electronic structure to reactivity : NHC-derived borenium catalysts as test case

Radhika Gupta

INSTITUT POLYTECHNIQUE DE PARIS

ÉCOLE POLYTECHNIQUE

IP PARIS

NNT : 2021IPPAX060

Thèse de doctorat

A computational journey from electronic structure to reactivity: NHC-derived borenium catalysts as test case

Thèse de doctorat de l'Institut Polytechnique de Paris
préparée à l'École Polytechnique

n°626 : Ecole Doctorale de l'Institut Polytechnique de Paris
(ED IP Paris)
Spécialité de doctorat: Chimie

Thèse présentée et soutenue à Palaiseau, 09/09/2021, par

Radhika Gupta

Composition du Jury :

Laurent El Kaïm Professeur, École Polytechnique (LSO)	Président
Paola Nava Maitresse de conférence, Aix-Marseille Université (iSm2)	Rapportrice
Vincent Tognetti Maitre de conférence, Université de Rouen (COBRA)	Rapporteur
Carine Clavaguéra Directrice de recherche, Université Paris Saclay (ICP)	Examinatrice
Eric Hénon Professeur, Université de Reims Champagne-Ardenne (ICMR)	Examinateur
Gilles Frison Chargé de recherche, Sorbonne Université (LCT)	Directeur de thèse

कर्मण्येवाधिकारस्ते मा फलेषु कदाचन।

मा कर्मफलहेतुर्भूर्मा ते सङ्गोऽस्त्वकर्मणि॥

२-४७, भगवद् गीता।

To work alone you have the right, and not to the fruits. Do not be impelled by the fruits of work. Nor have attachment to inaction.

Chapter 2, Verse 47, Bhagavad Gita

Dedicated to my teachers.

Acknowledgements

"It is easy to acknowledge, but almost impossible to realize for long, that we are mirrors whose brightness, if we are bright, is wholly derived from the sun that shines upon us."

– C.S. Lewis

The completion of my doctoral studies would not have been as fulfilling and successful had it not been for some wonderful people. To convey my appreciation towards them in mere words seems futile, but here I am, trying.

I would first like to express my heartfelt gratitude towards my supervisor, Dr. Gilles Frison, for his constant support, motivation and insight. Your guidance has been invaluable in shaping my thoughts as a scientist. I am also indebted to the members of the jury for their helpful suggestions and inputs that helped me write and defend the thesis better. I also thank Jacob S. Hirschi who was an internship student at LCM and contributed in some parts of the thesis – you were a pleasure to work with.

I take this opportunity to extend my thanks and warm regards to the members of LCM, specially, Cédric Tard (for being the best director!), Sophie Bourcier and Edith Nicol (for always helping me out when I was utterly confused), Gilles Alla (for all the help with the computers and more importantly, the little French conversations), Mérimée Thérèse and Sandra Schnakenbourg (for help with all the administrative paperwork).

I thank École Polytechnique for giving me the opportunity and means to work at LCM. Of course, none of the experiments would have been possible without the computational resources that were made available to me. For this, I am greatly obliged to Ecole Polytechnique, CINES and GENCI.

I want to express my deep appreciation for the friendships that were fostered here – Silvia Duran, Valeriu Cemortan, Amlan Roychowdhury and Ditipriya Hazra – you added sunshine to my days when the world was bleak.

The acknowledgements would not be complete without thanking my family and friends who encouraged and sustained me during difficult times. I owe everything I have achieved to my parents – Mr. Debashish Gupta and Mrs. Monalisa Gupta who worked endlessly to give me a

fair chance to succeed in life. I also want to thank my friends Aishwarya Mukherjee, Adrija Roy, Kangona Dey, Soumabrata Majumdar and Shrestha Banerjee for the endless hours of video-calling whenever I needed it and sometimes when they knew I needed it even without my asking. There's very little in life that cannot be overcome when you have an contingent of companions such as these.

Finally, I thank you, dear reader, for your interest in my thesis. I hope you find the read to be as engrossing as I found the work.

Résumé

La chimie computationnelle est maintenant omniprésente dans l'évaluation numérique des propriétés physiques et chimiques des molécules. C'est un outil de prédiction pour les chimistes théoriciens et un outil complémentaire en chimie organique et inorganique qui peut être utilisé pour éviter les expériences et synthèses ardues en laboratoire. La chimie computationnelle s'intéresse à la fois à la mesure des propriétés physiques et chimiques, et à l'évaluation de l'efficacité des méthodes théoriques à prédire ces valeurs.

Dans ce travail de thèse, nous explorons ces deux facettes pour le cas particulier des adduits de borénium dérivés de carbènes N-hétérocycliques (NHC). Ces composés sont reconnus pour leur rôle d'acides de Lewis en chimie, comme illustré pour leur rôle catalytique d'activation de petites molécules comme H_2. De plus, ces composés présentent des caractéristiques chimiques qui permettent de décomposer finement les transferts électroniques entre ses constituants borénium et carbone divalent (ligands NHC ou carbone). L'un des objectifs était d'explorer diverses méthodes de calcul pour évaluer les propriétés structurelles, thermodynamiques et cinétiques de ces composés borénium dérivés des NHC afin de vérifier la validité des approches de calcul. L'autre objectif était d'établir une relation structure-activité pour ces adduits, ouvrant la voie à la conception rationnelle *in silico* de catalyseurs nouveaux et plus performants.

Avec ces axes de recherche en tête, la thèse présente une première partie bibliographique suivie de trois autres parties. L'acidité de Lewis, la propriété thermodynamique la plus importante de ces adduits de borénium déficients en électrons, est contrôlée par deux interactions importantes - les donations σ et π du composé carboné divalent vers le borénium. La PARTIE A de la thèse est consacrée à l'évaluation de ces deux interactions en utilisant de nombreuses approches théoriques, permettant d'identifier les descripteurs les plus efficaces pour ces interactions. Si les différents descripteurs identifiés pour quantifier les interactions σ et π sont parfois correctement corrélés entre eux, dans certains cas, des niveaux de corrélation moins bons qu'attendus sont obtenus. Ces aspects ont été abordés avec une attention particulière dans cette thèse. La raison de l'absence de corrélation est considérée comme provenant de certaines différences conceptuelles fondamentales des méthodes, de

la définition de descripteurs particuliers ou d'une mauvaise interprétation des données. Néanmoins, certaines méthodes non ambiguës de quantification de ces deux interactions (donations σ et π) à l'aide d'outils de la chimie quantique ont été identifiées. La fiabilité de nos résultats computationnels a été renforcée par la comparaison avec des valeurs expérimentales issues de la littérature, lorsqu'elles étaient disponibles.

Dans la PARTIE B, l'évaluation par diverses approches calculatoires d'un autre concept chimique, l'acidité de Lewis, concept fondamental et pourtant quelque peu "imprécis", a été envisagée. Une fois encore, des descripteurs intéressants et pertinents de l'acidité de Lewis ont été identifiés et comparés entre eux. A partir de ces résultats, une relation quantitative entre les interactions σ et π, évaluées dans la partie précédente, et l'acidité de Lewis globale, évaluée par l'affinité des ions hydrure, a pu être établie. Cette partie permet donc d'apporter des réponses à deux questions importantes concernant ces catalyseurs de borénium dérivés de NHC: "Comment évaluer l'acidité de Lewis?" et "Comment corréler l'acidité de Lewis avec les propriétés structurelles de ces molécules?"

Enfin, la PARTIE C démontre par l'exemple la pertinence et l'utilité de disposer d'une échelle d'acidité de Lewis pour rationaliser et prédire la réactivité catalytique. Ici, l'activation du dihydrogène en utilisant les catalyseurs de borénium a été explorée. Nous avons montré que leur acidité de Lewis globale est corrélée avec l'énergie d'activation de H_2, établissant ainsi une relation directe entre la propriété thermodynamique de l'acidité de Lewis des catalyseurs et leur réactivité. De plus, l'énergie d'activation pour ces réactions et une combinaison linéaire des interactions σ et π montrent une même tendance pour l'ensemble des catalyseurs étudiés, établissant ainsi une relation structure-activité pour cet ensemble de molécules. Au final, nos résultats théoriques sont également corroborés par certaines données expérimentales, bien que la disponibilité de ces données soit assez limitée. Cela contribue à donner de la crédibilité à l'approche théorique utilisée dans cette thèse pour étudier divers aspects de ces composés chimiques très intéressants et par extension d'autres problèmes pertinents dans le domaine de la catalyse homogène.

Abstract

Computational chemistry is ubiquitous in the numerical evaluation of physical and chemical properties of molecules. It is a predictive tool for theoretical chemists and a complementary tool in organic and inorganic chemistry to avoid arduous laboratory experiments and syntheses. Computational chemistry is concerned with both measuring physical properties and evaluating how efficiently theoretical methods can predict these values.

In this work we explore both these facets in the context of N-Heterocyclic carbene (NHC) derived borenium adducts. These compounds are recognised for their role as Lewis acids in chemistry, as illustrated for their catalytic role for activating small molecules like H_2. Moreover, these compounds present chemical characteristics that allow to finely decompose the electronic transfers between its borenium and divalent carbon (NHC or carbone ligands) constituents. One part of the objectives was ro explore multifarious computational methods to evaluate various structural, thermodynamic and kintic properties of the NHC-derived borenium compounds to ascertain the validity of the computational approaches. The other objective was to establish a structure-activity relationship for these adducts computationally, paving the way to the rational in silico design of new and better catalysts.

With these themes in mind, the thesis presents an initial bibliographic account followed by three sections. Lewis acidity, the most significant thermodynamic property of these electron-deficient borenium adducts is controlled by two significant interactions – the σ and π-donation both from the divalent carbon compound to the borenium. PART A of the thesis is dedicated to the evaluation of these two interactions using numerous theoretical approaches, allowing to identify the most efficient descriptors for these interactions. While sometimes the various descriptors identified to quantify the σ and π-interactions correlate well with each other, in some cases sub-optimal correlation care obtained. These aspects have been addressed with particular emphasis in this thesis. The reason for the lack of correlations are seen to arise from some fundamental conceptual differences, definition of particular descriptors or misinterpretation of data. Nonetheless, some unambiguous methods of quantifying these two interactions (σ and π donations) using computational tools have been identified. The reliability of our computational results has been strengthened by comparison with available experimentally recorded values, wherever available.

In PART B, we try to evaluate another fundamental, and yet, somewhat 'fuzzy' chemical concept – Lewis acidity. Once again, some interesting and pertinent descriptors of Lewis acidity have been identified and compared with each other. Next, we attempt to establish a quantitative relationship the between the σ and π interactions, evaluated in the previous section, and the overall Lewis acidity, evaluated through hydride ion affinity. This section, therefore answers two important questions with respect to these NHC-derived borenium catalysts – "How to evaluate Lewis acidity? How to correlate it with the structural properties of these molecules?"

Finally, PART C is dedicated to exemplify the utility of having a scale of Lewis acidity. Here, the activation of H_2 using the borenium catalysts have been explored and the overall Lewis acidity is found to correlate with the energy of H_2 activation, thereby establishing a direct relationship between the thermodynamic property of Lewis acidity and their reactivity. Furthermore, the activation energy for these reactions also show a reasonable trend with a linear combination of σ and π-interactions, thereby establishing a structure-activity relationship for this set of molecules. In the end, our theoretical findings are also corroborated by some experimental data, although availability of such data is quite limited. This helps to give credibility to the theoretical approach used in this thesis to study various aspects of these very interesting chemical compounds and by extension other relevant problems in the field of chemical catalysis.

Contents

1. GENERAL INTRODUCTION

The word science originates from the Latin word *scientia* meaning knowledge and is presently defined as a systematic enterprise that *builds and organises knowledge* in the form of *testable explanations* and *predictions* about the universe.[1, 2] The 'organisation of knowledge' is brought about by the act of *measurement*. Measurement, according to Norman Campbell, is the act of assigning numbers to properties of an object or an event to represent its qualities with respect to other objects or events.[3] The measurement reveals some data – to explain which we construct *theories*. Theories are a set of rules that are said to govern the properties of a system.[4] In science, usually, theories can be expressed in terms of mathematical equations. While theories aim for as great a generality as possible, they often pose the threat of becoming too complicated to be applied to reality. For instance, it is wholly futile to apply quantum mechanics to understand the oscillation of a pendulum when the same results can be obtained through the use of simpler, 'approximate' equations, in this case by applying classical Newtonian mechanics. Therefore, often a theory must be simplified to widen its scope of applicability – giving rise to *models*. Conversely excessive "modelisation" of theories may sometimes render them qualitative. Therefore, for the sake of efficiency and simplicity, a compromise has to be made.

Quantum mechanics is a highly generalised theory that is universally applicable but is generally used to describe the physical properties of nature at atomic and molecular scale. According to quantum mechanics, the wavefunction is the key to all properties of matter and can be obtained by solving the Schrödinger equation. At this point we recall Dirac's famous words "The fundamental laws necessary for the mathematical treatment of a large part of physics and the whole of chemistry are thus completely known, and the difficulty lies only in the fact that application of these laws leads to equations that are too complex to be solved."[5] The electronic Schrödinger equation cannot be solved exactly for any system other than single-electron systems like the hydrogen atom. Therefore, some approximations have to be introduced and models are constructed to get to a solution as close to experimental reality as possible. Computational chemistry is the branch of chemical sciences that deals with the application of the exact quantum mechanical equations or an approximate model of it to materials and molecular systems through mathematical calculations to study the system at hand.

The foundation of computational chemistry was laid by the seminal work of Schrödinger in 1925 which was rapidly followed by the works of Paul Dirac, Hartree and Fock, Lennard Jones, Mulliken, Hund and Slater. However, realising their theories for moderate to large molecules was virtually impossible without unlocking the potential of electronic computers, which became available in the 1950s. Thus, the second half of the 20th century marks the beginning of the "age of computation". Since then the application of computers to chemical problems has grown so much so that today, it is almost *conventional* to accompany an experimental study with theoretical calculations. In addition, computational modelling plays an obvious role in weeding out chemically redundant endeavours, furthering the cause of green chemistry while also reducing time and effort significantly. Finally, of course, computational chemistry helps to bridge the gap between theoretical models and experimental observations. To *summarise*, the research in the field of computational chemistry can be broadly accommodated under two categories – (a) the evaluation of physical and chemical properties of molecular systems and materials and (b) improving the efficiency and reliability of computational tools in predicting the values associated with said properties.

In modern chemistry much of the ancient mysterious veil of alchemy has been lifted and this has been possible because of one key idea – structure-activity relationships. This means, for example, that the reaction pathway followed by a compound participating in a reaction is influenced by its geometric and electronic structure. Therefore, reaching the desired outcome from a reaction can be seen as largely relying on the ability to identify the correct 3-D geometry and electronic distribution of the starting reactants. In this thesis, our objective was to investigate to what extent such an approach can be a source of new knowledge. The structural properties and chemical activity of molecular species, as well as their relationships, was thus carefully investigated with the help of computational tools. Comparison between these modelling and available experimental data or empirical chemical concepts constitutes the second pillar of our project. Naturally, reactive molecules are preferable for such a study and chemistry offers those in spades – in the form of catalysts. At the same time, in order to evaluate the quality of results obtained from the computational approach relatively simple and easily interpretable interactions are desirable. The 'right' model sits at the confluence of all these various ideas and is a rare find.

The adduct noted hereafter **X**-BH_2^+ and formed between a divalent carbon compound (like N-heterocyclic carbenes and carbones) and positively charged borenium unit (BH_2^+) presents itself as an ideal candidate around which all our work was articulated (Figure 1-1), the structure of which is modified in our study by changing the nature of **X**. From a chemical point of view, these adducts have been shown to activate small molecules like H_2 by virtue of their Lewis acidity. However, such reports are sporadic at best and although it is quite evident that changing the nature of the carbenic backbone changes the Lewis acidity of the borenium adduct and therefore its activity, no quantitative relationship expounding it exists to the best of our knowledge.

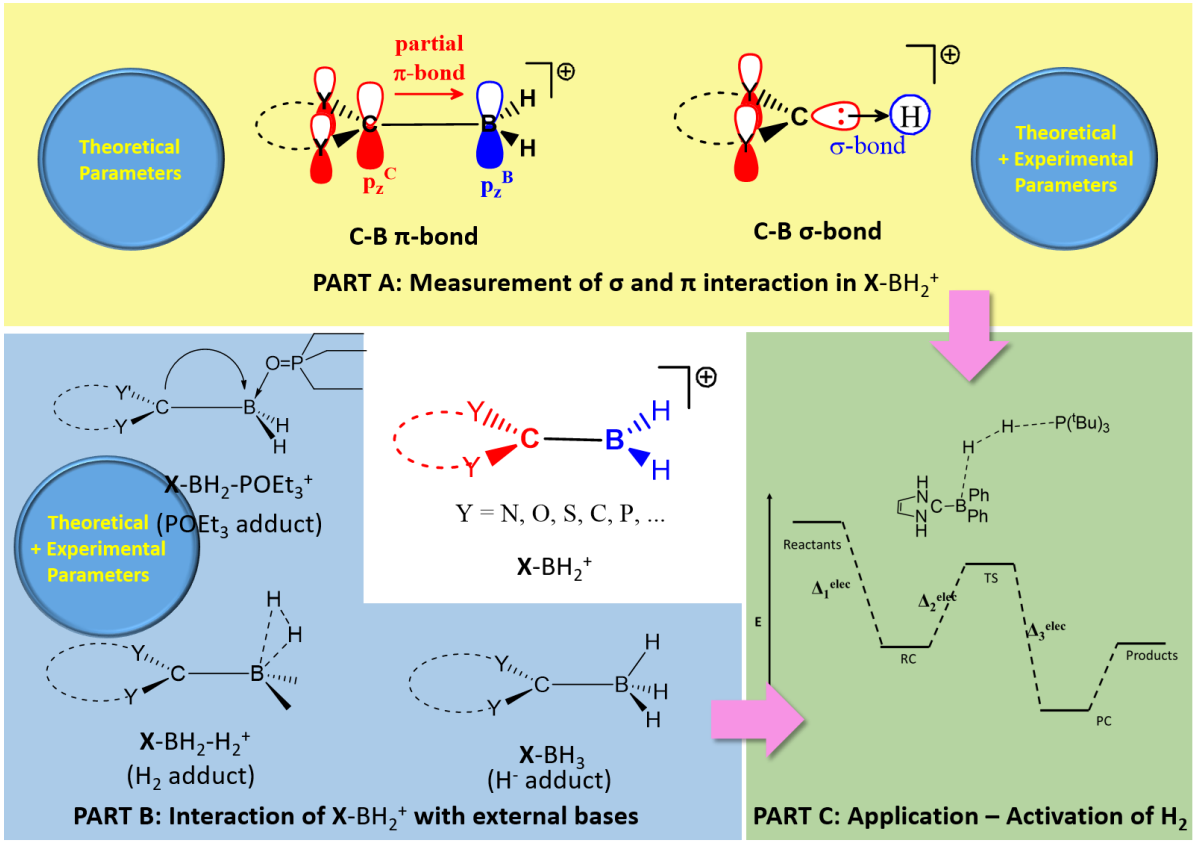

Figure 1-1: Graphical representation of the components of this thesis

From a theoretical point of view, this system provides a unique opportunity due to its inherent simplicity. Carbenes are normally treated as popular ligands in organometallic chemistry where they are coordinated to transition metals. The bonding situation in this case however is quite complicated – the link between the carbene carbon and the transition metal can be described as a cumulative effect of numerous interactions which can be difficult to completely segregate (σ/π donation, backdonation etc.). More easily understandable interactions are

present within carbene-borenium adducts. In particular, σ and π interactions in the carbene-boron linkage are simpler than in transition metal complexes because they are exclusively donations. Due to this, the relative ability of the divalent carbon compounds to donate electrons can be easily quantified.

Based on this qualitative description of the interactions within NHC-derived borenium adducts, the first part of the thesis (**PART A**) deals with the computational measurement of the σ- and π-interaction strengths of the C-B bond using various descriptors. The second part (**PART B**) is dedicated to the interaction of the Lewis acidic borenium with external bases in order to estimate the strength of the Lewis acidity of these adducts. In other words, can the thermodynamic properties of these borenium be explained by their structural properties? Finally, in the last part (**PART C**), the utility of the above-mentioned structural descriptors in predicting the reactivity of these Lewis acid catalysts in the activation of dihydrogen has been explored.

The thesis starts with chapter I which itself has two sections – 2A and 2B. The first part contains bibliographic details of carbenes followed by the theoretical basis of the various computational techniques employed in the thesis, with the objective of providing a rudimentary understanding of the kind of chemical systems we are dealing with as well as the tools employed to understand them. The reader is advised that the material covered in this chapter is in no way exhaustive and is directed to follow the articles, reviews and books cited for greater detail.

Chapter II and chapter III constitute the first part of the thesis where the objective is to provide a better understanding of the π- and σ-donating abilities of the divalent carbon compounds. Different theoretical and experimental parameters have been used to quantify these σ- and π-interactions, and the reliability of these various approaches has been questioned. More specifically, chapter II deals with the various computational models used to measure π-bond strength and comparison between these methods. The plethora of techniques that are used ubiquitously in chemical literature to measure the properties of a chemical bond are not necessarily equivalent and therefore may lead to discrepancies and misinterpretations. In our study we identified descriptors that adequately quantify the π-interaction, methods that quantify mainly the π-interaction but also have significant

contribution from other interactions in the molecule and descriptors that perform rather poorly in describing the π-bond strength.

In chapter III, we have relied on two experimental methods, both based on NMR, which are used in the literature to evaluate the σ-donating strength of divalent carbon compounds. Are these two experimental parameters comparable with each other and with theoretical descriptors? These are the questions addressed in this chapter. Reasonable correlations have been identified between selected calculated parameters and experimentally recorded values. This chapter also shows that not all the methods of evaluating σ-donation are equivalent.

Having in hand an accurate description of the electronic structure of the carbene-borenium adducts, based on the π- and σ-donating abilities of the carbene ligands, we focus in a second step on the reactivity of borenium. The first question addressed is whether the population of the boron p_z orbital, related to the π-interaction with the carbene ligand, provides a good measure of the Lewis acidity of the boron center. In chapter IV, the interactions of the borenium compounds with external bases like triethyl phosphineoxide ($POEt_3$) and hydride H^- have therefore been considered. From this investigation, hydride ion affinity (HIA) emerges as a scale of total Lewis acidity for the divalent-borenium adducts. The final section of Chapter V demonstrates the utility of these scales in real world applications – such as predicting the barrier of activation of H_2 by boreniums acting as the Lewis acid component in frustrated Lewis pairs.

Finally, the different statistical metrics using which the quality of correlation between two variables are measured are briefly discussed in the appendix.

References

1. Harper, D., Online Etymology Dictionary. Retrieved September 20, 2014 ed., https://www.etymonline.com/word/science

2. Wilson, E. O., The natural sciences. *Consilience: The Unity of Knowledge (Reprint ed.). New York, New York: Vintage* **1999**.

3. Tal, E., Measurement in Science. *The Stanford Encyclopedia of Philosophy (Fall **2020** Edition)* (Edward N. Zalta (ed.)).

4. Cramer, C. J., *Essentials of Computational Chemistry : Theories and Models*. West Sussex, England ; New York :J. Wiley, **2002**.

5. Paul Dirac Quotes. (n.d.). BrainyQuote.com. Retrieved June 29, from BrainyQuote.com https://www.brainyquote.com/quotes/paul_dirac_279318.

List of molecules

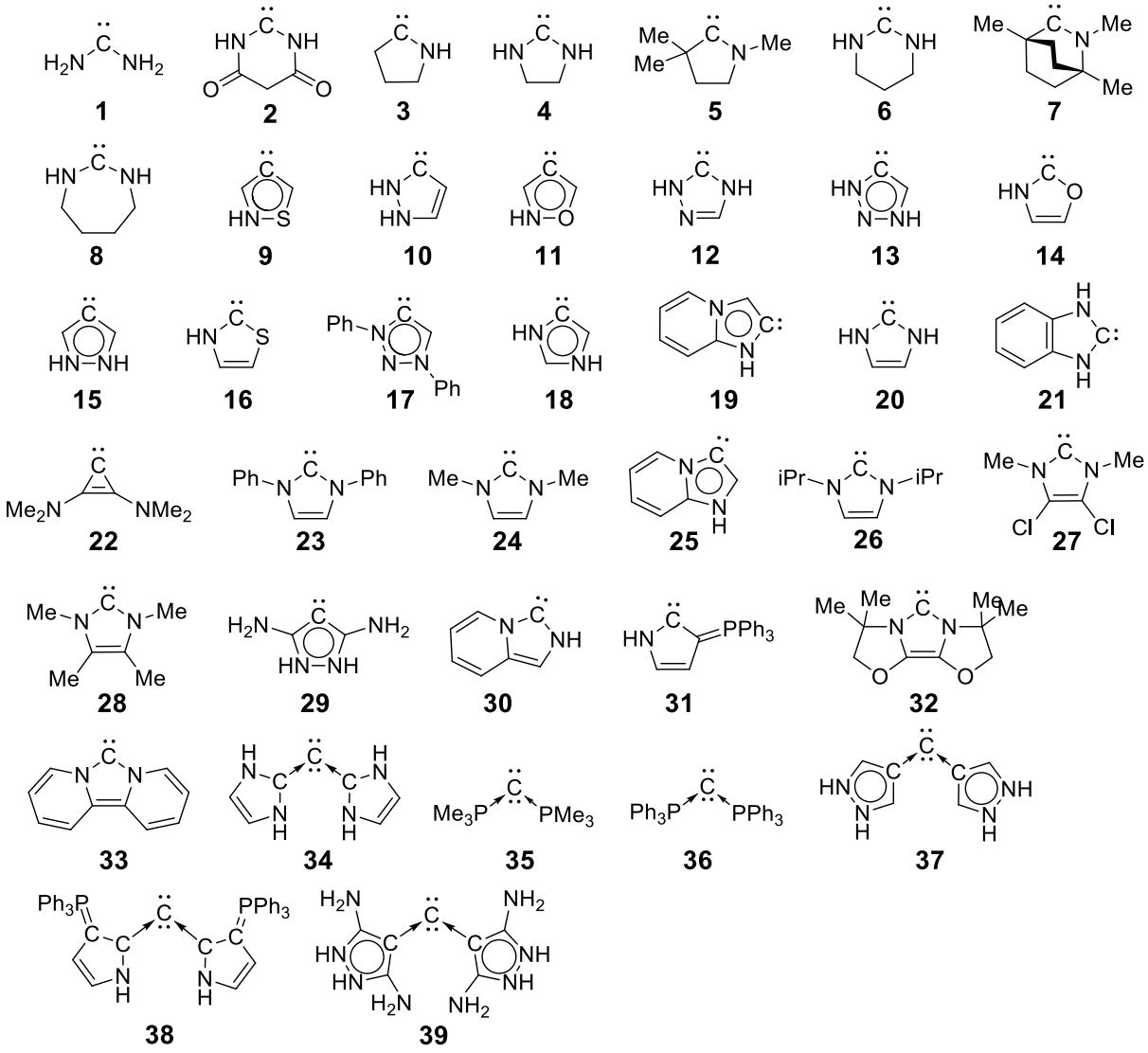

Scheme 1: list of main divalent carbon molecules studies in chapters II, IV and V of this thesis

2. CHAPTER I
Bibliography

Abstract

This chapter has two sections – 2A and 2B containing short bibliographic accounts of the two most important components of this thesis – divalent carbon compounds (including carbenes and carbones) and the various aspects of theoretical chemistry necessary to understand them. Readers already familiar with the subject matter can safely skip this chapter and come back to the topics as and when referenced in the following chapters. Others are invited to continue in the light of the knowledge that the topics have been dealt with brevity and are by no means exhaustive. For greater insight the readers are recommended to consult the cited texts.

2.1. Introduction

This chapter has two parts – the first part deals with the bibliographic description of carbenes and other divalent carbon compounds. In the next part, the chapter deals with the theoretical foundation and computational tools that are used in the description of the compounds in the following chapters of the thesis.

2A. Carbenes

Carbenes form a diverse and extremely important class of compounds in chemistry.[1] In our studies, the primary goal is to establish and understand relationships between the structure of catalysts with their reactivity. This objective was built around catalysts including various carbenic backbones and these compounds therefore play a significant role in this work. It is not possible to discuss all the interesting aspects of carbene chemistry in this text. Therefore, we pick and choose the topics most pertinent to our discussion. We start with the history of carbenes followed by a short description of their classification, including special classes called N-Heterocyclic carbenes (NHC) and carbones. Next, a brief discussion of their electronic structure and the various factors that influence it have been presented. Finally, we look at the most important applications of NHCs in chemistry, with particular emphasis on NHC-stabilised borenium ions which are used in activation of small molecules, like H_2.

2A.1. A Brief History of Carbenes

Carbenes are divalent carbon compounds with two non-bonding electrons, the carbon being characterised by a sextet instead of an octet. The history of divalent carbon compounds goes back more than 150 years from today. The first attempts to synthesise a carbene takes us as far back as 1835, when Dumas tried to synthesise the parent carbene – methylene ($:CH_2$) – by dehydration of apparent hydride, methanol ($CH_2.H_2O$).[2] It must be noted that at the time the tetravalency of carbon had not yet been established and therefore the existence of a divalent carbon was considered quite plausible.

The first assumption of the involvement of a carbene species as a reactive intermediate was made by Geuther and Hermann in 1855,[3] who suggested that the alkaline hydrolysis of

chloroform proceeds via the formation of dichlorocarbene. In 1897, Nef correctly suggested the same intermediate to be involved in the famed Reimer Tiemann reaction.[4] (Scheme 2-1)

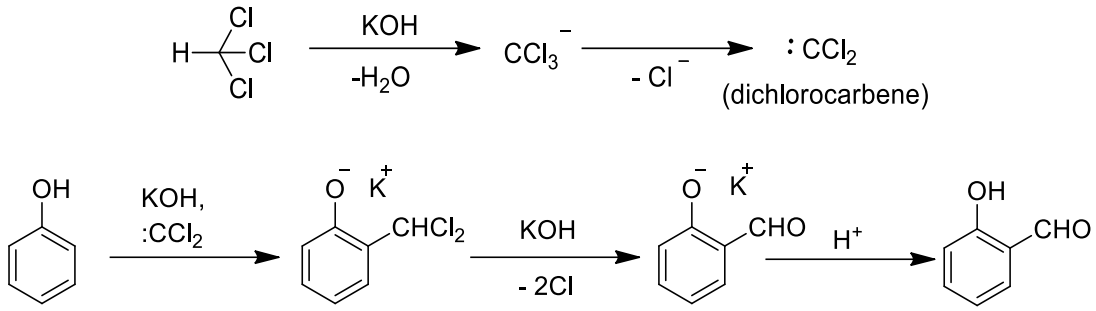

Scheme 2-1: Proposed reaction mechanism for Reimer Tiemann Reaction

In the early twentieth century (1920s and 30s) Staudinger, Kupfer,[5, 6] Curtius[7] all contributed to carbene chemistry by establishing that carbenes, generated from diazo compounds or ketenes, were highly reactive intermediates. The incomplete octet of the divalent carbon in these compounds was the reason behind their heightened reactivity. Note that at this time, the existence of free radicals had only finally been recognised and their popularity was growing rapidly.[8] Naturally, the carbene moiety was seen primarily as a diradical. The methylene radical was seen as a linear species with two electrons in two degenerate p-orbitals, indicating a triplet state.[9]

The mid-twentieth century saw carbenes being accepted as fleeting reaction intermediates as several reactions were discovered that could be mechanistically explained by the participation of a carbene species.[8] In 1953, Doering and Knox published an elegant synthesis of tropolones by an addition of methylene to substituted benzene.[10] The most outstanding contribution from Doering et al. came next year when they proved the existence of dibromo methylene ($:CBr_2$) in the first cyclopropanation reaction involving the addition of $:CBr_2$ to an alkene (Scheme 2-2).[11] However, these decades did not see too many attempts to synthesize or isolate carbenes, and whatever attempts were made had been unsuccessful.[12]

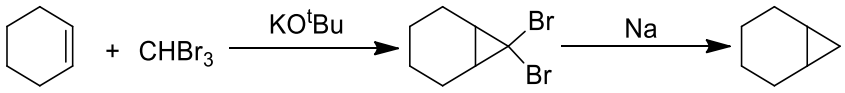

Scheme 2-2: Cyclopropanation via a methylene intermediate as proposed by Doering et al.[11]

By this time (1950s), however, an important development had begun. The upsurge in the popularity of these somewhat 'peculiar' carbon derivatives in synthetic chemistry drew the attention of theoretical chemists and physicists. Armed with increasing computational power,

stalwarts of *ab initio* theory like Pople and Lennard-Jones used theoretical calculations to determine geometric structures and properties of small molecules, including methylene (1951).[13] The shape of the carbene and how this affected the frontier orbitals became a matter of active research (Scheme 2-3).[14, 15] It was asserted that methylene could have two possible electronic structures - (1) one where the carbene is a singlet with a bent sp^2 hybridised C including a pair of electrons in the sp^2 hybridised orbital (σ) and a vacant p orbital (p_π) and the other (2) is a linear sp hybridised geometry where the two non-bonding electrons occupy two mutually perpendicular degenerate p orbitals – p_x and p_y – like the diradical indicated earlier (Scheme 2-3 indicates the two possible geometries). However, it was difficult to know for sure which of these represents the actual ground state without extensive mathematical calculations. In 1968 Hoffmann determined the minimum energy gap between the singlet and triplet states.[16]

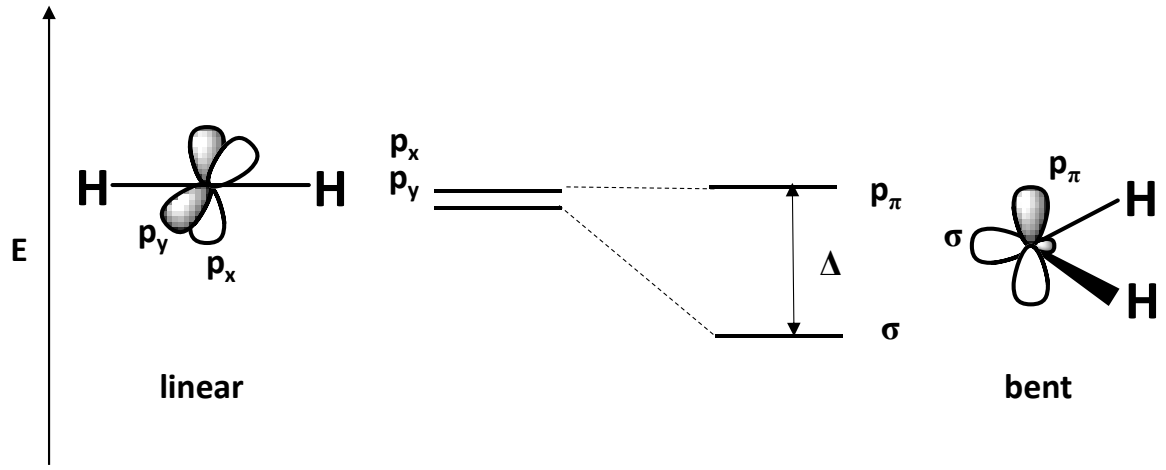

Scheme 2-3: Relationship between carbene bond angle and nature of frontier orbitals

Throughout the next two decades, numerous theoretical papers were published, calculating the exact geometries of methylene moieties like :CH_2, :CHF, :CHBr, :CF_2, :CCl_2, etc..[17] It became more evident that inductive and mesomeric effects go hand in hand in determining the energies associated with the possible electronic states. At around the same time carbenes were spectroscopically characterised in matrices at a few kelvins of temperature (1960s and 70s).[18] This enabled chemists to really isolate and 'see' carbenes for the first time. In 1989 a detailed study of the transient electrophilic and nucleophilic carbenes was reported by Moss.[19]

The debate over the ground state structure of methylene continued to rage on, now that spectroscopic data was available. Herzberg and co-workers published their spectroscopic study[20-22] of the electronic structure of methylene (1959-61) expounding it to be linear.[a] This turned out to be in complete contradiction of several *ab initio* calculations, all of which predicted a bent geometry, having an angle between 130-140°. The disparity with theoretically calculated values made it necessary to make more accurate spectroscopic measurements. The latest spectroscopic measurements by Jensen and Bunker show the angle to be 133.84±0.05° [23-25] which matches almost perfectly with the most extensive *ab initio* calculation that puts the value between 132 and 133°.[26] The accuracy that the theoretical methods displayed in predicting the correct geometry of methylene is considered one of the earliest successes of *ab initio* calculation and theoretical chemistry in general.[26]

In the meantime, the works of Breslow and Wanzlick in the 1950s indicated that the stability of carbenes increased phenomenally in the presence of amino substituents, although they were not able to isolate the monomeric carbenes.[27, 28] Finally, in the year 1964, Fischer and Maasböl synthesised and spectroscopically characterised a carbene species stabilised by bonding with a metal center for which they were awarded the coveted Nobel Prize in 1973 (Scheme 2-4(b)).[29] The first carbene-transition metal complex had actually already been synthesised by Chugaev as early as 1925 (Chugaev's red salt), but this work remained unrecognised for decades.[30] Only in the 1970s was the crystal structure of the compound solved and definitely proven to be a carbene-metal complex (Scheme 2-4(a)).[31]

The following decades saw the foundational work by Öfele and Lappert using carbenes as ligands in organometallic chemistry.[32, 33] But, by such time, a renewed interest caught chemists trying to isolate stable carbenes again. The first free, stable carbene- a (phosphino)(silyl)carbene – was claimed by Bertrand et al. in 1988,[34] breaking open the floodgates as it were. However, this particular species did not show any notable ability in binding transition metals. Finally, Arduengo's discovery of "a stable crystalline carbene" in

[a] The interpretation of the spectroscopic data was somewhat complicated – some subbands in the absorption spectrum that could conclusively prove the structure to be bent could not be observed due to predissociation. At the same time, most of the data obtained would be complementary to a linear methylene. However, they did mention that a methylene with a bond angle as low as 140 was indeed possible.

1991[35] ended the decades' long search, opening new and fascinating doors for generations of chemists to come. The carbene that Arduengo isolated is an imidazole-2-ylidene (Scheme 2-4(c)) and belongs to the class of the most popular carbenes in chemistry – the N-Heterocyclic carbenes (NHC). They bind transition metals, which makes them a popular ligand in catalyst design.

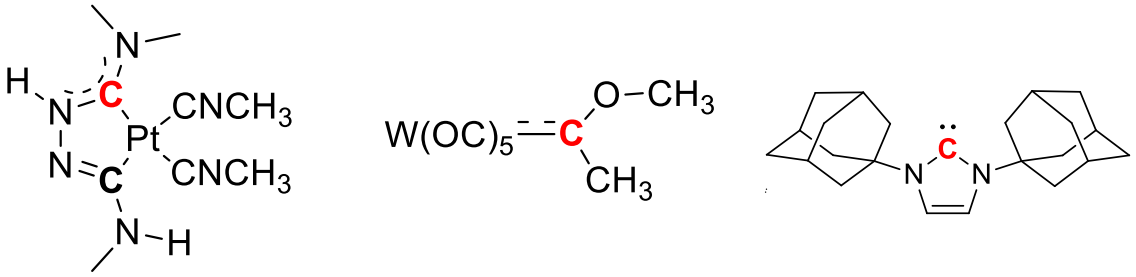

(a) **(b)** **(c)**

Scheme 2-4: (a) Chugaev's red salt (1925); (b) Fischer's Tungsten carbonyl carbene complex (1964); (c) Arduengo's carbene (1991) with the carbenic carbon represented in red in the structure

The history of carbene chemistry is a fascinating narrative and its development is a reflection of modern chemistry. It has seen exemplary contributions from the largely diversified fields of synthetic chemistry, spectroscopy and theoretical chemistry. But even during the discovery of the first 'bottle-able' carbenes (late 1980s), they were largely classified as chemical 'curiosities'.[36] However, the decades that followed saw carbenes, and particularly their organometallic adducts, shoot forward to the very forefront of catalytic chemistry. Carbenes constitute a very flexible class of reagents, whose chemistry can be manipulated to produce a range of effects including electrophilicity, nucleophilicity, radical-character etc. They can be ornamented with appropriate alkyl and/or aryl groups to produced stereospecificity. In fact, carbenes, which have been regarded as unstable reactive intermediates for more than a century, are now used to stabilise other highly-reactive species.[37] It has even made its mark in material science and medicinal chemistry.[38] Carbenes have been instrumental in pushing the boundaries of the chemical sciences - perhaps far beyond what Dumas had imagined 150 years ago, when he thought "Well, why not?"

Let us now take a look at the special class of N-Heterocyclic carbene and some carbones which are the main focus of our computational study.

2A.2. Classical N-Heterocyclic Carbenes or Arduengo Carbenes

N-Heterocyclic carbenes (NHC) can be defined as heterocyclic species containing a carbene carbon and at least one nitrogen atom within the ring.[38] This criteria covers many different classes of carbene compounds of various substitution patterns, ring sizes, degree of heteroatom stabilisation etc. However, most of the NHCs reported in chemical literature are derived from imidazolium salts and therefore are characterised by a five-member ring with the carbene carbon at placed in between two nitrogen atoms. The first carbene reported by Arduengo (Scheme 2-4(c)) is a representative example of this category – therefore these carbenes are also referred to as Arduengo carbenes and normal/classical N-Heterocyclic carbenes. NHCs form the most popular group among the persistent carbenes i.e., carbenes that show particular stability in their native forms. NHCs usually feature very bulky substituents adjacent to the carbene carbon, such as the adamentyl groups in the first carbene synthesised by Arduengo, generally to provide kinetic stability. NHCs are also usually singlet carbenes with a lone pair in sp^2 hybrid orbital and a vacant unhybridized p orbital (indicated as p_z in Scheme 2-5) perpendicular to it.

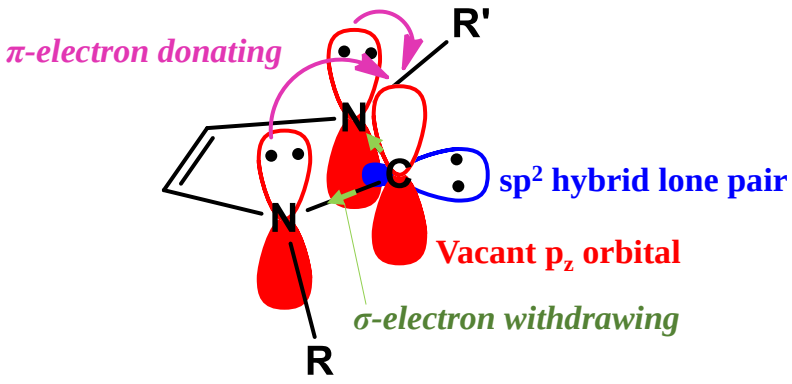

Scheme 2-5: Typical structure of an NHC with intra-molecular mesomeric and inductive effects highlighted in purple and green arrows respectively

Inductive and mesomeric effects are simultaneously responsible for the kinetic stability and multiplicity of the ground state of these molecules. The σ-electron withdrawing and π-electron donating effect of the neighbouring nitrogen atoms in Arduengo carbenes help to lower the energy of the sp^2 hybridised σ lone pair favouring the singlet state. Furthermore, their π-electron donating effect stabilises the vacant p_z orbital. The cyclic structure also forces the lone pair into a more s-character of its sp^2 type hybridation, thereby stabilising it. These effects have been discussed in more detail in Section 2A.4.

2A.3. Beyond Classical N-Heterocyclic Carbenes

Although the most popular carbenes today are still the Arduengo type, a large number of carbenes have been synthesised that do not belong to this category. A key feature in the Arduengo carbenes is the somewhat 'excessive' heteroatom stabilisation by ensuring the presence of two heteroatoms, at least one of which is nitrogen in the α-position of the carbene carbon.[39] The idea of a carbene that is not stabilised by two α-N atoms arose with the serendipitous discovery of C4 bonding in imidazolylidenes (Scheme 2-6).[40]

(a) Normal binding mode via C2
Imidazol-2-ylidene-M

(b) Abnormal binding mode via C4
Imidazol-4-ylidene-M

Scheme 2 -6: Binding modes of imidazolylidenes

Thus a large group of other, less-stabilised heterocyclic frameworks as well as acyclic carbenes lead to the preparation of carbenes in which the electronic and steric parameters are vastly different from Arduengo carbenes discussed above.[39] That includes carbenes that are stabilised by one or no heteroatoms adjacent to the carbonic carbon. There are several ways of classifying the carbenes available today, each method highlighting one crucial difference between its classes. The following are a few important categories that are ubiquitous in chemical literature.

Normal vs. Abnormal NHC

The term 'abnormal' was first proposed by Crabtree[41] to refer to imidazol-4-ylidenes in order to draw attention to the contrast of this species to their far more popular isomer imidazol-2-ylidenes (Scheme 2-6). The term refers to any case where the free ligand is mesoionic – meaning that it is not possible to write a completely uncharged resonance structure for such a neutral molecule, i.e. only resonances structures including at least one positive and one negative charges on some atoms can be drawn. This group of structures, called either abnormal carbenes or mesoionic carbenes (MIC) have several fundamental differences with NHCs in their free state.

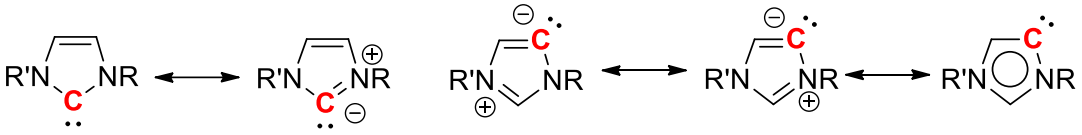

(a) Normal NHC **(b) Abnormal / Mesoionic carbenes**

Scheme 2-7: Resonance structures of (a) normal and (b) abnormal/mesoionic NHC

An MIC is characterised by exceptionally strong σ-donating ability, in a range that is normally not achievable by modification of classical NHCs alone. For instance, the TEP[b] for a normal NHC such as 1-isopropyl-3-methyl-4,5-diphenylimidazol-2-ylidene is 2039 cm^{-1} compared to 2047 cm^{-1} associated with the corresponding abnormal NHC (Scheme 2-8).[42]

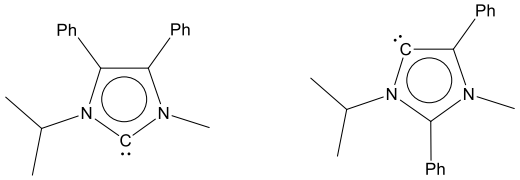

(a) **(b)**

TEP **2047 cm^{-1}** **2039 cm^{-1}**

Scheme 2-8: (a) 1-isopropyl-4,5-diphenyl-3methylimidazol-2-ylidene (b) 1-isopropyl-2,4-diphenyl-3-methylimidazol-5-ylidene

This enhanced donating ability can be rationalised by considering the fact that compared to NHCs, such molecules are missing a neighbouring N atom for the carbenic centre, making the sp^2 lone pair higher in energy, thus increasing its donating ability.

Remote vs. Non-remote NHC

An orthogonal method of classification of NHC considers the location of the heteroatom in the carbene. The so called remote NHCs feature no heteroatoms adjacent to the carbene carbon. Thus, remote carbenes may be normal or abnormal (Scheme 2-9). The first free remote carbene was prepared by Bertrand *et al.*[34] and the first remote NHC complexes were synthesised by Raubenheimer.[43] Calculations indicate a stronger metal-carbene bond for remote NHC compared to their non-remote analogues.[44]

[b] TEP or Tolmann electronic parameter is an experimental parameter designed to measure the electron donating ability of a ligand (L) by measuring the shift in stretching frequency of CO in $Ni(CO)_3L$ complex. It is discussed further in chapter II.

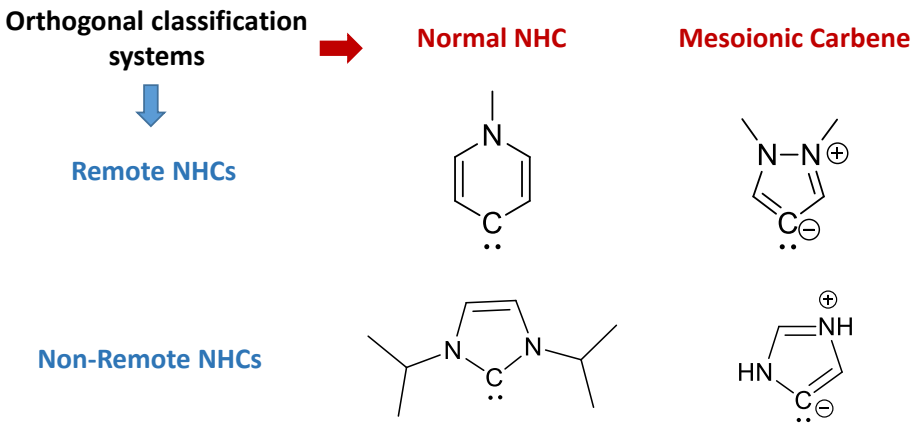

Scheme 2-9: Orthogonal classification of carbenes

Cyclic Alkyl Amino Carbenes (CAACs)

Bertrand et al. pioneered the synthesis of cyclic alkyl amino carbenes (CAACs or cAACs) which, for the purpose of this thesis are classified as NHCs.[45] In contrast to the carbene species mentioned earlier, CAACs are characterised by a single nitrogen atom next to the carbene carbon and an sp^3 hybridised alkyl carbon on the other side (Scheme 2-10). These carbenes are stable and crystalline, with distinct melting points, proving that one nitrogen is sufficient to stabilise an electron deficient carbene centre. When compared with saturated imidazol-2-ylidenes,[c] it was found that the presence of only one N makes these carbenes stronger σ-donors. At the same time, CAACs are better π-acceptors than Arduengo type carbenes.[46] In addition, the quaternary C and its substituents provide some stereoselectivity to CAACs compared to Arduengo carbenes.

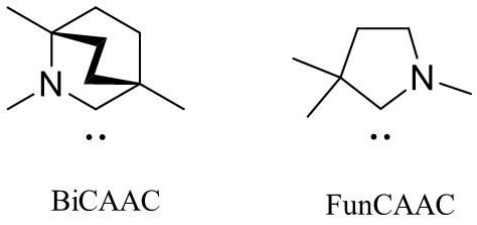

Scheme 2-10: Some representative examples of CAAC molecules, bicyclic CAAC (BiCAAC) and functionalised CAAC (FunCAAC).

[c] 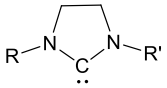

Saturated imidazol-2-ylidene

Carbones

Carbones form a separate category of ligands that are distinct from carbenes in the number of electron pairs on the carbon donor atom although both carbenes and carbones possess a sigma lone pair on the coordinating carbon centre. In carbones, denoted by CL_2, the divalent C(0) atom retains all four of its electrons as two lone pairs and accepts two pairs of electrons from its two neutral donor ligands (L) via coordinate covalent bonds.[47] Therefore a carbone is best represented as L→C←L. Depending on the nature of L, there can be different types of carbones. For example, when L= Phosphine we get carbodiphosphoranes (Scheme 2-11(a)), when L= NHC they are called carbodicarbenes (Scheme 2-11(b)) etc.

The two electron pairs in a carbone are of different symmetry and are non-degenerate – one is of σ symmetry (similar to the carbene lone pair) and the other pair is in the p_z orbital perpendicular to the valence plane having π symmetry. Carbones are not only versatile compounds in their own right, but they have been used in stabilising highly electron deficient systems such as BH_2^+[48] and $B_2H_5^+$[49] by virtue of the *two* lone pairs of electrons.

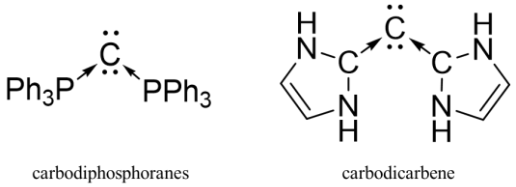

Scheme 2-11: Representative examples of (b) carbodiphosphoranes and (c) carbodicarbenes

In the following section we take a closer look at the various stereo-electronic effects that play a central role in the chemistry of these compounds.

2A.4. Electronic Structure of Carbenes

The ground state electronic structure (singlet or triplet) of carbenes and geometry (linear or bent) is a fundamental feature of carbenes and it dictates their reactivity, as we have already mentioned before.[50] This in turn depends upon the nature of the substituents and the mesomeric, inductive and steric effect it exerts on the carbene center. These factors are briefly discussed in the following sections:[50]

2A.4.1. Inductive effect

The electronegativity of substituents affects the multiplicity of carbenes. σ-electron withdrawing substituents favour the singlet over triplet state. Harrison et al. showed that the carbenes go from being a triplet to a singlet on changing the electronegativity of the substituents by varying from lithium to hydrogen and then finally to fluorine.[51] The effect can be easily rationalised by using molecular orbital diagrams for C_{2v} symmetry. σ-electron withdrawing substituents lower the energy of the lone pair (noted n_σ) by increasing its s character while the p_z orbital remains unchanged as a p_π MO of b_1 symmetry (n_p in Scheme 2-12). This increases the HOMO-LUMO gap, stabilising the singlet state relative to the triplet state.

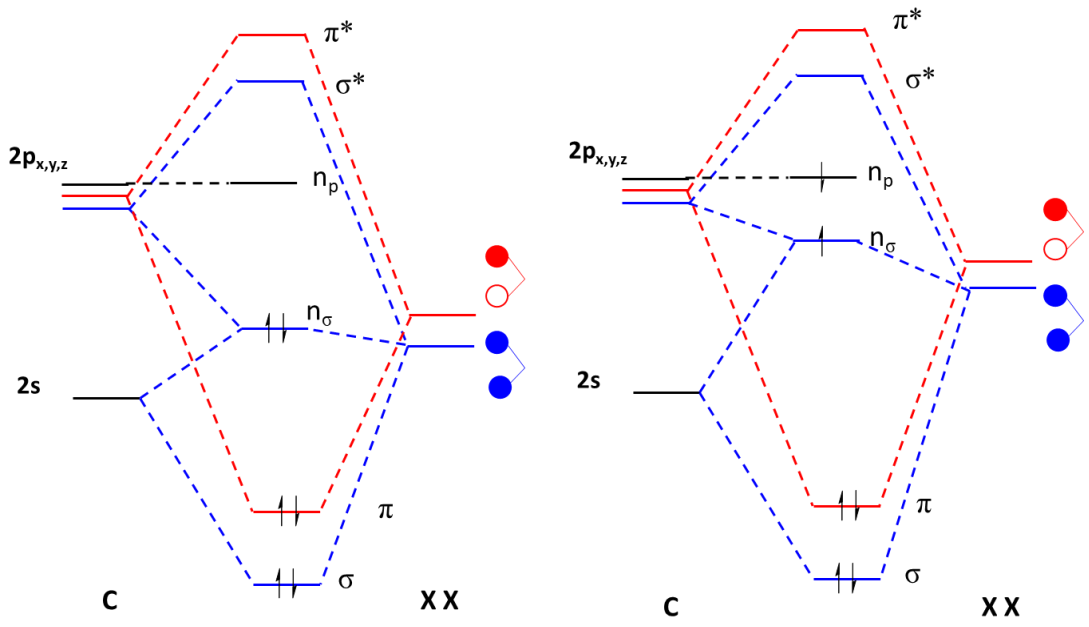

Scheme 2-12: Molecular orbital diagram of bent CX_2 showing inductive effect of highly electronegative substituents (left) and weakly electronegative or electropositive substituents (right)

2A.4.2. Mesomeric effect

The mesomeric effect plays a much more significant role in influencing the ground state electronic structure and geometry than the inductive effect. The substituents interacting with the carbene center can be classified into two categories – the π-electron donating groups denoted in Scheme 2-13 by L (-NR_2, -OR, -SR etc.) and can be characterised by a "high-energy" doubly occupied orbital, and the π-electron withdrawing groups denoted by Z (-COR, PR_3^+

etc.) characterised by a “low-energy” vacant orbital. Therefore the carbenes themselves can be classified into three categories – (L,L)-carbenes, (L,Z)-carbenes and (Z,Z)-carbenes.

The (L,L)-carbenes are predicted to be bent and in singlet state.[52, 53] The p_π orbital centred on the carbene carbon interacts with the combination of filled p orbitals on the neighbouring atoms – thereby generating a vacant LUMO of higher energy ($p_\pi(b_1)$). As the lone pair in the σ plane remains nearly unaffected, the energy gap between the HOMO and LUMO is effectively increased – leading to the singlet state. Arduengo carbenes (derivatives of imidazol-2-ylidenes) (Scheme 2-13 (a)), belong to this category.

Most (Z,Z)-carbenes are predicted to be linear, singlet carbenes. Here, the substituent vacant orbitals interact with the p_z orbital on the carbene carbon that lies parallel to it. The p_y orbital is not affected by this interaction and therefore the degeneracy of the p_y and p_z orbital is lost. Hence, these are singlet carbenes in spite of being linear. Such molecules are best described by two zwitterionic resonating structures, featuring a positive charge on the carbene carbon. Dicarbomethoxycarbenes and ‘masked’ diborylcarbenes are representative examples of this category (Scheme 2-13 (b)).

The quasi-linear (LZ) carbenes combine both these effects. The L substituent lone pair interacts with the vacant p_z orbital of the carbene while the filled p_y orbital of the carbene in turn interacts with the vacant orbital on the Z substituent. This forms something like a polarised allene system. Bertrand’s first (phosphine)(silyl)carbene falls under this category. (Scheme 2-13 (c))

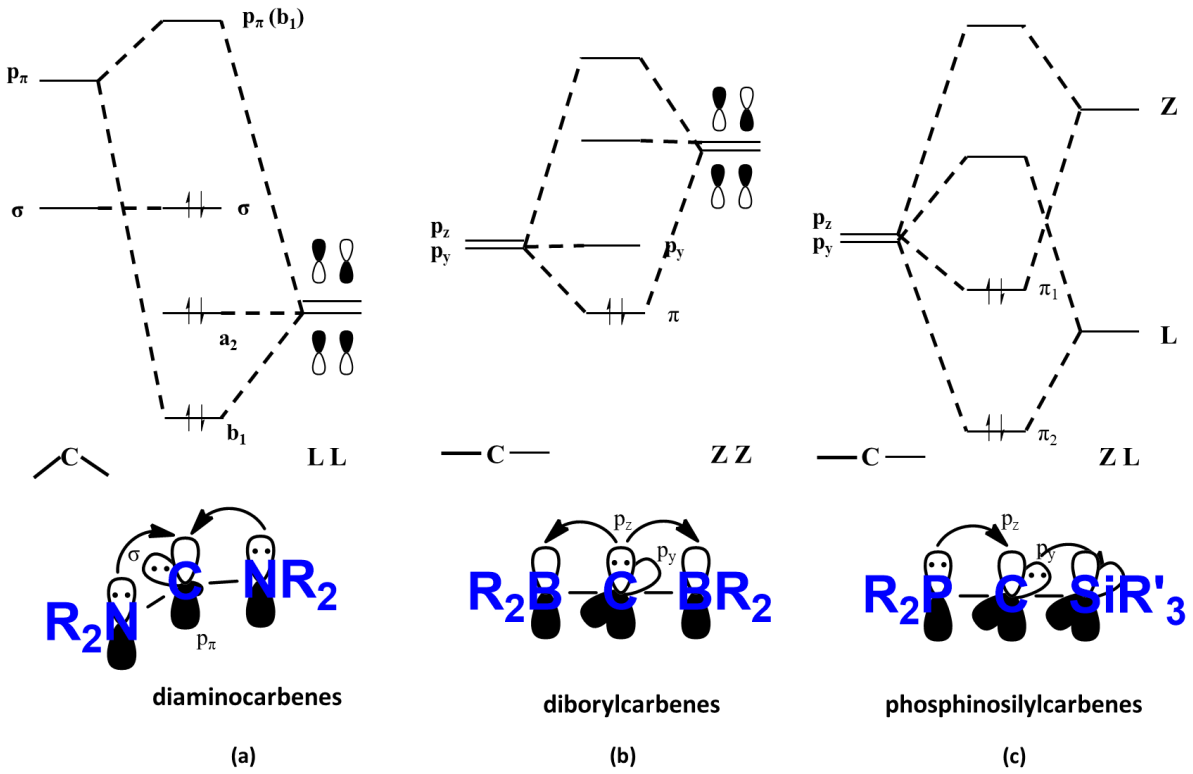

Scheme 2-13: Perturbation orbital diagram showing the influence of mesomeric effect of different substituents in carbenes.

2A.4.3. Steric Effect

Bulky substituents help to kinetically stabilise all kinds of carbenes by preventing dimerization (Wanzlick equilibrium).

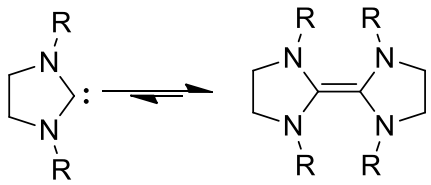

Scheme 2-14: Wanzlick equilibrium

In absence of significant electronic effects, steric effects also control the multiplicity of a carbene. Since the maximum stabilisation of a triplet carbene relative to a singlet carbene is when their frontier orbitals are degenerate, a linear geometry favours a triplet state. This point can be illustrated by the difference between dimethyl carbene, which has a bent singlet ground state, whereas di(tert-butyl)-carbene or diadamenyl carbene are triplets. N-Heterocyclic carbenes, being cyclic, are forced to stay in a bent geometry and therefore prefer the singlet state.[50]

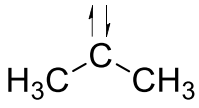

Bent dimethyl carbene

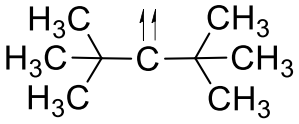

Linear di(t-butyl)carbene

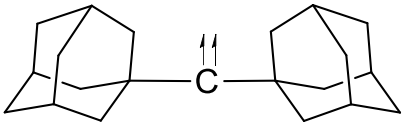

Linear diadamentylcarbene

Scheme 2-15: Some examples of linear and bent carbenes whose shape is mainly controlled sterically

2A.4.4. Measuring Steric and Electronic Properties

In the previous sections we have taken a look at the various divalent carbon compounds that are present in a chemist's arsenal. These include Arduengo's carbenes, CAACs, MICs, remote carbenes and carbones to name a few of the prominent categories. Each of these different classes represent a different combination of properties – some are significantly strong σ-donors (MICs), some are σ-donors and π-acceptors (Arduengo carbenes, cAACs), some are σ and π donors (carbones). In principle, by tuning the steric and electronic properties of these divalent carbon compounds each application (discussed in the following section) ought to have some tailor-made carbenes that are ideally suited to fulfil these roles. However, this is not a straightforward task. Terms like "strong" or "weak" donor have no quantitative value and, therefore, are somewhat arbitrary. Hence, quantification of the steric and electronic properties of these compounds is of primary importance.

The steric and electronic properties of these divalent carbon compounds can be measured using both experimental and theoretical methods. Among experimental methods most methods use a spectroscopic probe (a different ligand that when coordinated to the divalent carbon compound shows a change in its spectroscopic properties). The most popular of these methods have been mentioned briefly in the chart below. These factors have not been discussed here as they are elaborately explored in Chapter III of this thesis. Similarly, there are also various theoretical tools that also allow to measure these properties and some of them are listed in the chart below. These properties are mainly the tools used in our investigation and have been discussed in section 2B.9.

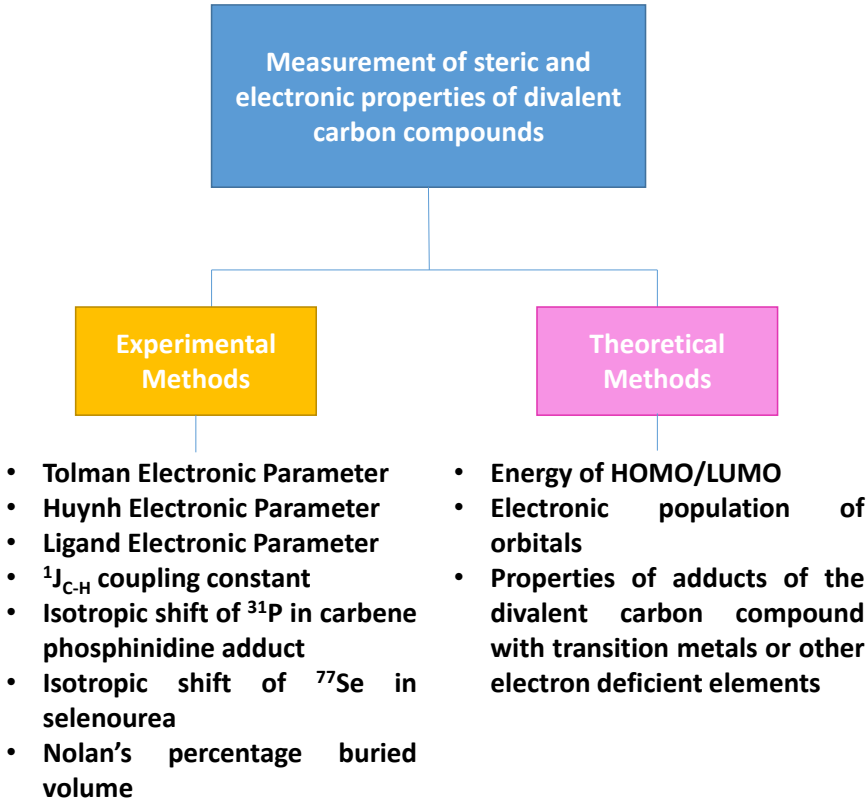

Scheme 2-16: Various experimental and theoretical methods to evaluate steric and electronic properties of divalent carbon compounds.

2A.5. Relationship between Structure and Activity

There is an intimate relationship between the structure of chemical compounds and their reactivity. In the previous section we have taken a look at the steric and electronic factors that influence the reactivity of NHCs, and by extension, carbones as well. In general, it is found that the presence of a heteroatom next to the carbene carbon increases the stability of the singlet carbene by stabilising the vacant p orbital of the carbene and at the same time lowering the energy of the lone pair. The bent Y-C-Y angle (Y = α-atoms to carbenic carbon) also stabilises the singlet state. Therefore, it is evident that reactivity of such compounds can be easily manipulated by varying the mentioned parameters through alterations in the carbenic backbone.

For instance, although the combination of strong σ-donation and weak π-acid puts NHCs within the same bracket as phosphines in some senses,[54] they have their own unique characteristics. NHCs and carbones have a highly directional sp^2 lone pair on carbon as compared with the non-directional s-type lone pair of phosphorus in phosphines. NHCs forms stronger bonds with metals (indicated by lower TEP values) forming more thermodynamically

stable complexes.[55] The stronger σ-donating ability is also testified by the higher proton affinity values associated with NHCs.[56-58] At the same time, the NHCs and carbones do not participate in π-backbonding as readily as phosphines (although this interaction cannot be ignored).[59-63] As a result, the electron density on the transition metal in an adduct is higher in one with an NHC or a carbone than with phosphines. Phosphines and NHCs are also quite different in terms of their steric effect. NHCs are generally considered more sterically demanding because the group points towards the metal centre. This could sometimes result in weaker carbon-metal bonds in spite of the higher donating ability of the carbenes.[64]

Similarly, study of electronic structures of Arduengo and mesoionic carbenes helps to explain the even greater donating ability of mesoionic carbenes. The vinylic character of mesoionic carbenes as well as absence of one α-N atom make them exceptionally strong σ-donors.

The backbone of NHCs can also be modified to tune the electron donation of NHCs and carbones. This is illustrated by a study comparing the gradual increase in electrophilic character going from a diaminocarbene (NHC), to a monoamino-amidocarbene (MAAC) and finally to a diamidocarbene (DAC).[65] The electron withdrawing carbonyl group in the backbone of MAAC and DAC makes the carbene carbon less electron rich and more prone to participating in electrophilic reactions like activation of C-H bond.[66] The gradual increase in electrophilicity is evidenced by the increasing trend of TEP values (Scheme 2-17).

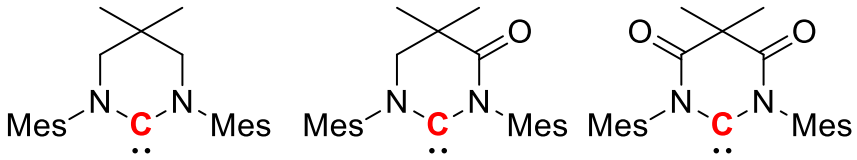

Scheme 2-17: Diaminocarbene (NHC), monoamido-amino carbene (MAAC) and diamido carbene (DAC) with their TEP values

These few examples and various other studies therefore clearly indicate that the structure of divalent carbon compounds is the key to understand and exploit their chemical characteristics. Theoretical studies focussing on structure activity relationships are useful in the design of catalysts that are required to be 'reactive, selective and enduring' at the same time.[67] Quantum chemical studies contributed to this field indirectly – through the calculation of molecular and material properties and reaction mechanisms. Broadly speaking, there are

two different approaches for catalyst design in computational chemistry – (a) study of reaction mechanism and (b) measurement of physical properties. While atomistic study of reaction mechanism provides detailed knowledge of the catalytic cycle but requires an atomistic treatment, physical-property based techniques allows one to survey large ranges of chemical space but the interpretation of such information may not be straightforward. Such physical property-based studies to establish a relationship between steric and electronic properties of phosphines and carbenes to measurable outcomes of catalyst modification such as yield, rate and selectivity have been conducted in particular by Fey and co-workers.[68] Numerous investigations have been made to study the electronic structure of carbenes and their adducts with transition metal complexes.[69-71] Frenking and co-workers have worked extensively on the bonding between main group and transition metal compounds employing EDA-NOCV analysis.[72] Sometimes theoretical studies also yield surprising information that can inspire further investigations. For instance, the study of NHC-Transition metal bonds by Cavallo and co-workers have revealed a surprising π-backdonation from d^0 metal centres.[73] This demands further studies with simpler systems.

In this thesis, our objective is to use computational tools to study the borenium adducts of the divalent carbon compounds. We particularly emphasise on the theoretical estimation of how their reactivity changes due to changes in the carbenic backbone, not just in a qualitative but also in a quantitative manner. Ideally, we wish there to have been *one* measurable *chemical parameter* pertaining to a chemical compound that correlates with *reactivity* (although that hardly ever is the case). This raises three important question – (1) which *chemical parameter* associated with the compound under investigation should be chosen? (2) which parameters should be chosen as measurable outcomes of catalyst modification? (3) and, finally, what is the measure of a "good" or "bad" correlation. In this work, we mainly attempt to answer the first question.

We turn our attention to a specific problem – the borenium adducts of divalent carbon compounds and their role as Lewis acids in activating small molecules (*vide infra*). Naturally, the chemical parameter that should to be quantified is Lewis acidity. For this, however, Lewis acidity has to be first defined and some quantifiable parameter pertaining to Lewis acidity has to be identified. Once this is achieved, this parameter is compared with a parameter associated with reactivity, usually the energy of activation for the reaction under question.

The quality of correlation is usually determined by the value of the square of the regression coefficient (R^2) corresponding to a linear fit, although other parameters (see Appendix) can give a more complete picture of parity or disparity between the two parameters being compared.

In the following section we take a brief look at the chemical history and significance of carbene-borenium adducts – how they appeared as plausible candidates for Frustrated Lewis pair (FLP)-based activation of hydrogen, why they hold particular promise in the field and how computational calculation of Lewis acidity can be a potential indicator for the design of more efficient catalysts.

2A.6. The Case for Carbene-Borenium Adducts

During the past few decades, global awareness and concern about environmental and fiscal cost of energy and material intensive chemical processes have been growing. Keeping that in mind, development of new, more environment friendly catalytic strategies have become a crucial demand in chemistry. Hydrogenation is one such catalytic process that has huge industrial application. Presently hydrogenation of unsaturated bonds employs highly effective transition metal-based catalysts in spite of their toxicity, cost, rarity and high carbon footprint. Naturally there has been an extensive pursuit of viable alternatives. One of the directions is the development to catalysts based on cheap, non-toxic transition metals like iron and cobalt as well as early metals such as titanium and calcium. The other way is to depend on organocatalysis, of which one example is FLP chemistry (*vide infa*).[74]

The NHCs present a remarkable similarity with transition metals themselves, having filled σ and vacant π frontier orbitals. Taking advantage of this, NHCs can be used in activating small molecules such as NH_3.[75] π-accepting NHCs such as CAACs are particularly suitable for such reactivity. Sterically encumbered NHCs (Lewis bases) like 1,3-di-tert-butylimidazolin-2-ylidene can be coupled with sterically encumbered Lewis acids like $B(C_6F_5)_3$ to form frustrated Lewis pairs (FLP) that cannot form an adduct together because of steric repulsion. They can, however, be used in splitting small molecules such as H_2 by polarising the molecule that finally leads to heterolytic cleavage of the H-H sigma bond.[76]

The first such report of metal-free hydrogen activation was published in 2006 where H_2 activation was carried out by a linked phosphino-borane by Stephan et al. (Scheme 2-18)[77]

The next year, they were able to use a similar species of the form $(Me_3C_6H_2)_2PH(C_6F_4)BH(C_6F_5)_2$ in the metal-free catalytic hydrogenation of imines and protected nitriles.[78] (Scheme 2-18)

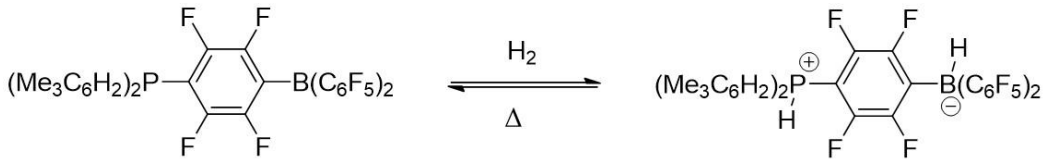

Scheme 2-18: Reversible hydrogen activation by linked phosphino-borane

This created the concept of FLP catalysis and eventual experimentation lead to a commendable broadening of substrate scope. However, the catalyst efficiency still cannot compete with transition metal-based catalysts. The difficulty of synthesis of electrophilic boranes presents quite a challenge to having a large family of such compounds so that a structure-activity relationship may be established.[148]

The catalytic cycle of imine hydrogenation, the reaction studied by Crudden et al., consists of two steps (Scheme 2-19).[90] The first step involves the polarisation and heterolytic cleavage of hydrogen molecule by the frustrated Lewis acid base pair – the imine acting as the Lewis base and the boron compound acting as the Lewis acid. For the catalysis to be complete, in the next step the hydride that had been accepted by the boronic Lewis acid is added to the C to the iminium ($C=NH^+$) bond, thus completing the addition of H_2 across the iminium double bond.

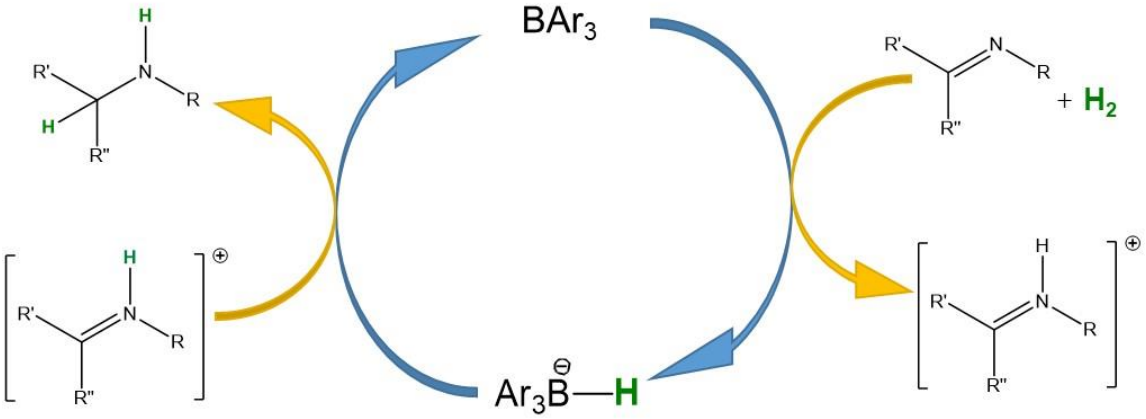

Scheme 2-19: The general catalytic cycle for FLP hydrogenation of imines

Some studies suggested that slight modification of the Lewis acid Lewis base pair in an FLP hydrogenation catalyst greatly influences the activity and selectivity. For instance, Soós and coworkers found that replacing one C_6F_5 group from $B(C_6F_5)_3$ by a bulkier mesityl group affects

the selectivity of the reaction.[79, 80] In fact, careful selection of the Lewis base in FLP hydrogenation has led to the expansion of substrate scope to include silyl enol ethers,[81] olefins,[82] aldehydes and ketones.[83, 84]

As far as work on optimising the Lewis acid is concerned, most FLP hydrogenation catalysts initially used a neutral boron compound (BR_3) as the Lewis acid. In order to maximise the Lewis acidity, the boron is attached to highly fluorinated substituents, e.g. $B(C_6F_5)_3$. However, the presence of such electronegative substituents deters hydride donation in the next step (Scheme 2-19), thereby slowing down the catalysis. In addition, boranes are also highly air- and moisture-sensitive and therefore present a synthetic challenge. A less explored, but important class of boron-based Lewis acids, the borenium ion, was introduced by Stephan et al. as a viable alternative to using neutral boron Lewis acids in FLP hydrogenations.[74]

Borenium is a trivalent boron cation. A considerable amount of Lewis acidity of these compounds is attributed to this positive charge. Nevertheless, these cationic borenium can be stabilised by coordination to sterically demanding groups or highly electron donating groups. A number of these species have been used as electrophiles in aromatic and aliphatic borylations and also as catalysts in hydroboration of alkenes.[85] The first instance of an NHC stabilised borenium was provided by Matsumoto and Gabbai who reported the synthesis and characterisation of $[(IMe)BMes_2]OTf$ (IMe = 1,3 dimethylimidazol-2-ylidine) in 2009.[86] A number of NHC-Borenium adducts have been synthesised since then.[87] At the same time the NHC-Borane have been proven to be strong reductants.[88, 89] So while NHC-borenium cations are strongly electrophilic, NHC-Borane adducts are efficient hydride donors. This combination of properties makes these adducts ideal for the FLP hydrogenation process mention above.

It follows from the studies conducted thus far that changing the nature of the NHC can dramatically change the electrophilicity of the NHC-borenium adduct – generating more (or less) efficient catalysts. Indeed, such an improvement takes place when the classical NHC in NHC-borenium adduct is replaced by a related divalent carbon compound – MIC. Crudden et al. show vast improvements in catalytic activity during the hydrogenation of aldimine, ketimines and N-heterocycles on using MIC stabilised boreniums in comparison to neutral boron compounds like $B(C_6F_5)_3$ or even NHC-stabilised boreniums due to the enhanced electrophilicity of MIC.[90]

While the effect of an NHC change on catalytic efficiency in NHC-borenium FLP hydrogenation catalysis has been observed by Crudden and others, the rationalisation and understanding of this phenomenon remains incomplete. With the aim of establishing a structure-activity relationship, we have selected these species as the core chemical target of our work. To generate better catalysts or have an efficient activation, one can assume that a stronger Lewis acidic borenium is required, and for the strongest Lewis acid, the NHC with the weakest π-donating ability must be ideal. The σ-donating ability of NHCs and carbones can also be determined by some theoretical and experimental method. In PART A of the thesis the efficiency of the various available methods to quantify σ and π donation in NHC and carbones have been explored. PART B of the thesis is dedicated to the measurement of Lewis acidity as a combination of σ and π effects quantified in PART A. At the final section, PART C, the relevance of parameters, such as the one we have at our disposal at the end of PART B, in predicting the reactivity of borenium based Lewis acids in activating small molecules like H_2 is explored.

2B. Electronic Structure Theory – A Brief Overview

In this thesis we use computational chemistry to study the properties of divalent carbon-borenium adducts. From a theoretical stand point, information about any system (like our NHC-borenium adduct) can be obtained from the knowledge of its wave function. We can arrive at an approximate wave function by solving the Schrödinger equation. There are several levels of approximations necessary to solve it and we briefly go over the various steps. Then finally we look at electron density as a fundamental variable, replacing the wave function. This is the basis of density functional theory. Finally, we take a look at some technical aspects for obtaining the most reliable solutions. This includes the choice of exchange correlation functionals and basis sets.

In this section, we discuss only the general theoretical frame work and approximations that are employed in computational chemistry to evaluate various properties associated with a chemical system. The exact application of the computational techniques to the divalent carbon compound-borenium adduct has been elaborated in the respective chapters.

2B.1. Solving the Schrödinger Equation

The first postulate of quantum mechanics posits that the state of a quantum mechanical system is completely described by a function $\boldsymbol{\Psi}$(x,t), x and t being the coordinates of space and time. The second postulate states that every physical observable in the universe can be represented by an operator in quantum mechanics. These operators are Hermitian and follow the eigenvalue equation for a set of eigen functions ('eigen' meaning 'characteristic'). In chemistry, one is almost always concerned with energy – the energy levels of atoms and molecules (electronic, vibrational…), energy change during chemical processes (ΔG, ΔH and so on), etc... Energy is given by the eigenvalues of the energy operator - the Hamiltonian operator (**H**). Therefore, in order to gain information about the energy levels of a system, we attempt to solve the following eigenvalue equation, better known as the Schrödinger equation:[91, 92]

$$\mathbf{H}\,\boldsymbol{\Psi}(\mathbf{x},\mathbf{t}) = \mathbf{E}\,\boldsymbol{\Psi}(\mathbf{x},\mathbf{t}) \qquad (1)$$

It can be shown that the expectation value of energy obtained from the solution of the eigenvalue equation of the time-independent Hamiltonian is independent of time. Further, the spin and orbital angular momentum for many molecular systems, as is the case for the

systems under study in this thesis, are non-coupled. Therefore, we mainly concern ourselves with the solution of *time-independent*, *non-relativistic* Schrödinger equation:

$$\mathbf{H}\,\Psi(\mathbf{x}) \;=\; \mathbf{E}\,\Psi(\mathbf{x}) \tag{2}$$

Here, the wavefunction **Ψ** is the total wavefunction that depends on the space and spin coordinates of both electrons and nuclei. The Hamiltonian operator ($\mathbf{H_{tot}}$) consists of the following 5 terms:

$$\begin{aligned}\mathbf{H_{tot}} \;&=\; -\sum_{i=1}^{N}\frac{1}{2}\nabla_i^2 - \sum_{A=1}^{M}\frac{1}{2M_A}\nabla_A^2 - \sum_{i=1}^{N}\sum_{A=1}^{M}\frac{Z_A}{\mathbf{r_{iA}}} + \sum_{i,j\ i<j}^{N}\frac{1}{\mathbf{r_{ij}}} + \sum_{A,B\ A<B}^{N}\frac{Z_A Z_B}{\mathbf{r_{AB}}} \\ &=\quad \mathbf{T_e} \quad + \quad \mathbf{T_N} \quad + \quad \mathbf{V_{Ne}} \quad + \quad \mathbf{V_{ee}} \quad + \quad \mathbf{V_{NN}}\end{aligned} \tag{3}$$

Where i and j are the electronic index, A and B are the atomic index, N is the total number of electrons, M is the total number of atoms, Z_A denotes the charge of atom A, $\mathbf{r_{ij}}$ (= $\mathbf{r_i} - \mathbf{r_j}$) is the distance between electrons i and j, $\mathbf{r_{iA}}$(= $\mathbf{R_A} - \mathbf{r_i}$) denotes the distance between electron i and atomic nucleus A, $\mathbf{r_{AB}}$ (= $\mathbf{R_A} - \mathbf{R_B}$) denotes the distance between atoms A and B and the Laplacian operators ∇_i^2 and ∇_A^2 involve differentiation with respect to the coordinates of the i^{th} electron and A^{th} atom respectively. The equation has been expressed in atomic units. The first term of equation (3) is the operator for the kinetic energy of the electrons ($\mathbf{T_e}$), the second term is the kinetic energy of the nuclei ($\mathbf{T_N}$), the third term is the coulombic attraction between electrons and nuclei ($\mathbf{V_{Ne}}$) while the fourth and fifth terms indicate the inter-electronic and inter-nuclear repulsion $\mathbf{V_{ee}}$ and $\mathbf{V_{NN}}$ respectively. The five terms together constitute the total Hamiltonian ($\mathbf{H_{tot}}$).

$\mathbf{H_{tot}}$ has several features of interest. Examination of the terms show that $\mathbf{T_e}$ and $\mathbf{V_{ee}}$ are independent of nuclear coordinates, they are constant for all iso-electronic systems. $\mathbf{T_N}$ and $\mathbf{V_{NN}}$ on the other hand have no dependence on electronic coordinates. The $\mathbf{V_{Ne}}$ potential energy term is special in this respect – it acts as the molecular signature in the expression of $\mathbf{H_{tot}}$ by coupling electronic and nuclear coordinates together.

2B.2. The Born Oppenheimer Approximation

The Born Oppenheimer approximation is central to quantum chemistry. Intuitively, one can say that nuclei, being many orders of magnitude heavier than electrons can be approximated to be stationary with respect to the electronic motion. This enables us to make some crucial

simplifications in the expression of $\mathbf{H_{tot}}$: the $\mathbf{T_N}$ term can be safely approximated to zero, $\mathbf{V_{NN}}$ becomes a constant that has no effect on the operator eigenfunctions and $\mathbf{V_{Ne}}$ now essentially has a parametric dependence on the nuclear coordinates (**R**). **r** represents the electronic coordinates in this case. So now, we can write the electronic Schrödinger equation:

$$\mathbf{H_{el}}\boldsymbol{\varphi}_{\mathbf{el}}(\mathbf{r},\{\mathbf{R}\}) = \mathrm{E}_{\mathrm{el}}\{\mathbf{R}\}\varphi_{\mathrm{el}}(\mathbf{r},\{\mathbf{R}\}) \tag{4}$$

where,

$$\mathbf{H_{el}}(\mathbf{r},\{\mathbf{R}\}) = \mathbf{T_e}(\mathbf{r}) + \mathbf{V_{Ne}}(\mathbf{r},\{\mathbf{R}\}) + \mathbf{V_{ee}}(\mathbf{r}) \tag{5}$$

By parametric dependence we mean that for different arrangements of the nuclei, φ_{el} is a different function of the electronic coordinates. Note that equation (4) would be exactly solvable if there were no electron-electron repulsion ($\mathbf{V_{ee}}$ = 0), i.e., for a non-interacting system. Although that is a very big approximation and not close to the exact solution at all, it becomes a good starting point for a 'guess' wave function for variational optimisation.

After solving the electronic problem, one can subsequently solve for the motion of nuclei by replacing the electronic coordinates by their average values, averaged over the electronic wave function. This then generates the nuclear Hamiltonian for the motion of the nuclei in the average field of electrons.

$$\mathbf{H_{nu}} = \mathbf{T_N} + \mathbf{V_{NN}} + < \mathbf{H_{el}} > \tag{6}$$

$\mathbf{V_{NN}}$ and $<\mathbf{H_{el}}>$ together constitute E_{tot} which provides the potential for nuclear motion. This function constitutes a Potential Energy Surface (PES) which is discussed further in section 2B.9.1.

We now concentrate on the solution of the electronic Schrödinger equation.

2B.3. Spin Orbitals and the Electronic Wave Function

An orbital is defined as a 1-electron wave function. A spatial orbital, $\psi(\mathbf{r})$, is a function of the position vector **r** and describes the spatial distribution of the electron. However, for a complete description of an electron, one must specify its spin. The total basis set for spin wave function consists of two orthonormal functions $\alpha(\boldsymbol{\omega})$ and $\beta(\boldsymbol{\omega})$. The wave function of an electron that can describe both its spatial distribution and spin is called a spin orbital, $\chi(\mathbf{x})$, where **x** represents both the space and spin coordinates. Each spatial orbital can have two spin orbitals:

$$\chi(\mathbf{x}) = \begin{cases} \psi(\mathbf{r})\alpha(\boldsymbol{\omega}) \\ \text{or} \\ \psi(\mathbf{r})\beta(\boldsymbol{\omega}) \end{cases} \tag{7}$$

Now that we know the appropriate wave function to describe a single electron, we attempt to describe the complete N-electron wave function for the electronic Hamiltonian $\mathbf{H_{el}}$. However, before considering the fully interacting system, if we were to first consider a system of N non-interacting electrons, the Hamiltonian would look something like this:

$$\mathbf{H_{non-int}} = \sum_{i=1}^{N} \mathbf{h}(i) \tag{8}$$

Where **h**(i) is an operator describing the kinetic energy and potential energy of an individual electron i. Here we have neglected the electron-electron repulsion completely and thus make the eigen value equation solvable. Now if the solutions form a set of eigenfunctions of the operator **h**(i), applying the non-interacting theorem, we can say that a product of the spin orbitals must be an eigen function of $\mathbf{H_{non-int}}$. Therefore, the Hartree product wave function φ_{el}^{HP} is an eigenfunction of $\mathbf{H_{non-int}}$:

$$\varphi_{el}^{HP} = \chi_1(\mathbf{x_1})\chi_2(\mathbf{x_2})\chi_3(\mathbf{x_3}) \dots \chi_N(\mathbf{x_N}) \tag{9}$$

φ_{el}^{HP} wave function however does not meet two indispensable requirements - it is neither anti-symmetrised, nor does it respect the indistinguishability of electrons. These requirements are, however, fulfilled by a Slater determinant:

$$\varphi_{el}(\mathbf{x_1 x_2} \dots \mathbf{x_N}) = \begin{pmatrix} \chi_1(\mathbf{x_1}) & \cdots & \chi_N(\mathbf{x_1}) \\ \vdots & \ddots & \vdots \\ \chi_1(\mathbf{x_N}) & \cdots & \chi_N(\mathbf{x_N}) \end{pmatrix} \tag{10}$$

The Slater determinant is an exact solution for $\mathbf{H_{non-int}}$ but certainly not so for the interacting Hamiltonian ($\mathbf{H_{el}}$). However, the Slater determinant represents a good starting point of the solution of the multi-electronic Schrödinger equation as it answers the chemical problem – "If I have N electrons and N orbitals, can I have *one* determinant that represents adequately the chemistry of the molecule?"

2B.4. The Hartree-Fock Approximation

Central to all attempts at solving the electronic Schrödinger equation is the Hartree-Fock approximation. It usually constitutes the first step towards more sophisticated

approximations (see Section 2B.5). However, solving the Hartree-Fock equations is beyond the scope of this text. Therefore, we only showcase the most important results in this section.

As mentioned before, Hartree-Fock aims to find a set of spin orbitals $\{\chi_a\}$ such that the single determinant of the form

$$|\varphi_{el}\rangle = |\chi_1\chi_2 \ldots \chi_a\chi_b \ldots \chi_N\rangle \tag{11}$$

is the best possible approximation to the ground state of the N-electron Hamiltonian $\mathbf{H_{el}}$. According to the variational principle, the best spin orbitals are the ones that minimise the electronic energy given by:

$$\begin{aligned} E_0^{HF} &= \langle\varphi_{el}|\mathbf{H_{el}}|\varphi_{el}\rangle = \sum_a \langle a|H|a\rangle + \frac{1}{2}\sum_{a,b}\langle ab||ab\rangle \\ &= \sum_a \langle a|H|a\rangle + \frac{1}{2}\left[\sum_{a,b}\langle ab|ab\rangle - \sum_{a,b}\langle ab|ba\rangle\right] \end{aligned} \tag{12}$$

Here, $|\chi_a\rangle$ has been represented as $|a\rangle$ in a shorthand notation. By systematic variation of $\{\chi a\}$ under the constraints that they remain orthonormal, i.e., $\langle a|b\rangle = \delta_{ab}$, one can obtain an equation that defines the best spin orbitals. These are obtained as a solution of the eigen value equation of the 1-electron Fock operator **f**.

$$\mathbf{f}|\chi_j\rangle = \varepsilon_j|\chi_j\rangle \tag{13}$$

f is expressed as:

$$f(\mathbf{1}) = h(\mathbf{1}) + \sum_{b\neq a} J_b(\mathbf{1}) - \sum_{b\neq a} K_b(\mathbf{1}) \tag{14}$$

The first term h(1) denotes the kinetic energy and potential energy attraction to the nuclei of an arbitrarily chosen electron 1:

$$h(\mathbf{1}) = -\frac{1}{2}\nabla_1^2 - \sum_A \frac{Z_A}{r_{1A}} \tag{15}$$

The next two terms are the coulomb and exchange integrals:

$$J_b(\mathbf{1}) = \int dx_2 \chi_b(\mathbf{2})\chi_b^*(\mathbf{2})r_{12}^{-1}, \quad K_b(1) = \int dx_2 \chi_a(\mathbf{2})\chi_b^*(\mathbf{2})r_{12}^{-1} \tag{16}$$

The coulomb term evaluates the 'classical' inter-electronic repulsion. It represents the average repulsion experienced by an electron in χ_a due to the N-1 electrons in other spin orbitals. The exchange term arises as a direct consequence of the anti-symmetry of Slater

determinants, a condition required by the very nature of fermions, and has no simple classical interpretation.

Note that equation (12) is expressed in the general spin orbital form. For a closed shell system, the equation can be spin-integrated to produce a set of equations in spatial functions (ψ). These spatial functions can then be expressed in a basis set of atomic orbitals.

$$\psi = \sum_{AO} c_i \upsilon_i \tag{17}$$

This is nothing but the well acquainted LCAO-MO approach brought to life by the Roothaan equations.[93, 94] More is discussed about the basis set of atomic orbitals in section 2B.7.

2B.5. Post Hartree-Fock

As mentioned in the previous section, the Hartree-Fock scheme is approximate by its very definition in being a single determinant method.[92,95] Although φ_{el} manages to capture a significant portion of the physics of the system, it never corresponds to the *exact* wave function. E_0^{HF} is always necessarily larger (less negative) than the exact energy E_0 due to the variational principle. The difference between these two energies, following Löwdin[96], 1959, is called the correlation energy.

$$E_C^{HF} = E_0 - E_0^{HF} \tag{18}$$

The correlation energy is a negative quantity and it constitutes the error that is introduced through the Hartree-Fock scheme. Hartree-Fock approximation treats inter-electronic interaction only in an average way. Electronic correlation is mainly caused by instantaneous repulsion of electrons, which is not factored into the Hartree-Fock potential. Pictorially put, the electrons can often get too close to each other in the Hartree-Fock scheme making the electron-electron repulsion term too large. This is called *dynamical electron* correlation as it is related to the actual movement of individual electrons. The second important contribution comes from *non-dynamical static correlation*. This arises from the fact that in some systems, the slater determinant is not a good approximation of the ground state wave function. Even kinetic energy and nuclear-electronic attraction term can have significant, albeit indirect, contributions to the correlation energy.[97] For example, if the average distance between electrons were to be too short at the Hartree-Fock level, it will lead to a kinetic energy that is too large and a nuclear-electron attraction that is too strong.

Within the purview of wave function-based techniques, a lot of work has been done and new methods continue to be developed in order to achieve more and more precise determination of the correlation energy. Some popular ones are briefly discussed in the following. The most economically viable method is using the second order perturbation theory to estimate correlation energy due to Møller and Plesset.[98] This level is often abbreviated as MP2. Møller–Plesset correction to the fourth order (MP4) is also quite popular although it is a lot more computationally expensive. Other methods are based on configuration interaction (CI)[99] and couple cluster approaches (CC).[100] Of course, in principle these theories could give us the exact wave functions, but in all cases some approximations have to be adopted. These include CISD, QCISD and CCSD where 'SD' stands for single and double excitations. Even more sophisticated methods include triple excitations to the last two methods mentions – QCISD(T) and CCSD(T). However, there is nothing called a free lunch in computational chemistry. As the accuracy of these methods go up, so does their computational cost and the ability to treat larger systems decreases. It should be noted here that wavefunction based approaches such as the ones mentioned above have not been employed for our thesis because the size of our systems are too large for these methods. Instead we employ density functional theory, the subject of the following section.

2B.6. Density Functional Theory

2B.6.1. Electron Density as the basic variable[101]

Up to this point we have focussed on wave function-based approaches in quantum mechanics. However, a serious difficulty of this approach is that the wave function, φ_{el}, is a 4N dimensional quantity and it cannot be determined experimentally. Most systems that one encounters in chemistry are too large to be treated by higher order wave-function based methods.

On the other hand, the Hamiltonian has only 1-electron (**T** and $\mathbf{V_{Ne}}$) and at most 2-electron ($\mathbf{V}_{ee}$) interactions in it. This encourages one to ask if a less complicated function can be used as the primary variable and one can still get away with it. The electron density ($\rho(\mathbf{r})$), defined as

$$\rho(\mathbf{r_1}) = \mathrm{N} \int \dots \int \left| \varphi_{\mathrm{el}}(\mathbf{x_1}, \mathbf{x_2} \dots \mathbf{x_N}) \right|^2 \mathrm{d}\mathbf{s_1} \mathrm{d}\mathbf{x_2} \dots \mathrm{d}\mathbf{x_N} \qquad (19)$$

is the probability of finding any of the N electrons within a volume element dr_1 but with arbitrary spin while the remaining N-1 electrons have arbitrary positions and spins in the state represented by φ_{el}. $\rho(\mathbf{r})$ is a three-dimensional quantity in physical space that can be used as a means to solve the Schrödinger equation. This is validated by the following arguments:

i. $\int \rho(\boldsymbol{r_1}) d\boldsymbol{r_1} = N$, i.e. the density integrates to the total number of electrons in the system.
ii. $\rho(\mathbf{r})$ has maxima at the position ($\mathbf{R_A}$) of the nuclei
iii. The density at the position of the nuclei contains information about nuclear charge.

Thus, the density already provides all the necessary quantities to construct a system specific Hamiltonian, as noted by E.B. Wilson.[95] Thus we lay the foundation of the density functional theory (DFT). Once again, an exhaustive discussion of DFT is far beyond the capacity of this text. Therefore, only the most important aspects have been briefly outlined here.

2B.6.2. The Hohenberg-Kohn Theorems[102]

The foundations of DFT as we know it today were laid with a landmark paper in 1964[103] expounding the two Hohenberg-Kohn theorems.

i. The first theorem states that the nuclear-electronic potential V_{Ne}, referred to as V_{ext}[d] (external potential) within the parlance of DFT, is a unique functional of density $\rho(\mathbf{r})$; and since $\mathbf{V_{ext}}(\mathbf{r})$ fixes $\mathbf{H}$, it implies that the full particle ground state is a unique functional of $\rho(\mathbf{r})$.

   $\rho_0(\mathbf{r}) \Rightarrow V_{ext} \Rightarrow \mathbf{H} \Rightarrow \phi_0 \Rightarrow E_0$

ii. The second theorem states that the functional that delivers the ground state energy of the system delivers the lowest energy if and only if the input density is the true ground state density, ρ_0.

   $E_0 \leq E[\rho']$

   Where ρ' indicates a trial density.

Although the first theorem clearly states that the energy E_0 can be expressed as a unique functional of ρ_0, it says nothing about its analytical form. E_0 can be decomposed into individual components as:

[d] V_{ext} can include all kinds of potentials that the system is subjected to, like external electric or magnetic fields, in addition to the coulombic nuclear-electron attraction potential. However, for our purposes $V_{Ne} = V_{ext}$

$$E_0[\rho_0] = T[\rho_0] + V_{ee}[\rho_0] + V_{ext}[\rho_0] \quad (20)$$

The expression of $E_0[\rho_0]$ has a system dependent part $V_{ext}[\rho_0]$ which can be expressed as purely nuclear electronic attraction:

$$V_{ext}[\rho_0] = V_{Ne}[\rho_0] = \int \rho_0(\mathbf{r})\mathbf{V}_{Ne}\, d\mathbf{r} \quad (21)$$

The remaining two terms in equation (20) are system independent. The lion's share of the kinetic energy component of the energy, $T[\rho_0]$, can be calculated from the wave function of a fictitious, non-interacting reference system with the same density as the real one, represented by the wave function φ_{KS}, using the Kohn-Sham approach: [104, 105]

$$T_S = -\frac{1}{2}\sum_{i=1}^{N}\langle\varphi_{KS}|\nabla^2|\varphi_{KS}\rangle \quad (22)$$

The remaining term of equation (20), V_{ee}, is not completely known. Part of it can be attributed to the classical coulombic electron-electron repulsion, J[ρ(r)], while the rest of it is grouped off, somewhat vaguely, as exchange correlation energy. The remainder of the kinetic energy component that cannot be estimated by T_S formula (i.e., $T[\rho] - T_S[\rho]$) is also included in this $\mathbf{V_{ee}}$ term.

$$V_{ee} = J[\rho(r)] + E_{XC}[\rho(r)] + T[\rho] - T_S[\rho] \quad (23)$$

The coulombic term J[ρ(r)] can be expressed as,

$$J[\rho(r)] = \frac{1}{2}\sum_{i,j}\iint \frac{1}{r_{ij}}\rho(r_i)\rho(r_j)dr_i\, dr_j \quad (24)$$

An exact expression for $E_{XC}[\rho]$ does not exist. The quest of a suitable exchange correlation functional is an elaborate chapter in the history of DFT. In this text, however, we adhere to the discussion of the functionals that are most relevant to the calculations described in the following chapters.

2B.6.3. Some Exchange Correlation Functionals[106]

$E_{XC}[\rho]$ can be thought to be composed of two components – the exchange and the correlation energy. This kind of formulation helps in designing accurate functionals.

$$E_{XC}[\rho] = E_X[\rho] + E_C[\rho] \quad (25)$$

Choosing a combination of basis set and functional, in other words, fixing the level of calculation is important to the admissibility of the results of a theoretical calculation. Usually, the results are benchmarked against reference data, which could be some experimental data if it is available or theoretical data calculated at very high level. The following encompass the functionals and basis sets (see next section) we use in our studies. The justification for these choices is mentioned later.

i. B3LYP (Becke-3-Lee-Yang-Parr Functional)[107]

   This is a functional that considers the dependence of the gradient of electron density in the formulation of the $E_{XC}[\rho]$, hence follows the generalised gradient approximation (GGA). B3LYP is a hybrid functional, meaning that a part of the exchange term is calculated using exact Hartree-Fock exchange. For B3LYP, this is 20%. B3LYP uses empirically derived parameters in formulating the functional to yield results that complement experimental data.

ii. M06 (Minnesota Functional, 2006)[108]

   The Minnesota functionals represent a family of metaGGA functionals. Meta-GGA functionals model the exchange correlation energy by including the kinetic energy density in addition to electron density and the gradient of electron density itself. MetaGGA functionals in general perform better than classical hybrid functionals in calculation of dispersion forces. M06 uses 27% exact Hartree-Fock exchange energy.

iii. PBE1PBE (Perdew–Burke-Ernzerhof Functional)[109]

   PBE1PBE is also a GGA functional that mixes Perdew–Burke-Ernzerhof exchange energy with 25% Hartree-Fock exchange energy along with full PBE correlation energy. Although PBE functionals do not use experimentally fitted parameters to include the gradient correction, it is known for its general applicability and fairly reliable results. The nomenclature of this functional actually refers to the fact that both exchange and correlation parts are included in the functional. PBE1PBE indicates “1 parameter hybrid” using PBE exchange and PBE correlation.

iv. ωB97XD functional

   Designed by Head-Gordon, this is a range separated version of Becke 97 functional with additional dispersion correction. The exchange energy constitutes 22% Hartree-Fock exchange in the short range and it is 100% in the long range.

2B.7. Basis Sets

A basis set is a set of mathematical functions from which the wave function is constructed. Molecular orbitals can be expressed as a linear combination of atomic orbitals. For a basis set to be truly complete, it must be infinite – however this is not practical. In reality a basis set is chosen to be large enough to represent the system accurately but it must be finite or sometimes small enough to have a manageable computational time. The original slater type orbital (STO) (which is the typical forms of an atomic orbital obtained from the hydrogen atom solution), as shown in equation (26), has a mathematical form the analytical solutions of the integrals of which are not available. Therefore, evaluating integrals involving STOs are quite expensive.

$$v_{abc}^{STO}(x,y,z) = Nx^a y^b z^c e^{-\zeta r} \tag{26}$$

As a work around, an STO is often expressed as a linear combination of Gaussian Type Orbitals (GTOs) thereby forming a contracted Gaussian function, which are much cheaper to compute.

$$v_{abc}^{GTO}(x,y,z) = Nx^a y^b z^c e^{-\zeta r^2} \tag{27}$$

Each orbital can be expressed by one (single zeta, minimal), two (double zeta), three (triple zeta) and so on contracted Gaussian function while each such function is expressed as a linear combination of individual GTOs (referred to as primitive Gaussian functions). Some of the most popular basis sets that have also been used in the following work include:

i. Pople Basis[110]

   Pople introduced the concept of a split valence basis set. Here the core is represented by a single contracted Gaussian function while the valence orbitals (where all the chemistry takes place) is represented by linear combinations of multiple contracted Gaussian functions. The basis set is written something like X-YZg. The X in the nomenclature stands for the number of primitive Gaussians used to represent the core atomic orbital. Two or three numbers following the hyphen (Y and Z) shows that the valence orbitals are represented by two contracted gaussian functions each – the first one composed of a linear combination of Y primitive Gaussian functions and the second one of Z primitive Gaussian functions. Accordingly, such basis sets are called valence double zeta or triple zeta basis sets. Sometimes additional polarisation functions and diffuse functions are added to the basis set depending upon the requirement of the system.

For example, we go on to use the 6-311G(d,p) basis set in chapters II and V. 6-311G(d,p) implies that the core is treated by 6 primitive Gaussians, the three numbers following the hyphen indicates that it is a triple zeta basis set that describes the valence shell of the atoms by 3 contracted Gaussians, each composed of 3, 1 and 1 primitive Gaussians respectively. The (d,p) indicates that a set of 5 d polarisation functions have been added for each 2nd row elements and a set of 3 p polarisation functions have been added to each hydrogen atom. This would mean, a carbon atom will be assigned 18 mathematical functions to represent its atomic orbitals.

ii. Karlsruhe Basis[111, 112]

The TZVP basis set has been used in works performed in chapter II, III, IV and V. This is a valence triple zeta basis set with added polarisation.

iii. Dunning Basis Sets[113]

These were developed by Dunning and co-workers particularly in order to converge post-Hartree-Fock calculation to complete basis set limit using empirical extrapolation techniques. The aug-cc-pVTZ basis set has been used in chapter III extensively. In this basis set, the valence electrons are represented by three contracted gaussians, hence "valence triple zeta". "aug" refers to the presence of extra diffuse functions and "p" indicates the presence of polarisation functions as well. These basis sets are correlation consistent (hence, "cc"), i.e. sets which include all functions in a given group as well as all functions in any higher groups.[152] They include successively larger shells of polarisation functions.

2B.8. Choice of Level of Calculation

Choosing a level of calculation for a computational study is not any easy decision to make and usually never has only *one* correct answer. As mentioned before, keeping the size of the system in mind, DFT based approaches were ideally suited. Next, two choices must be made – the functional and the basis set. The choice of functional and basis depends of a large number of factors. Usually a benchmark calculation can be performed to compare with experimentally obtained values, if it is available. Sometimes comparisons can also be made with high levels of calculations. For the molecules in this study, in general optimisation is performed initially using B3LYP functional and a triple zeta basis set (TZVP). However, the B3LYP functional does not always give reliable results.[149] Therefore, at least for the initial part of the study, the calculations were repeated using a different functional M06. No disparity is

observed in the results, indicating that both levels of calculation are acceptable. There remains the possibility of using a larger/better basis set to perform single point calculations. This is generally the case for NMR calculations which are highly sensitive to basis sets and ADF calculation which use slater type orbitals in their basis sets. For NMR calculation two types of basis sets/functional have been used in two different cases (Chapter III and IV) – B3LYP/aug-cc-PVTZ for ^{1}H NMR and PBE1PBE/6-31+G(d) for ^{31}P NMR calculation. The choice for NMR basis set is generally dictated by the size of the system and the accuracy of the calculation in reproducing experimental trends. For ETS-NOCV the corresponding triple zeta basis set composed of slater type orbitals (STO) that is closest to the triple zeta basis set used for optimisation is usually chosen.

2B.9. Computational Chemistry – Some Basic Concepts and Tools

The following section is dedicated to some essential concepts in computational chemistry which helps us understand the ground state wave function or density of molecular system as chemists. As Eugene Wigner appropriately reminds us: "It is nice to know that the computer understands the problem. But I would like to understand it too."[150]

To that end, a plethora of tools designed to extract essential chemical information from the mathematical solution of the Schrödinger equation are available to us today. Here we briefly discuss a small selection of these techniques that have been used in the course of this work.

2B.9.1. Potential Energy Surfaces

The concept of a potential energy surface, abbreviated to PES, arises from a suggestion made by French chemist René Marcelin by defining the state of a system by its distance and momentum coordinates and that a reaction may be regarded as the journey of a point over such a surface.[114] The PES we deal with is a 3N-6 (where N is the number of atoms in the molecule) dimensional hypersurface that is constructed by plotting the potential energy of a collection of atoms over all possible atomic arrangements for a given chemical formula. Each structure, a point on the PES, can be represented by the vector:

$$\mathbf{X} = (x_1, y_1, z_1, x_2, y_2, z_2 \dots x_i, y_i, z_i \dots x_N, y_N, z_N) \quad (28)$$

Where x_i, y_i and z_i are the coordinates of the i^{th} atom.

The complete PES of a polyatomic molecule can be hard to visualise because it involves a large number of dimensions. Therefore, it is conventional to take slices through the PES involving a single coordinate (e.g. a particular bond) or two coordinates (say, a bond and an angle) to obtain the relevant reduced-dimensionality potential energy curve or surface respectively.

From a computational point of view, many chemical problems can be reduced to an understanding of the PES.[115] Understanding the PES of a molecule helps us determine the relationship between potential energy and 3-D geometry of a molecule.[116, 117]

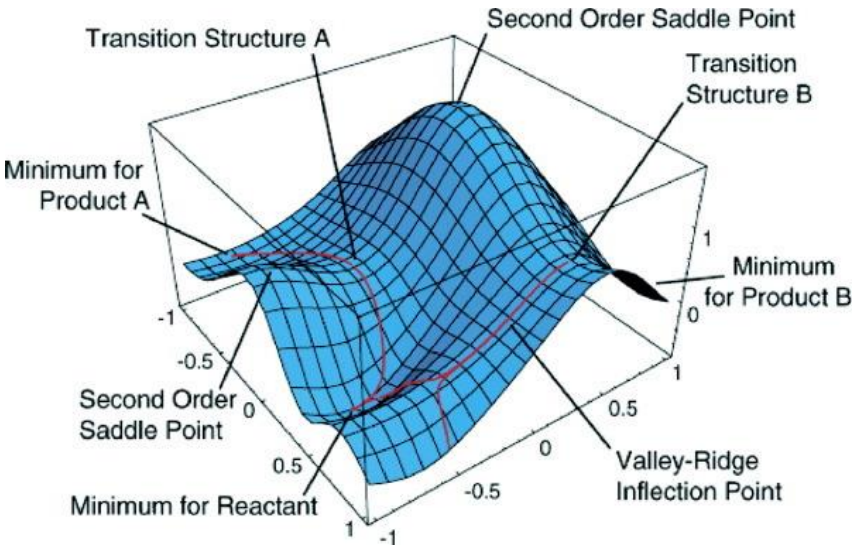

Figure 2-1: Model potential energy surface showing minima, transition state, second order saddle point and reaction paths (reproduced from paper by Schlegel)[115]

From figure 2-1, one can conceptualise a PES as a hilly landscape with peaks, valleys and mountain passes. Most frequently the 'structure of interest' is located in a valley i.e. this is a local minimum, or is a transition state between them. Such a point on a PES where the potential energy reaches a maximum or a minimum with respect to the visualised coordinates is called a stationary point. On the 3N-6 dimensional, fully explicit, PES a point that is a minimum with respect to all coordinates is a true minimum, one that is a minimum with respect to all but one coordinate is a 1st order saddle point and so on. Molecular conformations that have a finite lifetime in reality are usually located in the minima whereas those that are fleetingly short-lived, like a transition state are usually located at a 1st order saddle point. A molecule is expected to follow the intrinsic reaction coordinate (IRC), which is the lowest energy pathway, to travel from one minimum to the other (although this is rarely the case as these potential energy surfaces do not account for the dynamical effects), if it acquires enough potential energy to go over the transition state. For a transition state structure, the potential energy is a minimum with respect to all other coordinates except the IRC, with respect to which it is a maximum.

2B.9.2. Geometry Optimisation

The process of characterising a stationary point on the PES, i.e., ascertaining the said point is mathematically well-defined on the surface and then calculating its geometry and energy is called geometry optimisation.[116] The process usually involves providing a starting 'guess' structure (the more accurate the guess, the more efficient is the optimisation) to an algorithm

which then systematically changes the geometry until a stationary point has been found. The curvature of the PES with respect to the geometric parameters around this point is then examined to characterise the point as a minimum or some kind of saddle point.

The energy E of a molecular system under the Born-Oppenheimer approximation is a parametric function of the nuclear coordinates denoted by the vector **X** = (x_1,y_1, z_1 …,x_N, y_N, z_N). If we move from E(**X**) to E($\mathbf{X_1}$) on the PES, we can expand E($\mathbf{X_1}$) as a Taylor series around the point **X** as:

$$\mathrm{E}(\mathbf{X_1}) = \mathrm{E}(\mathbf{X}) + \mathbf{q}^{\dagger}\mathbf{f}(\mathbf{X}) + \frac{1}{2}\mathbf{q}^{\dagger}\mathbf{H}(\mathbf{X})\,\mathbf{q} + \ldots \tag{29}$$

Where $\mathbf{q} = (\mathbf{X_1} - \mathbf{X})$ and $\mathbf{q}^{\dagger}$is the adjoint of the column vector **q**.

The components of the gradient **f** are

$$\mathrm{f_i} = \frac{\partial \mathrm{E}(\mathbf{X})}{\partial \mathrm{x_i}} \tag{30}$$

and the components of Hessian **H** are

$$\mathrm{H_{ij}} = \frac{\partial^2 \mathrm{E}(\mathbf{X})}{\partial \mathrm{x_i}\,\partial \mathrm{x_j}} \tag{31}$$

Although the Taylor series has to be infinite to be exact, about the minima it can be approximated to the second order. Further, the first derivative at the minima should be 0. So, for $\mathbf{X} = \mathbf{X_e}$ the equation takes the form:

$$\mathrm{E}(\mathbf{X_1}) = \mathrm{E}(\mathbf{X_e}) + \frac{1}{2}\mathbf{q}^{\dagger}\mathbf{H}(\mathbf{X}_e)\,\mathbf{q} \tag{32}$$

In the same way

$$\mathbf{f}(\mathbf{X_1}) = \mathbf{f}(\mathbf{X}) + \mathbf{H}(\mathbf{X})\,\mathbf{q} \tag{33}$$

For the point $\mathbf{X_1} = \mathbf{X_e}$, $\mathbf{f}(\mathbf{X_e}) = 0$, therefore:

$$\mathbf{f}(\mathbf{X}) = -\mathbf{H}(\mathbf{X})\,\mathbf{q} \tag{34}$$

The solution of equation 34 is the starting point of the most efficient procedures to find extrema on the PES. Equation 34 can be further modified to:

$$\mathbf{q} = -\mathbf{H}^{-1}(\mathbf{X})\,\mathbf{f}(\mathbf{X}) \tag{35}$$

Putting $\mathbf{q} = (\mathbf{X_e} - \mathbf{X})$:

$$\mathbf{X_e} = \mathbf{X} - \mathbf{H^{-1}(X)}\,\mathbf{f(X)} \quad (36)$$

If we start with a guess geometry indicated by **X** on the potential energy hypersurface, the corresponding gradient f(**X**) can be easily estimated analytically while an approximate Hessian is often calculated using molecular mechanics. If follows that using equation (36), one can directly arrive at the minima $\mathbf{X_e}$**.** However, recalling that the Taylor series was approximated to the second order the first geometry we move to is usually not $\mathbf{X_e}$ but a different point **X'**. **X'** can be used as the new guess for equation (36) and this process is repeated iteratively until we arrive at a point where the difference of energy between two consecutive points falls below an arbitrary threshold and the geometry is said to be optimised. In some algorithms, this threshold is given by a minimum value of force or displacement.

The conditions for locating a transition state (TS) are far more complicated as a TS is a minimum with respect to all coordinates *but one*. Using the above algorithm, one usually arrives at the closest stationary point, therefore with a reasonably good guess for a TS, the algorithm will converge to the required TS geometry. Considering the importance of TS geometries, a number of more sophisticated algorithms exist to locate them. Some of these require the specification of the geometries of the two minima that the TS connects. Others require specifying the particular coordinate along which the energy is to be maximised while minimising with respect to all the rest. When this coordinate overlaps with one of the normal modes of the molecule, it defines a TS. In the end, locating a TS comes down to providing a good initial 'guess' and a reasonable Hessian matrix, since locating a TS is really concerned with distinguishing the local curvatures on a PES.[117]

2B.9.3. Frequency Calculation

Once a stationary point has been located on a PES, it must be characterised as a minimum, TS or a higher order saddle point by calculating the curvature of the PES at the stationary point. This leads to the calculation of the normal modes of vibration for the molecule. Normal modes are the simplest, linearly independent modes of vibrations in a molecule. A non-linear molecule has 3N-6 normal modes.

Considering the simple stretching in a diatomic molecule AB, the stretching frequency is given by the following formula:

$$\tilde{\upsilon} = \frac{1}{2\pi c}\sqrt{\frac{k}{\mu}} \tag{37}$$

where ũ represents wavenumber, k is the force constant, μ is the reduced mass of atoms A and B and c is the speed of light. Indeed, most oscillatory motions can be represented by analogous equations. This relation between frequency and force constant implies that it is possible to calculate the normal modes of vibration from the force constant matrix i.e., the Hessian (**H**). By diagonalizing the Hessian matrix, we decompose it into a product of 3 matrices:

$$\mathbf{H} = \mathbf{P}\,\mathbf{A}\,\mathbf{P}^{-1} \tag{38}$$

Here **P** is a matrix whose columns are directions for the force constants k designated in the diagonalized matrix **A**. The **P** matrix is the eigenvector matrix and the **A** matrix is the eigenvalue matrix from the diagonalization of **H**. Mass weighting the force constants gives the vibrational frequencies. Of course, it should be noted that the calculation of vibrational frequencies has physical significance at only stationary points and at the level of calculation at which the stationary point has been computed because (i) only near a stationary point the curvature of the PES can be approximated to be quadratic and (ii) using a different level of calculation would imply that the PES at two different levels of calculation are parallel, which may not necessarily be true.

While for a minimum on the PES all the normal modes are positive, i.e., for each vibrational mode, there is a restoring force making the motion oscillatory, for a TS, one of the vibrations, the one along the reaction coordinate is quite different. The vibration along this mode takes the TS towards the reactant or the product in an irreversible manner. The force constant, i.e., the derivative of the gradient at this point is *negative*, leading to an *imaginary frequency* along the IRC.

2B.9.4. NBO Analysis

Natural Bond Orbital (NBO) analysis is one of the most powerful tools that helps in 'translating' complex computational solutions of the Schrödinger wave equation into the simple language of chemical bonding by distilling information from delocalised molecular orbitals to localised 'natural' orbitals.[118-120] Natural orbitals are the eigen functions of the first order reduced density matrix operator **Γ**. The first order reduced density matrix (1-RDM) is a

close relative of the electron density (ρ(**r**)) but provides much more detailed information about the 1-electron subsystems within the N electron system represented by the complete wave function Ψ. It is defined as:

$$\gamma_1(r_1', r_1) = \mathrm{N} \int \Psi^*(\mathrm{r}_1', \mathrm{r}_2, \ldots \mathrm{r}_\mathrm{N}) \Psi(\mathrm{r}_1, \mathrm{r}_2, \ldots \mathrm{r}_\mathrm{N}) \, \mathrm{d}^3\mathrm{r}_2 \ldots \mathrm{d}^3\mathrm{r}_\mathrm{N} \tag{39}$$

The matrix γ_1(r', r) runs over two continuous indices. Its diagonal element (r' = r) corresponds to the electron density (γ_1(r, r) = ρ(r)). The first order reduced density operator (**Γ**) is simply the matrix representation γ_1. It is represented as:

$$\mathbf{\Gamma} = |\Psi(\mathrm{r}')\rangle\langle\Psi(\mathrm{r})| \tag{40}$$

since,

$$\begin{aligned} &\langle r_1', r_2, r_3 \ldots r_N | \mathbf{\Gamma} | r_1, r_2, r_3 \ldots r_N \rangle \\ &\quad = \langle r_1', r_2', r_3' \ldots r_N' | \Psi(\mathrm{r}') \rangle \langle \Psi(\mathrm{r}) | r_1, r_2, r_3 \ldots r_N \rangle \\ &\quad = \Psi^*(\mathrm{r}_1', \mathrm{r}_2, \ldots \mathrm{r}_\mathrm{N}) \Psi(\mathrm{r}_1, \mathrm{r}_2, \ldots \mathrm{r}_\mathrm{N}) \end{aligned} \tag{41}$$

This is a 1-electron projection operator of the full N-electron probability distribution. As shown by P.O. Lowdin,[96] the complete information presented by the 1-RDM can be obtained from its eigenorbitals, the 'natural' orbitals (θ_i) and their corresponding eigenvalues n_i.

$$\mathbf{\Gamma}.\theta_\mathrm{i} = \mathrm{n}_\mathrm{i}.\theta_\mathrm{i} \tag{42}$$

It is evident that θ_i, called natural orbitals, are defined completely by the wave function Ψ, and hence they are intrinsic and unique to the description of Ψ. The eigenvalue n_i represents the occupancy of the corresponding orbital θi.

Natural Atomic Orbitals (NAO) are localised, 1-centered atomic orbitals that can effectively be described as the natural orbital of an atom in a molecular environment. Natural bonding orbitals (NBO) are an orthonormal set of localised, 'maximum occupancy' orbitals of which leading N/2 orbitals (for closed-shell systems) give the most accurate-possible Lewis-like description of the N-electron system.

The NBO program delivers a succession of Natural Atomic Orbitals (NAO), Hybrid Orbitals (NHO) and Bonding Orbitals (NBO) from the initial Atomic Orbitals (AO). Each of these orbitals form a complete orthonormal basis set and are related to each other by non-singular transformations to the basis atomic orbitals (AO).

(AO) → NAO → NHO → NBO

It is worthwhile to note that this 'bottoms up' approach singularly helps to preserve the localisation of the starting NAOs to provide a chemically intuitive Lewis structure picture as opposed to the 'top down' approach of conventional MO based methods.

The program also provides bond order analysis through the Wiberg Bond Index (WBI).[121] WBI is defined as the electron population overlap between two atoms. It roughly indicates the number of electron pairs shared between two atoms in a molecule and it is known to have good agreement with empirical bond order.[122] WBI is given by:

$$W_{AB} = \sum_{\mu \in A} \sum_{\nu \in B} P_{\nu\mu}^2 \tag{43}$$

Where the summation runs over atomic orbitals μ of atom A and ν of atom B and $P_{\nu\mu}$ is the corresponding density matrix element.

The NBO program also provides the occupancy, i.e., the total number of electrons present in the orbitals for the 'best' Lewis structure chosen by the program. The electronic population can be evaluated in two ways using equation (42) with either NAOs or NBOs. One can directly note the occupancy of the NBOs or one can add the electronic occupancy of the NAOs that combine to form that particular NBO. The result from these two approaches should be identical.

The final noteworthy feature of NBO analysis is the perturbation theory energy analysis. This interaction is estimated by examining all possible overlaps between filled 'donor' NBOs (i) and empty 'acceptor' NBOs (j). The energy (E(2)) associated with this kind of localisation is given by:

$$E(2) = \Delta E_{ij} = q_i . \frac{F(i,j)^2}{(\varepsilon_i - \varepsilon_j)} \tag{44}$$

Where q_i is the occupancy of the donor orbital, ε_i and ε_j are respective orbital energies and F(i,j) is the off diagonal Fock matrix element between orbitals i and j.

2B.9.5. EDA-NOCV Analysis

EDA-NOCV analysis provides a chemically intuitive method of analysing the components of a chemical bond combining the extended transition state method for energy decomposition

analysis and the natural orbitals for chemical valence theory to further categorise the bonding orbital interaction into familiar components of σ, π or δ bonds.

Within the framework of Kohn-Sham MO methods, applying Morokuma's bond energy decomposition scheme,[123] the total bond energy between fragments of a molecule can be decomposed into various components. The total bond energy (ΔE) is divided into two major components. First we have the preparation energy of the two components (ΔE_{prep}), which can be further compartmentalised into the energy required for geometric deformation ($\Delta E_{prep,geo}$) i.e., the energy required to deform the fragments from their equilibrium geometry to the geometry they acquire in the molecule; and the energy required to promote the fragments to their valence electronic state ($\Delta E_{prep,el}$). In second place we have the energy of interaction between the two fragments (ΔE_{int}).

$$\Delta E = \Delta E_{prep} + \Delta E_{int} = \Delta E_{prep,geo} + \Delta E_{prep,el} + \Delta E_{int} \quad (45)$$

The ΔE_{int} is further broken down into three components – the electrostatic interaction (ΔV_{elst}), Pauli repulsion (ΔE_{pauli}) and orbital interaction (ΔE_{oi}). ΔV_{elst} corresponds to the classical electrostatic interaction between the two fragments as they are brought together from infinite separation while their densities remain frozen such that the final density is a simple superposition of the density of the component fragments. The Pauli repulsion (ΔE_{pauli}) is the energy for the combined wave function of the fragments to be transformed by anti-symmetrisation and renormalisation into an acceptable wave function for the complete molecule Ψ_0 which is associated with the density ρ_0. It represents the repulsion between occupied orbitals and is responsible for steric interaction. Finally, the wave function is allowed to relax completely into a fully converged wave function, Ψ, and the associated energy is called the orbital interaction (ΔE_{oi}). ΔE_{oi} comprises of electron pair bonding, charge transfer interaction and polarisation.

$$\Delta E_{int} = \Delta V_{elst} + \Delta E_{pauli} + \Delta E_{oi} \quad (46)$$

The orbital interaction component (ΔE_{oi}) can be expressed as:

$$\Delta E_{oi} = E[\rho] - E[\rho_0] \quad (47)$$

i.e., as the energy difference between the states Ψ_0 and Ψ. The difference between their densities, $\Delta\rho_{orb} = \rho - \rho_0$ is called the deformation density. In the NOCV approach,[124-127] the

deformation density can be expressed in terms of a orthonormal fragment spin orbitals (λ_i, i = 1, …, N):[128]

$$\Delta\rho_{orb} = \sum_{\mu}\sum_{\nu} \Delta P^{orb}_{\mu\nu} \lambda_\mu \lambda_\nu \tag{48}$$

Where $\Delta P^{orb}_{\mu\nu}$ are the components of the deformation density matrix. The NOCVs are now constructed by the diagonalization of the deformation density matrix expressed in the set of orthogonalized fragment spin-orbitals. Thus, the NOCVs satisfy the following equation

$$\Delta\rho^{i} C_i = \upsilon_i C_i \tag{49}$$

Where, C_i is a vector containing the coefficients that expand the Ψ_i (NOCVs) as a linear combination of λ_i (set of fragment orbitals). The deformation density $\Delta\rho_{orb}$ in turn can be expressed as sum of pair of complementary NOCVs (Ψ_k, Ψ_{-k}) corresponding to eigenvalues equal in magnitude but opposite in sign.

$$\Delta\rho_{orb}(r) = \sum_{k} \Delta\rho_k(r) = \sum_{k} \nu_k [\Psi_k(r)^2 - \Psi_{-k}(r)^2] \quad k = 1,2 \ldots \frac{N}{2} \tag{50}$$

The complementary pairs of NOCV signify channels of electronic charge transfer between fragments. Within the construct of the ETS-NOCV scheme it can be shown that

$$\Delta E_{oi} = \sum_{k} \Delta E^{orb}_{k} = \sum_{k} \nu_k \left(F^{TS}_{k} - F^{TS}_{-k}\right) \quad k = 1,2 \ldots \frac{N}{2} \tag{51}$$

Where F_k^{TS} and F_{-k}^{TS} are diagonal element of transition-state Kohn Sham matrix corresponding to the eigenvalues of ν_k and ν_{-k}. The overarching advantage of combining this scheme of energy decomposition with NOCV analysis is that not only can each $\Delta\rho_k(r)$ be visualised, but there is an energy contribution ΔE_k^{orb} associated with it.[129]

2B.9.6. QTAIM Analysis[130, 131]

The quantum theory of atoms in molecules is a theory that utilises electronic density (ρ) of molecules as a means of studying the nature of bonding in molecular systems. The electron density as mentioned in section 2B.6 is a quantum mechanical observable but may also be derived experimentally.

It is well understood that the electron density distribution in a molecule is a function of the forces acting within the molecule.[131-133] Analysing the surface of electron density reveals the

presence of maxima, minima and saddle points in the topology. The attractive forces of the nuclei form the most distinctive features of the topology – the density exhibits local maxima there. The points (r_c) at which the first derivative of electron density, $\rho(r_c)$, vanishes are called critical points (CP).

$$\nabla\rho(r_c) = \boldsymbol{i}\frac{\partial\rho}{\partial x} + \boldsymbol{j}\frac{\partial\rho}{\partial y} + \boldsymbol{k}\frac{\partial\rho}{\partial z} = 0 \tag{52}$$

Now, whether a CP is a maximum or a minimum is determined by the sign of the second derivative at this point. In 3-dimensional space, 9 such derivatives are possible which are represented in the format of a matrix called the Hessian of $\rho(r_c)$.

$$H = \begin{pmatrix} \frac{\partial^2\rho}{\partial x^2} & \frac{\partial^2\rho}{\partial x\partial y} & \frac{\partial^2\rho}{\partial x\partial z} \\ \frac{\partial^2\rho}{\partial y\partial x} & \frac{\partial^2\rho}{\partial y^2} & \frac{\partial^2\rho}{\partial y\partial z} \\ \frac{\partial^2\rho}{\partial z\partial x} & \frac{\partial^2\rho}{\partial z\partial y} & \frac{\partial^2\rho}{\partial z^2} \end{pmatrix} \tag{53}$$

The Hessian can be diagonalized by a unitary transformation to obtain the eigenvalues λ_1, λ_2, λ_3 which are also the three principle axes of curvature of $\rho(r_c)$. The sum of λ_1, λ_2, λ_3 is called the Laplacian of $\rho(r)$.

$$\nabla^2\rho(r_c) = \frac{\partial^2\rho(r_c)}{\partial x^2} + \frac{\partial^2\rho(r_c)}{\partial y^2} + \frac{\partial^2\rho(r_c)}{\partial z^2} = \lambda_1 + \lambda_2 + \lambda_3 \tag{54}$$

The CPs are characterised by a pair of numbers – the rank and signature (ω, σ). The rank is the number of non-zero eigenvalues and the signature is the algebraic sum of the sign of those eigen values. Based on this, there are 4 possible CPs of rank 3:

(3, -3) All curvatures are negative, the CP is a local maximum and is called **atomic critical point.** These indicate the location of the nuclei.

(3, -1) Two curvatures are negative and one is positive; ρ is maximum in a plane and minimum perpendicular to this plane- the CP is called a **bond critical point (BCP)**.

(3, +1) Two curvatures are positive and one is negative: ρ is minimum in a plane and maximum perpendicular to this plane – the CP is called a **ring critical point**

(3, +3) All the curvatures are positive, this is a local minimum of ρ – the CP is called a **cage critical point**

Information about the nature of a bond is usually obtained by measuring chemical indicators at the BCP. QTAIM analysis affords several different kinds of descriptors, both local and global, in the study of bonding patterns in molecules. Of these descriptors, those most pertinent to this report include the value of electron density at the BCP (ρ_{BCP}), the ellipticity of electron density at BCP (ε_{BCP}) and the Delocalisation Index (DI).

The electron density minimises at the BCP along the bond path while it is maximised in the two directions perpendicular to it. The accumulation of electron density at BCP (ρ_{BCP}) is inversely related to bond length and an approximate indicator of bond strength.[134, 135]

The ellipticity at BCP, ε_{BCP}, is a measure of the anisotropy of the electron density around the BCP. It measures the ratio of curvature of electron density (the two negative eigen values of the Hessian) in the two directions perpendicular to the direction of the bond (Figure 2-2).

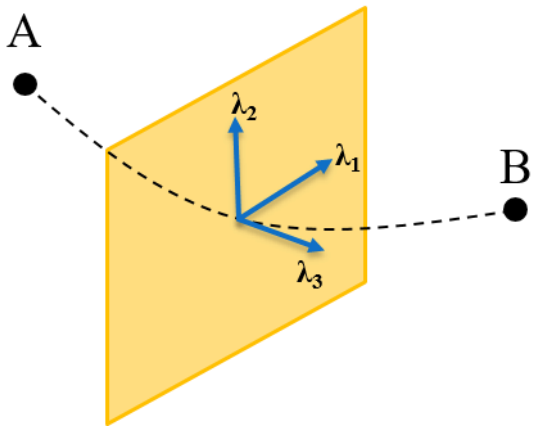

Figure 2-2: curvatures λ_1, λ_2, λ_3 along bond path connecting atoms A and B

ε_{BCP} is formulated as:

$$\varepsilon_{BCP} = \frac{\lambda_1}{\lambda_2} - 1 \text{ , where } |\lambda_1| \geq |\lambda_1| \qquad (55)$$

Typically, the shape of electron density is highly sensitive to its nature. For example, the ε_{BCP} of ethane (ε_{BCP} = 0.00), to ethylene (ε_{BCP} = 0.332) and acetylene (ε_{BCP} = 0.000)[136] changes with the anisotropy of the C-C linkage – the sigma bond in ethane is cylindrically symmetric, the π-bond in ethylene makes the electron density anisotropic, accumulating more electron in the π-plane than in the one perpendicular to it; whereas the two mutually perpendicular π-bonds in acetylene makes the electronic distribution isotropic once more. Naturally ellipticity has

been closely associated with π-character of a bond and used as a measure of electronic delocalisation in conjugated systems.[151]

QTAIM theory also provides a decomposition of the electronic density into molecular basins. Using this, we arrive at the delocalisation index (DI).[137, 138] DI is a measure of the number of electrons that are shared between two atoms or basins. It is directly related to bond order[138, 139] and is obtained from the integration of the Fermi hole density:

$$\mathrm{DI} = 2\mathrm{F}(\Omega,\Omega') = 2[\mathrm{F}^{\alpha}(\Omega,\Omega') + \mathrm{F}^{\beta}(\Omega,\Omega')] = -2\sum_{\mathrm{i,j}}^{\mathrm{N}} \mathrm{S_{ij}}(\Omega)\,\mathrm{S_{ij}}(\Omega') \qquad (56)$$

Where $S_{ij}(\Omega)$ is the overlap integral of α spin orbitals ϕ_i and ϕ_j over the atomic basin Ω and $F^{\alpha}(\Omega,\Omega')$ is the Fermi correlation for α electrons of atomic basin Ω delocalised into another atomic basin Ω'.

$$\mathrm{F}^{\alpha}(\Omega,\Omega') = -\sum_{\mathrm{i,j}}^{\mathrm{N}_{\alpha}} \mathrm{NS_{ij}}(\Omega)\,\mathrm{S_{ij}}(\Omega') \qquad (57)$$

2B.9.7. ELF[140, 141]

The electron localisation function (ELF) was originally introduced by Becke and Edgecombe[142-144] as a competitive alternative to partitioning the molecular space in terms of electron density (ρ(r)) as in Bader's QTAIM and instead uses conditional pair electron density. ELF helps in understanding the concept of pair electron localisation in the spirit of Lewis structures.[141] The probability density of finding two electrons of the same spin, simultaneously at positions 1 and 2 in a multi electronic system is given by the same-spin pair electron density:

$$\mathrm{P_2}(1,2) = \rho(1)\rho(2) - \left|\rho(1,2)\right|^2 \qquad (58)$$

Where ρ(1,2) is the one body spin density matrix of the Hartree-Fock determinant. The conditional probability density $P_{cond}(1,2)$ is the probability of finding an electron at position 2 if an electron of the same spin is located with certainty at position 1. This is obtained simply by dividing equation (58) by ρ(1).

$$\mathrm{P_{cond}}(1,2) = \rho(2) - \frac{\left|\rho(1,2)\right|^2}{\rho(1)} \qquad (59)$$

The short-ranged, spherical averaged conditional pair density can be approximated by the leading quadratic term of the Taylor series expansion of $P_{cond}(r,s)$

$$P_{cond}(r,s) \approx \frac{1}{3}\left[\tau - \frac{1}{4}\frac{(\nabla\rho)^2}{\rho}\right]s^2 \quad (60)$$

Where r and s denote the origin and radius of the averaged shell and τ is the positive kinetic energy density. Becke and Edgecombe defined the bracketed quantity in equation (60) as D_σ which contains all the information regarding electron localisation. D_σ is small where the possibility of finding a second electron of the same spin is low, i.e., the electron density is localised. However, the function D_σ can attain arbitrarily high values for delocalised densities. Therefore, the ELF was formulated where D_σ is referenced against the value of D_σ for a homogenous electron gas D_σ^0.

$$ELF = \frac{1}{1 + \left(\frac{D_\sigma}{D_\sigma^0}\right)^2} \quad (61)$$

In this way $0 \leq ELF \leq 1$ and the closer the value of ELF is to 1, the higher is the electron localisation. For single determinantal wave functions, ELF can be treated in terms of excess local kinetic energy density from Pauli Repulsion. Following this, regions of high/low ELF are associated with low/high Pauli repulsion. ELF is larger in regions where orbitals are localised and small at the borders of these regions.

In the spirit of Bader's segregation of electron density into atomic basin within a molecule, the ELF function can be treated in an analogous manner as electron density to create ELF basins. The derivative of the ELF function with respect to the coordinates helps to identify the maxima of this function – this corresponds to maximum probability of electron pair and are called attractors. Basins are formed surrounding the attractors. Depending upon the nature of attractor within the basin, the basin can be core (corresponding to nuclear positions), valence or composite (containing both core and valence attractors). Depending upon the number of core basins that have a common boundary with it, the valence basins can be assigned a 'synaptic order'. Accordingly, the valence basins can be asynaptic , monosynaptic, disynaptic of polysynaptic. Asynaptic basins correspond to unusual chemical entities such as F centres in surface chemistry, monosynaptic basins correspond to lone pairs, disynaptic basins are signatures of two-centred bonds while polysynaptic basins represent multicentred

bonds. The population of the basins correspond to the density of the cores, and strengths of the bonds respectively.[141]

2B.9.8. NMR[117]

Nuclear Magnetic resonance spectroscopy is one of the most widely used spectroscopic techniques in chemistry today. However, initially theoretical prediction of the NMR spectrum of a molecule lagged significantly compared to experimental work. The primary reason behind this is that it is much more difficult to model the interaction between a wave function and a magnetic field than it is with an electric field. Notwithstanding, commendable progress has been made in this field particularly with DFT.

NMR measurements assess the energy difference between a system in the presence and absence of an external magnetic field. There are two different NMR parameters that are reported abundantly in characterising a molecule – the chemical shift (δ) and the spin-spin coupling constant (J). In the case of NMR there are two magnetic fields of interest – the external magnetic field of the instrument and the internal magnetic field generated by the nuclear spin. The chemical shift is measured as a 2^{nd} order derivative of energy with respect to the external magnetic field and the nuclear magnetic moment whereas the spin-spin coupling constant is measured as the 2^{nd} order derivative of energy w.r.t. the nuclear magnetic moments of the two nuclei in question. However, these integrals are much more difficult to calculate because the magnetic field perturbs the kinetic energy term of the Hamiltonian.

The properties of the perturbed kinetic energy operator are such that an origin must be specified, defining the coordinate system for the calculation. This origin is called the 'gauge origin'. In order to avoid errors due to the gauge origin two methods have been extensively used in the literature. The GIAO (Gauge Independent Atomic Orbitals) method incorporates the gauge origin in the basis functions itself, thereby making it possible to make all matrix elements composed of these basis functions independent of it. The other method is IGLO (Independent Gauge for Localised Orbital), designed to minimise errors due to some MOs being too far away from the gauge origin. The GIAO method has been implemented in all the NMR calculations performed in the following chapters.

Another complication with NMR calculations is that the results are highly sensitive to the size of the basis sets used. However, increasing the size of the basis set arbitrarily also renders the calculation more and more expensive. To strike a reasonable balance the use of locally dense basis sets (LDBS) have gained more and more popularity.[145-147] Within the constraints of the LDBS approximation, the nuclei for which the chemical shifts and coupling constant need to be calculated are computed using a large basis set while the rest of the atoms are treated with a smaller basis set without incurring a severe blow to the quality of the results obtained. The NMR chemical shifts are also sensitive to the presence of solvents. Including a solvent often results in better correlation with experimentally recorded values.

2.2. Conclusion

In this chapter we have mainly explored the chemical compounds – NHCs and carbones- that are the entities of interest in this work as well as the various computational tools that have been used extensively to explore the various properties of these divalent carbon borenium adducts. The specific cases for the compounds discussed have not been dealt with in this chapter and instead have been addressed as and when they come up. Specific details of calculations have also similarly been discussed specifically where necessary.

References

1. Hahn, F. E., Introduction: Carbene Chemistry. *Chemical Reviews* **2018,** *118* (19), 9455-9456.
2. Dumas, J. B.; Peligot, E. M. Mémoire sur l'esprit de bois et sur les divers composés éthérés qui en proviennent. l'Académie des Sciences, Paris. Imprimerie de E-J Bailly et Co, Place Sornbonne. **1834**.
3. Hermann, M., Ueber die bei der technischen Gewinnung des Broms beobachtete flüchtige Bromverbindung. *Justus Liebigs Annalen der Chemie* **1855,** *95* (2), 211-225.
4. Nef, J. U., Ueber das zweiwerthige Kohlenstoffatom. (Vierte Abhandlung.) Die Chemie des Methylens. *Justus Liebigs Annalen der Chemie* **1897,** *298* (2-3), 202-374.
5. Staudinger, H.; Kupfer, O., Versuche zur Darstellung von Methylenderivaten. *Berichte der deutschen chemischen Gesellschaft* **1911,** *44* (3), 2194-2197.
6. Staudinger, H.; Kupfer, O., Über Reaktionen des Methylens. III. Diazomethan. *Berichte der deutschen chemischen Gesellschaft* **1912,** *45* (1), 501-509.
7. Buchner, E.; Curtius, T., Ueber die Einwirkung von Diazoessigäther auf aromatische Kohlenwasserstoffe. *Berichte der deutschen chemischen Gesellschaft.* **1885,** *18* (2), 2377-2379.
8. Kirmse, W., *Carbene chemistry* (Second Edition) Vol. 1. Academic Press. New York, London. **1971**.
9. Mulliken, R. S., The Interpretation of Band Spectra Part III. Electron Quantum Numbers and States of Molecules and Their Atoms. *Reviews of Modern Physics* **1932,** *4* (1), 1-86.
10. Doering, W. v. E.; Knox, L. H., Synthesis of Substituted Tropolones. *Journal of the American Chemical Society* **1953,** *75* (2), 297-303.
11. von E. Doering, W.; Hoffmann, A. K., The Addition of Dichlorocarbene to Olefins. *Journal of the American Chemical Society* **1954,** *76* (23), 6162-6165.
12. Bertrand, G.; Jerabek, P.; Hegemann, J.; Authmann, A., *History of Carbene Chemistry*. Paul Jerabek, Julian Hegemann, Andreas Authmann: **2011**.
13. Lennard–Jones, J.; Pople, J. J., A survey of the principles determining the structure and properties of molecules. Part 1.—The factors responsible for molecular shape and bond energies. *Discussions of the faraday society*. **1951,** *10*, 9-18.
14. Pople, J. A.; Raghavachari, K.; Frisch, M. J.; Binkley, J. S.; Schleyer, P. V. R., Comprehensive theoretical study of isomers and rearrangement barriers of even-electron polyatomic molecules HmABHn (A, B = carbon, nitrogen, oxygen, and fluorine). *Journal of the American Chemical Society* **1983,** *105* (21), 6389-6399.
15. Walsh, A. D., 466. The electronic orbitals, shapes, and spectra of polyatomic molecules. Part I. AH2 molecules. *Journal of the Chemical Society (Resumed)* **1953,** (0), 2260-2266.
16. Hoffmann, R.; Zeiss, G. D.; Van Dine, G. W., The electronic structure of methylenes. *Journal of the American Chemical Society* **1968,** *90* (6), 1485-1499.
17. Bauschlicher, C. W.; Schaefer, H. F.; Bagus, P. S., Structure and energetics of simple carbenes methylene, fluoromethylene, chloromethylene, bromomethylene,

difluoromethylene, and dichloromethylene. *Journal of the American Chemical Society* **1977,** *99* (22), 7106-7110.

18. Sander, W.; Bucher, G.; Wierlacher, S., Carbenes in matrixes: spectroscopy, structure, and reactivity. *Chemical Reviews* **1993,** *93* (4), 1583-1621.

19. Moss, R. A., Carbenic reactivity revisited. *Accounts of Chemical Research* **1989,** *22* (1), 15-21.

20. Herzberg, G.; Shoosmith, J., Spectrum and Structure of the Free Methylene Radical. *Nature* **1959,** *183* (4678), 1801-1802.

21. Herzberg, G. ; Sciences, P., The Bakerian Lecture, The spectra and structures of free methyl and free methylene. *Proceedings of the Royal Society of London A*. **1961,** *262* (1310), 291-317.

22. Herzberg, G.; Johns, J. W. C., The spectrum and structure of singlet CH2. *Proceedings of the Royal Society of London. Series A. Mathematical and Physical Sciences* **1966,** *295* (1441), 107-128.

23. Bunker, P. R.; Jensen, P.; Kraemer, W. P.; Beardsworth, R., The potential surface of X̃ 3B1 methylene (CH2) and the singlet–triplet splitting. *The Journal of Chemical Physics* **1986,** *85* (7), 3724-3731.

24. Jensen, P.; Bunker, P. J. , The potential surface and stretching frequencies of X̃ 3 B 1 methylene (CH2) determined from experiment using the Morse oscillator-rigid bender internal dynamics Hamiltonian. *The journal of chemical physics*. **1988,** *89* (3), 1327-1332.

25. Jensen, P.; Bunker, P. R., The potential surface and stretching frequencies of X̃ 3B1 methylene (CH2) determined from experiment using the Morse oscillator-rigid bender internal dynamics Hamiltonian. *The Journal of Chemical Physics* **1988,** *89* (3), 1327-1332.

26. Shavitt, I., Geometry and singlet-triplet energy gap in methylene: a critical review of experimental and theoretical determinations. *Tetrahedron.***1985,** *41* (8), 1531-1542.

27. Breslow, R., On the mechanism of thiamine action. IV. 1 Evidence from studies on model systems. *Journal of American Chemical Society.***1958,** *80* (14), 3719-3726.

28. Wanzlick, H. W. Nucleophile Carben-Chemie. *Angewandte Chimie*. **1962,** *74* (4), 129-134.

29. Fischer, E.; Maasböl, A. J, On the existence of a tungsten carbonyl carbene complex. *Angewandte chimie international edition.***1964,** *3* (8), 580-581.

30. Tschugajeff, L.; Skanawy-Grigorjewa, M.; Posnjak, A.; Skanawy-Grigorjewa, M., Über Die Hydrazin-Carbylamin-Komplexe des Platins.*Zeitschrift für anorganische und allgemeine Chemie.***1925,** *148* (1), 37-42.

31. Yusenko, K. V.; Zadesenets, A. V.; Baidina, I. A.; Shubin, Y. V.; Vasil'chenko, D. B.; Korenev, S. V., Re-determination of the crystal structure and investigation of thermal decomposition of the Chugaev's salt, [Pt(NH3)5Cl]Cl3·H2O. *Journal of Structural Chemistry* **2006,** *47* (4), 735-739.

32. Öfele, K., 1, 3-Dimethyl-4-imidazolinyliden-(2)-pentacarbonylchrom ein neuer Übergangsmetall-carben-komplex. *Journal of organometallic chemistry* **1968,** *12* (3), P42-P43.

33. Cardin, D.; Cetinkaya, B.; Lappert, M., Transition metal-carbene complexes. *Chemical reviews*. **1972,** *72* (5), 545-574.
34. Igau, A.; Grutzmacher, H.; Baceiredo, A.; Bertrand, G., Analogous. alpha.,. alpha.'-bis-carbenoid, triply bonded species: synthesis of a stable. lambda. 3-phosphino carbene-. lambda. 5-phosphaacetylene. *Journal of the Americal Chemical Society*. **1988,** *110* (19), 6463-6466.
35. Arduengo III, A. J.; Harlow, R. L.; Kline, M., A stable crystalline carbene. *Journal of the American Chemical Society.***1991,** *113* (1), 361-363.
36. Diez-Gonzalez, S., N-heterocyclic carbenes: From Laboratory Curiosities to Efficient Synthetic Tools. Editor: Silvia Diez-Gonzalez **2011**.
37. Martin, C. D.; Soleilhavoup, M.; Bertrand, G., Carbene-stabilized main group radicals and radical ions. *Chemical Science* **2013,** *4* (8), 3020-3030.
38. Hopkinson, M. N.; Richter, C.; Schedler, M.; Glorius, F., An overview of N-heterocyclic carbenes. *Nature* **2014,** *510* (7506), 485-496.
39. Schuster, O.; Yang, L.; Raubenheimer, H. G.; Albrecht, M., Beyond Conventional N-Heterocyclic Carbenes: Abnormal, Remote, and Other Classes of NHC Ligands with Reduced Heteroatom Stabilization. *Chemical Reviews* **2009,** *109* (8), 3445-3478.
40. Vivancos, A. n.; Segarra, C.; Albrecht, M., Mesoionic and related less heteroatom-stabilized N-heterocyclic carbene complexes: synthesis, catalysis, and other applications. *Chemical Review*. **2018,** *118* (19), 9493-9586.
41. Perrin, L.; Clot, E.; Eisenstein, O.; Loch, J.; Crabtree, R. H., Computed Ligand Electronic Parameters from Quantum Chemistry and Their Relation to Tolman Parameters, Lever Parameters, and Hammett Constants. *Inorganic Chemistry* **2001,** *40* (23), 5806-5811.
42. Chianese, A. R.; Kovacevic, A.; Zeglis, B. M.; Faller, J. W.; Crabtree, R. H., Abnormal C5-Bound N-Heterocyclic Carbenes: Extremely Strong Electron Donor Ligands and Their Iridium(I) and Iridium(III) Complexes. *Organometallics* **2004,** *23* (10), 2461-2468.
43. Meyer, W. H.; Deetlefs, M.; Pohlmann, M.; Scholz, R.; Esterhuysen, M. W.; Julius, G. R.; Raubenheimer, H. G., Preparation and characterisation of palladium, platinum and manganese di(organo)carbene complexes from quinolinone and quinolinium precursors. *Dalton Transactions* **2004,** (3), 413-420.
44. Schneider, S. K.; Julius, G. R.; Loschen, C.; Raubenheimer, H. G.; Frenking, G.; Herrmann, W. A., A first structural and theoretical comparison of pyridinylidene-type rNHC (remote N-heterocyclic carbene) and NHC complexes of Ni(ii) obtained by oxidative substitution. *Dalton Transactions* **2006,** (9), 1226-1233.
45. Lavallo, V.; Canac, Y.; Präsang, C.; Donnadieu, B.; Bertrand, G., Stable Cyclic (Alkyl)(Amino)Carbenes as Rigid or Flexible, Bulky, Electron-Rich Ligands for Transition-Metal Catalysts: A Quaternary Carbon Atom Makes the Difference. *Angewandte Chemie International Edition* **2005,** *44* (35), 5705-5709.
46. Soleilhavoup, M.; Bertrand, G., Cyclic (Alkyl)(Amino)Carbenes (CAACs): Stable Carbenes on the Rise. *Accounts of Chemical Research* **2015,** *48* (2), 256-266.

47. Petz, W.; Frenking, G., Carbodiphosphoranes and Related Ligands. In *Transition Metal Complexes of Neutral eta1-Carbon Ligands*, Chauvin, R.; Canac, Y., Eds. Springer Berlin Heidelberg: Berlin, Heidelberg, **2010**, 49-92.
48. Inés, B.; Patil, M.; Carreras, J.; Goddard, R.; Thiel, W.; Alcarazo, M., Synthesis, Structure, and Reactivity of a Dihydrido Borenium Cation. *Angewandte Chemie International Edition* **2011,** *50* (36), 8400-8403.
49. Petz, W.; Öxler, F.; Neumüller, B.; Tonner, R.; Frenking, G., Carbodiphosphorane C(PPh3)2 as a Single and Twofold Lewis Base with Boranes: Synthesis, Crystal Structures and Theoretical Studies on [H3B{C(PPh3)2}] and [{(μ-H)H4B2}{C(PPh3)2}]+. *European Journal of Inorganic Chemistry* **2009,** (29-30), 4507-4517.
50. Bourissou, D.; Guerret, O.; Gabbaï, F. P.; Bertrand, G., Stable Carbenes. *Chemical Reviews* **2000,** *100* (1), 39-92.
51. Harrison, J. F., Electronic structure of carbenes. I. Methylene, fluoromethylene, and difluoromethylene. *Journal of the American Chemical Society* **1971,** *93* (17), 4112-4119.
52. Schoeller, W. W., When is a singlet carbene linear? *Journal of the Chemical Society, Chemical Communications* **1980,** (3), 124-125.
53. Pauling, L., The structure of singlet carbene molecules. *Journal of the Chemical Society, Chemical Communications* **1980,** (15), 688-689.
54. Crabtree, R. H., NHC ligands versus cyclopentadienyls and phosphines as spectator ligands in organometallic catalysis. *Journal of Organometallic chemistry* **2005,** *690* (24-25), 5451-5457.
55. Crudden, C. M.; Allen, D. P., Stability and reactivity of N-heterocyclic carbene complexes. *Coordination Chemistry Reviews* **2004,** *248* (21), 2247-2273.
56. Liu, M.; Yang, I.; Buckley, B.; Lee, J. K., Proton Affinities of Phosphines versus N-Heterocyclic Carbenes. *Organic Letters* **2010,** *12* (21), 4764-4767.
57. Tonner, R.; Heydenrych, G.; Frenking, G., First and Second Proton Affinities of Carbon Bases. *ChemPhysChem* **2008,** *9* (10), 1474-1481.
58. Jolly, C. A.; Chan, F.; Marynick, D. S., Calculated inversion barriers and proton affinities for P(CH3)3 and P(C6H5)3. *Chemical Physics Letters* **1990,** *174* (3), 320-324.
59. Hu, X.; Tang, Y.; Gantzel, P.; Meyer, K., Silver Complexes of a Novel Tripodal N-Heterocyclic Carbene Ligand: Evidence for Significant Metal−Carbene π-Interaction. *Organometallics* **2003,** *22* (4), 612-614.
60. Hu, X.; Castro-Rodriguez, I.; Olsen, K.; Meyer, K., Group 11 Metal Complexes of N-Heterocyclic Carbene Ligands: Nature of the MetalCarbene Bond. *Organometallics* **2004,** *23* (4), 755-764.
61. Garrison, J. C.; Simons, R. S.; Kofron, W. G.; Tessier, C. A.; Youngs, W. J., Synthesis and structural characterization of a silver complex of a mixed-donor N-heterocyclic carbene linked cyclophane. *Chemical Communications* **2001,** (18), 1780-1781.
62. Díez-González, S., *N-heterocyclic carbenes: from laboratory to curiosities to efficient synthetic tools*. Cambridge, United Kingdom. Royal Society of Chemistry. **2016** .

63. Wilson, D. J. D.; Couchman, S. A.; Dutton, J. L., Are N-Heterocyclic Carbenes "Better" Ligands than Phosphines in Main Group Chemistry? A Theoretical Case Study of Ligand-Stabilized E2 Molecules, L-E-E-L (L = NHC, phosphine; E = C, Si, Ge, Sn, Pb, N, P, As, Sb, Bi). *Inorganic Chemistry* **2012,** *51* (14), 7657-7668.
64. Hillier, A. C.; Sommer, W. J.; Yong, B. S.; Petersen, J. L.; Cavallo, L.; Nolan, S. P., A combined experimental and theoretical study examining the binding of N-heterocyclic carbenes (NHC) to the Cp*RuCl (Cp* = eta(5)-C5Me5) moiety: Insight into stereoelectronic differences between unsaturated and saturated NHC ligands. *Organometallics* **2003,** *22* (21), 4322-4326.
65. Blake, G. A.; Moerdyk, J. P.; Bielawski, C. W., Tuning the Electronic Properties of Carbenes: A Systematic Comparison of Neighboring Amino versus Amido Groups. *Organometallics* **2012,** *31* (8), 3373-3378.
66. Hudnall, T. W.; Bielawski, C. W., An N,N'-Diamidocarbene: Studies in C−H Insertion, Reversible Carbonylation, and Transition-Metal Coordination Chemistry. *Journal of the American Chemical Society* **2009,** *131* (44), 16039-16041.
67. Ess, D.; Gagliardi, L.; Hammes-Schiffer, S., Introduction: Computational Design of Catalysts from Molecules to Materials. *Chemical Reviews* **2019,** *119* (11), 6507-6508.
68. Durand, D. J.; Fey, N., Computational Ligand Descriptors for Catalyst Design. *Chemical Reviews* **2019,** *119* (11), 6561-6594.
69. Häller, L. J. L.; Page, M. J.; Erhardt, S.; Macgregor, S. A.; Mahon, M. F.; Naser, M. A.; Vélez, A.; Whittlesey, M. K., Experimental and Computational Investigation of C−N Bond Activation in Ruthenium N-Heterocyclic Carbene Complexes. *Journal of the American Chemical Society* **2010,** *132* (51), 18408-18416.
70. Sun, F.; Yin, T.; Wang, Y.; Feng, A.; Yang, L.; Wu, W.; Yu, C.; Li, T.; Wei, D.; Yao, C., A combined experimental and computational study of NHC-promoted desulfonylation of tosylated aldimines. *Organic Chemistry Frontiers* **2020,** *7* (3), 578-583.
71. de Brito Sá, É. Computational study of Iron carbenes and their reactivity with olefins. *Universitat Autonoma de Barcelona*. Barcelona, Spain. **2018**.
72. Lein, M.; Szabó, A.; Kovács, A.; Frenking, G., Energy decomposition analysis of the chemical bond in main group and transition metal compounds. *Faraday Discussions* **2003,***124* (0), 365-378.
73. Jacobsen, H.; Correa, A.; Costabile, C.; Cavallo, L., π-Acidity and π-basicity of N-heterocyclic carbene ligands. A computational assessment. *Journal of Organometallic Chemistry* **2006,** *691* (21), 4350-4358.
74. Farrell, J. M.; Hatnean, J. A.; Stephan, D. W., Activation of Hydrogen and Hydrogenation Catalysis by a Borenium Cation. *Journal of the American Chemical Society* **2012,** *134* (38), 15728-15731.
75. Moerdyk, J. P.; Bielawski, C. W., Alkyne and Reversible Nitrile Activation: N,N'-Diamidocarbene-Facilitated Synthesis of Cyclopropenes, Cyclopropenones, and Azirines. *Journal of the American Chemical Society* **2012,** *134* (14), 6116-6119.

76. Kolychev, E. L.; Theuergarten, E.; Tamm, M., N-Heterocyclic Carbenes in FLP Chemistry. In *Frustrated Lewis Pairs II: Expanding the Scope*, Erker, G.; Stephan, D. W., Eds. Springer Berlin Heidelberg: Berlin, Heidelberg, **2013**; 121-155.
77. Welch, G. C.; San Juan, R. R.; Masuda, J. D.; Stephan, D. W. J. s., Reversible, metal-free hydrogen activation. **2006,** *314* (5802), 1124-1126.
78. Chase, P. A.; Welch, G. C.; Jurca, T.; Stephan, D. W., Metal-Free Catalytic Hydrogenation. *Angewandte Chemie International Edition* **2007,** *46* (42), 8050-8053.
79. Erős, G.; Mehdi, H.; Pápai, I.; Rokob, T. A.; Király, P.; Tárkányi, G.; Soós, T., Expanding the Scope of Metal-Free Catalytic Hydrogenation through Frustrated Lewis Pair Design. *Angewandte Chemie International Edition* **2010,** *49* (37), 6559-6563.
80. Erős, G.; Nagy, K.; Mehdi, H.; Pápai, I.; Nagy, P.; Király, P.; Tárkányi, G.; Soós, T., Catalytic Hydrogenation with Frustrated Lewis Pairs: Selectivity Achieved by Size-Exclusion Design of Lewis Acids. *Chemistry – A European Journal* **2012,** *18* (2), 574-585.
81. Wang, H.; Fröhlich, R.; Kehr, G.; Erker, G., Heterolytic dihydrogen activation with the 1,8-bis(diphenylphosphino)naphthalene/B(C6F5)3 pair and its application for metal-free catalytic hydrogenation of silyl enol ethers. *Chemical Communications* **2008,** (45), 5966-5968.
82. Greb, L.; Oña-Burgos, P.; Schirmer, B.; Grimme, S.; Stephan, D. W.; Paradies, J., Metal-free Catalytic Olefin Hydrogenation: Low-Temperature H2 Activation by Frustrated Lewis Pairs. *Angewandte Chemie International Edition* **2012,** *51* (40), 10164-10168.
83. Mahdi, T.; Stephan, D. W., Enabling Catalytic Ketone Hydrogenation by Frustrated Lewis Pairs. *Journal of the American Chemical Society* **2014,** *136* (45), 15809-15812.
84. Scott, D. J.; Fuchter, M. J.; Ashley, A. E., Nonmetal Catalyzed Hydrogenation of Carbonyl Compounds. *Journal of the American Chemical Society* **2014,** *136* (45), 15813-15816.
85. Prokofjevs, A.; Boussonnière, A.; Li, L.; Bonin, H.; Lacôte, E.; Curran, D. P.; Vedejs, E., Borenium Ion Catalyzed Hydroboration of Alkenes with N-Heterocyclic Carbene-Boranes. *Journal of the American Chemical Society* **2012,** *134* (29), 12281-12288.
86. Matsumoto, T.; Gabbaï, F. P., A Borenium Cation Stabilized by an N-Heterocyclic Carbene Ligand. *Organometallics* **2009,** *28* (15), 4252-4253.
87. Curran, D. P.; Solovyev, A.; Makhlouf Brahmi, M.; Fensterbank, L.; Malacria, M.; Lacôte, E., Synthesis and Reactions of N-Heterocyclic Carbene Boranes. *Angewandte Chemie International Edition* **2011,** *50* (44), 10294-10317.
88. Horn, M.; Mayr, H.; Lacôte, E.; Merling, E.; Deaner, J.; Wells, S.; McFadden, T.; Curran, D. P., N-heterocyclic carbene boranes are good hydride donors. *Organic letter*. **2012,** *14* (1), 82-85.
89. Lindsay, D. M.; McArthur, D., The synthesis of chiral N-heterocyclic carbene–borane and –diorganoborane complexes and their use in the asymmetric reduction of ketones. *Chemical Communications* **2010,** *46* (14), 2474-2476.
90. Eisenberger, P.; Bestvater, B. P.; Keske, E. C.; Crudden, C. M., Hydrogenations at Room Temperature and Atmospheric Pressure with Mesoionic Carbene-Stabilized Borenium Catalysts. *Angewandte Chemie International Edition* **2015,** *54* (8), 2467-2471.

91. Hinde, R. J., Quantum Chemistry, 5th Edition (by Ira N. Levine). *Journal of Chemical Education* **2000,** *77* (12), 1564.
92. Szabo, A.; Ostlund, N. S., *Modern quantum chemistry: introduction to advanced electronic structure theory*. New York. Dover Publication. **1996**.
93. Roothaan, C. C. J., New Developments in Molecular Orbital Theory. *Reviews of Modern Physics* **1951,** *23* (2), 69-89.
94. Hall, G. G.; Lennard-Jones, J. E., The molecular orbital theory of chemical valency VIII. A method of calculating ionization potentials. *Proceedings of the Royal Society of London. Series A. Mathematical and Physical Sciences* **1951,** *205* (1083), 541-552.
95. Koch, W., Holthausen, M.C., *A Chemist's Guide to Density Functional Theory (2nd Edition)*. Weinheim, Germany. Wiley. **2001**.
96. Löwdin, P. O., Quantum Theory of Many-Particle Systems. I. Physical Interpretations by Means of Density Matrices, Natural Spin-Orbitals, and Convergence Problems in the Method of Configurational Interaction. *Physical Review* **1955,** *97* (6), 1474-1489.
97. Baerends, E. J.; Gritsenko, O. V., A Quantum Chemical View of Density Functional Theory. *The Journal of Physical Chemistry A* **1997,** *101* (30), 5383-5403.
98. Møller, C.; Plesset, M. S., Note on an Approximation Treatment for Many-Electron Systems. *Physical Review* **1934,** *46* (7), 618-622.
99. David Sherrill, C.; Schaefer, H. F., The Configuration Interaction Method: Advances in Highly Correlated Approaches. In *Advances in Quantum Chemistry*, Löwdin, P.O.; Sabin, J. R.; Zerner, M. C.; Brändas, E., Eds. Academic Press: **1999**; Vol. 34, pp 143-269.
100. Bartlett, R. J.; Musiał, M., Coupled-cluster theory in quantum chemistry. *Reviews of Modern Physics* **2007,** *79* (1), 291-352.
101. The Electron Density as the Basic Variable: Early Attempts. In *A Chemist's Guide to Density Functional Theory.* Weinheim, Germany. Wiley. **2001**; pp 29-32.
102. The Hohenberg-Kohn Theorems. In *A Chemist's Guide to Density Functional Theory (2nd Edition)*, Weinheim, Germany. Wiley. **2001**; pp 33-40.
103. Hohenberg, P.; Kohn, W., Inhomogeneous Electron Gas. *Physical Review* **1964,** *136* (3B), B864-B871.
104. Kohn, W.; Sham, L. J., Self-Consistent Equations Including Exchange and Correlation Effects. *Physical Review* **1965,** *140* (4A), A1133-A1138.
105. The Kohn-Sham Approach. In *A Chemist's Guide to Density Functional Theory (2nd Edition)*, Weinheim, Germany. Wiley. **2001**; pp 41-64.
106. The Quest for Approximate Exchange-Correlation Functionals. In *A Chemist's Guide to Density Functional Theory (2nd Edition)*. Weinheim, Germany. Wiley. **2001**; 65-91.
107. Stephens, P. J.; Devlin, F. J.; Chabalowski, C. F.; Frisch, M. J., Ab Initio Calculation of Vibrational Absorption and Circular Dichroism Spectra Using Density Functional Force Fields. *The Journal of Physical Chemistry* **1994,** *98* (45), 11623-11627.
108. Zhao, Y.; Truhlar, D. G., A new local density functional for main-group thermochemistry, transition metal bonding, thermochemical kinetics, and noncovalent interactions. *The Journal of Chemical Physics* **2006,** *125* (19), 194101.

109. Perdew, J. P.; Burke, K.; Ernzerhof, M., Generalized Gradient Approximation Made Simple. *Physical Review Letters* **1996,** *77* (18), 3865-3868.
110. Ditchfield, R.; Hehre, W. J.; Pople, J. A., Self-Consistent Molecular-Orbital Methods. IX. An Extended Gaussian-Type Basis for Molecular-Orbital Studies of Organic Molecules. *The Journal of Chemical Physics* **1971,** *54* (2), 724-728.
111. Zheng, J.; Xu, X.; Truhlar, D. G., Minimally augmented Karlsruhe basis sets. *Theoretical Chemistry Accounts* **2011,** *128* (3), 295-305.
112. Hellweg, A.; Rappoport, D., Development of new auxiliary basis functions of the Karlsruhe segmented contracted basis sets including diffuse basis functions (def2-SVPD, def2-TZVPPD, and def2-QVPPD) for RI-MP2 and RI-CC calculations. *Physical Chemistry Chemical Physics* **2015,** *17* (2), 1010-1017.
113. Kendall, R. A.; Dunning, T. H.; Harrison, R. J., Electron affinities of the first-row atoms revisited. Systematic basis sets and wave functions. *The Journal of Chemical Physics* **1992,** *96* (9), 6796-6806.
114. Edmiston, C.; Krauss, M., Configuration-Interaction Calculation of H3 and H2. *The Journal of Chemical Physics* **1965,** *42* (3), 1119-1120.
115. Schlegel, H. B., Exploring potential energy surfaces for chemical reactions: An overview of some practical methods. *Journal of Computational Chemistry* **2003,** *24* (12), 1514-1527.
116. Lewars, E., *Computational Chemistry: Introduction to the Theory and Applications of Molecular and Quantum Mechanics*. **2011**; 1-664.
117. Cramer, C. J., *Essentials of computational chemistry : theories and models (2nd Edition)*. West Sussex, England ; New York. Wiley, **2002**.
118. Weinhold, F.; Landis, C. R., *Valency and Bonding: A Natural Bond Orbital Donor-Acceptor Perspective*. Cambridge University Press: Cambridge, **2005**.
119. Weinhold, F.; Landis, C. R.; Glendening, E. D., What is NBO analysis and how is it useful? *International Reviews in Physical Chemistry* **2016,** *35* (3), 399-440.
120. Parr, R. G. In *Density Functional Theory of Atoms and Molecules*, Horizons of Quantum Chemistry, Dordrecht, **1980**; Fukui, K.; Pullman, B., Eds. Springer Netherlands: Dordrecht, **1980**; 5-15.
121. Wiberg, K. B., Application of the pople-santry-segal CNDO method to the cyclopropylcarbinyl and cyclobutyl cation and to bicyclobutane. *Tetrahedron* **1968,** *24* (3), 1083-1096.
122. Mayer, I., Bond order and valence indices: A personal account. *Journal of Computational Chemistry* **2007,** *28* (1), 204-221.
123. Kitaura, K.; Morokuma, K., A new energy decomposition scheme for molecular interactions within the Hartree-Fock approximation. *International Journal of Quantum Chemistry* **1976,** *10* (2), 325-340.
124. Mitoraj, M.; Michalak, A., Applications of natural orbitals for chemical valence in a description of bonding in conjugated molecules. *Journal of Molecular Modeling* **2008,** *14* (8), 681-687.

125. Michalak, A.; Mitoraj, M.; Ziegler, T., Bond Orbitals from Chemical Valence Theory. *The Journal of Physical Chemistry A* **2008,** *112* (9), 1933-1939.
126. Mitoraj, M.; Michalak, A., Donor–Acceptor Properties of Ligands from the Natural Orbitals for Chemical Valence. *Organometallics* **2007,** *26* (26), 6576-6580.
127. Mitoraj, M.; Michalak, A., Natural orbitals for chemical valence as descriptors of chemical bonding in transition metal complexes. *Journal of Molecular Modeling* **2007,** *13* (2), 347-355.
128. Mitoraj, M. P.; Zhu, H.; Michalak, A.; Ziegler, T., On the origin of the trans-influence in square planar d8-complexes: A theoretical study. *International Journal of Quantum Chemistry* **2009,** *109* (14), 3379-3386.
129. te Velde, G.; Bickelhaupt, F. M.; Baerends, E. J.; Fonseca Guerra, C.; van Gisbergen, S. J. A.; Snijders, J. G.; Ziegler, T., Chemistry with ADF. *Journal of Computational Chemistry* **2001,** *22* (9), 931-967.
130. Kumar, P. S. V.; Raghavendra, V.; Subramanian, V., Bader's Theory of Atoms in Molecules (AIM) and its Applications to Chemical Bonding. *Journal of Chemical Sciences* **2016,** *128* (10), 1527-1536.
131. Bader, R. F. W., Atoms in molecules. *Accounts of Chemical Research* **1985,** *18* (1), 9-15.
132. Bader, R. F. W., A quantum theory of molecular structure and its applications. *Chemical Reviews* **1991,** *91* (5), 893-928.
133. Bader, Atoms in Molecules: A Quantum Theory Oxford University. *International series of monographs in Chemistry*, **1990**.
134. Gibbs, G. V.; Ross, N. L.; Cox, D. F.; Rosso, K. M.; Iversen, B. B.; Spackman, M. A., Pauling bond strength, bond length and electron density distribution. *Physics and Chemistry of Minerals* **2014,** *41* (1), 17-25.
135. Popelier, P. L. A., Characterization of a Dihydrogen Bond on the Basis of the Electron Density. *The Journal of Physical Chemistry A* **1998,** *102* (10), 1873-1878.
136. Carlos Silva, L.; Angel, R. d. L., Bond Ellipticity as a Measure of Electron Delocalization in Structure and Reactivity. *Current Organic Chemistry* **2011,** *15* (20), 3576-3593.
137. Matta, C. F.; Hernández-Trujillo, J., Bonding in Polycyclic Aromatic Hydrocarbons in Terms of the Electron Density and of Electron Delocalization. *The Journal of Physical Chemistry A* **2003,** *107* (38), 7496-7504.
138. Matta, C. F.; Boyd, R. J., An Introduction to the Quantum Theory of Atoms in Molecules. In *The Quantum Theory of Atoms in Molecules*, **2007**; 1-34.
139. Bader, R. F. W.; Heard, G. L., The mapping of the conditional pair density onto the electron density. *The Journal of Chemical Physics* **1999,** *111* (19), 8789-8798.
140. Steinmann, S. N.; Mo, Y.; Corminboeuf, C., How do electron localization functions describe π-electron delocalization? *Physical Chemistry Chemical Physics* **2011,** *13* (46), 20584-20592.

141. Fuentealba, P.; Chamorro, E.; Santos, J. C., Chapter 5 Understanding and using the electron localization function. In *Theoretical and Computational Chemistry*, Toro-Labbé, A., Ed. Elsevier: **2007**; (19), 57-85.
142. Becke, A. D.; Edgecombe, K. E., A simple measure of electron localization in atomic and molecular systems. *The Journal of Chemical Physics* **1990,** *92* (9), 5397-5403.
143. Silvi, B.; Savin, A., Classification of chemical bonds based on topological analysis of electron localization functions. *Nature* **1994,** *371* (6499), 683-686.
144. Savin, A.; Silvi, B.; Colonna, F., Topological analysis of the electron localization function applied to delocalized bonds. *Canadian Journal of Chemistry* **1996,** *74* (6), 1088-1096.
145. Chesnut, D. B.; Moore, K. D., Locally dense basis sets for chemical shift calculations. *Journal of Computational Chemistry* **1989,** *10* (5), 648-659.
146. Reid, D. M.; Kobayashi, R.; Collins, M. A., Systematic Study of Locally Dense Basis Sets for NMR Shielding Constants. *Journal of Chemical Theory and Computation* **2014,** *10* (1), 146-152.
147. Sanchez, M.; Provasi, P. F.; Aucar, G. A.; Sauer, S. P. A., On the Usage of Locally Dense Basis Sets in the Calculation of NMR Indirect Nuclear Spin–Spin Coupling Constants: Vicinal Fluorine–Fluorine Couplings. In *Advances in Quantum Chemistry*, Academic Press: **2005**; (48) 161-183.

148. Farrell, J. M.; Posaratnanathan, R. T.; Stephan, D. W., A family of N-heterocyclic carbene-stabilized borenium ions for metal-free imine hydrogenation catalysis. *Chemical Science* **2015,** *6* (3), 2010-2015.

149. Zhang, I. Y.; Wu, J.; Xu, X., Extending the reliability and applicability of B3LYP. *Chemical Communications* **2010,** *46* (18), 3057-3070

150. Wigner, E., Artificial Atoms, *Physics Today* **1993,** *46*, 24.

151. Carlos Silva, L.; Angel, R. d. L., Bond Ellipticity as a Measure of Electron Delocalization in Structure and Reactivity. *Current Organic Chemistry* **2011,** *15* (20), 3576-3593.

152. Dunning, T. H., Gaussian basis sets for use in correlated molecular calculations. I. The atoms boron through neon and hydrogen. *The Journal of Chemical Physics* **1989,** *90* (2), 1007-1023.

PART A – Measurement of Structural Parameters of NHC-derived Borenium

3. CHAPTER II
Computational Investigation of C→B π-bond in NHC-derived Borenium Catalysts

Abstract

Our investigations start with the question of how to quantify the π-bond. Literature points out there are numerous methods to achieve this goal, but are these methods equivalent? A family of compounds, including a dihydrido borenium cation stabilized by various divalent C donor ligands, has been designed for that purpose. Numerous approaches could indeed be achieved to estimate the partial π-bond that exists between the carbon and boron atoms in these species.

Quantum chemical calculations and NBO, ETS-NOCV, QTAIM and ELF interpretative approaches have been carried out on these compounds. Numerous descriptors of the C-B π-bond strength obtained from orbital localization, energy partitioning or topological methods as well as from structural and chemical parameters have been calculated for 39 C-donor ligands including N-heterocyclic carbenes and carbones. Comparison of the results allows the identification of *relative* and *absolute* descriptors of the π interaction. Excellent correlations are obtained for both families of descriptors. This enables the establishment of a π-donation capability scale and shows that the interpretative methods, despite their conceptual differences, describe the same chemical properties. These results also reveal noticeable shortcomings in these popular methods, and some precautions that need to be taken to interpret their results adequately.

3.1. Introduction

Chemical bonds, among other "fuzzy" chemical concepts[1, 2], are not univocally defined and their quantification is not straightforward because they are not a quantum mechanical observable. However, chemical bonding is a key concept in chemistry, a cornerstone of this science.[3, 4] There is little doubt that the concept of a chemical bond is quite useful to chemists and has led to the development of constructive ideas when appropriately used and defined. After all, the justification of concepts lies in their successful application rather than in firm proofs.[1] Some may even claim that the success of chemistry is due to how flexible and fuzzy the concept of a bond is.[5]

Numerous approaches have been developed in order to describe, classify and measure chemical bonds. Various properties of a chemical bond can be evaluated experimentally or theoretically. In this chapter, our work is focused on the study of the strength of π-interaction in NHC-derived borenium adducts (*vide infra*). A large variety of methods are available to quantify such interactions; however, these methods are not necessarily equivalent. Here, a comparison of such methods is presented and the most reliable methods are established as standard for measuring the strength of π-donation for the following stages of the thesis.

The work presented in this chapter has been published as "Comparison of Chemical and Interpretative Methods: The Carbon-Boron π-bond as a Test Case" with similar text and figures.[6] Additional data pertaining to this work is available as supporting information for this paper.

3.1.1. Experimental Parameters

A significant amount of information pertaining to the chemical bond can be obtained from experimental data, although it is quite difficult to quantify a chemical bond. The bond length, which from the chemist's point of view should be approximately correlated to its strength, can indeed be empirically related to a bond index[7] or compared to the sum of the covalent radii of the atoms involved.[8] The activation barrier associated to the rotation around the bond allows to differentiate a single bond (free rotation) from a double bond (strong rotation barrier). Thermochemical measurements and electronic spectroscopy also provide information about bond strength. Bond order, a concept that pre-dates the quantum era, can be a little more complicated to derive experimentally, but nevertheless, can be obtained from

experimental quantities using approximate formulae.[1] For example,[9] the force constant (calculated from IR stretching frequencies), bond equilibrium distance and the number of valence electrons in the shell of the participating atoms have been fitted in a formula to produce an expected bond order for a set of diatomic molecules and it is conceivable that the same study can be applied to the whole periodic table and polyatomic molecules. Although it is not possible to decompose bond energy into its physically meaningful components through any experimental technique, an indirect way is to use experimental electronic densities into theoretical decomposition schemes. The problem with this is that it is quite difficult to obtain accurate experimental densities.[1]

3.1.2. Theoretical Parameters

The advent of theoretical and computational chemistry has made it possible to have straightforward access to the above-mentioned parameters by calculation, and simultaneously has led to the development of methods for bond analysis. To determine the properties of a bond (e.g. bond order) within a molecule, one of the simplest methods is to have an appropriate description of the atoms within the molecule. This can be achieved mainly by two different methods[10] – the first is based upon using atom centered basis sets i.e., via a partitioning of the Hilbert space that is composed of basis functions used to describe the wave function. The bond order for π-bond in the Hückel framework defined by Coulson,[11] the Wiberg Bond Index (WBI)[12] and the Mayer bond order[13] are prominent examples derived from this approach.[14] Bonding analysis can also result from different procedures leading to localized molecular orbitals[15-17] or natural orbitals,[18] leading to methods such as the Localized orbital bonding analysis (LOBA) method[19, 20] and the well-known natural bonding orbital (NBO) method.[21] The most serious drawback of the Hilbert space is that since the methods are focused on atom-centered basis sets, the results produced can be strongly basis set dependent.[1]

The second method to define atoms in molecules is by partitioning electron density (real space), which albeit leads to reduced basis set sensitivity. Within such partitioning schemes the atoms may have sharp (Bader's QTAIM theory)[22] or fuzzy, interpenetrating (Hirshfield)[23] boundaries. The real space partitioning of molecular space may also be achieved by using functions of electronic density and/or its derivatives. The electron localization function (ELF),[24, 25] the localized orbital locator (LOL),[26] non-covalent interaction (NCI)[27] index and the

density overlap regions indicator (DORI)[28] are prominent examples in this category. While ELF and LOL depend upon kinetic energy of electrons, NCI partitions molecular space using reduced density gradient while DORI uses the single-Exponential decay detector. Again, an interesting picture of the chemical bond can also be obtained through the variations in isotropic magnetic shielding around a molecule[29] or with the charge displacement analysis method.[30]

The strength of a bond can be determined by calculating the bond dissociation energy (BDE). While experimental determination of the BDE is notoriously difficult, theoretical methods are well-suited for the purpose. Chemical bond analysis can also be performed using energy decomposition approaches, such as the extended transition state (ETS)[31, 32] or the energy decomposition analysis (EDA)[33] methods, possibly combined with the natural orbitals for chemical valence (NOCV) theory,[34] and the symmetry-adapted perturbation theory (SAPT) scheme.[35] Another fundamentally different approach that quantifies the internal energy of a bond (the energy between two fragments within the molecule) is obtained from the interacting quantum fragments (IQF) approach.[36, 37] In addition to methods mentioned above, the somewhat random partitioning of Hamiltonian exchange and kinetic energy terms (which do not have an intuitive physical meaning) results in numerous other competing decomposition schemes.[38]

Finally, although force constants are known not to properly match the bond strengths,[39] derived methods such as the concept of adiabatic internal vibrational modes,[40] or the local stretching force[41] and compliance constants[42] also provide noteworthy chemical bond descriptors.

3.1.3. Controversies in Literature - Do these parameters complement each other?

These numerous interpretative methods are widely used in the literature to provide insights into the nature of chemical bonds.[4, 43-50] However, this plethora of methods, while of value in providing complementary visions of the same subject,[51-53] is also troublesome, in the sense that contradictory descriptions can result, leading to many controversies in the literature. For instance, there are conflicting views in describing the bonding situation in carbonyl complexes of alkaline earth metals[10, 54, 55] as well as in describing metal-ligand bonds as in the case of

cAACs binding to coinage transition metals.[56, 57] In the case of recognizing multiple bonds, like in the cases of galium[58] or boron[59, 60] there are several conflicting views. Description of weak bonds such as hydrogen bonding interactions,[61-66] or rotational barrier about a single bond as in the case of ethane where the explanation for its preferred conformation be rationalized by steric repulsion or hyperconjugation[67, 68] are also a few instances where no unified narrative is available. In some cases, there is no significant discrepancy between two different approaches, but the agreement is far from perfect. A noteworthy example is given in a recent study in which the internal π-donation to the carbene center for 15 *N*-heterocyclic carbenes (NHC) has been estimated through NBO and ETS-NOCV approaches.[69] Despite the relevance of the two selected descriptors, the coefficient of determination (R^2) is no higher than 0.89. If these computational approaches indeed represent powerful tools in studying the electronic structure of molecules, one has to investigate the source of such discrepancies.

Depending on the theoretical model used, the numerical differences between several bond descriptors may result from many factors, such as the comparison of descriptors which might not be related to the same chemical concept, the misuse of methods, the misinterpretation of the results or the existence of conceptual problems in the definition of the descriptors. It is currently difficult to distinguish between these different assumptions and opinions may differ,[48, 70] even if numerous efforts have been made to compare various methods, to analyze their differences and to propose unified approaches.[71-74]

3.1.4. C-B π-bond as a Test Case

The ability to establish cross correlations (or a lack thereof) between these different approaches would, however, provide a better knowledge of the nature of the calculated descriptors and the chemical concept under investigation. This could even help in the development of new interpretative methods. The focus of this chapter lies on the modeling of the π-interaction between neutral divalent carbon-donor compounds and cationic dihydrido borenium BH_2^+ moiety through various theoretical approaches, and to examine if a unified qualitative as well as quantitative description of this interaction can be provided. Borenium cations R_2BL^+ are well-known boron Lewis acids.[75] These boron species have been used in numerous catalytic processes.[76-79] They are stabilized through electronic π-donation from the π-cloud of the boron substituents,[80-83] and neutral divalent carbon-donor compounds, such as normal NHC,[84-89] mesoionic NHC[90] and carbones,[91] have all been used for

this purpose (Scheme 3-1). The donation takes place from the filled π-cloud to the vacant p orbital localized on boron that lies parallel to it, denoted by p_z^B or p_{vac}^B. For dihydrido borenium (R = H), only the two-electrons σ-donor ligand L provides partial mitigation of their electron deficiency and consequently their stabilization requires strong π-donors.[92, 93] DFT studies on [C-donor ligand-BR_2]$^+$ borenium reveal a short CB bond reflecting a partial double-bond character due to C→B π-electronic transfer.[86, 88, 91-95] Beyond structural parameters, various theoretical indicators have been used to analyze the electronic structure of these and other related compounds,[96-98] among them are the nature of the highest occupied and lowest unoccupied molecular orbitals (HOMO/LUMO), the atomic charges, the energy associated to the σ- and π-donation through energy decomposition analysis of the B-C bond, and the Wiberg bond index between these two atoms. However, only a handful of studies using such indicators to compare the bonding situation in borenium complexes exist in chemical literature. The comparison of the bonding in various complexes between carbones $(PPh_3)_2C$ and EH_2^q (E^q = Be, B^+, C^{2+}, N^{3+}, O^{4+}) has been performed with the ETS-NOCV approach.[94] Recently, a combination of energy decomposition analysis methods has been used to clarify the theoretical measurement of the π-interactions strength within main group-NHC complexes, including NHC-borenium complexes.[99] Based on these previous studies, C-donor ligand - dihydrido borenium complexes, in which the π-interaction between the two fragments is limited to the C→B π-donation, appear as ideal models to assess the relevance of π-bond descriptors. The strength of this π interaction has a direct consequence on the Lewis acidity of the B center, which in turn, affects its efficiency as a catalyst.

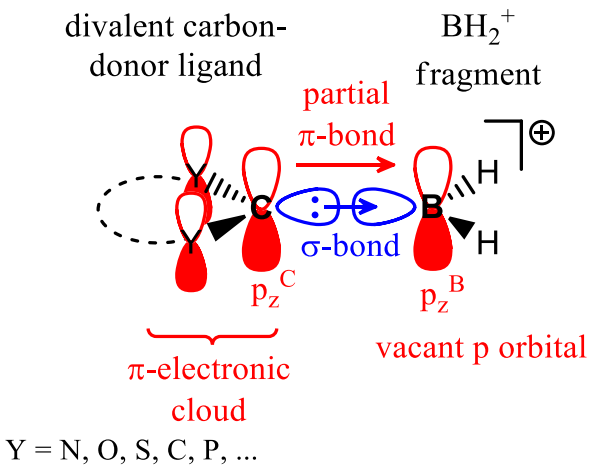

Scheme 3-1. Schematic description of the σ- and π-interaction in carbene and related compounds – BH_2^+ complexes

3.2. Geometric Structure

For this section of the study, 39 divalent carbon compounds, shown on page 13, have been chosen. These include normal NHC (**1**-**2**, **4**, **6**, **8**, **10**, **12**, **14**, **16**, **20**-**24**, **26**-**28**, **30**-**33**), mesoionic NHC (**9**, **11**, **13**, **15**, **17**-**19**, **25**, **29**), cyclic alkyl amino carbenes (cAAC **3**, **5**, **7**), carbodiphosphoranes (**35**-**36**) and carbodicarbenes (**34**, **37**-**39**), which have been selected so as to ensure a wide variety of geometrical structures and electronic properties.[100-103] Optimisation has been performed using Gaussian09 package.[127] A more detailed description of each of these categories of divalent carbon compounds has been provided in Sections 2A.2-2A.3. All of them, with the exception of **5**, **7**, **17**, **23**-**24**, **26**-**28** and **32**, are unsubstituted or "parent" molecules, preventing steric interference in the electronic analysis of their BH_2^+ complexes, also shortening computation time simultaneously.

Scheme 3-1 illustrates the general electronic structure of these adducts. The divalent carbon atom of **1**-**39** is linked to two atoms, denoted as Y, on either side. Y includes C, N, O, S etc. Depending on if Y is the same on both side or not, the carbene may be symmetric (as is the case for **1**-**2**, **4**, **6**, **8**, **22**, **23**, **24**, **26**-**29**, **32**-**39**) or unsymmetrical, respectively. These divalent carbon compounds are in their singlet state and therefore possess an sp^2 hybridised lone pair located in the Y-C-Y plane. **1**-**39** bind to the BH_2^+ moiety to form the borenium cations **X**-BH_2^+ (**X** = **1**-**39**) by dative donation of this lone pair to form a σ-bond. Geometry optimization of **X**-BH_2^+ (**X** = **1**-**39**) was carried out at the DFT B3LYP/TZVP without any symmetry constraints. Each stationary point has been characterized with frequency analysis and shows the correct number of negative eigenvalues (zero for a local minimum and one for a transition state). Furthermore, in order to ensure that the results obtained are not dependent on the level of calculation used, geometry optimizations were also carried out for all the divalent carbon-borenium adducts with the M06 functional[104] and the 6-311G(d,p)[105, 106] basis set (Table 1). The results obtained, concerning bond lengths, barrier of rotation (ΔE_{rot}) (*vide infra*) energy barrier or NBO analysis, show an excellent agreement between B3LYP and M06 data, therefore only B3LYP data are presented in the text. Geometry optimisation leads to minimum on the potential energy surface for which the BH_2 and Y_2C moiety are coplanar or almost coplanar (Scheme 3-2 left),[e] except for **3**, **5** and **7** (vide infra). This planar conformation

[e] The largest deviation is observed for **8**-BH_2^+ with Y-C-B-H dihedral angle of 13.8 degrees, due to the non-planarity of the NHC moiety.

will be noted hereafter as $\mathbf{X}^{//}$-BH_2^+. In addition to the σ-B-C bond formed by the donation of the in-plane lone pair of the carbon atom to the vacant sp^2-orbital of the boron atom (Scheme 3-2), this planarity supports the existence of a partial π-bond, the strength of which is supposed to depend on the nature of the π-system of the divalent donor ligand. The average B-C bond length of the optimized $\mathbf{X}^{//}$-BH_2^+ is around 1.54 Å. Comparison between experimental and theoretical structures is only possible for $\mathbf{36}^{//}$-BH_2^+, revealing a very nice agreement between the 1.494 Å calculated value for the C-B bond length and the 1.503 Å experimental value obtained from X-ray structure analysis.[134]

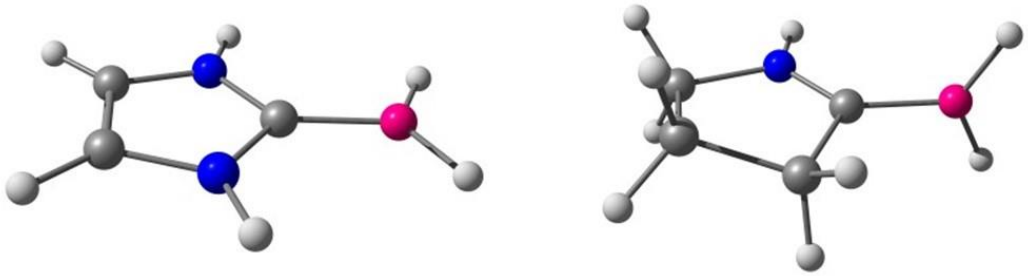

20-BH_2^+ **3**-BH_2^+

Scheme 3-2: Ground state geometry of two representative carbenes – **20**-BH_2^+ on the left and **3**-BH_2^+ (right); Carbon atoms have been represented in grey, Nitrogen atoms in blue, Boron atoms in pink and Hydrogen atoms in white.

The $\mathbf{X}^{//}$-BH_2^+ conformation of **X**-BH_2^+ (**X** = **3**, **5**, **7**) is a transition state for the rotation around the C-B bond, whereas the BH_2 and Y_2C moiety are mutually perpendicular (Y-C-B-H dihedral angle around 90°) in the ground state. This conformation is noted as $\mathbf{X}^{\perp}$-BH_2^+ in the following (Scheme 3-2right). The bond lengths calculated for $\mathbf{X}^{//}$-BH_2^+ in the case of **3**, **5** and **7** is around 1.6 Å, which is significantly higher than the average and amongst the longest C-B bond lengths in the group. This result suggests weak π-donation capability for **3**, **5** and **7**. Furthermore, in addition to σ- and π-donations, it is likely that there are other weak electronic or steric interactions between the BH_2 and the C-donor ligand in the **X**-BH_2^+ complexes.

Table 1. Rotational barrier and optimized geometrical data for $\mathbf{X}^{//}$-BH_2^+, $\mathbf{X}^{\perp}$-BH_2^+ and **X**-BH_3(**X** = **1**-**39**) computed at the B3LYP/TZVP and M06/6-311G(d,p) levels.

	B3LYP				M06		
X	$d_{C\text{-}B}$ (Å) in $\mathbf{X}^{//}$-BH_2^+	$d_{C\text{-}B}$ (Å) in $\mathbf{X}^{\perp}$-BH_2^+	$d_{C\text{-}B}$ (Å) in **X**-BH_3	ΔE_{rot} (kJ/mol)	$d_{C\text{-}B}$ (Å) in $\mathbf{X}^{//}$-BH_2^+	$d_{C\text{-}B}$ (Å) in $\mathbf{X}^{\perp}$-BH_2^+	ΔE_{rot} (kJ/mol)
1	1.60582	1.59498	1.59633	10.63	1.60063	1.58697	10.43
2	1.60726	1.58851	1.56868	5.14	1.60329	1.58068	3.96
3	1.60236	1.55936	1.56761	-13.22	1.59826	1.55463	-13.39
4	1.59078	1.58528	1.58690	9.81	1.58761	1.57868	8.02
5	1.59730	1.56124	1.59723	-15.92	1.59325	1.55556	-16.04
6	1.58779	1.59168	1.59811	19.40	1.58467	1.58400	18.43
7	1.59982	1.56129	1.58701	-28.60	1.59746	1.55550	-29.59
8	1.58831	1.59599	1.60234	21.92	1.58618	1.58721	21.03
9	1.55962	1.57967	1.61876	30.31	1.55531	1.57414	29.17
10	1.56142	1.57734	1.58804	26.78	1.56010	1.57183	23.42
11	1.55817	1.57968	1.61541	29.40	1.55522	1.57473	27.23
12	1.56433	1.58886	1.58550	29.75	1.56389	1.58231	25.46
13	1.55599	1.58392	1.59795	34.21	1.55416	1.57821	30.99
14	1.56361	1.59158	1.57303	27.30	1.56317	1.58507	23.33
15	1.55058	1.57499	1.61606	33.81	1.54774	1.57022	31.39
16	1.55656	1.58154	1.58388	33.97	1.55533	1.57635	30.98
17	1.54594	1.57814	1.60381	30.19	1.54502	1.57283	26.78
18	1.54269	1.58164	1.60002	45.95	1.54080	1.57646	42.78
19	1.54323	1.57729	1.59251	42.98	1.54153	1.57200	39.50
20	1.54771	1.58778	1.58907	44.90	1.54645	1.58214	40.24
21	1.54891	1.58536	1.58261	42.26	1.54895	1.57923	37.37
22	1.53567	1.53978	1.58764	18.52	1.53964	1.53670	11.92
23	1.54253	1.58545	1.59813	28.39	1.54228	1.58035	22.19
24	1.53858	1.58489	1.59430	43.82	1.53855	1.57857	41.38
25	1.52665	1.57917	1.59743	59.02	1.52491	1.57379	56.41
26	1.53780	1.58272	1.60404	39.29	1.53794	1.57605	36.12
27	1.53697	1.58691	1.59981	46.54	1.53662	1.58047	44.29
28	1.53172	1.58310	1.60162	50.08	1.53213	1.57705	46.56
29	1.51190	1.57224	1.61110	76.85	1.50864	1.56736	78.04
30	1.51982	1.58503	1.58801	69.21	1.52007	1.57912	63.79
31	1.51812	1.56960	1.60551	59.45	1.51784	1.56683	49.84
32	1.51239	1.57858	1.60156	66.14	1.51319	1.57328	60.43
33	1.49786	1.58152	1.59206	91.18	1.49740	1.57620	87.25
34	1.49813	1.57890	1.64144	114.19	1.49533	1.57233	112.86
35	1.49091	1.57915	1.69041	121.30	1.49224	1.57275	114.99
36	1.49436	1.58923	1.69881	95.52	1.49563	1.58246	89.83
37	1.48392	1.56351	1.63883	129.76	1.48052	1.55789	129.58
38	1.47575	1.56739	1.60821	129.14	1.47574	1.56513	101.21
39	1.47195	1.56144	1.64133	172.75	1.46841	1.55261	165.65

3.3. π-bonding descriptors based on chemical insight

From a chemist's point of view, there are several features that distinguish a double bond from a single bond. The most important of these features include (a) the bond length – a double bond is generally shorter than a single bond,[7, 107-111] although there also exist simultaneously some arguments against this general empirical rule;[112-114] and (b) a significant energy barrier associated with the rotation around a bond.[115-117] To estimate these characteristics for our system, we calculated the energy barrier ΔE_{rot} associated with the rotation around the C-B bond, i.e., the energy required to go from $\mathbf{X}^{//}$-BH_2^+ to $\mathbf{X}^{\perp}$-BH_2^+, as illustrated in Scheme 3-3.

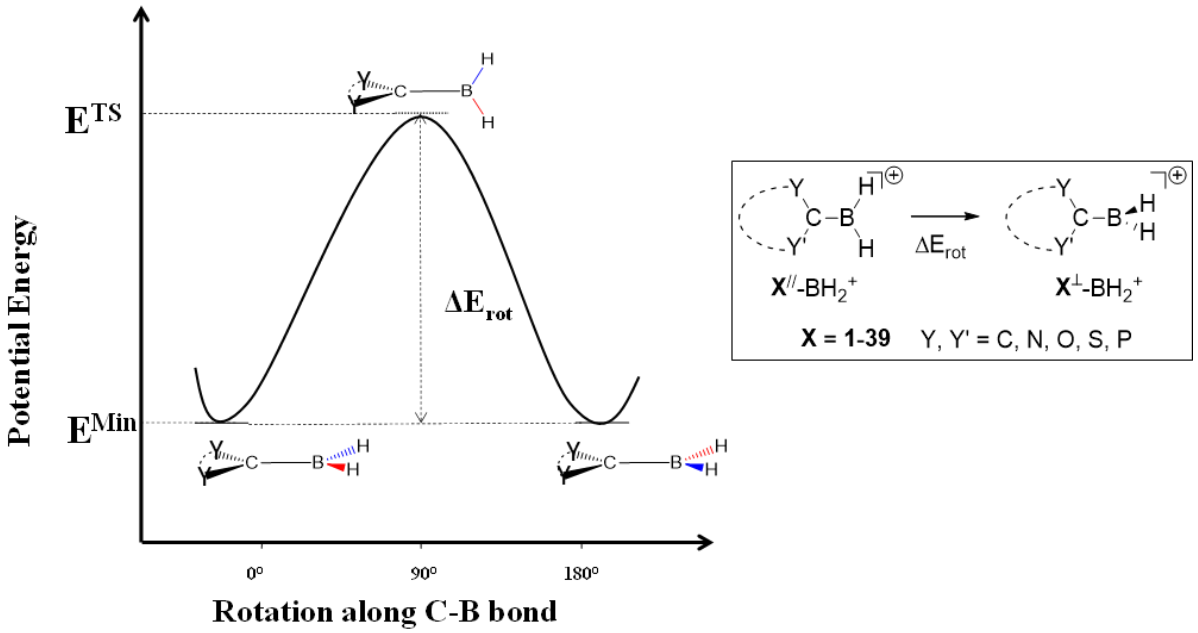

Scheme 3-3: Rotation along the C-B bond

In all cases except **3**, **5** and **7**, $\mathbf{X}^{\perp}$-BH_2^+ is a transition state for this rotation and ΔE_{rot} has a positive value which range from 5 kJ/mol for **2** to 172 kJ/mol for **39**. For **3**, **5** and **7**, a negative value is obtained (between -29 and -13 kJ/mol). This wide range of values confirms the structural diversity of compounds **1**-**39** in terms of π-donation capability. At the same time, the change from $\mathbf{X}^{//}$-BH_2^+ to $\mathbf{X}^{\perp}$-BH_2^+ induces in most cases, a slight increase in the B-C bond length (average increase for the positive values of B-C bond length being 0.046 Å), in line with the cancellation of the π-transfer to the vacant p_{vac}^B orbital, which is responsible for the partial double bond character. A slight decrease is however observed for **1**-**5** and **7** (around average values -0.025 Å).

In agreement with the chemical expectation, Figure 3-1A indicates that there is a rough match between the C-B bond length ($d_{C\text{-}B}$) in $\mathbf{X}^{//}\text{-}BH_2^+$ and the energy barrier ΔE_{rot} associated with the rotation around the C-B bond. This correlation is only fairly good (R^2 = 0.86), indicating that these descriptors do not measure exactly the same chemical property. This discrepancy may be due to the fact that $d_{C\text{-}B}$ includes both the π- and the σ-interactions whereas ΔE_{rot} characterizes only the latter and measures an evolution from $\mathbf{X}^{//}\text{-}BH_2^+$ to $\mathbf{X}^{\perp}\text{-}BH_2^+$. In order to resolve these differences, the C-B bond elongation $\Delta d_{C\text{-}B}$ during the rotation of the BH_2 group has been considered (Figure 3-1B). A correlation is again obtained, but it is not better than the one observed previously (R^2 = 0.84). A similar correlation (R^2 = 0.82, Figure 3-1C) is obtained by considering the C-B bond elongation when the H^- anion is added to $\mathbf{X}^{//}\text{-}BH_2^+$ to form the donor-acceptor $\mathbf{X}\text{-}BH_3$ complex. The larger C-B bond length in $\mathbf{X}\text{-}BH_3$ compared to $\mathbf{X}^{\perp}\text{-}BH_2^+$, as well as the moderately good correlation between $\Delta d_{C\text{-}B}$ to reach these two complexes from $\mathbf{X}^{//}\text{-}BH_2^+$ (R^2 = 0.81, Figure 3-1D), indicate that these two ways of considering a purely σ-bond are not equivalent. It is likely that the interaction between **X** and the rotated BH_2^+ or BH_3 groups in these complexes is not only a σ-interaction, but also includes other component such as an electronic transfer from the **X** σ-system to the vacant p-orbital of the rotated BH_2^+ group in $\mathbf{X}^{\perp}\text{-}BH_2^+$ (*vide infra*). This first approach therefore does not provide an unbiased measure of the π-donation capability of **X**.

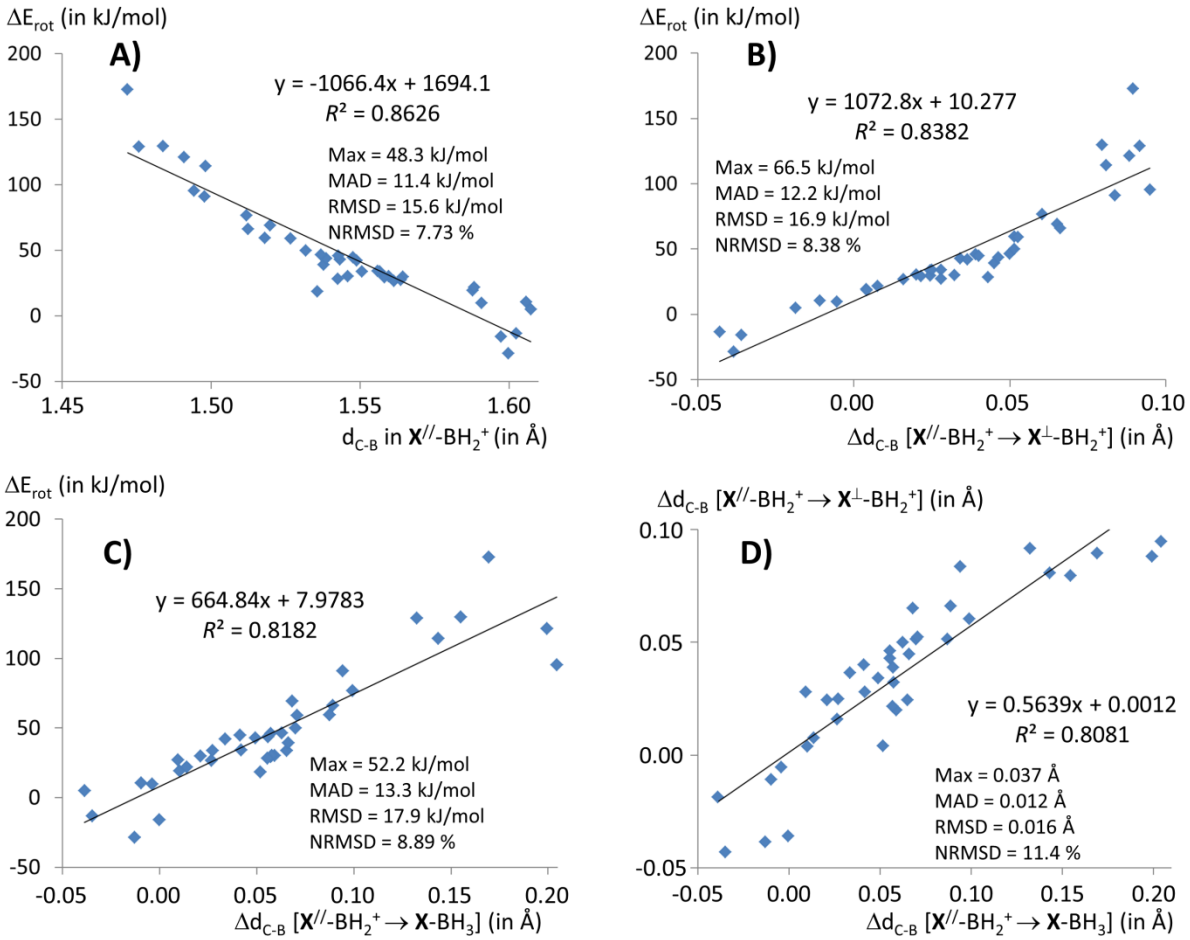

Figure 3-1: Correlation plots for **X**-BH_2^+ complexes computed at the B3LYP/TZVP level between: the energy barrier ΔE_{rot} associated with the rotation around the C-B bond *vs*. the C-B bond length ($d_{C\text{-}B}$) in $\mathbf{X}^{//}$-BH_2^+ (A); ΔE_{rot}*vs*. the change in the C-B bond length ($\Delta d_{C\text{-}B}$) when going from $\mathbf{X}^{//}$-BH_2^+ to $\mathbf{X}^{\perp}$-BH_2^+ (B) and **X**-BH_3 (C); $\Delta d_{C\text{-}B}$ when going from $\mathbf{X}^{//}$-BH_2^+ to $\mathbf{X}^{\perp}$-BH_2^+*vs.* to **X**-BH_3 (D). Linear regression equation, coefficients of determination (R^2), maximum absolute deviations (Max), mean absolute deviations (MAD), root mean square deviations (RMSD) and normalized RMSD (NRMSD) are reported.[f]

3.4. π-bonding descriptors based on the NBO Approach

Electronic structures obtained at the B3LYP/TZVP level were explored by means of natural bond orbital (NBO) analysis[128] using the NBO6 program.[129-130] The NBO method is a multistep localization process which provides a quantitative description of the electronic structure in terms of natural atomic orbitals (NAOs) and natural bond orbitals (NBOs). NBOs are localized 1- or 2-center orbitals which give the 'best' Lewis structure corresponding to the total electron density (See Section 2B.9.4 for further details). In the framework of the NBO analysis, the C→B π-donation in $\mathbf{X}^{//}$-BH_2^+ complexes can be characterized through several indicators. In all

[f] A short account of the different statistical analysis method to determine the spread of values has been provided in Appendix 1.

$\mathbf{X}^{//}$-BH_2^+ and $\mathbf{X}^{\perp}$-BH_2^+ complexes, the boron atom is involved in 7 or 8 valence Lewis and non-Lewis NBOs. This includes 2 σ_{BH} bonding and 2 σ^*_{BH} antibonding orbitals, 1 σ_{CB} bonding and 1 σ^*_{CB} antibonding orbitals, and either 1 unfilled valence nonbonding orbital of 'lone vacancy' type (LV(B)) or 1 π_{CB} bonding and 1 π^*_{CB} antibonding orbitals. The occupancy-weighted symmetric orthogonalization method used to generate the NAOs allows to compute the Wiberg bond index (WBI).

We compute the WBI which is known to have good agreement with empirical bond order. Values of WBI between 0.83 ($\mathbf{2}^{//}$-BH_2^+) and 1.43 ($\mathbf{39}^{//}$-BH_2^+) have been obtained. Comparisons between WBI and the C-B bond length show similar trend, but with moderate correlation (R^2 = 0.82 Figure 3-2).

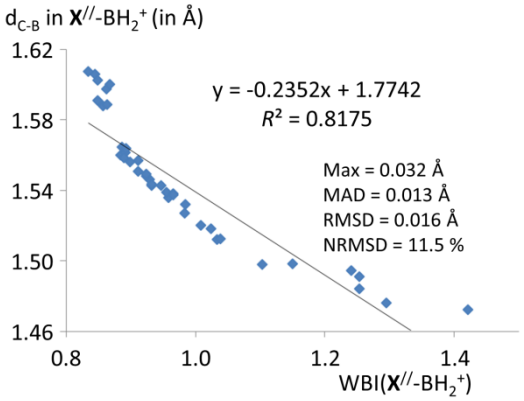

Figure 3-2: Correlation plots for $\mathbf{X}^{//}$-BH_2^+ complexes computed at the B3LYP/TZVP level between the C-B bond length ($d_{C\text{-}B}$) and the C-B WBI in $\mathbf{X}^{//}$-BH_2^+.

A better correlation is observed between WBI ($\mathbf{X}^{//}$-BH_2^+) and ΔE_{rot} (R^2 = 0.90, Figure 3-3 A). For $\mathbf{X}^{\perp}$-BH_2^+ complexes for which approximately a single C-B bond is expected, the WBI ranges as anticipated from 0.84 to 0.92. A revised π-bond order can be estimated by calculating the difference between the WBI obtained for $\mathbf{X}^{//}$-BH_2^+ and $\mathbf{X}^{\perp}$-BH_2^+ (ΔWBI).[g] ΔWBI lies between -0.06 and 0.50, which confirms the diverse π-donation capability of **1**-**39**.

[g] WBI values have also been calculated for$\mathbf{X}$-BH_3 complexes, and the use of these values leads to similar analyses to the ones obtained with $\mathbf{X}^{\perp}$-BH_2^+.

Table 2. C-B Bond descriptors computed with the NBO methods at the B3LYP/TZVP and M06/6-311G(d,p) levels for $\mathbf{X}^{//}$-BH_2^+ (**X** = **1**-**39**).

	B3LYP			M06		
X	C-B WBI	pop($^{//}p_{vac}^{B}$) (e)	$E^{//}_{del}$ (kJ/mol)	C-B WBI	pop($^{//}p_{vac}^{B}$) (e)	$E^{//}_{del}$ (kJ/mol)
1	0.8451	0.02743	26.09142	0.8446	0.02336	23.30488
2	0.8339	0.02749	25.83620	0.8280	0.02254	23.07058
3	0.8494	0.03033	26.50982	0.8420	0.02561	23.22120
4	0.8487	0.03347	29.47628	0.8447	0.02792	27.03701
5	0.8624	0.03743	31.80677	0.8495	0.03334	29.48046
6	0.8578	0.04178	35.22510	0.8508	0.03539	31.25030
7	0.8674	0.04497	36.20834	0.8544	0.03966	33.49710
8	0.8637	0.04651	39.73963	0.8547	0.03951	34.48453
9	0.8846	0.07606	60.33328	0.8707	0.06766	56.10326
10	0.8920	0.07051	55.88569	0.8792	0.05917	48.63063
11	0.8895	0.07114	58.19944	0.8781	0.06141	52.68493
12	0.8866	0.07188	54.91918	0.8796	0.05879	47.46748
13	0.8992	0.07568	60.00274	0.8899	0.06413	53.51754
14	0.8923	0.07781	56.27480	0.8920	0.06409	49.78123
15	0.9114	0.08350	66.02770	0.8964	0.07223	59.65547
16	0.9112	0.08806	66.24109	0.9050	0.07617	60.17429
17	0.9297	0.09725	73.52125	0.9163	0.08429	66.55070
18	0.9322	0.09875	75.10280	0.9207	0.08553	68.01929
19	0.9323	0.10168	74.95218	0.9184	0.08760	67.39587
20	0.9239	0.10410	74.49612	0.9136	0.08776	65.55910
21	0.9239	0.10940	73.68442	0.9107	0.09121	63.94407
22	0.9585	0.11928	80.29514	0.9302	0.09447	65.29550
23	0.9472	0.12159	85.50841	0.9385	0.10793	77.98139
24	0.9550	0.12453	87.28661	0.9420	0.10578	76.85590
25	0.9831	0.13381	96.21108	0.9675	0.11728	87.60459
26	0.9656	0.13403	92.90154	0.9515	0.11628	83.41222
27	0.9663	0.14072	95.44541	0.9518	0.12209	84.88081
28	0.9842	0.15275	103.70462	0.9674	0.13141	91.30743
29	1.0338	0.16329	115.70015	1.0082	0.14561	106.49535
30	1.0088	0.17409	116.59134	0.9916	0.15057	103.42430
31	1.0242	0.18120	126.13505	1.0014	0.16464	115.39054
32	1.0386	0.21058	145.56554	1.0182	0.18557	128.44462
33	1.1040	0.23917	156.63222	1.0857	0.21283	142.32713
34	1.1508	0.27298	182.67762	1.1096	0.24603	167.17590
35	1.2536	0.28031	214.95718	1.2140	0.25748	200.62280
36	1.2414	0.28057	210.50122	1.2065	0.26801	209.39665
37	1.2543	0.34780	230.07816	1.2202	0.32188	214.25009
38	1.2959	0.40675	282.44510	1.2537	0.38307	284.04758
39	1.4223	0.45728	326.67835	1.3903	0.44199	315.85853

Table 3. C-B Bond descriptors computed with the NBO methods at the B3LYP/TZVP and M06/6-311G(d,p) levels for $\mathbf{X}^{\perp}$-BH_2^+ (**X** = **1**-**39**).

	B3LYP			M06		
X	C-B WBI	pop($^{\perp}p_{vac}^{B}$) (e)	$E^{\perp}_{del}$ (kJ/mol)	C-B WBI	pop($^{\perp}p_{vac}^{B}$) (e)	$E^{\perp}_{del}$ (kJ/mol)
1	0.8657	0.00762	11.01647	0.8724	0.00679	9.61483
2	0.8650	0.01712	13.86996	0.8674	0.01488	12.01226
3	0.9096	0.02398	26.01193	0.9040	0.01889	23.45132
4	0.8634	0.00993	11.80306	0.8676	0.00851	10.28846
5	0.9039	0.02939	33.41761	0.8947	0.02579	26.44706
6	0.8624	0.00936	11.91185	0.8642	0.00825	10.32193
7	0.9004	0.04207	43.85669	0.8914	0.03780	40.00741
8	0.8591	0.01554	16.90336	0.8596	0.01486	15.59377
9	0.8493	0.01107	13.86159	0.8405	0.00896	14.84065
10	0.8715	0.01158	14.27162	0.8696	0.00916	14.12100
11	0.8535	0.01126	14.01640	0.8482	0.00879	13.61055
12	0.8617	0.01169	11.39722	0.8689	0.00968	11.82398
13	0.8611	0.01054	12.38046	0.8623	0.00833	12.37209
14	0.8672	0.00634	8.39310	0.8790	0.00563	7.43915
15	0.8648	0.01206	15.71092	0.8570	0.00936	14.38878
16	0.8770	0.01255	16.69416	0.8783	0.01216	17.43054
17	0.8689	0.02779	22.17938	0.8689	0.02569	20.30495
18	0.8686	0.00905	11.79888	0.8682	0.00723	10.28427
19	0.8736	0.00979	12.48087	0.8718	0.00781	13.32604
20	0.8706	0.00763	9.73617	0.8743	0.00639	8.43076
21	0.8729	0.00828	10.20896	0.8769	0.00679	8.72364
22	0.9225	0.04279	40.51367	0.9180	0.03814	38.40075
23	0.8681	0.04906	33.49710	0.8713	0.05804	41.27098
24	0.8731	0.01664	18.24224	0.8789	0.01503	16.38873
25	0.8729	0.01092	13.62310	0.8727	0.00913	11.87838
26	0.8745	0.03328	29.78590	0.8798	0.02761	24.75254
27	0.8698	0.02089	21.50158	0.8741	0.01855	18.87402
28	0.8767	0.02100	22.37185	0.8810	0.01877	19.85308
29	0.8761	0.01492	18.48491	0.8653	0.01086	16.23810
30	0.8742	0.00907	11.25914	0.8806	0.00802	10.02486
31	0.8935	0.03215	26.63953	0.8855	0.04892	39.96975
32	0.8766	0.02261	20.64804	0.8817	0.02423	21.46392
33	0.8782	0.01160	13.82812	0.8862	0.00969	11.56039
34	0.8687	0.02235	21.52668	0.8546	0.01804	20.14596
35	0.8628	0.03368	40.03251	0.8522	0.03623	40.72706
36	0.8446	0.06873	70.07363	0.8326	0.06980	72.35391
37	0.8928	0.01977	27.22110	0.8819	0.01505	23.27978
38	0.8875	0.07144	68.72220	0.8722	0.07569	84.10677
39	0.9210	0.03455	37.13718	0.9163	0.07091	66.24109

Small negative values are obtained for **3**, **5** and **7** for which the "perpendicular" conformer is more stable than the planar one. The ΔWBI parameter, which accounts for both the interaction in $\mathbf{X}^{//}$-BH_2^+ and $\mathbf{X}^{\perp}$-BH_2^+ complexes, as is the case with ΔE_{rot}, leads as expected to an improved but still imperfect correlation (R^2 = 0.92, Figure 3-3 B).

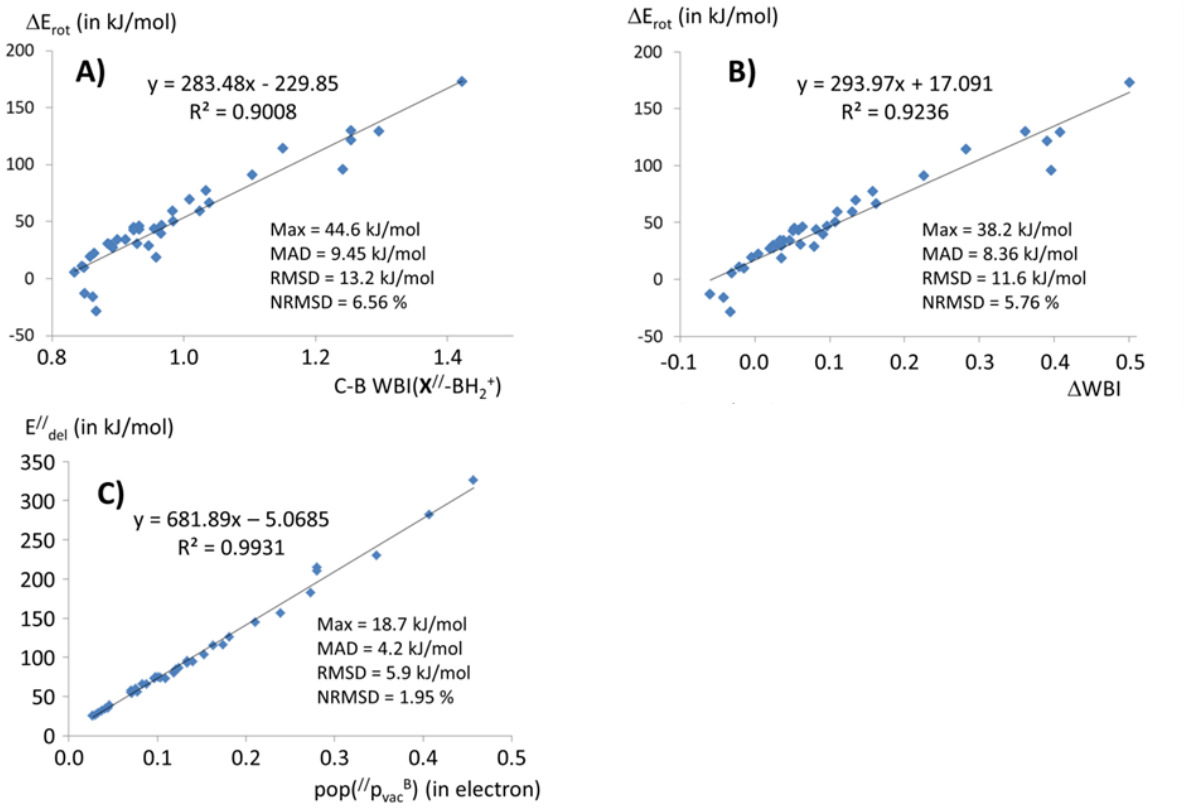

Figure 3-3: Correlation plots for **X**-BH_2^+ complexes computed at the B3LYP/TZVP level between various descriptors obtained with the NBO method.

WBI was originally designed as a quantitative measure of the electronic population occupying bonding molecular orbital.[12] Similarly, the electronic population of the p_{vac}^B orbital,[100, 118] noted as pop($^{//}p_{vac}^B$), is expected to measure the π-donation strength from **X** to BH_2^+ in $\mathbf{X}^{//}$-BH_2^+ complexes. Indeed, by construction, the p_{vac}^B orbital is utterly empty for the BH_2^+ fragment alone, whereas in the $\mathbf{X}^{//}$-BH_2^+ conformation, its population can only come from the π-type orbitals of the **X** moiety. Pop($^{//}p_{vac}^B$) values range from 0.027 to 0.457 electron (Table 2) again illustrating the diversity of π-donation properties of ligands **1**-**39**. The NBO6 program includes a module ($del option) that allows to remove specific electronic interactions and to measure their energy contribution. This allows to determine the energetic cost of deleting some vacant NBOs. This "deletion" energy, noted $E^{//}_{del}$, has been computed for the $\mathbf{X}^{//}$-BH_2^+

conformer by removing the p_{vac}^{B} orbital, thus cancelling any possibility of π-electronic donation from **X** to BH_2^+. In practice, this is done by deleting the Lewis vacant NBO orbital on boron (LV(B)) as well as any Rydberg orbital on B having the same spatial direction as LV(B) and subject to a significant increase in their electronic population when only LV(B) is deleted. It is noteworthy that pop($^{//}p_{vac}^{B}$) and $E^{//}_{del}$ correlate almost perfectly with each other (R^2 = 0.99, Figure 3-3 C, Table 2 and 3). These NBO electronic population and energetic parameters therefore measure the same chemical property. By construction of these descriptor, we assume that they measure the *intrinsic* strength of π-interaction. Even if they seem to reliably quantify the π-donation capability of the divalent C-donor ligand, showing as expected, a significantly higher π-donation for carbones compared to most NHCs, at this stage, it is not possible to guarantee that these NBO-based indicators are reference data for intrinsic π-bond strengths. This outstanding linear correlation is nevertheless expected to be restrained to bonds between two defined atoms, here boron and carbon atoms, and probably cannot be extended to all bonds. To a lesser extent, the WBI allows also a suitable quantification of the *intrinsic* π-bond, as very good correlation between the C-B bond WBI and either pop($^{//}p_{vac}^{B}$) or $E^{//}_{del}$ is observed (R^2> 0.975, Figure 3-4 A & B).

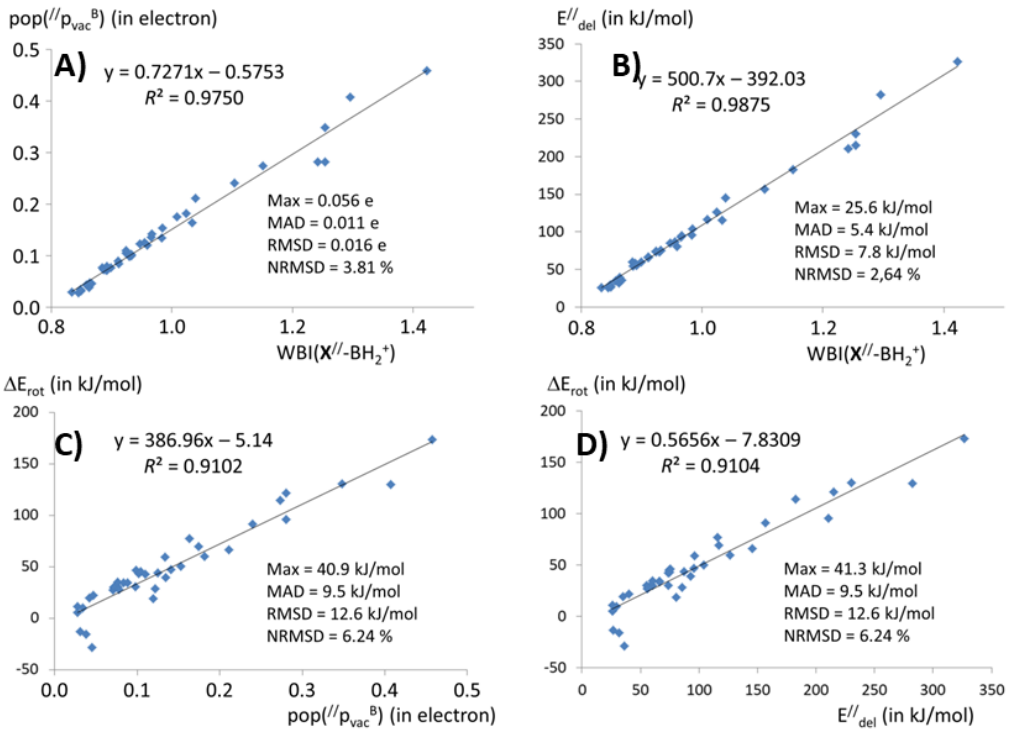

Figure 3-4: Correlation plots for $\mathbf{X}^{//}$-BH_2^+ complexes computed at the B3LYP/TZVP level between C-B bond WBI, pop($^{//}p_{vac}^{B}$), $E^{//}_{del}$ and ΔE_{rot}.

The above parameters calculated with the NBO method do not correlate satisfactorily with the previously calculated descriptors based on chemical insight. Indeed, an R^2 value of 0.91 is obtained when comparing ΔE_{rot} and pop($^{//}p_{vac}^{B}$) or $E^{//}_{del}$ (Figure 3-4 C & D). This reveals the conceptual difference between the *intrinsic* and the *relative* strength of the π-interaction. The latter, measured by ΔE_{rot}, results from the energy difference between the planar ($\mathbf{X}^{//}$-BH_2^+) and the perpendicular ($\mathbf{X}^{\perp}$-BH_2^+) conformations. To confirm this assumption, the $\mathbf{X}^{\perp}$-BH_2^+ conformers have been used to compute the pop($^{\perp}p_{vac}^{B}$) and $E^{\perp}_{del}$ values (Table 3). In the $\mathbf{X}^{\perp}$-BH_2^+ conformation, the p_{vac}^{B} orbital is coplanar with the **X** moiety and perpendicular to the B-C bond, inducing non-zero overlap between this p orbital and the σ backbone of **X**. The pop($^{\perp}p_{vac}^{B}$) values, which range between 0.006 and 0.071 electron, reveals weak in-plane π-type electronic donation from **X** to p_{vac}^{B}, in agreement with our previous assessment. The deletion of this p orbital leads to $E^{\perp}_{del}$ which nicely correlate with pop($^{\perp}p_{vac}^{B}$) (R^2 = 0.94, Figure 3-5 A). Assuming that the interactions between the B-H bonds and the σ-system of **X** in $\mathbf{X}^{//}$-BH_2^+ and those between the B-H bonds and the π-system of **X** in $\mathbf{X}^{\perp}$-BH_2^+ are weak (or similar), and that the B-C σ-bond strength is weakly affected by the rotation of the BH_2 group, ΔE_{rot} is expected to be equivalent to the difference between $E^{//}_{del}$ and $E^{\perp}_{del}$. This is nicely confirmed by the very good correlation obtained between ΔE_{rot} and ($E^{//}_{del} - E^{\perp}_{del}$) ($R^2$ = 0.97, Figure 3-5 D). The descriptors $\Delta E_{del} = E^{//}_{del} - E^{\perp}_{del}$ and $\Delta pop(p_{vac}^{B}) = pop(^{//}p_{vac}^{B}) - pop(^{\perp}p_{vac}^{B})$ are therefore reliable measures of the *relative* strength of the π-interaction, whose reference is ΔE_{rot}. So, it is no surprise that these parameters correlate well (R^2> 0.95) with each other (Figure 3-5 Band C). It should be noted that the absolute values of ΔE_{rot} and ΔE_{del} are different, the former being significantly lower than the latter. Features of the NBO approach, which allows only bonding interactions to be calculated and does not cover antibonding contributions,[119] explains the systematic overestimation of ΔE_{del}.

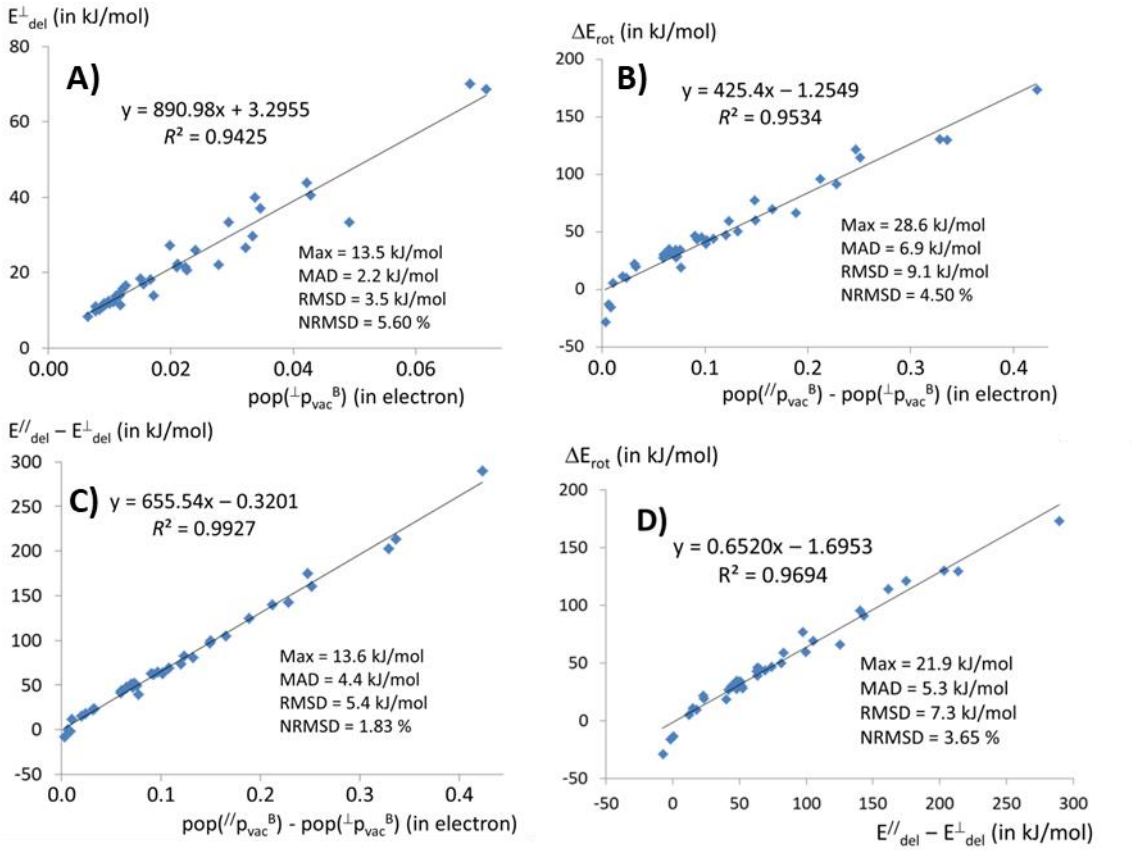

Figure 3-5: Correlation plots for $\mathbf{X}^{//}$-BH_2^+ and $\mathbf{X}^{\perp}$-BH_2^+ complexes computed at the B3LYP/TZVP level between $E^{\perp}_{del}$ and $pop(^{\perp}p_{vac}{}^{B})$, and between $\Delta pop(p_{vac}{}^{B})$, ΔE_{del} and ΔE_{rot}.

3.5. π-bonding descriptors based on the ETS-NOCV approach

The ETS-NOCV method allows to calculate the energy and to identify the nature of the different orbital interactions between two fragments in a molecule – in our case we split the **X**-BH_2^+ adduct into BH_2^+ and the divalent carbon compound. Diagonalization of the deformation density matrix due to bonding provides eigenvectors named natural orbitals for chemical valence (NOCVs). Pairs of NOCV, having opposite eigenvalues υ_i and $-\upsilon_i$ and for which an energy ΔE_i is associated, are obtained. They enable to visualize the deformation of the density associated with each interaction and to determine its nature. Therefore, the total orbital interaction between fragments is partitioned into several chemically interpretable interactions ($NOCV_i$) for which energy (ΔE_i) and charge transfer (υ_i) are quantified. NOCV analysis coupled with energy decomposition has been discussed in greater detail in Section 2B.9.5. The calculations were performed using ADF2017.[131-132]

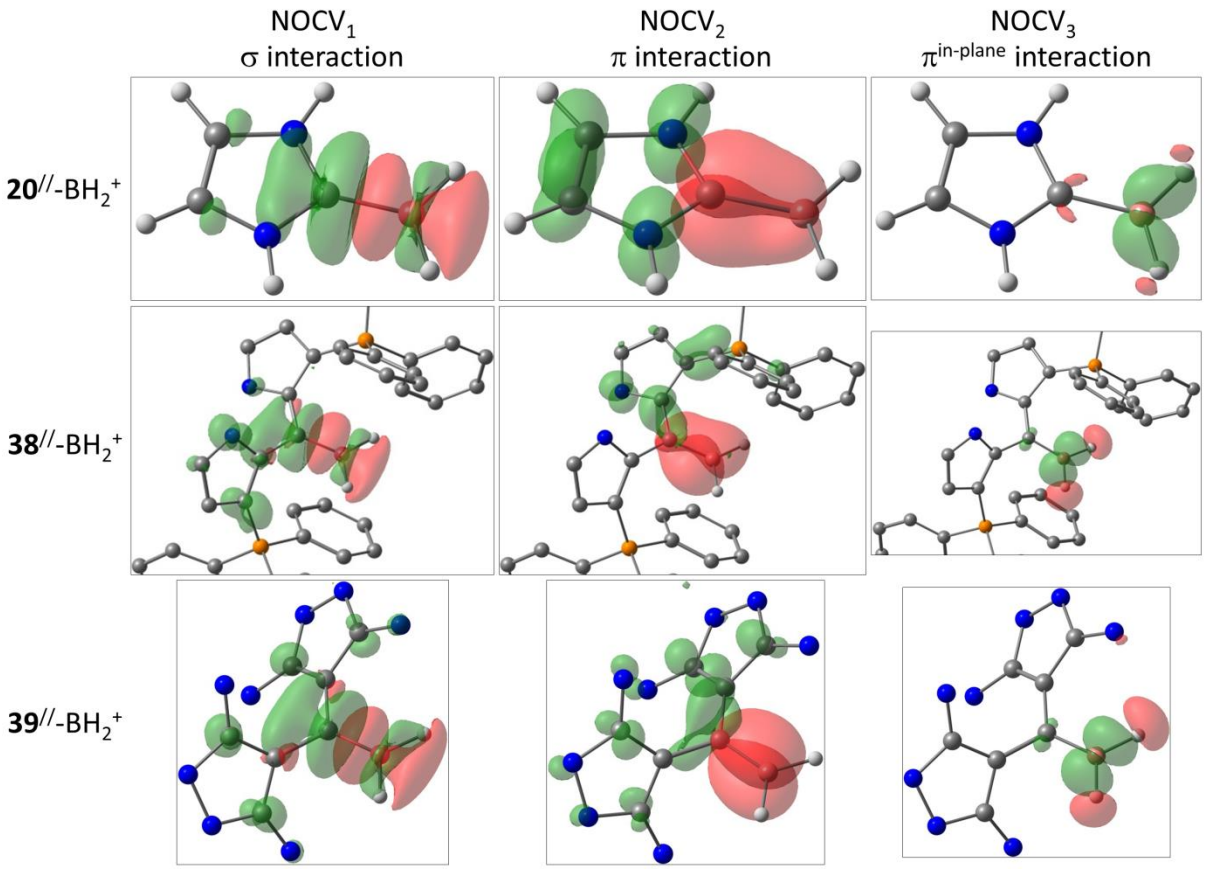

Figure 3-6: Deformation densities associated with the orbital interactions in **X**$^{//}$-BH_2^+ (**X** = **20**, **38** and **39**). The charge flow of the electronic density is green → red. For **X**=**38** and **39**, H atoms, except BH_2, have been omitted for clarity. Isosurface value: 0.003 a.u.

All **X**$^{//}$-BH_2^+ complexes showed similar features regarding the description of the bonding between C-donor and borenium within **X**$^{//}$-BH_2^+. Three main contributions accounting for about 90% of the total orbital interaction can be identified in the deformation density (Figure 3-6, Table 4). The first pair of NOCV, $NOCV_1$, is the strongest contribution. It corresponds to a σ-type interaction which can be described as the **X**→BH_2^+ σ-donation.

Table 4. ETS-NOCV results (energies in kJ/mol) for the C-B bond in $\mathbf{X}^{//}$-BH_2^+ (**X** = **1**-**39**) calculated at the B3LYP/TZ2P level after geometry optimization at the B3LYP/TZVP level.

					σ–interaction		π–interaction		$\pi^{\text{in-plane}}$ interaction	
X	ΔE_{int}	ΔE_{elstat}	ΔE_{Pauli}	ΔE_{orb}	υ_1	ΔE_1	υ_2	ΔE_2	υ_3	ΔE_3
1	-668.2	-625.5	648.7	-691.4	0.79450	-577.4	0.27435	-55.2	0.09236	-12.9
2	-598.3	-546.5	622.3	-674.1	0.75168	-534.3	0.33030	-66.9	0.10417	-16.0
3	-692.8	-647.1	654.0	-699.7	0.78106	-567.3	0.30547	-59.4	0.12817	-15.9
4	-695.6	-652.3	658.9	-702.3	0.77608	-567.1	0.31741	-66.5	0.06509	-14.5
5	-726.4	-656.4	676.6	-746.6	0.79600	-583.0	0.34212	-69.5	0.14250	-13.3
6	-732.2	-694.5	685.2	-722.8	0.77549	-575.4	0.34469	-73.2	0.10907	-13.8
7	-746.4	-671.3	686.2	-761.3	0.80120	-581.0	0.38734	-79.9	0.13696	-12.3
8	-742.9	-696.0	693.0	-739.9	0.78595	-585.3	0.34913	-74.8	0.11453	-13.8
9	-775.1	-650.5	690.7	-815.3	0.84977	-636.6	0.40690	-108.3	0.09739	-11.3
10	-754.8	-701.0	701.4	-755.2	0.77357	-579.3	0.42731	-105.6	0.10011	-13.6
11	-761.9	-695.7	699.5	-765.6	0.79090	-593.6	0.40012	-102.9	0.10535	-12.2
12	-647.3	-610.4	669.7	-706.7	0.73413	-537.3	0.43111	-102.7	0.09533	-17.6
13	-720.0	-672.2	695.3	-743.1	0.75655	-564.7	0.43214	-110.1	0.09806	-15.3
14	-652.5	-614.6	663.1	-701.1	0.72564	-527.5	0.46926	-108.6	0.08140	-19.1
15	-828.4	-751.6	724.8	-801.5	0.81245	-617.6	0.42265	-111.7	0.10584	-11.2
16	-685.7	-617.2	682.0	-750.6	0.74911	-551.5	0.50054	-127.9	0.10626	-18.4
17	-788.5	-698.1	716.9	-807.3	0.76994	-579.2	0.49091	-127.5	0.12018	-15.5
18	-796.6	-741.0	730.4	-786.0	0.77049	-587.1	0.47829	-127.4	0.09899	-15.3
19	-813.6	-736.9	731.2	-807.9	0.76694	-584.1	0.54599	-143.5	0.10034	-14.2
20	-715.8	-676.2	709.4	-749.0	0.73779	-552.4	0.50977	-128.9	0.09003	-16.6
21	-717.7	-657.4	706.7	-766.9	0.73827	-550.9	0.57928	-142.0	0.08933	-15.6
22	-800.8	-675.5	698.4	-823.7	0.78756	-585.4	0.57196	-149.7	0.13357	-10.2
23	-770.5	-683.1	719.9	-807.3	0.75105	-558.2	0.56586	-146.9	0.12576	-15.9
24	-759.6	-697.0	738.2	-800.9	0.75601	-573.2	0.55874	-147.1	0.09730	-15.7
25	-832.9	-750.2	757.1	-839.8	0.77219	-593.5	0.57896	-159.3	0.10162	-16.7
26	-786.3	-706.8	751.3	-830.8	0.76556	-582.6	0.56561	-151.7	0.09657	-17.7
27	-731.6	-636.0	726.2	-821.8	0.76189	-572.6	0.59789	-159.9	-0.09384	-18.1
28	-794.7	-719.1	757.8	-833.3	0.75639	-576.6	0.61251	-166.3	0.09478	-17.9
29	-902.5	-808.5	820.2	-914.3	0.82866	-657.2	0.57441	-170.1	0.11078	-15.7
30	-766.0	-683.4	749.2	-831.8	0.73668	-560.6	0.68750	-192.8	0.08362	-17.4
31	-946.9	-847.0	822.3	-922.2	0.79250	-625.6	0.64238	-184.9	0.13759	-14.2
32	-822.1	-716.1	774.5	-880.5	0.75231	-578.0	0.70683	-207.7	0.09208	-15.8
33	-816.4	-691.0	784.0	-909.5	0.73833	-568.8	0.82096	-254.3	0.07799	-18.8
34	-963.7	-777.2	840.8	-1027.2	0.88225	-698.8	0.68723	-227.7	0.09413	-14.8
35	-959.5	-713.1	816.0	-1062.4	0.90648	-721.0	0.60790	-217.4	0.15754	-14.0
36	-968.2	-659.6	796.3	-1104.9	0.93721	-731.8	0.61061	-214.8	0.16247	-10.4
37	-1171.6	-961.5	912.8	-1122.9	0.91158	-743.1	0.78328	-275.5	0.09858	-17.5
38	-1167.7	-810.5	880.0	-1237.2	0.94150	-699.4	0.97701	-402.3	0.08164	-16.1
39	-1195.3	-913.1	947.4	-1229.6	0.96032	-780.4	0.85000	-334.2	0.20093	-20.6

Table 5. ETS-NOCV results (energies in kJ/mol) for the C-H bond in **X**-H^+ (**X** = **1**-**39**) calculated at the B3LYP/TZ2P level after geometry optimization at the B3LYP/TZVP level.[h]

				σ–interaction		π–interaction		$\pi^{\text{in-plane}}$ interaction	
X	ΔE_{int}	ΔE_{elstat}	ΔE_{orb}	υ_1	ΔE_1	υ_2	ΔE_2	υ_3	ΔE_3
1	-1093.1	-279.7	-813.4	0.72348	-707.4	0.20381	-51.0	0.09766	-23.4
2	-1020.3	-214.9	-805.3	0.68296	-661.9	0.26026	-66.1	0.11776	-21.4
3	-1115.4	-306.0	-809.4	0.70123	-680.6	0.22008	-53.2	0.13546	-35.0
4	-1111.7	-305.6	-806.1	0.70032	-680.7	0.22879	-59.1	0.11055	-26.6
5	-1152.4	-308.7	-843.8	0.71055	-691.1	0.23467	-58.0	0.13692	-35.0
6	-1150.2	-335.2	-815.0	0.69448	-680.5	0.23992	-61.5	0.11418	-26.3
7	-1178.8	-318.3	-860.5	0.71701	-694.7	0.25486	-63.1	0.13067	-33.1
8	-1163.2	-329.6	-833.6	0.70691	-694.4	0.23558	-60.6	0.11664	-26.5
9	-1164.8	-276.0	-888.8	0.78806	-761.0	0.23321	-67.4	0.09841	-23.9
10	-1149.1	-329.9	-819.2	0.69841	-680.0	0.27916	-76.8	0.10406	-25.7
11	-1149.1	-323.4	-825.7	0.71682	-696.2	0.24937	-70.8	0.10622	-26.6
12	-1036.3	-253.0	-783.3	0.66999	-647.5	0.27550	-74.7	0.10823	-24.8
13	-1106.1	-303.1	-803.0	0.68506	-664.9	0.27754	-78.7	0.10327	-25.7
14	-1046.1	-264.6	-781.5	0.66819	-645.0	0.30222	-78.5	0.10093	-22.2
15	-1214.6	-368.0	-846.6	0.73428	-714.3	0.25077	-72.1	0.10378	-26.4
16	-1069.3	-251.9	-817.3	0.68674	-663.1	0.31742	-87.8	0.12430	-31.6
17	-1174.9	-315.8	-859.1	0.69365	-674.3	0.30927	-86.4	0.11530	-24.5
18	-1177.5	-356.2	-821.3	0.69530	-677.7	0.29413	-83.9	0.10267	-25.3
19	-1197.9	-353.1	-844.8	0.68793	-670.7	0.36934	-101.9	0.10248	-26.2
20	-1097.3	-301.4	-795.9	0.67057	-651.3	0.30921	-84.7	0.10173	-23.9
21	-1103.2	-285.5	-817.7	0.66986	-649.6	0.37047	-98.1	0.10103	-24.9
22	-1166.8	-311.9	-854.9	0.72142	-683.6	0.32656	-91.1	0.13433	-36.1
23	-1155.9	-298.5	-857.4	0.68285	-662.2	0.33950	-94.1	0.12660	-16.2
24	-1136.8	-306.5	-830.3	0.68503	-667.2	0.31555	-88.6	0.09959	-23.6
25	-1200.3	-351.8	-848.4	0.69449	-676.3	0.34409	-96.8	0.10300	-25.8
26	-1163.5	-312.7	-850.8	0.69131	-674.2	0.31178	-88.2	0.10022	-22.8
27	-1102.8	-252.5	-850.3	0.69995	-678.1	0.32620	-90.8	0.10372	-23.8
28	-1164.5	-322.8	-841.7	0.68533	-667.3	0.33419	-93.4	0.10163	-24.0
29	-1241.0	-372.8	-868.2	0.73587	-716.7	0.28322	-85.3	0.10466	-26.3
30	-1122.5	-289.5	-833.0	0.67275	-652.3	0.39482	-110.8	0.09463	-22.7
31	-1309.6	-417.3	-892.3	0.70829	-692.0	0.35069	-97.8	0.12889	-20.0
32	-1162.7	-305.6	-857.1	0.68846	-667.0	0.36278	-102.7	0.09883	-23.0
33	-1146.8	-282.4	-864.4	0.67623	-654.7	0.45259	-134.8	0.08668	-21.4
34	-1271.5	-345.5	-926.0	0.78445	-759.5	0.28110	-84.6	0.08673	-21.7
35	-1236.3	-266.4	-969.9	0.84980	-810.9	0.21922	-65.8	0.12611	-33.4
36	-1258.8	-220.4	-1038.5	0.88505	-838.5	0.22515	-65.3	0.12793	-31.5
37	-1455.2	-515.8	-939.4	0.77139	-759.3	0.35766	-105.3	0.08752	-22.4
38	-1435.7	-390.2	-1045.5	0.83473	-811.8	0.39123	-99.8	0.07935	-18.9
39	-1423.0	-425.1	-997.9	0.83627	-806.6	0.41739	-117.8	0.07857	-19.5

[h] $\Delta E_{Pauli} = 0$ for all complexes.

Table 6. ETS-NOCV results (energies in kJ/mol) for the C-B bond in $\mathbf{X}^{\perp}$-BH_2^+ (**X** = **1**-**39**) calculated at the B3LYP/TZ2P level after geometry optimization at the B3LYP/TZVP level.

					σ–interaction		π–interaction		$\pi^{\text{in-plane}}$ interaction	
X	ΔE_{int}	ΔE_{elstat}	ΔE_{Pauli}	ΔE_{orb}	υ_1	ΔE_1	υ_2	ΔE_2	υ_3	ΔE_3
1	-662.1	-618.2	660.8	-704.7	0.80333	-594.5	0.26161	-39.7	0.13996	-26.3
2	-592.1	-533.5	618.6	-677.2	0.75915	-540.7	0.30451	-51.1	0.19909	-31.8
3	-708.1	-672.5	707.8	-743.3	0.78331	-591.7	0.31084	-49.6	0.23487	-49.0
4	-686.8	-646.2	664.2	-704.8	0.78301	-576.8	0.27288	-46.7	0.16851	-31.8
5	-738.1	-677.7	722.6	-783.0	0.80009	-607.7	0.31032	-53.9	0.23605	-46.1
6	-713.1	-675.5	676.9	-714.5	0.78598	-583.2	0.26834	-46.5	0.16440	-30.6
7	-764.5	-693.5	735.8	-806.8	0.81110	-614.6	0.31239	-53.0	0.24395	-50.1
8	-719.7	-669.1	678.2	-728.8	0.79814	-592.8	0.25914	-44.5	0.17501	-31.3
9	-745.3	-624.0	659.8	-781.1	0.86257	-638.0	0.25361	-54.7	0.18273	-36.0
10	-728.8	-674.9	672.8	-726.7	0.78580	-581.6	0.30170	-60.4	0.17702	-34.9
11	-731.6	-668.4	667.6	-730.8	0.79997	-590.9	0.26461	-56.3	0.17853	-36.8
12	-617.8	-581.1	634.7	-671.4	0.74881	-538.1	0.29893	-57.4	0.17555	-30.7
13	-686.4	-639.1	653.6	-700.9	0.76905	-561.4	0.29295	-60.6	0.17095	-33.0
14	-630.6	-589.3	622.9	-664.1	0.74787	-533.4	0.32528	-61.0	0.13981	-24.2
15	-795.9	-723.0	688.2	-761.1	0.82273	-614.9	0.26500	-58.2	0.18290	-38.2
16	-650.9	-587.4	644.8	-708.3	0.76567	-553.3	0.33110	-67.3	0.19866	-40.6
17	-759.3	-664.9	671.2	-765.7	0.78412	-578.6	0.31263	-67.7	0.21702	-33.3
18	-754.0	-700.3	673.8	-727.5	0.78655	-582.1	0.30199	-65.0	0.16630	-32.4
19	-775.1	-701.2	679.1	-753.0	0.78423	-582.9	0.36631	-78.0	0.17185	-33.7
20	-672.9	-635.2	651.1	-688.8	0.75763	-550.4	0.31748	-64.1	0.15395	-28.4
21	-678.9	-621.6	651.2	-708.4	0.75940	-552.2	0.36514	-73.7	0.15709	-29.3
22	-775.0	-661.2	680.2	-794.0	0.79593	-591.5	0.34021	-76.4	0.27862	-65.6
23	-739.8	-634.9	659.4	-764.2	0.77127	-561.7	0.33201	-69.4	0.25926	-36.6
24	-709.1	-648.6	673.5	-734.0	0.78039	-574.5	0.31860	-66.7	0.15822	-28.3
25	-774.2	-698.4	681.0	-756.8	0.79174	-587.1	0.33993	-73.7	0.17077	-33.0
26	-736.4	-656.8	685.6	-765.1	0.78909	-585.1	0.31023	-66.0	0.19303	-31.5
27	-674.8	-587.9	654.2	-741.1	0.78740	-573.5	0.32413	-68.5	0.16569	-29.0
28	-735.2	-667.6	682.2	-749.8	0.78371	-579.2	0.32987	-69.8	0.16608	-29.6
29	-817.5	-733.9	720.2	-803.9	0.83875	-638.7	0.29775	-68.8	0.19052	-39.1
30	-695.4	-625.2	652.9	-723.2	0.76453	-555.5	0.38196	-81.8	0.15102	-27.6
31	-888.1	-789.9	738.0	-836.3	0.81469	-620.8	0.36023	-76.8	0.23440	-40.6
32	-738.2	-647.3	673.4	-764.3	0.78398	-577.0	0.35414	-77.2	0.17956	-30.2
33	-718.3	-620.4	658.1	-756.0	0.77269	-563.1	0.43203	-98.6	0.14625	-26.5
34	-837.2	-696.3	722.0	-862.9	0.90296	-678.7	0.33362	-71.2	0.16688	-31.7
35	-819.8	-599.0	675.6	-896.4	0.92708	-683.8	0.34615	-61.5	0.25545	-61.9
36	-856.2	-563.6	656.5	-949.1	0.94658	-683.4	0.34630	-55.4	0.30036	-67.9
37	-1029.1	-908.0	815.0	-936.1	0.91268	-723.2	0.43142	-92.4	0.18355	-38.3
38	-1006.2	-743.6	766.1	-1028.7	0.98183	-738.5	0.52346	-108.9	0.28378	-43.3
39	-1024.4	-815.1	817.8	-1027.1	0.99851	-774.2	0.54924	-119.4	0.24908	-37.4

The second deformation density $NOCV_2$ displays a π-type interaction: the π charge flow from the C-donor ligand to the vacant p orbital of the boron atom, p_{vac}^{B}, suggests that it corresponds to the π-donation. The third contribution $NOCV_3$ corresponds to a π-type interaction located in the Y_2C-BH_2 plane.

Surprisingly, neither the flow of electron density associated with the π-donation, $\Delta q^{//}_{\pi} = \upsilon^{//}_{2}$, nor the energy associated with the π-donation interaction, $\Delta E^{//}_{\pi} = \Delta E^{//}_{2}$, provide a very good correlation with pop($^{//}p_{vac}^{B}$) or $E^{//}_{del}$, respectively (Figures 3-7A and B). Do these non-perfect correlations illustrate a disagreement between the NBO and ETS-NOCV methods?

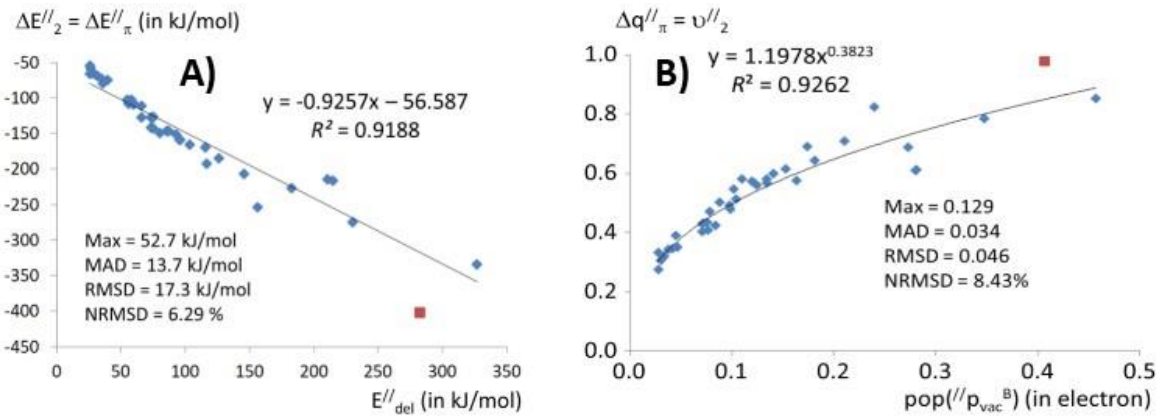

Figure 3-7. Correlation plots for **X**$^{//}$-BH_2^+ complexes between various descriptors obtained with the NBO and ETS-NOCV methods. The brown square corresponds to **X** = **38** and is not included in the trendlines. Power function has been selected as it provides the largest R^2 value for the pop($^{//}p_{vac}^{B}$) vs. $\Delta q^{//}_{\pi}$ correlation.

It should be noted that the π-type interaction corresponding to the second deformation density has been shown to include not only the contribution of the π-donation but also the π-polarization of the C-donor fragment, i.e. the reorganization of π-electron density inside **X** due to the formation of the σ-bond.[99] Thus, the previous non-satisfactory correlations could also be explained by a misinterpretation of the ETS-NOCV results. To investigate this hypothesis, the ETS-NOCV π-donation energy ($\Delta E^{//}_{\pi}$) calculated for **X**$^{//}$-BH_2^+ complexes has been adjusted. The corrected ETS-NOCV π-donation energy ($\Delta E^{//}_{\pi\ corr}$) is obtained by deduction of the π-contribution calculated by the same approach for **X**-H^+ complexes from $\Delta E^{//}_{\pi}$ (Table 5 and Figure 3-8).[99]

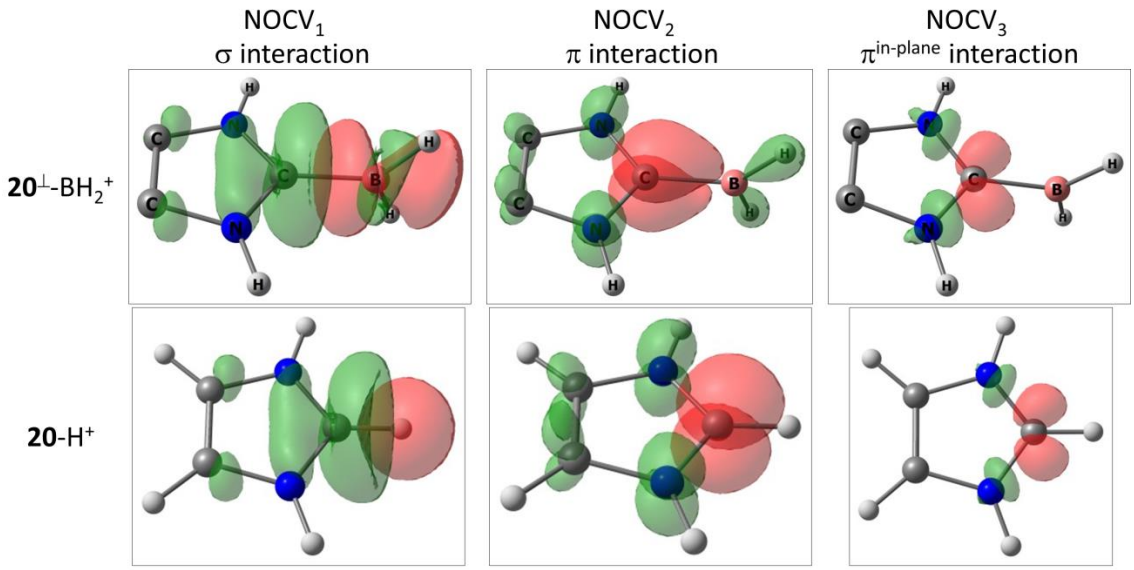

Figure 3-8. Deformation densities associated with the orbital interactions in **20**$^{\perp}$-BH_2^+ and **20**-H^+. The charge flow of the electronic density is green → red. Isosurface value: 0.003 a.u.

Gratifyingly, a much better linear correlation is obtained between $\Delta E^{//}{}_{\pi\ corr}$ and $E^{//}{}_{del}$. The only outlier is the **38**$^{//}$-BH_2^+ complex and by excluding this complex the correlation is excellent (R^2 = 0.99, Figure 3-9A), which validates the hypothesis and demonstrates that the intrinsic strength of the π-interaction can also be calculated by the ETS-NOCV method provided that the polarization of the fragments has been taken into account. Similarly, a strong quadratic correlation is obtained between pop($^{//}p_{vac}{}^{B}$) and $\Delta q^{//}{}_{\pi\ corr} = \upsilon^{//}{}_2 - \upsilon_2$(**X**-$H^+$) ($R^2$ = 0.99, Figure 3-9B). However, the non-linearity of the correlation remains to be explained. From a chemical point of view, these results confirm the π-donation capability scale of the divalent C-donor ligands calculated with the NBO method.

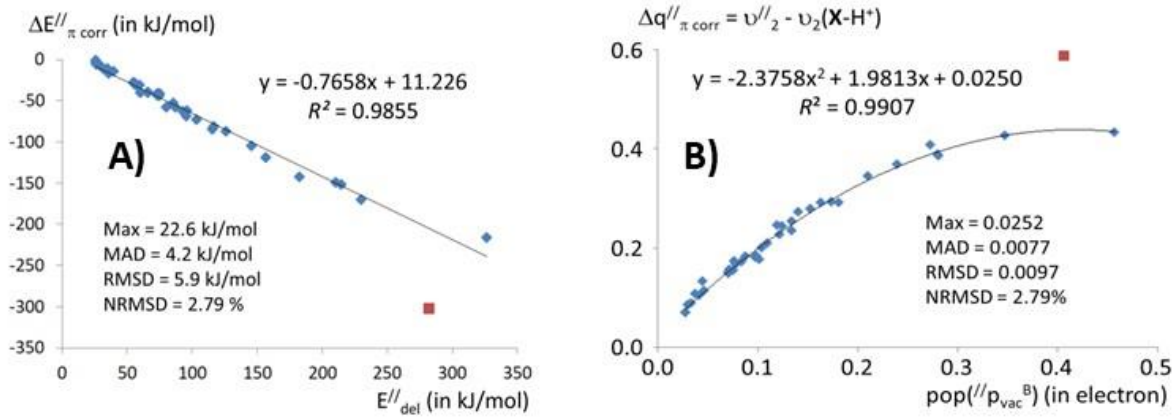

Figure 3-9: Correlation plots for **X**-BH_2^+ complexes between various descriptors obtained with the NBO and ETS-NOCV methods after applying correction for polarisation. The brown square corresponds to **X** = **38** and is not included in the trendlines. Quadratic function has been selected as it provides the largest R^2 value for the pop($^{//}p_{vac}{}^{B}$) vs. $\Delta q^{//}{}_{\pi\ corr}$ correlations

Analysis of deformation densities enables to explain the discrepancy observed for complex **38**$^{//}$-BH_2^+ with the ETS-NOCV method. With respect to the bisector plane of the **X**$^{//}$-BH_2^+ complexes, which is perpendicular to the complex plane and goes through the B-C axis, the deformation densities corresponding to the σ- and π-interactions (Figure 3-6) are symmetrical, in the sense that they involve both moieties of the C-donor ligand in an equivalent manner. This characteristic is observed for all complexes, except **38**$^{//}$-BH_2^+ for which the charge depletion of one moiety of **38** is observed only for $NOCV_1$, whereas the other part is involved only in $NOCV_2$ (Figure 3-6). Moreover, with respect to the plane defined by the C-BH_2 moiety, the inflow part of the deformation density in $NOCV_2$ for **38**$^{//}$-BH_2^+ is not perfectly symmetrical, contrary to what is observed for all other complexes. These visualizations suggest that $NOCV_1$ and $NOCV_2$ do not fit exactly with purely σ- and π-interactions, respectively, but that σ- and π-interactions are partly combined in these two NOCVs. Thus, the σ-interaction in **38**$^{//}$-BH_2^+ would be underestimated, while the π-interaction would be overestimated, explaining its outlier behavior.

The same polarization correction approach can be used to estimate the *relative* strength of the π-interaction through the ETS-NOCV method. To that end, the ETS-NOCV $\pi^{\text{in-plane}}$-donation energy ($\Delta E^{\perp}_{\pi\ \text{in-plane}}$) has been calculated for **X**$^{\perp}$-BH_2^+ complexes. Without correction of the polarization, $E^{//}_{del} - E^{\perp}_{del}$ and ΔE_{rot} correlates modestly with $\Delta E^{//}_{\pi} - \Delta E^{\perp}_{\pi\ \text{in-plane}}$ (R^2 = 0.91 and 0.87 respectively, Figure 3-10A and C). The correlation is improved significantly by applying a polarization correcting on both $\Delta E^{//}_{\pi}$ and $\Delta E^{\perp}_{\pi\ \text{in-plane}}$ (R^2 = 0.97 and 0.94, Figure 3-10 B and D).

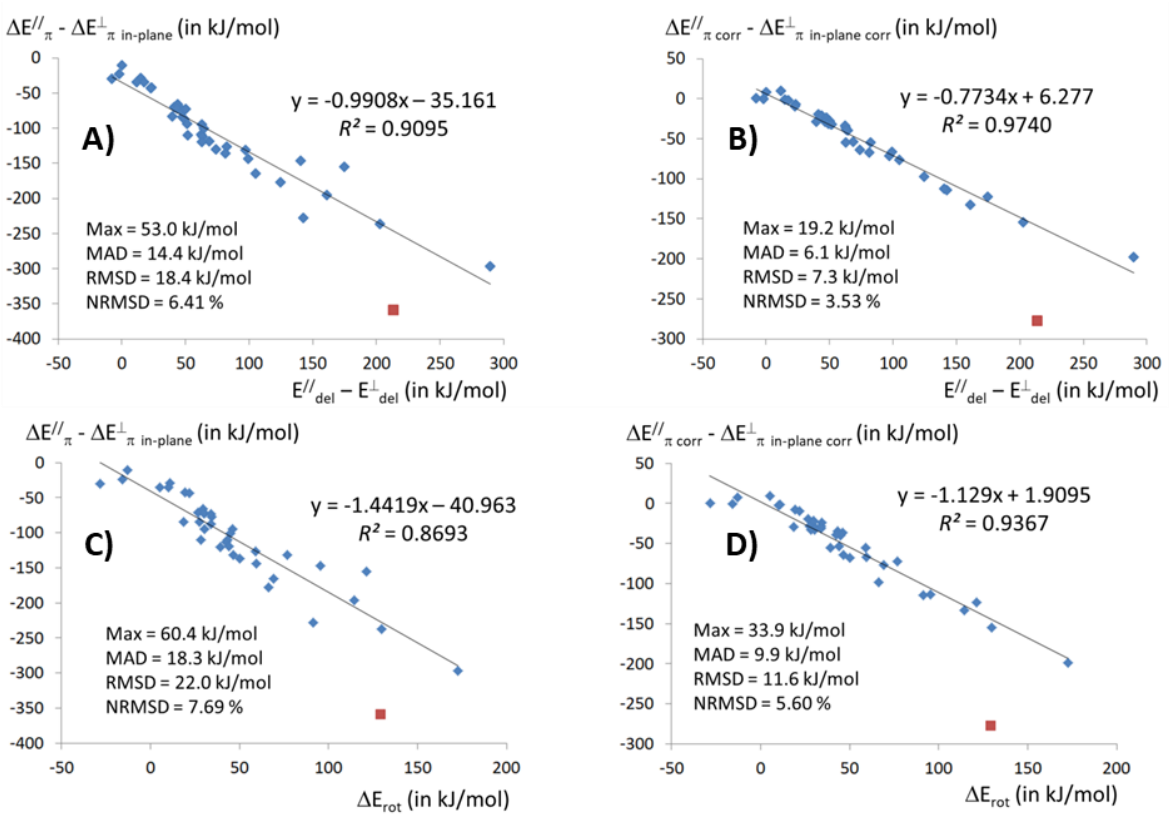

Figure 3-10: Correlation plots for **X**-BH_2^+ complexes between various descriptors obtained with the DFT, NBO and ETS-NOCV methods, where the brown square corresponds to **X** = **38** and is not included in the trendlines.

3.6. π-bonding descriptors based on the QTAIM approach

As elaborated in Section 2B.9.6, the QTAIM method provides a partition of the molecular space into atomic basins. To illustrate it, the molecular graph and the electronic density contour map in the molecular plane of **33**$^{//}$-BH_2^+ is depicted in Figure 3-11A. Calculations were performed using Multiwfn.[133]

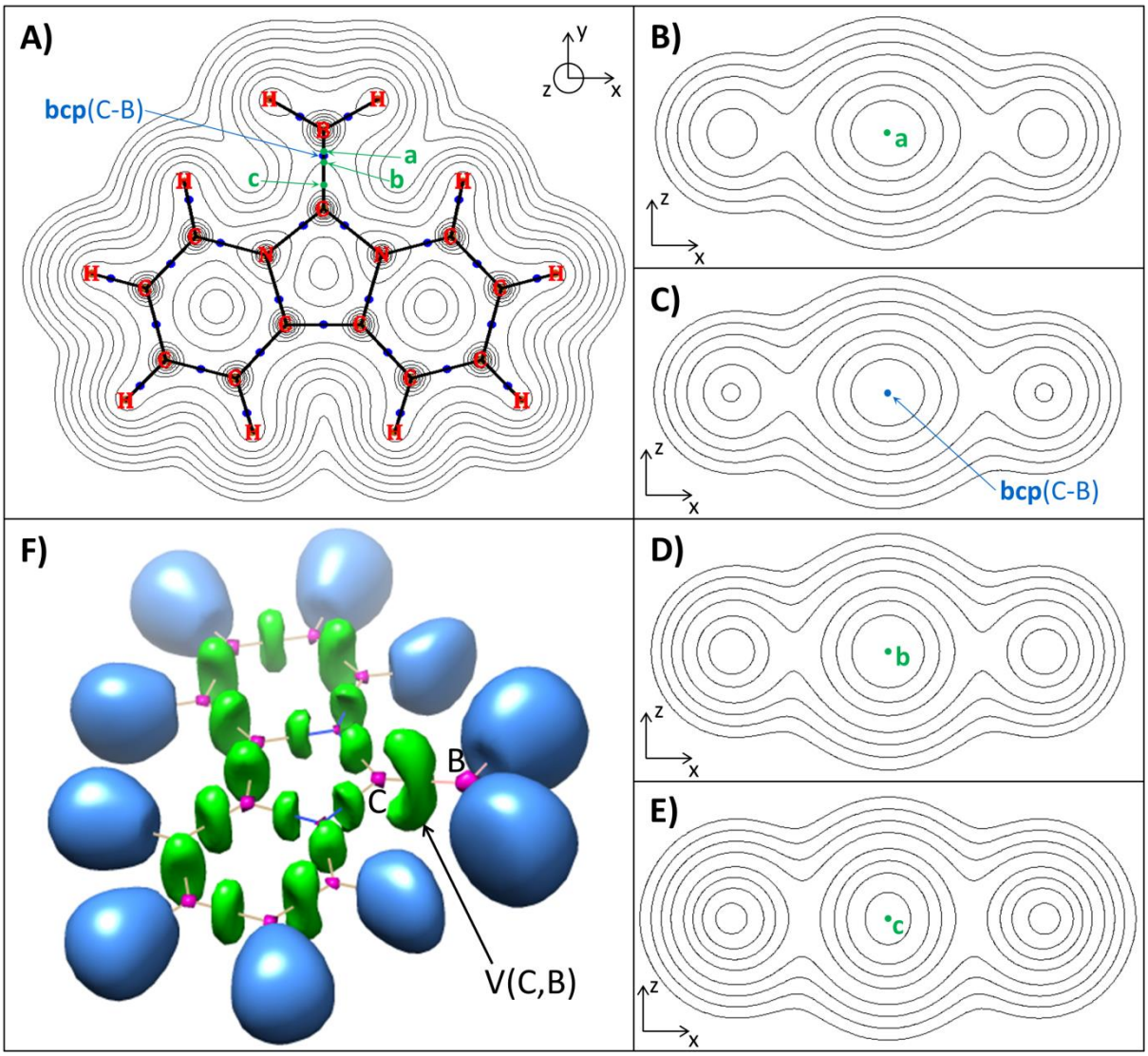

Figure 3-11: QTAIM molecular graph (blue points and bold black lines represent bond critical points and bond paths, respectively. The bcp of the C-B bond path is highlighted) and contour map of ρ in the molecular plan of **33**$^{//}$-BH_2^+ (A); contour map of ρ of **33**$^{//}$-BH_2^+ in a xz plane containing the point a corresponding to the largest negative ε_{corr} value along the C-B bond path (B), the carbon-boron bcp (C), the point b of the C-B bond path defined by $\varepsilon_{corr}(b) = 0$ (D) and the point c corresponding to the largest positive ε_{corr} value along the C-B bond path (E) (see Figure **3-15** for the variation of ε_{corr} along the C-B bond path for **33**$^{//}$-BH_2^+); isosurface (0.80) ELF representation for **33**$^{//}$-BH_2^+ (color code: magenta = core, green = disynaptic valence, light blue = protonated disynaptic).

This method affords the possibility of estimating the π-bond strength using different descriptors, which can be either local or global. Local chemical indices include the charge density ρ and the ellipticity ε derived from characteristics of the density at the bond critical point (bcp), and the Delocalization Index (DI) corresponds to the global index. It is well known that ρ_{bcp} and DI can be used to estimate the bond order.[120-122] More precisely, a logarithmic relationship was proposed between ρ_{bcp} and the bond order estimated by DI:[121] DI =

exp[A(ρ_{bcp} – B)]. At the B3LYP/TZVP level of calculation, the data points for the C-B bond in the 39 **X**$^{//}$-BH_2^+ complexes fit reasonably well to this equation with A = 10.4644, B = 0.1725 and R^2 = 0.92. A quadratic regression slightly improves the correlation with R^2 = 0.94 (Figure 3-12 A and B. Comparison between indices $\rho^{//}_{bcp}$ or DI$^{//}$ and those previously calculated clearly shows that the delocalization index provides more valuable information. This is reflected in a good linear correlation between DI$^{//}$ and $E^{//}_{del}$(R^2 = 0.94, Figure 3-12 C). Other measures of the *intrinsic* strength of the π-interaction, such as pop($^{//}p_{vac}^{B}$) and $\Delta E^{//}_{\pi\ corr}$ give similar correlation with respect to DI$^{//}$ (respectively R^2 = 0.95 and 0.94 excluding **38**$^{//}$-BH_2^+, Figure 3-12 E and F). Conversely, other indicators, such as $d_{C\text{-}B}$, $\Delta E^{//}_{\pi}$ or ΔE_{rot} for which a lower performance for estimating the *intrinsic* strength of the π-interaction has been shown above, give lower correlations (R^2 = 0.88, 0.92 and 0.92, respectively, not displayed). Similarly, ΔDI, calculated as the difference between the delocalization indexes DI$^{//}$ and DI$^{\perp}$ computed respectively for **X**$^{//}$-BH_2^+ and **X**$^{\perp}$-BH_2^+, turns out to be a good measure of the *relative* strength of the π-interaction, as revealed by the good correlation between ΔDI and ΔE_{rot} (R^2 = 0.96, Figure 3-12 D).

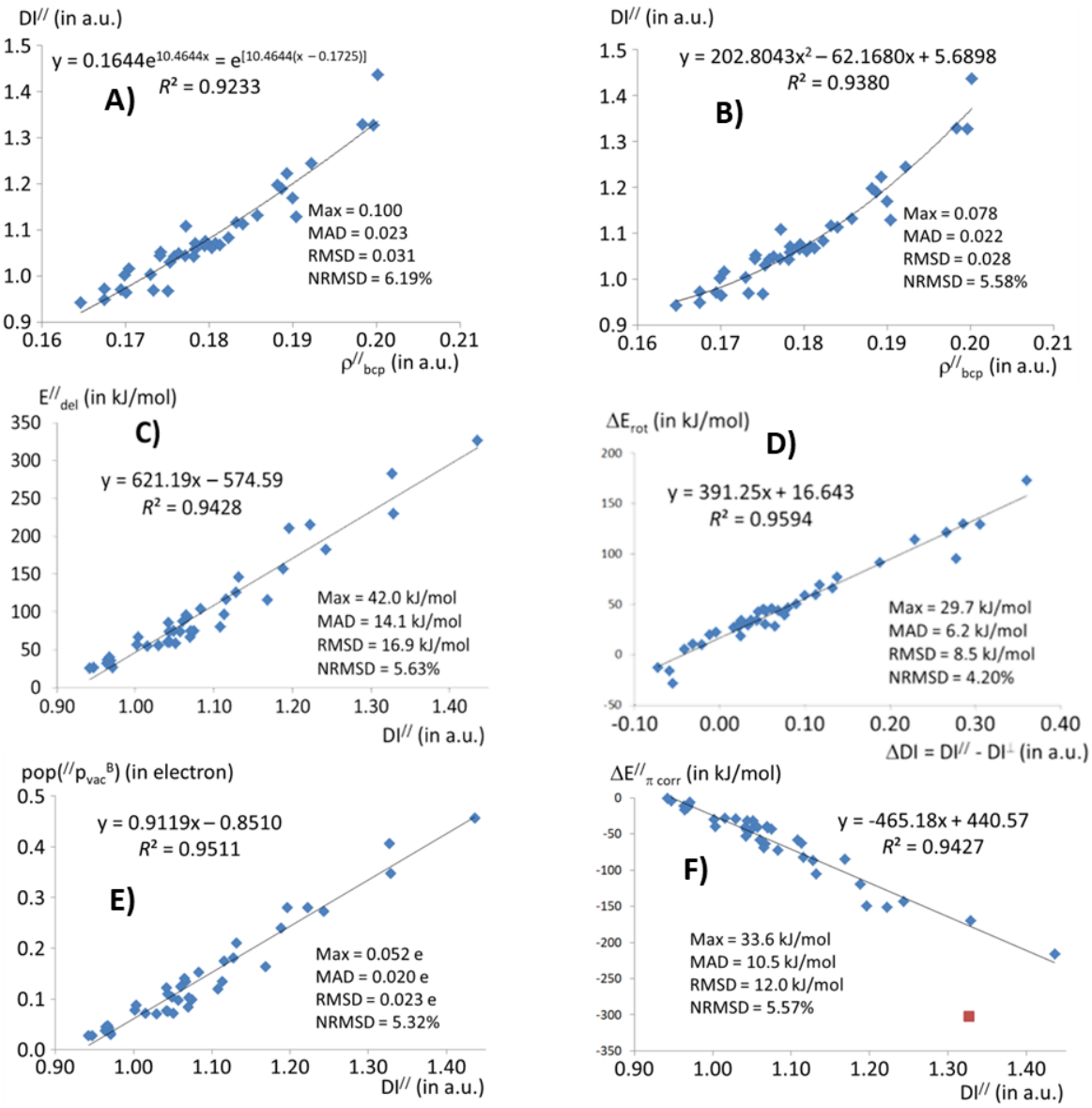

Figure 3-12: Correlation plots for **X**-BH_2^+ complexes between various descriptors obtained with the DFT, NBO, QTAIM and ETS-NOCV methods.

The ellipticity of the electron density at the bond critical points, ε_{bcp}, is a parameter computed in the framework of the AIM analysis.[123] This parameter provides a quantitative measurement of the anisotropy of the electron density at the bcp. This measure of the deviation of the charge distribution of the bond from axial symmetry is provided by the ratio between the two negative curvatures λ_1 and λ_2 of ρ at the bond critical point: $\varepsilon_{bcp} = \lambda_1 / \lambda_2 - 1$ (with $|\lambda_1| > |\lambda_2|$). Therefore, the ellipticity has been logically associated with the π character of bonds. For a single bond, $\varepsilon_{bcp} = 0$ because $\lambda_1 = \lambda_2$. For double bonds, the decrease of the density in the direction of the π-system should be smaller than that in the σ-plane of the bond. Consequently, the π-direction defines the λ_2 curvature which leads to $\varepsilon_{bcp} > 0$, ε_{bcp} being at

maximum for bonds of order 2. On this basis, it seems satisfactory to obtain a significant linear correlation between ε_{bcp} and $E^{//}_{del}$ (R^2 = 0.92, Figure 3-13). This trend is however highly surprising because an ellipticity close to zero is obtained for molecules which possess a large π-interaction whereas molecules with low $E^{//}_{del}$ values show large ε_{bcp} values.

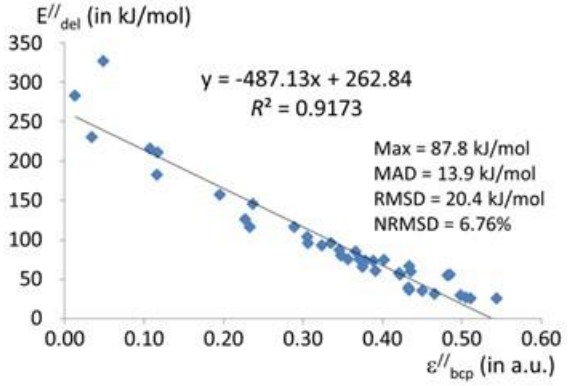

Figure 3-13: Correlation plots for **X**-BH_2^+ complexes between $E^{//}_{del}$ and ε_{bcp}

In order to explain this unexpected result, we focus our study on three representative cases: **1**$^{//}$-BH_2^+, **21**$^{//}$-BH_2^+ and **37**$^{//}$-BH_2^+, which show small, medium and large π-interaction respectively. The calculation for these complexes of the ellipticity $\varepsilon(d) = \lambda_1(d) / \lambda_2(d) - 1$ (with $|\lambda_1(d)| > |\lambda_2(d)|$) along the C-B bond, at the distance d from the C atom, reveals two maxima around d = 0.4 and 1.1 Å separated by a minimum value close to zero and located near the middle of the C-B bond (Figure 3-14 A, B and C). A similar result is obtained for the planar conformation of CH_2-BH_2^+ which possesses a pure σ-CB bond as its π-system is empty (Figure 3-14 D). On the other hand, this result differs strongly from what is obtained for the CC double bond in CH_2=CH_2 or the CB double bond in CH_2=BH_2^-, for which a single maximum is calculated along the bond (Figure 3-14 E and F).

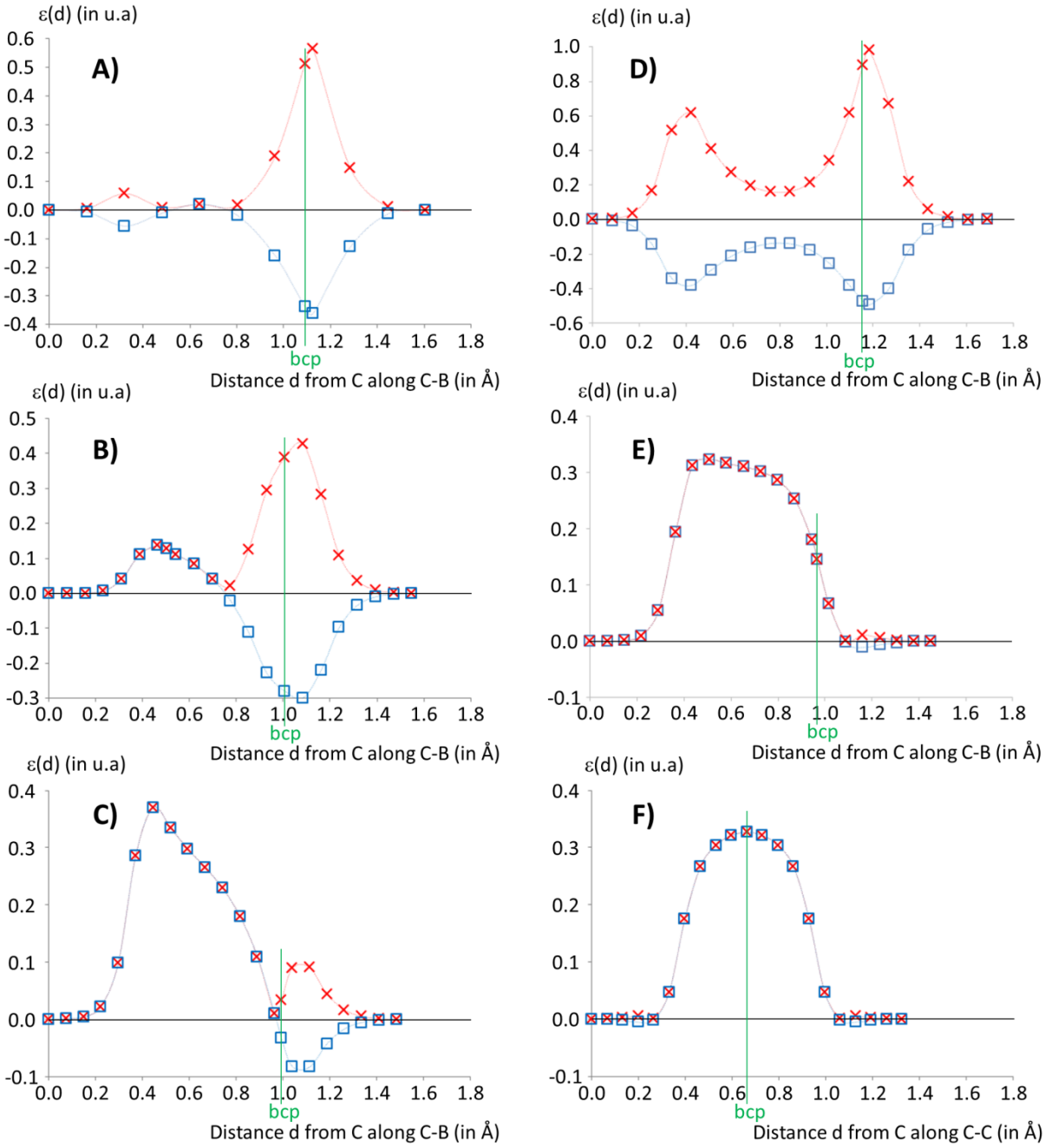

Figure 3-14: Variation of ellipticity indices $\varepsilon(d) = \lambda_1(d) / \lambda_2(d) - 1$ (with $|\lambda_1(d)| > |\lambda_2(d)|$) (red cross) and $\varepsilon_{corr}(d) = \lambda_{\pi\ in\text{-}plane}(d) / \lambda_\pi(d) - 1$ (blue square), calculated at the distance d from the C atom along the C-B or C-C bond for A) $\mathbf{1}^{//}$-BH_2^+, B) $\mathbf{21}^{//}$-BH_2^+, C) $\mathbf{37}^{//}$-BH_2^+, D) $CH_2^{//}$-BH_2^+, E) CH_2=BH_2^- and F) CH_2=CH_2.

These findings are explained by a thorough examination of the negative eigenvalues $\lambda_1(d)$ and $\lambda_2(d)$ ($|\lambda_1(d)| > |\lambda_2(d)|$) of $\Delta\rho(d)$ along the bond. For the sake of clarity, the curvature of $\rho(d)$ along the π direction is named $\lambda_\pi(d)$, while the curvature in the plane of the molecule along the axis perpendicular to the bond is noted $\lambda_{\pi\ in\text{-}plane}(d)$. We also define $\varepsilon_{corr}(d) = \lambda_{\pi\ in\text{-}plane}(d) / \lambda_\pi(d) - 1$. For CH_2=CH_2 and CH_2=BH_2^-, as expected, $\lambda_2(d) = \lambda_\pi(d)$ at the bcp and its neighbourhood, which means that $\varepsilon(d) = \varepsilon_{corr}(d)$ (Figure 3-14). However, this is not the case

close to the bond ends where $\lambda_1(d) = \lambda_\pi(d)$ and $\varepsilon(d) \neq \varepsilon_{corr}(d)$. More precisely, $\varepsilon_{corr}(d)$ turns negative, which is an indication that the decrease of the density is faster in the π-direction than in the plane of the molecule. We assume that this is due to the proximity of the C-H and B-H σ-bond. Similarly, differences between ε(d) and $\varepsilon_{corr}(d)$ are observed for $\mathbf{X}^{//}$-BH_2^+ complexes. This is also illustrated by the contour map of ρ at various planes perpendicular to the B-C bond (Figure 3-11 B-E). This assumption enables us to explain the 2 maxima of ε(d) obtained for CH_2-BH_2^+, which do not reflect any π system of the molecule but the presence of the C-H and B-H bonds at both bond ends. As the C-B bond is polarized, due to the low boron electronegativity, the bcp is located approximately at 2/3 of the CB bond, on the boron side, i.e. in the region of greatest influence of the B-H bonds. ε_{bcp} is thus large even if the C-B bond in CH_2-BH_2^+ is not a double bond. The influence of the rising π-donation from $\mathbf{1}^{//}$-BH_2^+ to $\mathbf{21}^{//}$-BH_2^+ and $\mathbf{37}^{//}$-BH_2^+ is thus clearly visible when calculating $\varepsilon_{corr}(d)$ along the B-C axis, with an increasing maximum located on the C atom side (Figures 3-14 A-C). The local character of ε_{bcp} does not allow this feature to be distinguished, and, on the contrary, this descriptor can be misleading because it does not distinguish the direction of the curvatures λ_1 and λ_2. Attempts to use $\varepsilon_{corr}(d)$ as a π-bond descriptor were unsuccessful. With respect to $E^{//}_{del}$, the best correlation, using the maximum of $\varepsilon_{corr}(d)$, gives only a poor correlation with $R^2 = 0.79$ (Figure 3-15B).

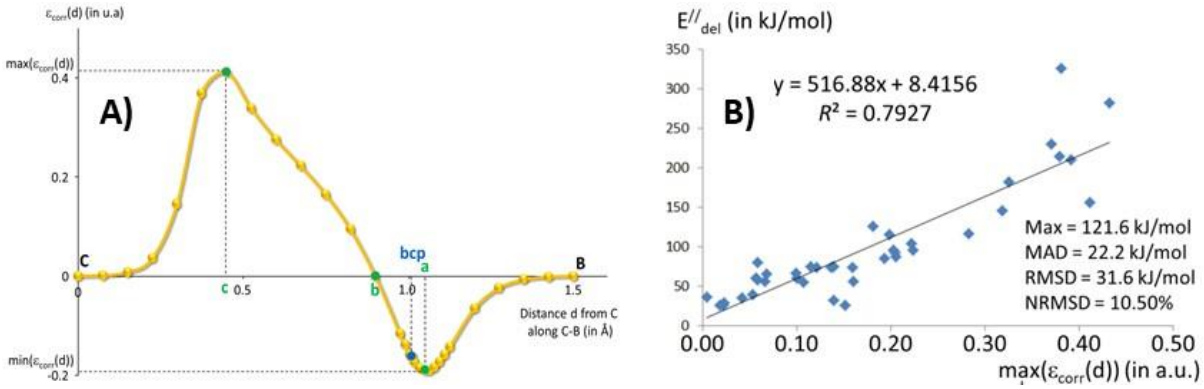

Figure 3-15: A) Evolution of $\varepsilon_{corr}(d)$ along C-B bond for $\mathbf{33}^{//}$-BH_2^+; B) Correlation between maximum of $\varepsilon_{corr}(d)$ and $E^{//}_{del}$

3.7. π-bonding descriptors based on the ELF approach

The topological analysis of the electron localization function (ELF) provides a partition of the molecular space into core and valence basins (Figure 3-11 E) (discussed in Section 2B.9.7).

This method allows the study of chemical bonds as a one-to-one correspondence between the valence basins, and lone pairs or Lewis-type bonds has been achieved.[25] The ELF method was previously used to study the interaction between NHC and main group fragments.[124-126] Integration of the electronic density over the basin corresponding to the C-B bond, V(C,B), is used to calculate the population of the C-B bond in $\mathbf{X}^{//}$-BH_2^+, $pop^{//}[V(C,B)]$. As expected, this population reflects the *intrinsic* π character of the bond, as shown by the correlation with $E^{//}_{del}$. The best fit is obtained with a logarithmic relationship (R^2 = 0.94, Figure 3-16 A). Calculation of the difference in the population of the C-B bond in $\mathbf{X}^{//}$-BH_2^+ and $\mathbf{X}^{\perp}$-BH_2^+, Δpop = $pop^{//}[V(C,B)] - pop^{\perp}[V(C,B)]$, gives a much weaker correlation with respect to ΔE_{rot} (R^2 = 0.81, Figure 3-16 B), showing that Δpop is not a good descriptor for measuring the *relative* strength of the π-interaction.

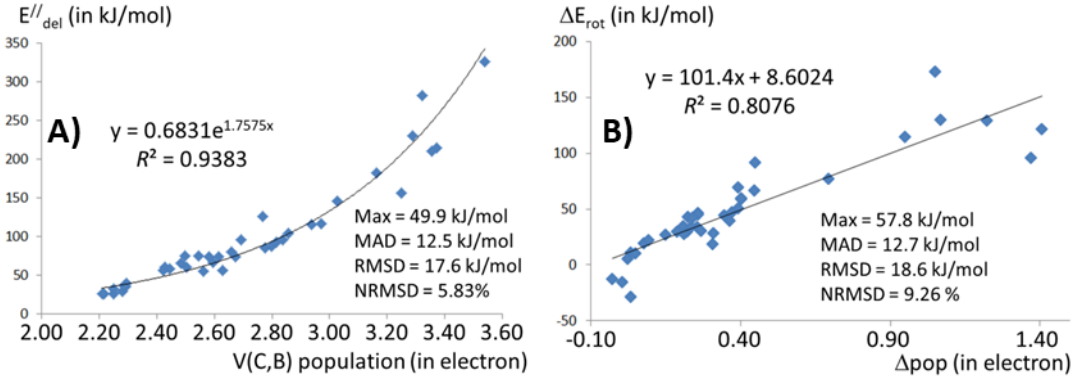

Figure 3-16: Correlation plots for **X**-BH_2^+ complexes between various descriptors obtained with the DFT, NBO and ELF methods.

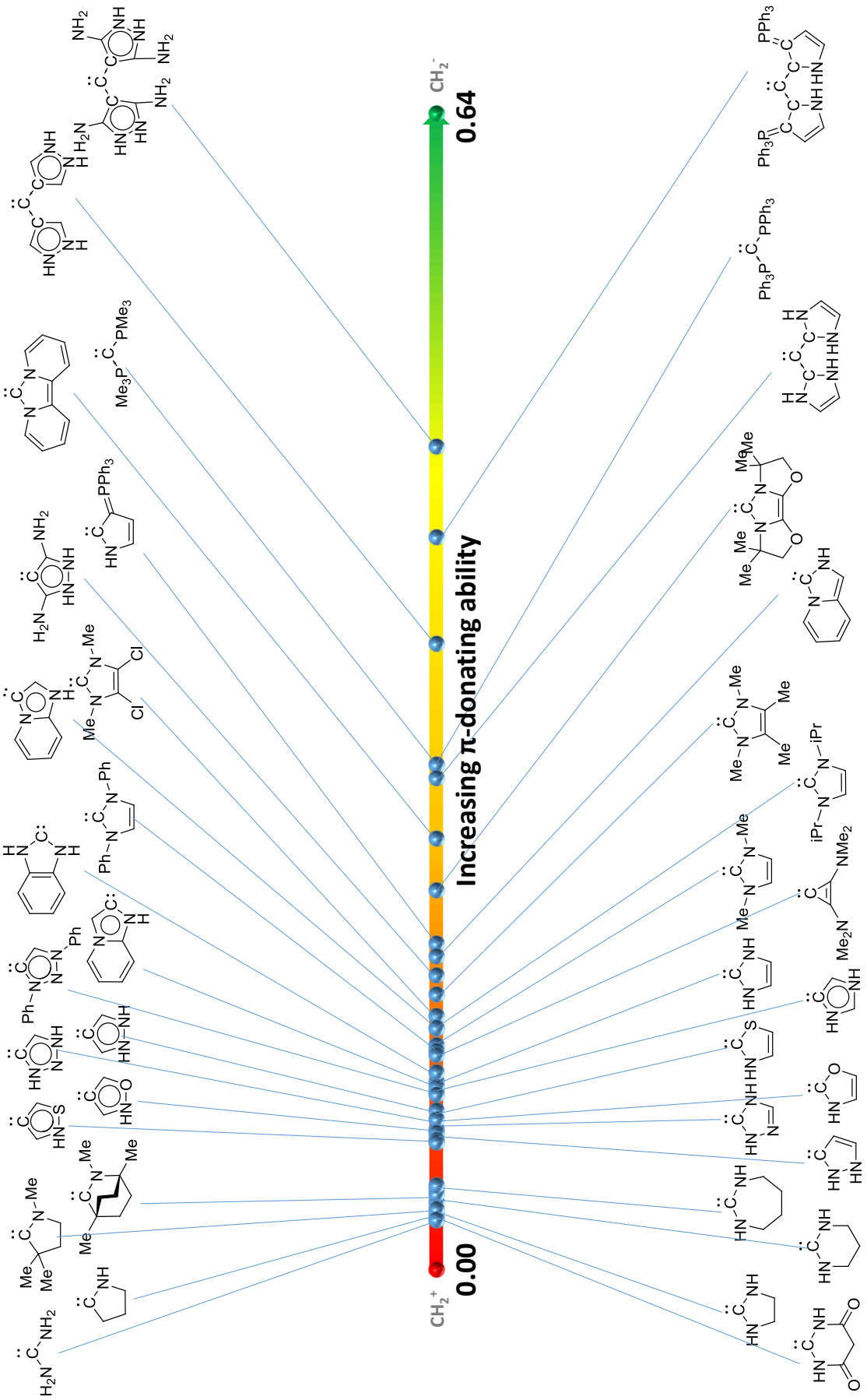

Figure 3-17: Scale of π-donating ability of 1-39 in $X^{///}$-BH_2^+ based on pop($^{///}p_{vac}{}^{B}$)

3.8. Chemical Interpretation of the π-donation Scale

The different modelling methods enable the calculation of π-bond descriptors which correlate very well with each other (R^2 between 0.94 and 0.99) and therefore appear to describe the same chemical property. They thus give a quantitative scale of increasing π-donation ability of **X** ligands from **1** to **39** (Figure 3-17). This scale indicates that carbodiphosphoranes and carbodicarbenes are the strongest π-donors whereas saturated NHC, NHCs with π-withdrawing substituents and cAAC ligands are weaker π-donors and the unsaturated ones lie in between. While the carbones form a separate group, showing that using them, one can achieve a π-donating ability that is normally not available by simple modification of carbenes, it is evident that the classical NHCs, cAACs or mesoionic carbenes are located in a shared chemical space and no hard lines can be drawn between them at least with respect to their π-donating ability. Carbenes derived from related structures form clusters, located relatively closer together on the scale of π-donation, showing that substitutions with alkyl or aryl groups have low impact, certainly less than that of structural modifications. E.g. carbenes **20**, **23**, **24**, **26** are all imidazole-2-ylidenes that lie within the short range of 0.104 to 0.134, varied by the N substitution. On the π-donation scale, they are arranged in increasing order of π-donation, going from H to Ph, Me, iPr (isopropyl group), in congruence with chemical intuition.

3.9. Conclusions

In the course of this work, the comparison between five modeling approaches based on DFT calculations (Optimized structure, NBO, ETS-NOCV, QTAIM and ELF) for estimating the magnitude of the π-donation has been achieved. Chemical systems, combining various divalent C-donor ligands with a BH_2^+ borenium group, have been designed. They include a partial CB π-bond resulting from a π-donation that is not biased by any other π-interaction between the two fragments and toward the boron atom. The intensity of the π-bond has been estimated from a wide selection of indicators and compared with each other. In some cases the correlations are already quite good. However, sometimes they require adjustments from the standard calculations commonly used in the literature, in particular for ETS-NOCV and QTAIM approaches. The use of these methods without these corrections leads to lower correlations (R^2< 0.92), or even to disagreements that may suggest that these methods diverge, which is not the case. In detail, the conclusions are as follows:

- A π-bond is characterized by 2 families of indicators: *intrinsic* and *relative* π-bond strength descriptors. Correlations between these two families are moderate (R^2 around 0.90).
- *Intrinsic* indicators describe the intensity of the π-bond in the molecule under study, whereas *relative* indicators measure the difference between the molecule with the π-interaction and the same molecule in a conformation which prevents this interaction.
- The reference *relative* indicator is the rotational barrier around the π-bond ΔE_{rot}. The bond lengths give at best an approximate indication of the strength of the π-bond.
- The NBO method provides three descriptors with moderately good (Wiberg Bond Index WBI) to very good (atomic π-population and NBO energetic analysis through the deletion of selected NBOs) performance to measure the π-bond strength. However, the absolute value of the π-bond energy is systematically overestimated by this approach.
- The π-donation-type NOCV eigenvalue and energy failed to give reliable measure of the π-bond strength. A significantly enhanced accuracy is obtained by correcting the previous values from the polarization of the π-system associated with the π-interaction, showing that NOCV chemical interpretation should be made with caution.
- Although the ETS-NOCV approach does not usually require symmetrical molecules to dissociate σ- and π-contributions, a case has been identified where this method fails and mixes σ- and π-interactions.
- The Delocalization Index (DI) provided by the QTAIM approach reproduces accurately the π-bond strength, contrary to the density value at the bond critical point ρ_{bcp}, which gives less relevant correlations. The ellipticity ε_{bcp} fails drastically for these dative π-bonds, due to the influence of the neighboring σ-bonds which reverse the role of the eigenvalues of the density curvature.
- The bond population given by the ELF method gives a reasonable correlation, but only for the *intrinsic* π-bond strength.

At the end of this study we have quantified the C→B dative π-bond through various computational parameters and additionally identified the parameters that are most 'reliable' in quantifying this interaction. We have constructed a scale for π-acidity of these divalent carbon compounds. The first question we may ask at this point is that can a similar study be

conducted with respect to σ-donating ability of the divalent carbon compounds? This is the subject of the following chapter. After that we may further ask what are the exact contributions of σ and π-donating strengths of the divalent carbon compounds towards the total acidity of the NHC-derived borenium adducts and can these factors be related to the reactivity of these molecules?

References

1. Gonthier, J. F.; Steinmann, S. N.; Wodrich, M. D.; Corminboeuf, C., Quantification of "fuzzy" chemical concepts: a computational perspective. *Chemical Society Reviews* **2012,** *41* (13), 4671-4687.
2. Grunenberg, J., Ill-defined chemical concepts: The problem of quantification. *International Journal of Quantum Chemistry* **2017,** *117* (9), e25359.
3. Pauling, L., The Nature of the Chemical Bond. *Cornell university press Ithaca (3rd Edition).* New York. Cornell University Publication. **1960**.
4. Zhao, L.; Hermann, M.; Schwarz, W. H. E.; Frenking, G., The Lewis electron-pair bonding model: modern energy decomposition analysis. *Nature Reviews Chemistry* **2019,** *3* (1), 48-63.
5. Alvarez, S.; Hoffmann, R.; Mealli, C., A Bonding Quandary—or—A Demonstration of the Fact That Scientists Are Not Born With Logic. *Chemistry – A European Journal* **2009,** *15* (34), 8358-8373.
6. Gupta, R.; Rezabal, E.; Hasrack, G.; Frison, G., Comparison of Chemical and Interpretative Methods: the Carbon–Boron π-Bond as a Test Case**. *Chemistry – A European Journal* **2020,** *26* (71), 17230-17241.
7. Gordy, W., Dependence Of Bond Order and Of Bond Energy Upon Bond Length. *Journal of Chemical Physics* **1947,** *15* (5), 305-310.
8. Pyykko, P.; Atsumi, M., Molecular Double-Bond Covalent Radii for Elements Li-E112. *Chemistry-a European Journal* **2009,** *15* (46), 12770-12779.
9. Jules, J. L.; Lombardi, J. R., Toward an experimental bond order. *Journal of Molecular Structure: THEOCHEM* **2003,** *664-665*, 255-271.
10. Zhao, L.; Pan, S.; Holzmann, N.; Schwerdtfeger, P.; Frenking, G., Chemical Bonding and Bonding Models of Main-Group Compounds. *Chemical Reviews* **2019,** *119* (14), 8781-8845.
11. Coulson, C. A., The electronic structure of some polyenes and aromatic molecules VII Bonds of fractional order by the molecular orbital method. *Proceedings of the Royal Society of London Series a-Mathematical and Physical Sciences* **1939,** *169* (938), 413-428.
12. Wiberg, K. B., Application Of Pople-Santry-Segal CNDO Method to Cyclopropylcarbinyl and Cyclobutyl Cation and to Bicyclobutane. *Tetrahedron* **1968,** *24* (3), 1083-1096.
13. Mayer, I., Charge, Bond Order and Valence in the ab initio SCF Theory. *Chemical Physics Letters* **1983,** *97* (3), 270-274.
14. Mayer, I., Bond order and valence indices: A personal account. *Journal of Computational Chemistry* **2007,** *28* (1), 204-221.
15. Boys, S. F., Construction of Some Molecular Orbitals to be Approximately Invariant for Changes from One Molecule to Another. *Reviews of Modern Physics* **1960,** *32* (2), 296-299.
16. Pipek, J.; Mezey, P. G., A Fast Intrinsic Localization Procedure Applicable for Abinitio and Semiempirical Linear Combination of Atomic Orbital Wave-Functions. *Journal of Chemical Physics* **1989,** *90* (9), 4916-4926.

17. Edmiston, C.; Ruedenberg, K., Localized Atomic and Molecular Orbitals. *Reviews of Modern Physics* **1963,** *35* (3), 457-465.
18. Lowdin, P. O., Quantum Theory of Many-Particle Systems .1. Physical Interpretations by Means of Density Matrices, Natural Spin-Orbitals, and Convergence Problems In The Method Of Configurational Interaction. *Physical Review* **1955,** *97* (6), 1474-1489.
19. Rhee, Y. M.; Head-Gordon, M., A delicate electronic balance between metal and ligand in Cu-P-Cu-P diamondoids: Oxidation state dependent plasticity and the formation of a singlet diradicaloid. *Journal of the American Chemical Society* **2008,** *130* (12), 3878-3887.
20. Thom, A. J. W.; Sundstrom, E. J.; Head-Gordon, M., LOBA: a localized orbital bonding analysis to calculate oxidation states, with application to a model water oxidation catalyst. *Physical Chemistry Chemical Physics* **2009,** *11* (47), 11297-11304.
21. Glendening, E. D.; Landis, C. R.; Weinhold, F., Natural bond orbital methods. *Wiley Interdisciplinary Reviews-Computational Molecular Science* **2012,** *2* (1), 1-42.
22. Bader, R. F. W., Atoms in molecules. *Accounts of Chemical Research* **1985,***18* (1), 9-15.
23. Hirshfeld, F. L., Bonded-atom fragments for describing molecular charge densities. *Theoretica chimica acta* **1977,** *44* (2), 129-138.
24. Becke, A. D.; Edgecombe, K. E., A Simple Measure of Electron Localization in Atomic and Molecular-Systems. *Journal of Chemical Physics* **1990,** *92* (9), 5397-5403.
25. Silvi, B.; Savin, A., Classification of Chemical-Bonds Based on Topological Analysis of Electron Localization Functions. *Nature* **1994,** *371* (6499), 683-686.
26. Schmider, H. L.; Becke, A. D., Chemical content of the kinetic energy density. *Journal of Molecular Structure: THEOCHEM* **2000,** *527* (1), 51-61.
27. Johnson, E. R.; Keinan, S.; Mori-Sanchez, P.; Contreras-Garcia, J.; Cohen, A. J.; Yang, W., Revealing Noncovalent Interactions. *Journal of the American Chemical Society* **2010,** *132* (18), 6498-6506.
28. de Silva, P.; Corminboeuf, C., Simultaneous Visualization of Covalent and Noncovalent Interactions Using Regions of Density Overlap. *Journal of Chemical Theory and Computation* **2014,** *10* (9), 3745-3756.
29. Karadakov, P. B.; Horner, K. E., Exploring Chemical Bonds through Variations in Magnetic Shielding. *Journal of Chemical Theory and Computation* **2016,** *12* (2), 558-563.
30. Bistoni, G.; Belpassi, L.; Tarantelli, F., Advances in Charge Displacement Analysis. *Journal of Chemical Theory and Computation* **2016,** *12* (3), 1236-1244.
31. Ziegler, T.; Rauk, A., CO, CS, N2, PF3, and CNCH3 As Sigma-Donors and Pi-Acceptors - Theoretical-Study By The Hartree-Fock-Slater Transition-State Method. *Inorganic Chemistry* **1979,** *18* (7), 1755-1759.
32. Ziegler, T.; Rauk, A., Theoretical-Study of The Ethylene-Metal Bond in Complexes Between Cu+, Ag+, Au+, Pt0, or Pt2+ and Ethylene, Based on The Hartree-Fock-Slater Transition-State Method. *Inorganic Chemistry* **1979,** *18* (6), 1558-1565.
33. Morokuma, K., Molecular Orbital Studies of Hydrogen Bonds .3. C=O H-O Hydrogen Bond in H2CO H2O and H2CO 2H2O. *Journal of Chemical Physics* **1971,** *55* (3), 1236-1244.

34. Mitoraj, M. P.; Michalak, A.; Ziegler, T., A Combined Charge and Energy Decomposition Scheme for Bond Analysis. *Journal of Chemical Theory and Computation* **2009,** *5* (4), 962-975.
35. Jeziorski, B.; Moszynski, R.; Szalewicz, K., Perturbation-Theory Approach to Intermolecular Potential-Energy Surfaces of van-der-Waals Complexes. *Chemical Reviews* **1994,** *94* (7), 1887-1930.
36. Pendás, A. M.; Blanco, M. A.; Francisco, E., Chemical fragments in real space: Definitions, properties, and energetic decompositions. *Journal of Computational Chemistry* **2007,** *28* (1), 161-184.
37. Tiana, D.; Francisco, E.; Blanco, M. A.; Macchi, P.; Sironi, A.; Martín Pendás, A., Bonding in Classical and Nonclassical Transition Metal Carbonyls: The Interacting Quantum Atoms Perspective. *Journal of Chemical Theory and Computation* **2010,** *6* (4), 1064-1074.
38. Mayer, I., Energy partitioning schemes: a dilemma. *Faraday Discussions* **2007,** *135* (0), 439-450.
39. Kaupp, M.; Danovich, D.; Shaik, S., Chemistry is about energy and its changes: A critique of bond-length/bond-strength correlations. *Coordination Chemistry Reviews* **2017,** *344*, 355-362.
40. Kraka, E.; Cremer, D., Characterization of CF Bonds with Multiple-Bond Character: Bond Lengths, Stretching Force Constants, and Bond Dissociation Energies. *ChemPhysChem* **2009,** *10* (4), 686-698.
41. Setiawan, D.; Kalescky, R.; Kraka, E.; Cremer, D., Direct Measure of Metal-Ligand Bonding Replacing the Tolman Electronic Parameter. *Inorganic Chemistry* **2016,** *55* (5), 2332-2344.
42. Brandhorst, K.; Grunenberg, J., How strong is it? The interpretation of force and compliance constants as bond strength descriptors. *Chemical Society Reviews* **2008,** *37* (8), 1558-1567.
43. Pecher, L.; Tonner, R., Deriving bonding concepts for molecules, surfaces, and solids with energy decomposition analysis for extended systems. *Wiley Interdisciplinary Reviews-Computational Molecular Science* **2019,** 9:e1401.
44. Zhao, L.; von Hopffgarten, M.; Andrada, D. M.; Frenking, G., Energy decomposition analysis. *Wiley Interdisciplinary Reviews-Computational Molecular Science* **2018,** 8: e1345.
45. Lepetit, C.; Fau, P.; Fajerwerg, K.; Kahn, M. L.; Silvi, B., Topological analysis of the metal-metal bond: A tutorial review. *Coordination Chemistry Reviews* **2017,** *345*, 150-181.
46. Weinhold, F.; Landis, C. R.; Glendening, E. D., What is NBO analysis and how is it useful? *International Reviews in Physical Chemistry* **2016,** *35* (3), 399-440.
47. Dognon, J.-P., Theoretical insights into the chemical bonding in actinide complexes. *Coordination Chemistry Reviews* **2014,** *266*, 110-122.
48. Andres, J.; Ayers, P. W.; Boto, R. A.; Carbo-Dorca, R.; Chermette, H.; Cioslowski, J.; Contreras-Garcia, J.; Cooper, D. L.; Frenking, G.; Gatti, C.; Heidar-Zadeh, F.; Joubert, L.; Martin Pendas, A.; Matito, E.; Mayer, I.; Misquitta, A. J.; Mo, Y.; Pilme, J.; Popelier, P. L. A.; Rahm, M.; RamosCordoba, E.; Salvador, P.; Schwarz, W. H. E.; Shahbazian, S.; Silvi, B.; Sola,

M.; Szalewicz, K.; Tognetti, V.; Weinhold, F.; Zins, E.-L., Nine questions on energy decomposition analysis. *Journal of Computational Chemistry* **2019,***40* (26), 2248-2283.

49. Bader, R. F. W., A Quantum-Theory of Molecular-Structure and Its Applications. *Chemical Reviews* **1991,** *91* (5), 893-928.

50. Dutta, S.; Maity, B.; Thirumalai, D.; Koley, D., Computational Investigation of Carbene-Phosphinidenes: Correlation between P-31 Chemical Shifts and Bonding Features to Estimate the pi-Backdonation of Carbenes. *Inorganic Chemistry* **2018,** *57* (7), 3993-4008.

51. Corts-Guzman, F.; Bader, R. F. W., Complementarity of QTAIM and MO theory in the study of bonding in donor-acceptor complexes. *Coordination Chemistry Reviews* **2005,** *249* (5-6), 633-662.

52. Fugel, M.; Hesse, M. F.; Pal, R.; Beckmann, J.; Jayatilaka, D.; Turner, M. J.; Karton, A.; Bultinck, P.; Chandler, G. S.; Grabowsky, S., Covalency and Ionicity Do Not Oppose Each Other-Relationship Between Si-O Bond Character and Basicity of Siloxanes. *Chemistry-a European Journal* **2018,** *24* (57), 15275-15286.

53. Fugel, M.; Beckmann, J.; Jayatilaka, D.; Gibbs, G. V.; Grabowsky, S., A Variety of Bond Analysis Methods, One Answer? An Investigation of the Element-Oxygen Bond of Hydroxides HnXOH. *Chemistry-a European Journal* **2018,** *24* (23), 6248-6261.

54. Wu, X.; Zhao, L.; Jin, J.; Pan, S.; Li, W.; Jin, X.; Wang, G.; Zhou, M.; Frenking, G., Observation of alkaline earth complexes M(CO)(8) (M = Ca, Sr, or Ba) that mimic transition metals. *Science* **2018,** *361* (6405), 912-916.

55. Landis, C. R.; Hughes, R. P.; Weinhold, F., Comment on "Observation of alkaline earth complexes M(CO)(8)(M = Ca, Sr, or Ba) that mimic transition metals". *Science* **2019,** *365* (6453):eaay2355.

56. Landis, C. R.; Hughes, R. P.; Weinhold, F., Bonding Analysis of TM(cAAC)(2) (TM = Cu, Ag, and Au) and the Importance of Reference State. *Organometallics* **2015,** *34* (13), 3442-3449.

57. Jerabek, P.; Roesky, H. W.; Bertrand, G.; Frenking, G., Coinage Metals Binding as Main Group Elements: Structure and Bonding of the Carbene Complexes TM(cAAC)(2)) and TM(cAAC)(2) (+) (TM = Cu, Ag, Au). *Journal of the American Chemical Society* **2014,** *136* (49), 17123-17135.

58. Xie, J. M.; Grev, R. S.; Gu, J. D.; Schaefer, H. F.; Schleyer, P. V.; Su, J. R.; Li, X. W.; Robinson, G. H., The nature of the gallium-gallium triple bond. *Journal of the American Chemical Society* **1998,** *120* (15), 3773-3780.

59. Klinkhammer, K., How Can One Recognize a Triple Bond between Main Group Elements? *Angewandte Chemie-international Edition.* **1997,** *36*, 2320-2322.

60. Molina Molina, J.; Dobado, J. A.; Heard, G. L.; Bader, R. F. W.; Sundberg, M. R., Recognizing a triple bond between main group atoms. *Theoretical Chemistry Accounts* **2001,** *105* (4), 365-373.

61. Weinhold, F.; Klein, R. A., Improved General Understanding of the Hydrogen-Bonding Phenomena: A Reply. *Angewandte Chemie-International Edition* **2015,** *54* (9), 2600-2602.

62. Frenking, G.; Caramori, G. F., No Need for a Re-examination of the Electrostatic Notation of the Hydrogen Bonding: A Comment. *Angewandte Chemie-International Edition* **2015,** *54* (9), 2596-2599.
63. Weinhold, F.; Klein, R. A., Anti-Electrostatic Hydrogen Bonds. *Angewandte Chemie-International Edition* **2014,** *53* (42), 11214-11217.
64. Stone, A. J.; Szalewicz, K., Reply to "Comment on 'Natural Bond Orbitals and the Nature of the Hydrogen Bond'" *Journal of Physical Chemistry A* **2018,** *122* (2), 733-736.
65. Weinhoid, F.; Glendening, E. D., Comment on "Natural Bond Orbitals and the Nature of the Hydrogen Bond". *Journal of Physical Chemistry A* **2018,** *122* (2), 724-732.
66. Stone, A. J., Natural Bond Orbitals and the Nature of the Hydrogen Bond. *Journal of Physical Chemistry A* **2017,** *121* (7), 1531-1534.
67. Bickelhaupt, F. M.; Baerends, E. J., The case for steric repulsion causing the staggered conformation of ethane. *Angewandte Chemie-International Edition* **2003,** *42* (35), 4183-4188.
68. Weinhold, F., Rebuttal to the Bickelbaupt-Baerends case for steric repulsion causing the staggered conformation of ethane. *Angewandte Chemie-International Edition* **2003,** *42* (35), 4188-4194.
69. Andrada, D. M.; Holzmann, N.; Hamadi, T.; Frenking, G., Direct estimate of the internal Pi-donation to the carbene centre within N-heterocyclic carbenes and related molecules. *Beilstein J Org Chem* **2015,** *11*, 2727-2736.
70. Ayers, P. L. a.; Boyd, R. J. b.; Bultinck, P.; Caffarel, M. d.; Carbo-Dorca, R. e.; Causa, M. f.; Cioslowski, J. g.; Contreras-Garcia, J. h.; Cooper, D. L. i.; Coppens, P. j.; Gatti, C. k.; Grabowsky, S. l.; Lazzeretti, P. m.; Macchi, P. n.; Martin Pendas, A. o.; Popelier, P. L. A. p.; Ruedenberg, K. r.; Rzepa, H. s.; Savin, A. h.; Sax, A. t.; Schwarz, W. H. E. u.; Shahbazian, S. w.; Silvi, B. h.; Sola, M. e.; Tsirelson, V. x., Six questions on topology in theoretical chemistry. *Computational and Theoretical Chemistry* **2015,** *1053*, 2-16.
71. Weinhold, F., Natural bond critical point analysis: Quantitative relationships between natural bond orbital-based and QTAIM-based topological descriptors of chemical bonding. *Journal of Computational Chemistry* **2012,** *33* (30), 2440-2449.
72. Weinhold, F., Natural bond orbital analysis: A critical overview of relationships to alternative bonding perspectives. *Journal of Computational Chemistry* **2012,** *33* (30), 2363-2379.
73. Sola, M., Why Aromaticity Is a Suspicious Concept? Why? *Frontiers in Chemistry* **2017,** (5), 22.
74. Solà, M., Connecting and combining rules of aromaticity. Towards a unified theory of aromaticity. *WIREs Computational Molecular Science* **2019,** *9* (4), e1404.
75. Piers, W. E.; Bourke, S. C.; Conroy, K. D., Borinium, Borenium, and Boronium Ions: Synthesis, Reactivity, and Applications. *Angewandte Chemie International Edition* **2005,** *44* (32), 5016-5036.
76. Farrell, J. M.; Hatnean, J. A.; Stephan, D. W., Activation of Hydrogen and Hydrogenation Catalysis by a Borenium Cation. *Journal of the American Chemical Society* **2012,** *134* (38), 15728-15731.

77. De Vries, T. S.; Prokofjevs, A.; Vedejs, E., Cationic Tricoordinate Boron Intermediates: Borenium Chemistry from the Organic Perspective. *Chemical Reviews* **2012,** *112* (7), 4246-4282.
78. Eisenberger, P.; Crudden, C. M., Borocation catalysis. *Dalton Transactions* **2017,** *46* (15), 4874-4887.
79. Rao, B.; Kinjo, R., Boron-Based Catalysts for C-C Bond-Formation Reactions. *Chemistry-an Asian Journal* **2018,** *13* (10), 1279-1292.
80. Ingleson, M. J., Fundamental and Applied Properties of Borocations. In *Synthesis and Application of Organoboron Compounds*, Fernandez, E.; Whiting, A., Eds. **2015**; (49), 39-71.
81. Franz, D.; Szilvasi, T.; Poethig, A.; Inoue, S., Isolation of an N-Heterocyclic Carbene Complex of a Borasilene. *Chemistry-a European Journal* **2019,** *25* (47), 11036-11041.
82. Fustier-Boutignon, M.; Nebra, N.; Mezailles, N., Geminal Dianions Stabilized by Main Group Elements. *Chemical Reviews* **2019,** *119* (14), 8555-8700.
83. Radcliffe, J. E.; Dunsford, J. J.; Cid, J.; Fasano, V.; Ingleson, M. J., N-Heterocycle-Ligated Borocations as Highly Tunable Carbon Lewis Acids. *Organometallics* **2017,** *36* (24), 4952-4960.
84. Matsumoto, T.; Gabbaï, F. P., A Borenium Cation Stabilized by an N-Heterocyclic Carbene Ligand. *Organometallics* **2009,** *28* (15), 4252-4253.
85. McArthur, D.; Butts, C. P.; Lindsay, D. M., A dialkylborenium ion via reaction of N-heterocyclic carbene-organoboranes with Bronsted acids-synthesis and DOSY NMR studies. *Chemical Communications* **2011,** *47* (23), 6650-6652.
86. Mansaray, H. B.; Rowe, A. D. L.; Phillips, N.; Niemeyer, J.; Kelly, M.; Addy, D. A.; Bates, J. I.; Aldridge, S., Modelling fundamental arene-borane contacts: spontaneous formation of a dibromoborenium cation driven by interaction between a borane Lewis acid and an arene pi system. *Chemical Communications* **2011,** *47* (45), 12295-12297.
87. Prokofjevs, A.; Boussonnière, A.; Li, L.; Bonin, H.; Lacôte, E.; Curran, D. P.; Vedejs, E., Borenium Ion Catalyzed Hydroboration of Alkenes with N-Heterocyclic Carbene-Boranes. *Journal of the American Chemical Society* **2012,** *134* (29), 12281-12288.
88. Tay, M. Q. Y.; Murugesapandian, B.; Lu, Y.; Ganguly, R.; Rei, K.; Vidović, D., Dihaloborenium cations stabilized by a four-membered N-heterocyclic carbene: electron deficiency compensation by asymmetric structural changes. *Dalton Transactions* **2014,** *43* (41), 15313-15316.
89. Farrell, J. M.; Schmidt, D.; Grande, V.; Wuerthner, F., Synthesis of a Doubly Boron-Doped Perylene through NHC-Borenium Hydroboration/C-H Borylation/Dehydrogenation. *Angewandte Chemie-International Edition* **2017,** *56* (39), 11846-11850.
90. Eisenberger, P.; Bestvater, B. P.; Keske, E. C.; Crudden, C. M., Hydrogenations at Room Temperature and Atmospheric Pressure with Mesoionic Carbene-Stabilized Borenium Catalysts. *Angewandte Chemie International Edition* **2015,** *54* (8), 2467-2471.
91. Münzer, J. E.; Oña-Burgos, P.; Arrabal-Campos, F. M.; Neumüller, B.; Tonner, R.; Fernández, I.; Kuzu, I., Difluoroborenium Cation Stabilized by Hexaphenyl-

Carbodiphosphorane: A Concise Study on the Molecular and Electronic Structure of [(Ph3P)2C⇉BF2][BF4]. *European Journal of Inorganic Chemistry* **2016,** (24), 3852-3858.
92. Inés, B.; Patil, M.; Carreras, J.; Goddard, R.; Thiel, W.; Alcarazo, M., Synthesis, Structure, and Reactivity of a Dihydrido Borenium Cation. *Angewandte Chemie International Edition* **2011,** *50* (36), 8400-8403.
93. Lafage, M.; Pujol, A.; Saffon-Merceron, N.; Mezailles, N., BH3 Activation by Phosphorus-Stabilized Geminal Dianions: Synthesis of Ambiphilic Organoborane, DFT Studies, and Catalytic CO2 Reduction into Methanol Derivatives. *ACS Catalysis* **2016,** *6* (5), 3030-3035.
94. Celik, M. A.; Frenking, G.; Neumueller, B.; Petz, W., Exploiting the Twofold Donor Ability of Carbodiphosphoranes: Theoretical Studies of (PPh3)(2)C -> EH2 (q) (E-q=Be, B+, C2+, N3+, O4+) and Synthesis of the Dication (Ph3P)(2)C = CH2 (2+). *ChemPlusChem* **2013,** *78* (9), 1024-1032.
95. Frenking, G.; Hermann, M.; Andrada, D. M.; Holzmann, N., Donor-acceptor bonding in novel low-coordinated compounds of boron and group-14 atoms C-Sn. *Chemical Society Reviews* **2016,** *45* (4), 1129-1144.
96. Ai Nhung, N. T.; Huynh, T. P. L.; Son, P.; Duc, H.; Quang, D.; Pham, V.; Dang, H., Theoretical assessment of donor–acceptor complexes [X(PPh3)2 → AlH2]+ (X = C–Pb): structures and bonding. *Theoretical Chemistry Accounts* **2019,** *138*.
97. Sato, K.; Tan, T. T. Y.; Schäfers, F.; Hahn, F. E.; Stephan, D. W., Imidazole-stabilized, electron-deficient boron cations. *Dalton Transactions* **2017,***46* (47), 16404-16407.
98. Tsai, H.-C.; Lin, Y.-F.; Liu, W.-C.; Lee, G.-H.; Peng, S.-M.; Chiu, C.-W., N-Heterocyclic Silylene Coordinated Dialkyl Borenium Equivalent. *Organometallics* **2017,** *36* (20), 3879-3882.
99. Rezabal, E.; Frison, G., Estimating pi Binding Energy of N-Heterocyclic Carbenes: The Role of Polarization. *Journal of Computational Chemistry* **2015,** *36* (8), 564-572.
100. Han Vinh, H.; Frison, G., Electronic Structural Trends in Divalent Carbon Compounds. *Journal of Organic Chemistry* **2013,** *78* (2), 328-338.
101. Bernhammer, J. C.; Frison, G.; Han Vinh, H., Electronic Structure Trends in N-Heterocyclic Carbenes (NHCs) with Varying Number of Nitrogen Atoms and NHC-Transition-Metal Bond Properties. *Chemistry-a European Journal* **2013,** *19* (38), 12892-12905.
102. Huynh, H. V., Electronic Properties of N-Heterocyclic Carbenes and Their Experimental Determination. *Chemical Reviews* **2018,** *118* (19), 9457-9492.
103. Munz, D., Pushing Electrons-Which Carbene Ligand for Which Application? *Organometallics* **2018,** *37* (3), 275-289.
104. Zhao, Y.; Truhlar, D. G., The M06 suite of density functionals for main group thermochemistry, thermochemical kinetics, noncovalent interactions, excited states, and transition elements: two new functionals and systematic testing of four M06-class functionals and 12 other functionals. *Theoretical Chemistry Accounts* **2008,** *120* (1), 215-241.
105. McLean, A. D.; Chandler, G. S., Contracted Gaussian basis sets for molecular calculations. I. Second row atoms, Z=11–18. *The Journal of Chemical Physics* **1980,** *72* (10), 5639-5648.

106. Krishnan, R.; Binkley, J. S.; Seeger, R.; Pople, J. A., Self-consistent molecular orbital methods. XX. A basis set for correlated wave functions. *The Journal of Chemical Physics* **1980,** *72* (1), 650-654.
107. Badger, R. M., A relation between internuclear distances and bond force constants. *The Journal of Chemical Physics.* **1934,** *2* (3), 128-131.
108. Badger, R. M., The relation between the internuclear distances and force constants of molecules and its application to polyatomic molecules. **1935,** *3* (11), 710-714.
109. Gordy, W. , A relation between bond force constants, bond orders, bond lengths, and the electronegativities of the bonded atoms. *The Journal of Chemical Physics*. **1946,** *14* (5), 305-320.
110. Pauling, L., Atomic Radii and Interatomic Distances in Metals. *Journal of the American Chemical Society* **1947,** *69* (3), 542-553.
111. Pauling, L., Interatomic Distances and Bond Character in the Oxygen Acids and Related Substances. *The Journal of Physical Chemistry* **1952,** *56* (3), 361-365.
112. Kraka, E.; Larsson, J. A.; Cremer, D. J.; In *Chemical Spectroscopy* Grunenberg, J., Ed.; Wiley: New York, N., USA, Generalization of the Badger rule based on the use of adiabatic vibrational modes. **2010**, 105-149.
113. Kaupp, M.; Metz, B.; Stoll, H., Breakdown of Bond Length-Bond Strength Correlation: A Case Study. *Angewandte Chemie International Edition* **2000,** *39* (24), 4607-4609.
114. Gibbs, G. V.; Hill, F. C.; Boisen, M. B.; Downs, R. T., Power law relationships between bond length, bond strength and electron density distributions. *Physics and Chemistry of Minerals* **1998,** *25* (8), 585-590.
115. Modarresi-Alam, A. R.; Najafi, P.; Rostamizadeh, M.; Keykha, H.; Bijanzadeh, H.-R.; Kleinpeter, E., Dynamic 1H NMR Study of the Barrier to Rotation about the C−N Bond in Primary Carbamates and Its Solvent Dependence. *The Journal of Organic Chemistry* **2007,** *72* (6), 2208-2211.
116. Wiberg, K. B.; Rablen, P. R., Why Does Thioformamide Have a Larger Rotational Barrier Than Formamide? *Journal of the American Chemical Society* **1995,** *117* (8), 2201-2209.
117. Jubert, A. H.; Della Vedova, C. O.; Aymonino, P. , Theoretical Calculation of the Rotational Barrier, Valence Force Constants and Experimental Electronic Spectrum of Chlorocarbonylsulphenyl Chloride (ClC (O) SCl). *Croatia Chemic Acta.***1987,** *60* (2), 207-213.
118. Tay, M. Q. Y.; Ilic, G.; Werner-Zwanziger, U.; Lu, Y.; Ganguly, R.; Ricard, L.; Frison, G.; Carmichael, D.; Vidovic, D., Preparation, Structural Analysis, and Reactivity Studies of Phosphenium Dications. *Organometallics* **2016,** *35* (4), 439-449.
119. Rogachev, A. Y.; Hoffmann, R., Hypervalent Compounds as Ligands: I-3-Anion Adducts with Transition Metal Pentacarbonyls. *Inorganic Chemistry* **2013,** *52* (12), 7161-7171.
120. Bader, R. F. W.; Tang, T. H.; Tal, Y.; Bieglerkonig, F. W., Properties of Atoms and Bonds in Hydrocarbon Molecules. *Journal of the American Chemical Society* **1982,** *104* (4), 946-952.
121. Matta, C. F.; Hernández-Trujillo, J., Bonding in Polycyclic Aromatic Hydrocarbons in Terms of the Electron Density and of Electron Delocalization. *The Journal of Physical Chemistry A* **2003,** *107* (38), 7496-7504.

122. Outeiral, C.; Vincent, M. A.; Martin Pendas, A.; Popelier, P. L. A., Revitalizing the concept of bond order through delocalization measures in real space. *Chemical Science* **2018,** *9* (25), 5517-5529.
123. Bader, R. F. W.; Slee, T. S.; Cremer, D.; Kraka, E., Description of Conjugation and Hyperconjugation in Terms of Electron Distributions. *Journal of the American Chemical Society* **1983,** *105* (15), 5061-5068.
124. Frison, G.; Sevin, A., A DFT/electron localization function (ELF) study of the bonding of phosphinidenes with N-heterocyclic carbenes. *Journal of Physical Chemistry A* **1999,** *103* (50), 10998-11003.
125. Frison, G.; Sevin, A., Substituent effects in polarized phosphaalkenes: a theoretical study of aminocarbene-phosphinidene adducts. *Journal of Organometallic Chemistry* **2002,** *643*, 105-111.
126. Frison, G.; Sevin, A., Theoretical study of the bonding between aminocarbene and main group elements. *Journal of the Chemical Society-Perkin Transactions 2* **2002,** (10), 1692-1697.

127. M.J. Frisch, G.W. Trucks, H.B. Schlegel, G.E. Scuseria, M.A. Robb, J.R. Cheeseman, G. Scalmani, V. Barone, B. Mennucci, G.A. Petersson, H. Nakatsuji, M. Caricato, X. Li, H.P. Hratchian, A.F. Izmaylov, J. Bloino, G. Zheng, J.L. Sonnenberg, M. Hada, M. Ehara, K. Toyota, R. Fukuda, J. Hasegawa, M. Ishida, T. Nakajima, Y. Honda, O. Kitao, H. Nakai, T. Vreven, J.A. Montgomery Jr, J.E. Peralta, F. Ogliaro, M. Bearpark, J.J. Heyd, E. Brothers, K.N. Kudin, V.N. Staroverov, R. Kobayashi, J. Normand, K. Raghavachari, A. Rendell, J.C. Burant, S.S. Iyengar, J. Tomasi, M. Cossi, N. Rega, J.M. Millam, M. Klene, J.E. Knox, J.B. Cross, V. Bakken, C. Adamo, J. Jaramillo, R. Gomperts, R.E. Stratmann, O. Yazyev, A.J. Austin, R. Cammi, C. Pomelli, J.W. Ochterski, R.L. Martin, K. Morokuma, V.G. Zakrzewski, G.A. Voth, P. Salvador, J.J. Dannenberg, S. Dapprich, A.D. Daniels, Ö. Farkas, J.B. Foresman, J.V. Ortiz, J. Cioslowski, D.J. Fox, Gaussian, Inc., Wallingford CT, Gaussian 09, Revision D.01, **2013**.

128. E.D. Glendening, C.R. Landis, F. Weinhold, *WIREs Comput. Mol. Sci*. **2012**, *2*, 1-42.

129. E.D. Glendening, J.K. Badenhoop, A.E. Reed, J.E. Carpenter, J.A. Bohmann, C.M. Morales, C.R. Landis, F. Weinhold, NBO 6.0; Theoretical Chemistry Institute, University of Wisconsin,Madison, WI, **2013**.

130. E.D. Glendening, C.R. Landis, F. Weinhold, *J. Comput. Chem.***2013**, *34*, 1429-1437.

131. G. Te Velde, F.M. Bickelhaupt, E.J. Baerends, C. Fonseca Guerra, S.J.A. Van Gisbergen, J.G. Snijders, T. Ziegler, *J. Comput. Chem.***2001**, *22*, 931-967.

132. *ADF2017*, SCM, Theoretical Chemistry, Vrije Universiteit, Amsterdam, The Netherlands, http://www.scm.com.

133. T. Lu, F. Chen, *J. Comp. Chem.***2012**, *33*, 580-592.

134. Matsumoto, T.; Gabbaï, F. P., A Borenium Cation Stabilized by an N-Heterocyclic Carbene Ligand. *Organometallics* **2009,** *28* (16), 4898-4898.

4. CHAPTER III
Computational Investigation of σ-donating Ability of Carbenic Compounds

Abstract

In the previous chapter the C→B dative π-bond strength was measured using various computational methods and the tools best suited to evaluate this interaction were identified. This chapter similarly concerns itself with the σ-donating ability of divalent carbon compounds. The C-H bond of 81 different azolium cations have been examined, the significant expansion in the examined set of molecules arising from inclusion of a large number of molecules for which the value of some experimental descriptor of σ-donation has been recorded. Although a large variety of experimental parameters are regularly used to quantify the σ-donation or total electron donation of carbenes and carbones, we focus on two NMR based descriptors – $^{1}J_{C\text{-}H}$ coupling constant and Huynh's electronic parameter (HEP) as these are plentiful in literature and can also be calculated computationally. Other than this, several theoretically calculated parameters like proton affinity, energy of the sp^2 hybridised lone pair, energy associated with σ donation from ETS-NOCV analysis have been computed and compared with the above-mentioned experimental descriptors.

4.1. Introduction

Divalent carbon compound, like N-Heterocyclic carbenes (NHC) and carbones have been prized for their electron donating ability in chemistry for a very long time. Initially NHCs were believed to be purely σ-donors.[1-4] However, subsequent studies have established that they have non-negligible π-acceptor properties,[5-8] and when the situation is conducive, they even have the ability to act as π-donors.[9, 10] The latter has been extensively illustrated in Chapter II of the thesis for divalent carbon compound-borenium adducts. The inherent symmetry and relative simplicity of the system chosen for the study, makes it easier to separate and understand the σ and π interactions from one another. However, this is not a general case. In most cases the stereo electronic properties measured are a cumulative effect of multiple interactions in the molecule, including orbital relaxations (σ-donation/back-donation, π-donation/back-donation, etc.), steric repulsion or dispersion.

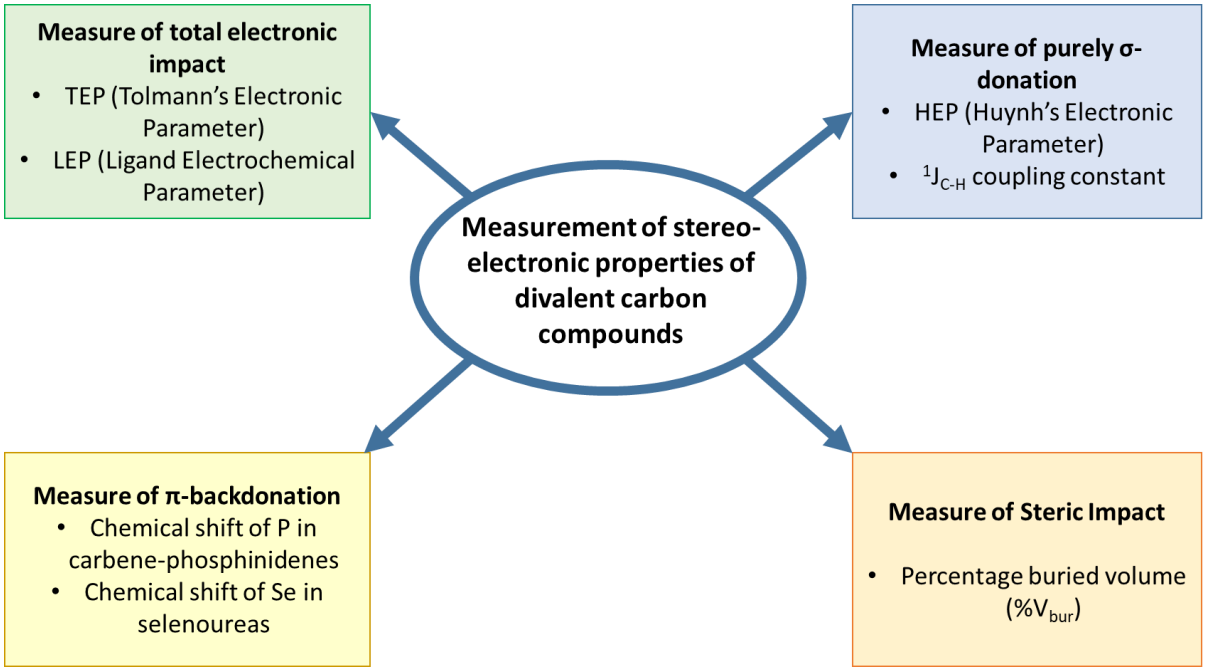

Figure 4-1: Classification of various experimental methods of measuring stereo-electronic properties of divalent carbon compounds

The vastly varying electronic properties of divalent carbon compounds need to be ordered as different electronic environments are suitable for different applications.[11, 12] Over the years various experimental techniques as well as theoretical approaches have been developed to quantify these electronic properties (Figure 4-1). These techniques can be roughly classified based on the property they quantify, although as mentioned before, it is not always possible

to completely segregate the various interaction in a molecule. Some descriptors quantify only the steric impact of the divalent carbon compound, some quantify the 'net' electron donation including both σ and π effects while some other parameters are supposed to classify only the σ donation or π-backdonation (Figure 4-1). In the following segment we take a brief look at these various descriptors.

4.1.1. Experimental Methods

i. Percent buried volume ($\%V_{bur}$)

Developed by Nolan, Cavallo and co-workers, the 'percent buried volume' parameter is used as a measure of the steric impact of NHCs and carbones.[13-15] Contrary to phosphines, the other class of very popular ligands used in organometallic complexes, the NHCs do not coordinate in a 'cone-shaped' manner. Instead, the substituents point towards the metal centre, creating a greater steric impact. Therefore, the Tolman cone angle, commonly used to measure the steric impact of phosphines, is not reliable to characterize NHC and has been replaced by $\%V_{bur}$ which is defined as the percentage of a sphere occupied, or, 'buried' by the ligand on coordination to a metal located at the centre of the sphere. This value can be obtained from X-Ray crystallographic data or theoretical calculation on the free carbene, an organometallic complex of the carbene or from its azolium salt (i.e. its protonated form). However, care must be taken to compare results only from similar sources.

ii. Tolman Electronic Parameter (TEP)

The Tolman electronic parameter had also been originally designed to measure the electron donating ability of phosphine ligands but it is equally applicable in the cases of divalent carbon compounds like NHCs and carbones.[16] This approach is based on the change in the stretching frequency of the carbonyl ligand (CO) in $[Ni(CO)_3L]$ tetrahedral complex due to change in the electronic properties of L.

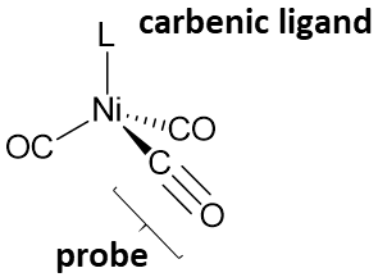

Figure 4-2: Complex studied to measure Tolman electronic parameter

The CO group, which is a very strong π-acceptor, is quite sensitive to the total electron density on the metal centre which engages in metal to carbonyl back-bonding. Naturally, the stronger the ligand L is as an electron donor, the greater the weakening of the C≡O triple bond, lowering its stretching frequency. In addition to the sensitivity of the CO group another advantage of this method is the ease of preparing $[Ni(CO)_3L]$ complexes (L = phosphine or NHC). The drawback of this method is the high toxicity of $Ni(CO)_4$, from which the $[Ni(CO)_3L]$ is synthesised. Therefore, alternative approaches using cis-$[MX(CO)_2(L)]$ (X = halide) where M = Rhodium(I) or Iridium(I) have been suggested.[17-20] Disparity in recorded values using any of these complexes may arise due to resolution of spectrometer used and solvent.[21, 22]

iii. Huynh's Electronic Parameter (HEP)

Huynh's method [23-25] of quantifying electronic properties of NHCs (as well as other ligands) utilises another spectroscopic method – nuclear magnetic resonance (NMR) spectroscopy. This method is based on the ^{13}C NMR chemical shift analysis of trans-$[Pd(Br)_2(^iPr_2\text{-Bimy})L]$ complex. The chemical shift of the carbene carbon of the $^iPr_2$-Bimy reporter ligand is influenced by the nature of the trans-standing ligand of interest, L, in the complex. Therefore, by recording the chemical shift of the carbene carbon on the reporter carbene, the electron donating ability of the ligand L can be measured. It has been found that a stronger donating ligand induces a downfield shift of the probe nucleus while a weak donor results in an upfield shift.

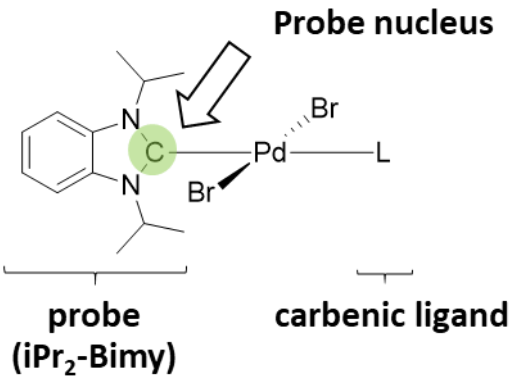

Figure 4-3: Typical HEP complex

This behaviour can be rationalised by considering the following, rather technical, point:[24] The carbene atoms of free NHCs generally exhibit downfield signals > 200 ppm. The magnitude of the downfield shift is approximately inversely proportional to the singlet-triplet (S-T) energy gap, i.e. the likeliness for an S-T transition by promoting an electron from the σ (NHC-lone pair) to the initially vacant p_π orbital of the NHC.[26] This process has the strongest contribution to the paramagnetic shielding term, which in turn leads to the downfield shift. Thus, an NHC with large S-T separation (e.g. unsaturated imidazolin-2-ylidenes) would exhibit smaller chemical shift compared to those with a smaller S-T gap (e.g. saturated imidazolidin-2-ylidene). Now, the metal coordination of NHCs occur via donation of their carbene lone pair, therefore removing the possibility of the S-T transition completely. This is why a significant upfield shift of the carbene atom is observed upon complexation. In light of this knowledge, let us consider the complex trans-[Pd(Br)$_2$(^{i}Pr$_2$-Bimy)L] (Figure 4-3). A stronger trans donor L would weaken the Pd-^{i}Pr$_2$-Bimy bond more effectively, leading to a larger contribution of "free" ^{i}Pr$_2$-Bimy character, which leads to a downfield shift.

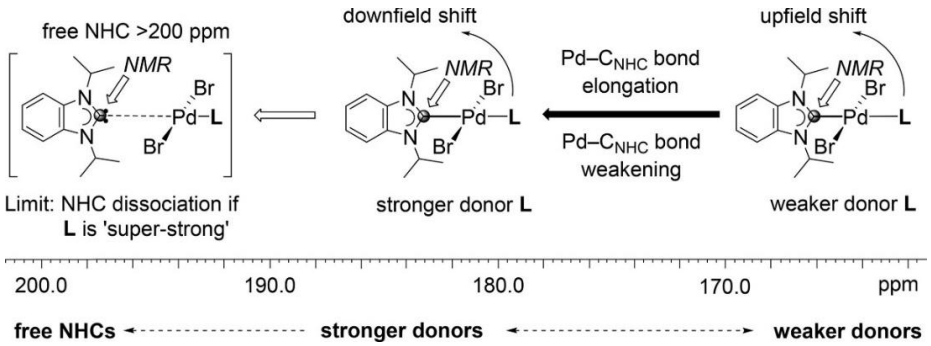

Figure 4-4: Mechanism of determination of Huynh's electronic parameter, the figure has been taken from Huynh's review[24]

This scaling method is relatively young and to ensure the validity of comparisons all complex probes have been measured in $CDCl_3$ while also making sure the $CDCl_3$ solvent signal appears at 77.7 ppm in all cases. This makes the HEP scale quite uniform and thus easy to compare with other measures of donating ability of ligands. In cases where the Pd(II) complexes cannot be synthesised, alternative gold(I) probe [Au($^{i}Pr_2$-Bimy)L] can be synthesised and a simple equation exists that allows the conversion between the two scales.[27] Another important feature of HEP is that because it utilises Pd(II) metal centre, which is a strong Lewis acid, metal to ligand back-donation is virtually insignificant. Therefore, it has been claimed that the HEP essentially measures the σ-donating ability of the ligands.[25]

iv. $^{1}J_{C\text{-}H}$ Heteronuclear Coupling Constants of Azolium Salts

The most recent method to evaluate electronic properties of NHCs also utilises ^{13}C NMR spectroscopy. Ganter proposed that the $^{1}J_{C\text{-}H}$ coupling constant of azolium salts, which is the complex of the NHC with a proton (H^+), could indicate the σ-donating ability of the respective NHCs.[6] The magnitude of the $^{1}J_{C\text{-}H}$ coupling constants which is related to the s-character of the C-H bond is inversely proportional to the σ-donor strength of the NHC.[24, 28, 29] This means that a weak σ-donor has a large coupling constant and a strong σ-donor has a small coupling constant. Only a few instances of recorded data exist in this regard.[6, 30-35] The simplicity of forming a complex with a proton offers the further advantage of avoiding any additional interactions like π-donations or back-donations which are almost always present in transition metal complexes of NHCs. This means that the only orbital interaction present is a σ-donation from the NHC to the H^+.

However, the data reveals that the azolium salts investigated differ in counteranion and the analyses were done in different deuterated solvents. Both of these factors can possibly affect the C-H coupling constants of the azolium salts.[36] Nevertheless, this method holds promise for the ease of access to the azolium salts.

v. Lever Electronic Parameter (LEP)

Introduced by Alfred Beverley Philip Lever in 1990, this method uses electrochemistry to determine the electronic properties of ligands.[37] This is called

the ligand electrochemical parameter, E_L. The thermodynamics of the oxidation/reduction undergone by the metal centre while coordinated to the ligand determines the magnitude of E_L. It is determined by measuring the redox potential of $Ru^{2+/3+}$ metal complexes containing the ligand of interest, although other metals have also been tried.[38] The E_L values do not exactly measure the ligand's donor strength, but reflect the ability of different ligands to stabilise different oxidation states of a metal. A ligand with small E_L value stabilises more strongly the high oxidation state of the metal (Ru^{3+}) than one with a larger E_L value. Therefore, the E_L value is somewhat indirectly related to ligand donor strength.[39]

This method has generally been applied to classical Werner type ligands e.g. H_2O, NH_3, Cl^-, CN^- while there are relatively few examples involving NHCs. The redox potentials for NHC-ruthenium complexes[40-42] are too few to have a detailed comparison of the various NHCs. However, significantly more data is available for rhodium and iridium complexes. Comparing this data allows the determination of remote substituent effects on the donating ability of N,N'-diaryl substituted imidazolin and imidazolidin-2-ylidenes and also corroborates that saturated imidazolidin-2-ylidenes are stronger donor than unsaturated imidazolin-2-ylidenes.

This method too has its shortcomings – it can be applied only to reversible or quasi-reversible redox processes and it cannot be applied to redox non-innocent ligands. This limits its application to NHCs and other divalent carbon compounds.

vi. NMR Spectroscopy of Carbene-Phosphinidene Adducts and Selenourea

The use of ^{31}P chemical shift in carbene-phosphinidene adducts to measure the π-accepting ability of a carbene was suggested by Bertrand and co-workers in 2013.[7] Inspired by Bertrand, Ganter suggested the use of ^{77}Se NMR chemical shift of much easily synthesizable selenourea for the same purpose the same year.[6] The idea behind using these complexes is that they can be represented by two extreme resonance forms – **A** and **C**.

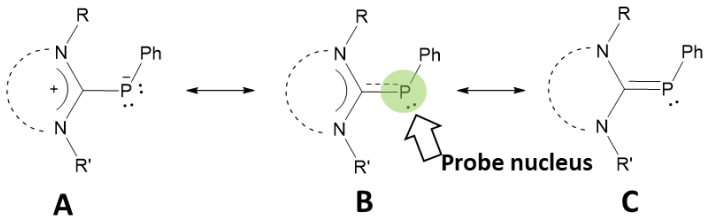

Resonance forms of Carbene-phosphinidene adducts

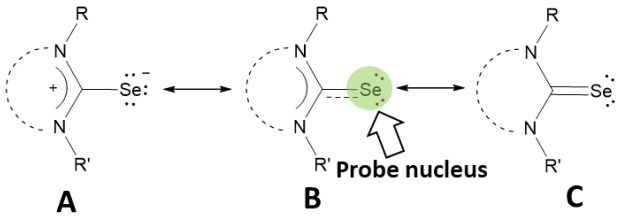

Resonance forms of selenourea

Figure 4-5: Resonance forms of carbene-phosphinidene adducts and selenoureas

The resonance form **A** shows primarily σ-donation and the form **C** has both significant σ-donation and π-backdonation. A strong π-acceptor is expected to have a greater contribution of resonance form **C** than a weaker π-acceptor. Therefore, for a strong π-acceptor, the P or Se nucleus is expected to be more deshielded leading to a downfield shift of the respective signals.

4.1.2. Theoretical Methods

There are various theoretical methods that can be used to quantify the sigma donor ability of divalent carbon compounds which are only briefly touched upon in this section. The most common parameter to measure C-H bond strength is proton affinity, which is calculated as the difference of electronic energy between the protonated and free divalent carbon compound. The formulation of proton affinity implies that this energy term includes the energy of geometric distortion. Geometric parameters like bond length and bond index give some notion of the strength of C-H bond that is formed. Methods to measure the σ-donor strength is to evaluate the energy of the σ lone pair. These factors have been discussed in greater detail with respect to the molecules we have studied in section 4.4.

In the previous chapter we computed the strength of the C→B π bond using a variety of theoretical methods only. In this chapter our objective is to achieve something similar with respect to the σ-donating ability of carbenes and carbones i.e., we calculate the sigma donating ability of divalent carbon compounds using various parameters and compare them

to see if they quantify the same chemical entity or not. Moreover, this time we focused on theoretical calculation of experimentally measured parameters with respect to σ-donation of these compounds. The sigma donating ability for these molecules is measured with respect to the simplest Lewis acid, H^+ because other than being easy to calculate, carbene-H^+ adducts, also referred to as azolium cations, have been investigated extensively in chemistry and a lot of experimental data recording their characteristics are available in chemical literature (*vide infra*). In addition, the corresponding Huynh's complexes have also been investigated to characterise the carbene-Pd bond and the σ-donating ability with respect to these complexes. Large number of experimental data means there will be larger number of molecules for our case study.

Of the various experimental methods described above, two methods based on NMR spectroscopy, have been included in our comparisons – the $^1J_{C\text{-}H}$ coupling constant and Huynh's electronic parameter (HEP). This is because the NMR chemical shifts of Huynh's complexes and coupling constants of C-H bonds of azolium salts both claim to quantify σ-donating ability of carbenes. These experimental descriptors have been compared with each other and the various theoretical descriptors as well in an attempt to arrive at a unified description of the σ-donating ability of carbenes/carbones.

4.2. Geometry Optimisation and NMR Calculation

For this chapter the results pertaining to a total of 81 different protonated divalent carbon compounds (**X**-H^+) have been presented (Scheme 4-2, Page 140-142). The list of divalent carbon compounds selected for this study include molecules **1**-**39** studied previously in (**X** = **38** was not included because **X**-H^+ could not be optimised) and molecules for which experimental parameters are available. 20 molecules originate from Ganter's paper (**X** = **40**-**59**),[6] 16 molecules from Huynh's papers (**X** = **60**-**75**)[23, 27, 43-45] and 7 molecules from other publications that have reported experimental results for azolium salts (X = **76**-**81**).[6, 30-35] The additional molecules explored in this study have been included as experimental data measuring their σ-donation capacity (i.e., $^1J_{C\text{-}H}$ coupling constant and HEP) are available for these molecules while such data is present only for 3 instances in our previous set. The molecules and their protonated forms have been optimised, as in the previous chapter, at B3LYP/TZVP level of theory using Gaussian09[46] and population analysis has been conducted

using NBO6 program at the same level.[47, 48] The energy decomposition analysis for the C-H bond has been conducted using the ADF2017 package[49, 50] at B3LYP/TZ2P level.

The σ-donating ability of the divalent carbon compounds is expected to be related to the nature (more specifically the electronegativity) of the neighbouring atoms (Y) as well the Y-C-Y bond angles as well as the total charge of the molecules. Keeping these factors in mind, we have introduced a nomenclature for the set of azolium cations explored in this chapter that help to highlight the most important features of the molecules, based on which they have been classified into different categories. Based on other differences in the molecules put in the same category following the previous scheme, they have been further divided into subcategories. Some examples of this nomenclature have been shown in Scheme 4-1.

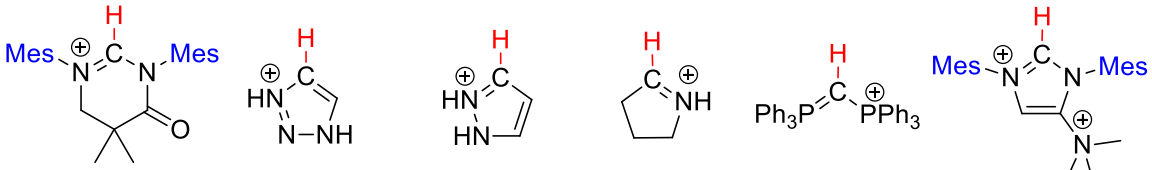

54 NN6 **13** NC5a **10** NC5b **3** NC5c **36** LL0 **81** NN5a+

Scheme 4-1: Some exemplary **X**-H$^+$ studied in this chapter and the classes they belong to

The nomenclature consists of 3 to 4 characters – the first two are capitalised letters, the third is a number and the fourth character, when present, is a small letter (a, b or c). The first two letters indicated the atoms α to the carbene carbon in the case of carbenes and for carbones these are indicated specifically by the uppercase L, and the number indicates the size of ring containing the carbene carbon (a 0 is used for acyclic molecule), the fourth lowercase alphabet indicates different subcategories of carbenes belonging to the same group according to the first three characters. Sometimes an additional charge is present indicating that the molecule actually has +2 charge instead of the usual +1 of azolium salts of neutral carbenes. For example, the code 'NN6' indicates a carbene with two α-nitrogen atoms in a 6-member ring, such as **X** = **54**. Similarly 'NC5a' indicates a 5-member carbene with the carbene carbon flanked by one nitrogen and one carbon on either side and a indicates that the carbene is a 1,2,3-triazolin-5-ylidene derivative whereas 'NC5b' indicates a carbene derived from 1,2-diethylindazolin-3-ylidene, such as **X** = **10**. In all, there are a total of 16 categories and 20 subcategories among the molecules studied in this chapter.

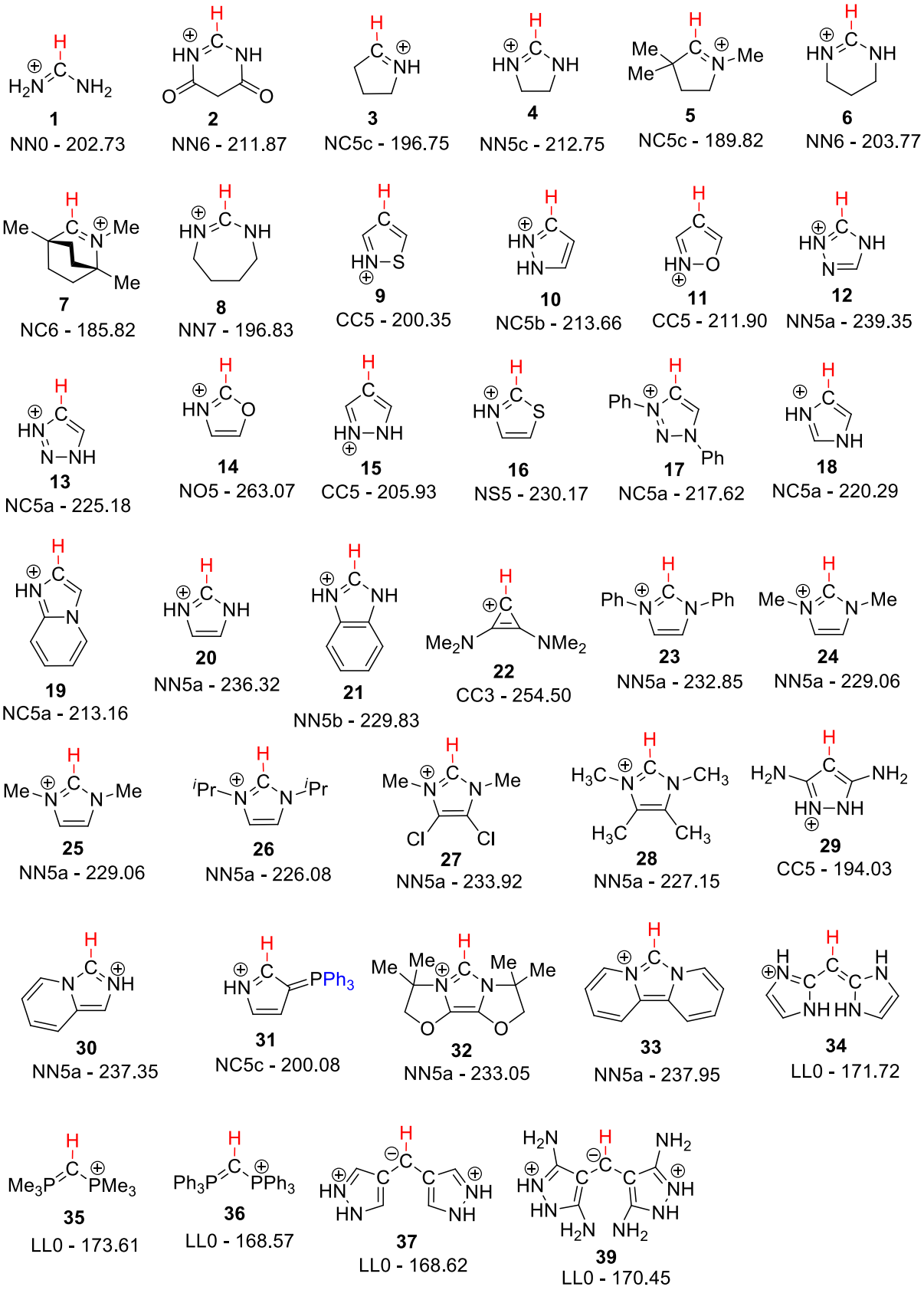

Scheme 4-2: **X**-H$^+$ molecules included in this work with given nomenclature and calculated $^1J_{C\text{-}H}$ coupling constant in ppm at the B3LYP/(aug)-cc-pVTZ//B3LYP/TZVP level (**X** = **1** -**39**) (continued on next page)

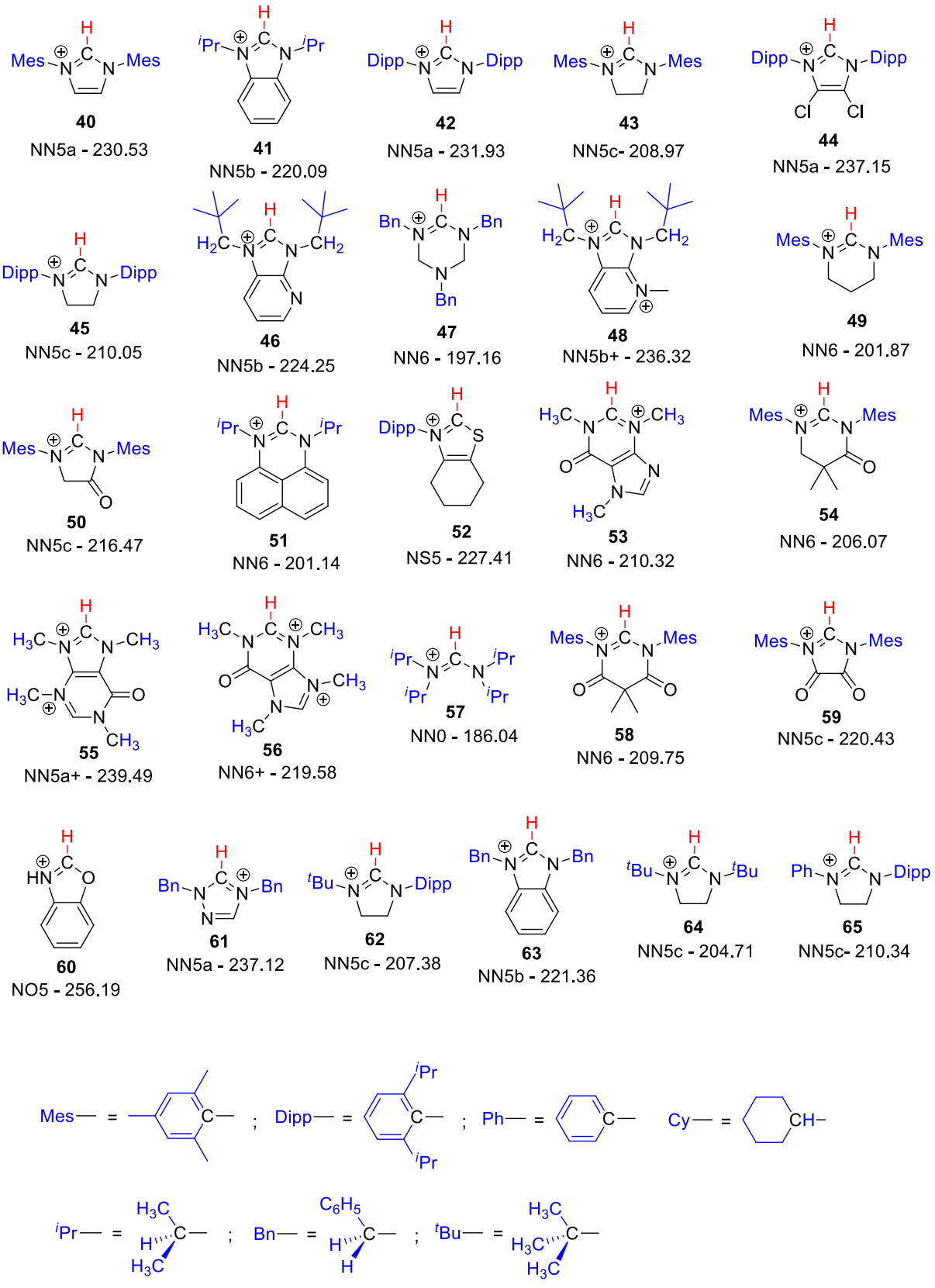

Scheme 4-2: **X**-H$^+$ molecules included in this work with given nomenclature and calculated $^1J_{C\text{-}H}$ coupling constant in ppm at the B3LYP/(aug)-cc-pVTZ//B3LYP/TZVP level (**X** = **40** -**65**) (continued on next page)

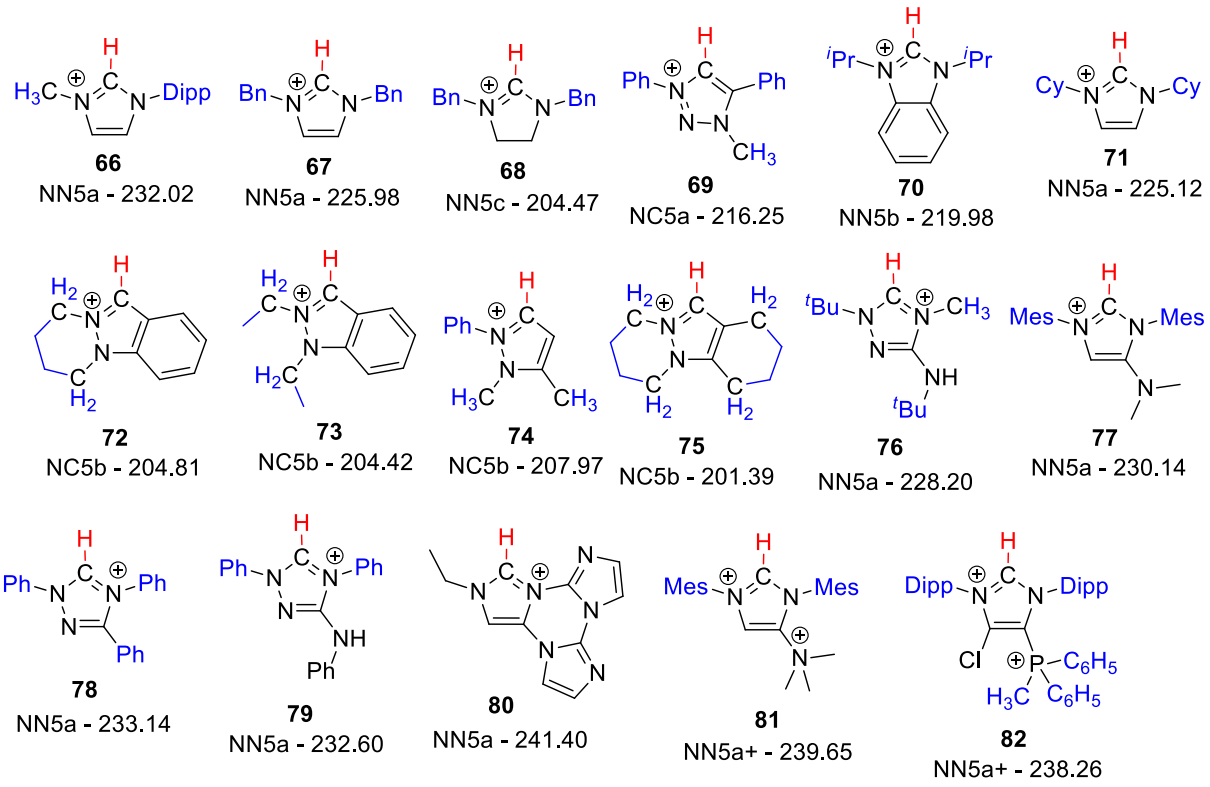

Scheme 4-2: **X**-H$^+$ molecules included in this work with given nomenclature and calculated $^1J_{C\text{-}H}$ coupling constant in ppm at the B3LYP/(aug)-cc-pVTZ//B3LYP/TZVP level (**X** = **66**-**82**)

NMR calculation have been performed using Gaussian 09 suit of programs. Large basis sets such as aug-CC-pVTZ[51] are required for accurate NMR calculations. However, NMR calculations can be quite computationally demanding and often for experimentally realistic molecules which have very large substituents the SCF convergence is difficult to reach, rendering the complete calculation intractable. Consequently, the difficulty of carrying out all NMR calculations with the aug-cc-pVTZ basis, as envisaged, led us to adapt the size of the basis set used. Most often, the substituents fulfil a steric role and their contribution to the electronic environment of the centre at which electron density is being calculated is minimal. With this in mind, it is therefore conceivable to approximate the electronic behaviour of the large substituents by modelling them at an accuracy lesser than that used for the centre at which the isotropic shielding or coupling constant is being measured. This corresponds to the locally dense basis set (LDBS) approximation.[52-54] In our study, for the azolium cations without substituents corresponding to 39 cases (**X** = **1**-**30**, **32**-**39**, **60**, **80**), all the atoms have been treated with a full basis set, i.e., their NMR isotropic shielding and coupling constants have been calculated at B3LYP/aug-CC-pVTZ level. For the rest of the molecules the LDBS approximation has been made, where all atoms of substituents of the carbene ring, except

the linkage atom, have been treated with the cc-pVTZ basis set while the rest of the atoms have been treated using aug-cc-pVTZ. The atoms treated with complete aug-cc-pVTZ basis set are shown in black and red and those treated with the cc-pVTZ basis set have been shown in blue in schemes 4-2 and 4-3. This level of calculation will be noted B3LYP/(aug)-cc-pVTZ hereafter. For a moderately sized **X**-H$^+$ molecule where **X** = **26**, this LDBS approximation reduces the number of atomic orbitals from 1390 (full aug-cc-pVTZ basis set) to 963 ((aug)-cc-pVTZ basis set), making the calculation for all molecules feasible.

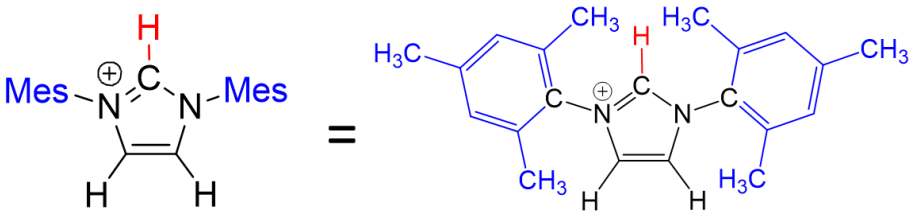

Scheme 4-3: An example of applying locally dense basis set (LDBS) in **X**-H$^+$ (**X** = **40**), the atoms in black and red are calculated with the aug-cc-pVTZ basis set and those in blue are calculated with cc-pVTZ.

The effects of this approximation have been quantified. For 9 **X**-H$^+$ molecules (**X** = **5**, **7**, **17**, **23**, **26**-**28**, **32**, **35**) which are neither too large nor too small (number of atoms in the set ranging from 28 to 68 and number of atomic orbitals ranging between 963 and 2,212 after applying the LDBS approximation), the ^{1}H NMR isotropic shielding of the proton attached to the carbene carbon (H in red in Scheme 4-2) and the $^1J_{C\text{-}H}$ coupling constant of the corresponding C-H bond has been calculated using the full aug-cc-pVTZ basis set as well as applying the LDBS approximation (Scheme 4-4). The root mean square deviation (RMSD) of the isotropic shielding calculated by the two methods is found to be 0.0026 ppm while that for the $^1J_{C\text{-}H}$ coupling constant has been found to be 0.014 Hz – showing that the LDBS approximation induces negligible errors in the calculation. This is demonstrated in the following scheme 4-4.

Molecules	^{13}C Isotropic shielding		$^{1}J_{C-H}$ coupling constant	
X-H^{+}	B3LYP/aug-cc-pVTZ	B3LYP/(aug)-cc-pVTZ	B3LYP/aug-cc-pVTZ	B3LYP/(aug)-cc-pVTZ
X	(ppm)	(ppm)	(Hz)	(Hz)
17	23.21	23.21	217.62	217.64
26	23.73	23.72	226.08	226.09
35	31.16	31.17	173.61	173.65
28	23.87	23.87	227.15	227.15
27	23.85	23.85	233.92	233.92
23	23.37	23.37	232.85	232.87
32	24.50	24.51	233.05	233.08
7	22.82	22.82	185.82	185.82
5	23.51	23.51	189.82	189.81

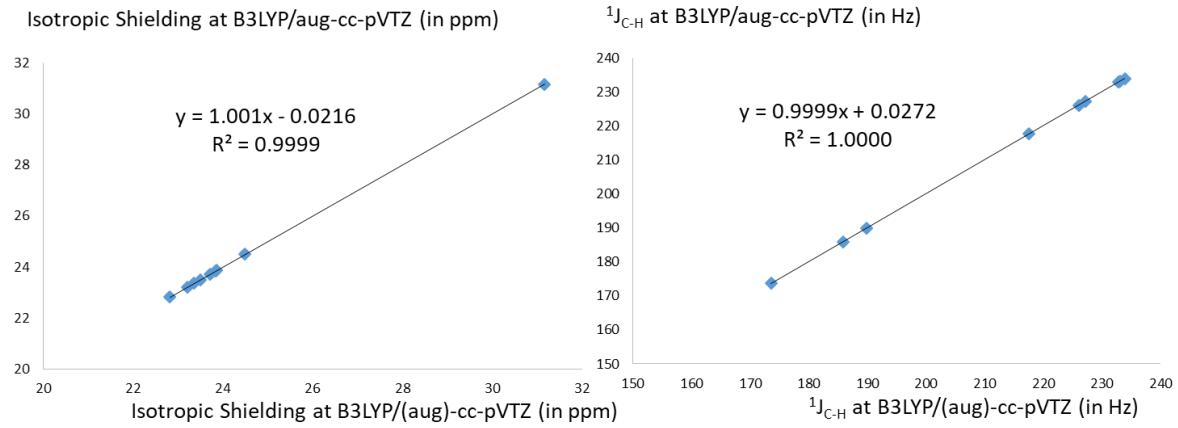

Scheme 4-4 Theoretically calculated values of ^{13}C chemical shift and $^{1}J_{C-H}$ coupling constants using LDBS approximation (B3LYP/(aug)-cc-pVTZ) and complete basis set (B3LYP/aug-cc-pVTZ).

The second step was to ensure that the results that are obtained through theoretical calculation is corroborated by experimental results. This has been performed for all azolium cations, corresponding to **X**-H^{+} (**X** = **33**, **40** – **44**, **47**, **49**, **52** – **56**, **76** – **82**), for which both experimental chemical shift of the carbene carbon and $^{1}J_{C-H}$ coupling constant are available from literature.[6] Two sets of calculations were made at the B3LYP/(aug)-cc-pVTZ level, including solvent effect or without it. Solvent effect has been introduced with the polarizable continuum model PCM for DMSO or $CHCl_3$ depending on the solvent used experimentally for each cation. The theoretical values were correlated with the experimental results. The quality of correlation is quite good for the estimation of both the isotropic shielding (R^2 = 0.97-0.98; Figure 4-6) and coupling constant (R^2 = 0.93-0.96), being slightly better in the presence of solvent effect in each case. The larger discrepancy is observed for $^{1}J_{C-H}$ values of 4 molecules (**X** =**41**, **52**, **53**, **56**) for which the same experimental value has been provided ($^{1}J_{C-H}$ = 218 ppm). All attempts to reproduce this result have failed. In fact, it has been noted that 4 molecules

with very different chemical environment having the same $^{1}J_{C\text{-}H}$ coupling constants seems unlikely.[24]

These results validate our approach to compute chemical shift and coupling constant in azolium salts and give confidence to the reliability of our results from DFT based theoretical predictions. The reliable prediction of $^{1}J_{C\text{-}H}$ by DFT is the basis to further comparing this property with other experimental and theoretical properties presented in this chapter.

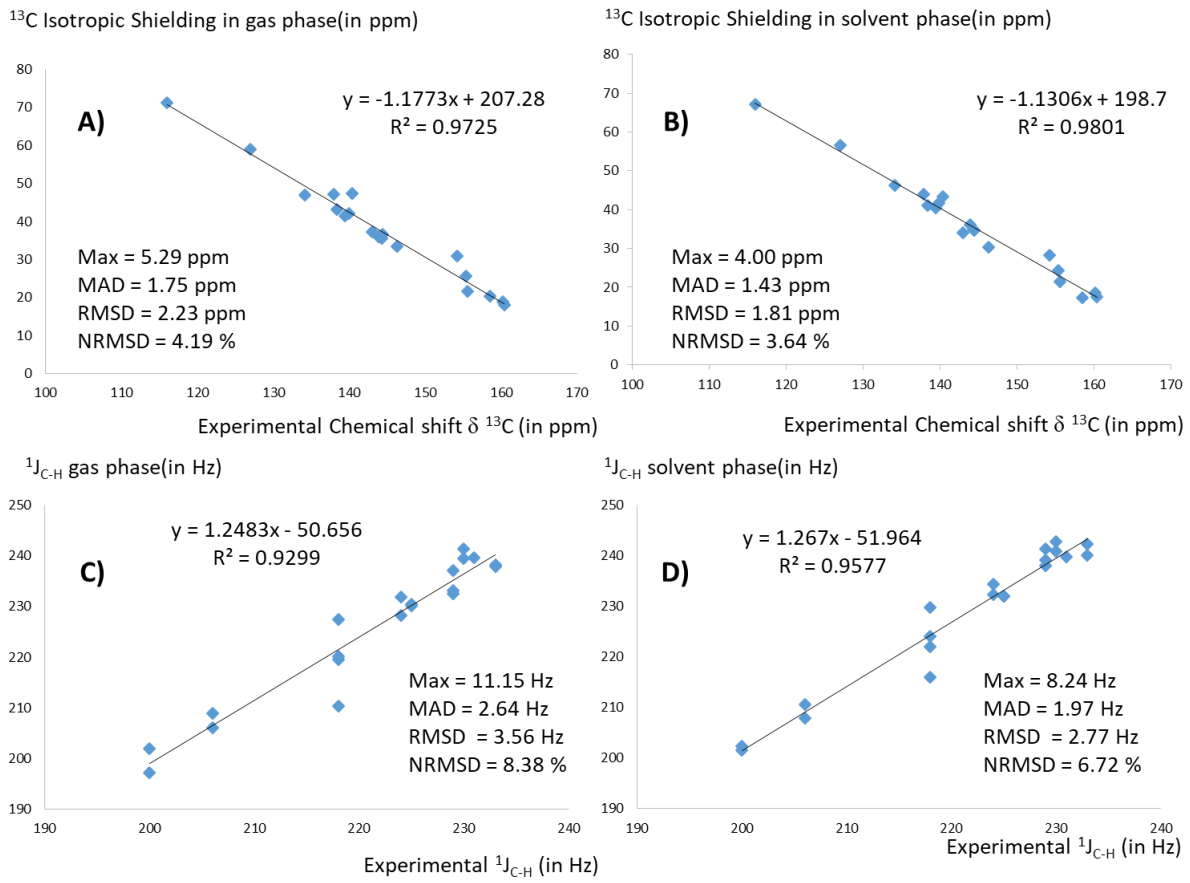

Figure 4-6: Correlation between experimental and theoretical NMR parameters – ^{13}C chemical shift of carbene carbon in **X**-H^{+} and $^{1}J_{C\text{-}H}$ coupling constant of the $C_{carbene}$-H bond in gas phase and condensed phase for **X** = **33, 40** – **44, 47, 49, 52** – **56, 76** – **82**

4.3. $^1J_{C\text{-}H}$ vs. Huynh Electronic Parameter (HEP)

Like the $^1J_{C\text{-}H}$ coupling constant of the previous section, Huynh's electronic Parameter (HEP) is another experimental measure of the σ-donating ability. However, only in very few case both the C-H coupling constant and the HEP have been recorded, which makes comparing the experimental data from these two parameters almost impossible. For the set of molecules considered in this study, only in three cases (**X** = **40**, **42**, **43**) both HEP and experimentally recorded $^1J_{C\text{-}H}$ coupling constants are available. While computing $^1J_{C\text{-}H}$ coupling constant is quite straight forward and reliable, computing the HEP values pertaining to a molecule is rather complicated because of the involvement of the metal centre (Pd^{2+}) as well as the larger size of the system. Therefore, we propose to theoretically calculate the $^1J_{C\text{-}H}$ values for the molecules for which experimental HEP values have been documented and compare the two parameters that claim to describe the same property. Thus, the coupling constants for 21 **X**-H^+ molecules (**X** = **26**, **40**, **42 – 43**, **45**, **60 – 75**) have been calculated in condensed phase (PCM($CHCl_3$)), applying LDBS approximation where necessary. The correlation between theoretical $^1J_{C\text{-}H}$ coupling constant and the reported experimental HEP values unfortunately shows very poor correlation (R^2 = 0.304). Clearly, the Huynh electronic parameter and C-H coupling constant do not correlate with each other and do not actually indicate the same chemical property.

In order to understand the differences between C-H and C-Pd bond, ETS-NOCV calculations were performed for both azolium cations and Pd-complexes. It was seen that the σ donation measured by ETS-NOCV analysis of the $C_{carbene}$-H bond in azolium cations does not correlate with the σ-donation of the $C_{carbene}$-Pd bond of the corresponding HEP complexes (R^2 = 0.1191 Figure 4-7 A). Similarly, no correlation exists between the energy of interaction (E_{int}), calculated from EDA analysis using ADF software, for the $C_{carbene}$-H bond and $C_{carbene}$-Pd bond (R^2 = 0.0048, Figure 4-7). This indicates that the C-H bond and the C-Pd bond are fundamentally different in character (R^2 = 0.0048). However, one cannot conclude if one or either of these parameters unequivocally denote σ-donating ability of **X** without further investigation.

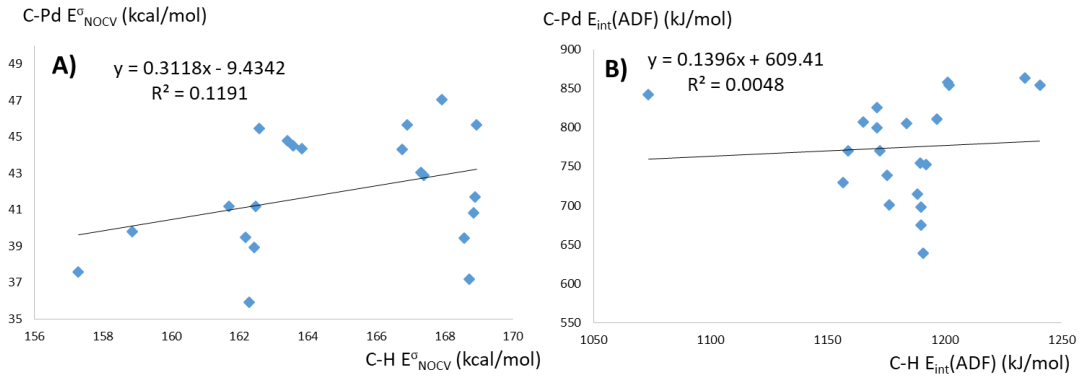

Figure 4-7: Correlation of different descriptors of σ-bond strength involving the $C_{carbene}$ atom in azolium salt and Pd complexes

A closer inspection of the correlation between $^{1}J_{C\text{-}H}$ and HEP reveals some more insight about the $^{1}J_{C\text{-}H}$ coupling constant and its dependence on the s-character of the C-H σ-bond and has been discussed later. Identifying the individual carbenes in Figure 4-8 A, to analyse the correlation between the C-H coupling constant and HEP further, reveals that carbenes belonging to the same category as defined in Section 4.2 cluster together. The combination of α-atoms to the carbene carbon ($C_{carbene}$), denoted by the letter 'Y', shows that the least electronegative combination, (N and C) are found at the top left corner of the graph, while the most electronegative combination, (N and O) is at the diametrically opposite bottom right corner. The more electronegative combination of atoms forces more s-character into the C-H bond, thus leading to stronger C-H bond and higher $^{1}J_{C\text{-}H}$ value.

Further, the unsaturated carbenes (green) are at the bottom left corner while the ones with aromatic stabilisation are located more to the right. As a result of the different levels of aromaticity of the carbenic ring, the C-C bond opposite to $C_{carbene}$ has different bond orders and therefore bond lengths, leading to a change in the Y-C-Y bond angle (Y = α-atom to $C_{carbene}$ like N, O, C) as well. This is one of the important factors that can change the hybridisation of $C_{carbene}$ and consequently, the s-character of the carbene lone pair. Indeed, in each individual subcategory (NN5a, NN5b and NN5c; NC5a and NC5b) of graph A a decreasing trend Y-C-Y bond angle has been observed (Figure 4-8 B) in line with an increase of the $^{1}J_{C\text{-}H}$ coupling constant. Therefore, one may say that $^{1}J_{C\text{-}H}$ coupling constant is influenced by the electronegativity of the atom α to $C_{carbene,}$ i.e., Y and the Y-C-Y bond angle – both of which are cumulatively reflected in the s character of the carbene lone pair. However, the correlations in the various subcategories are not perfect, possibly due to the existence of other factors

(eg. steric bulk of the substituents on Y etc.). Understanding the HEP on the other hand proves to be more complicated and it has been discussed further in the next section.

A combination of the two experimental methods of quantifying σ-bond strength, $^{1}J_{C\text{-}H}$ and HEP, while not correlated with each other, successfully categorise the 21 molecules that have been separated into non-overlapping categories in the chemical space defined by these two parameters. The $^{1}J_{C\text{-}H}$ coupling constant shows a very narrow range of variation for each category while their HEP values are widely spaced out. This perhaps reflects a greater sensitivity of the HEP scale towards ring substituents than the $^{1}J_{C\text{-}H}$ scale. The same characteristic is revealed in the comparison between the C-H and C-Pd σ-bonds, where C-Pd bonds show greater variation in value compared to C-H bonds. Further investigation is necessary to understand these aspects of $^{1}J_{C\text{-}H}$ and HEP scales.

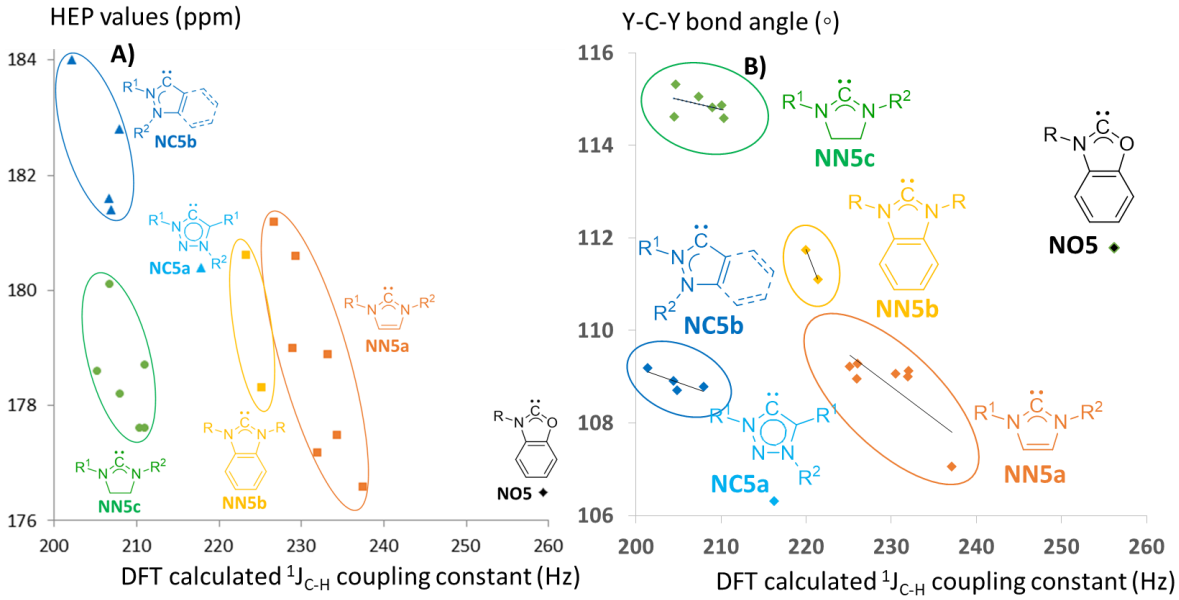

Figure4-8: Correlation between (A) two indicators of σ-donation – experimental Huynh's electron parameter (HEP) and calculated $^{1}J_{C\text{-}H}$ coupling constant and (B) Y-C-Y bond angle with $^{1}J_{C\text{-}H}$ coupling constant.

4.4. Understanding Huynh's Electronic Parameter using ETS-NOCV Analysis

We use ETS-NOCV analysis to understand HEP by studying the various energetic components of the **X**-Pd bond and Probe-Pd bond (Figure 4-3) for the same 21 molecules as in the previous section. Geometries optimization of all Pd complexes have been performed at the ωB97XD/def2-SVP level. This level has been selected as it gives the best results, compared to several levels of calculation tested out. The root mean square deviation of various geometric parameters calculated for a test set of 5 molecules (**X** = **64**, **67**, **70**, **71**, **74**) has been calculated at these various levels (Figure 4-9). ωB97XD/def2-SVP gives reasonably low RMSD for the parameters tested.

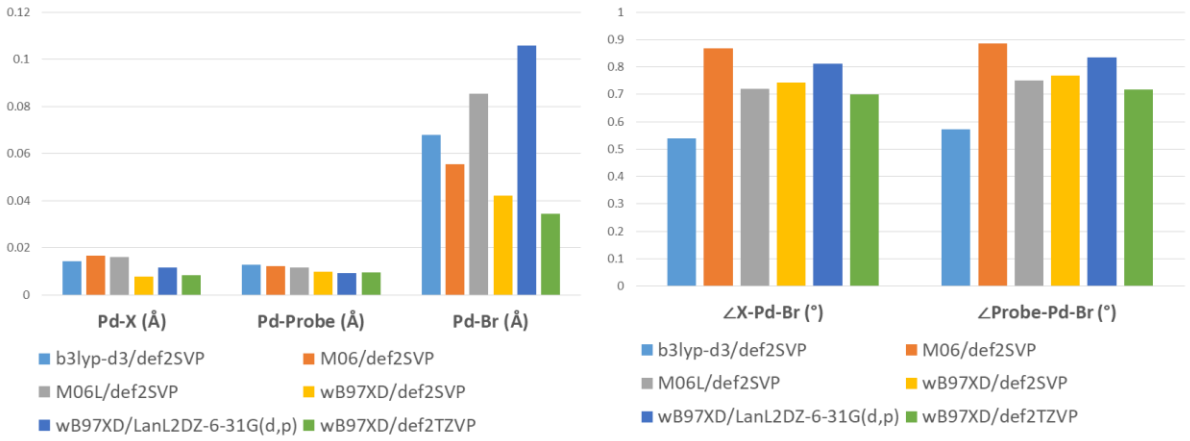

Figure 4-9: Bar graph comparing the RMSD of geometric parameters (x-axis) from experimental values, according to various levels of computation

The ETS-NOCV single point calculations have been performed at both B3LYP/TZ2P level as well as M06/TZ2P level to account for potential errors due to dispersion effects. The first two NOCVs arising from the orbital interaction component of the **X**-Pd bond have been illustrated in the figure below. The first component, denoted by E^{σ}_{NOCV}(**X**-Pd), clearly indicates the σ-donation from **X** to Pd^{2+} (average = 49.2 kcal/mol) while the second component, denoted by E_{pol}, represents a combination of π-back-donation and polarisation interaction and remains almost constant (average = 6.6 kcal/mol) for all the molecules. A similar ETS-NOCV analysis is conducted with the NHC-Probe bond as well (Figure 4-10 C and D). It should be noted that the strength of polarisation is not altogether insignificant in this case, however the σ donation is the primary interaction. The energy of σ-donation from **X** to Pd^{2+} correlates well with the energy of σ-donation from Pd^{2+} to the probe, denoted by E^{σ}_{NOCV}(Pd-Probe) (Figure 4-10 E).

This correctly reflects the HEP hypothesis – the stronger the donation for the NHC, the weaker the donation for the probe. At least for these E_{σ}^{NOCV} interactions, either functional – B3LYP and M06 no significant differences. The results presented here are from the B3LYP/TZ2P level of calculation. As HEP claims to measure purely the σ-donation of **X** to Pd, we expected to find a correlation between E^{σ}_{NOCV}(**X**→Pd) and the HEP values. However, only a moderate correlation was obtained with an R^2 value of 0.72 (Figure 4-10 F). Particularly significant deviations are observed for **X** = **66** and **75**, although the reason for this is not quite clear to us yet. Excluding these points leads to a large improvement in R^2 value, which rises to 0.88. At the same time, it should be noted that the R^2 coefficient is a parameter that is highly sensitive to the range of values included in the correlation. It is notoriously difficult to obtain high R^2 values for a small range of values as is the case for HEP.

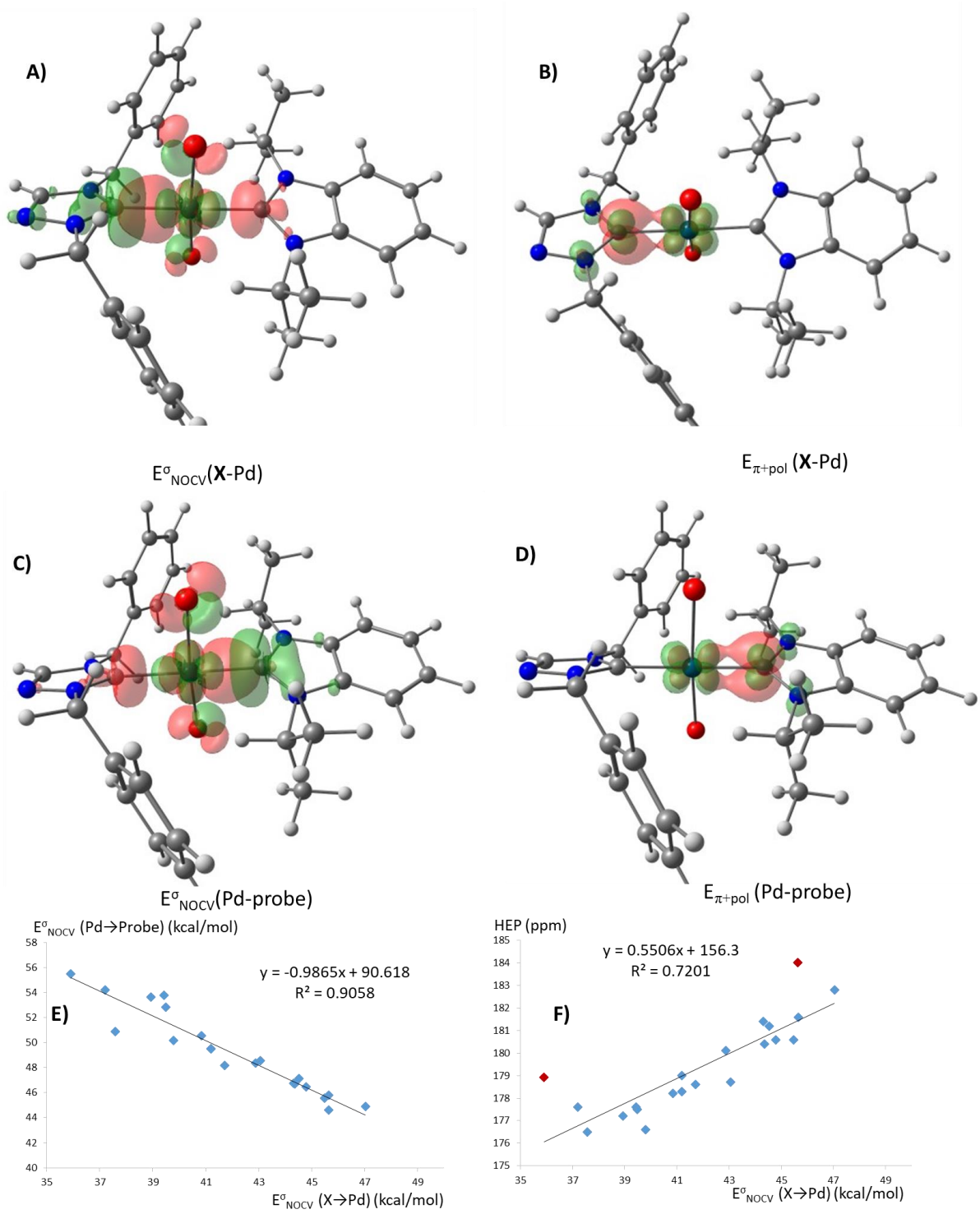

Figure 4-10: A) and B) represent deformation density associated with orbital interaction in HEP complexes for **X**-Pd bond (**X** = **30**). C) and D) represent the same with respect to the Pd-probe bond. The charge flow of electron density is green → red. Isosurface value = 0.003; E) and F) represent correlations between various elements of ETS-NOCV analysis of the HEP complexes and HEP values.

4.5. $^1J_{C-H}$ vs. Other Theoretical Descriptors of σ-donation

We have shown above that $^1J_{C-H}$ and HEP do not correspond to the same chemical property and find that HEP approximately describes the σ-donation as measured by NOCV analysis. To better understand what $^1J_{C-H}$ describe, in this section, we tried to identify which theoretically calculated property can be related to them. We therefore decide to compare them with other computed parameters describing in one way or another the strength of the sigma donation. This has been done for all the 81 molecules indicated in scheme 4-2.

Various theoretical parameters can be related to the σ-donating ability of divalent carbon compounds studied. The selected ones are presented below:

- The strength of the C-H bond resulting from the protonation of a divalent carbon compound **X** is expected to be linked to the σ-donation ability of **X**, through its carbon lone pair, with respect to the simplest Lewis acid, H^+. The electronic energy of the C-H bond has been calculated by two approaches; (i) the interaction energy (E_{int}), or vertical deprotonation energy, has been obtained using both ADF (at B3LYP/TZ2P level) and Gaussian 09 (electronic energies of optimised geometries of **X**-H^+ and associated single point calculations of **X** at B3LYP/TZVP level). Both levels give very similar values and only B3LYP/TZVP values will be discussed; (ii) the proton affinity (E_{PA} = E(**X**-H^+) – E(**X**)), or relaxed protonation energy, also calculated at the B3LYP/TZVP level. The geometric distortion to form a proton adduct being small (average value 24.8 kJ/mol) compared to the C-H bond strength, as expected, the proton affinity and interaction energy are very strongly correlated (R^2 = 0.9965, Figure 4-11A).
- ETS-NOCV analysis allows to extract the σ-donation component, E^{σ}_{NOCV}, from the orbital interaction energy. This amounts to remove from the interaction energy between **X** and the Lewis acid the electrostatic interaction term, the Pauli repulsion term and the other orbital interaction terms. When the Lewis acid is the proton, the Pauli repulsion term is zero and the other orbital interaction terms are much smaller compared to the σ-interaction and almost invariant. The correlation between the NOCV energy of σ-donation for the $C_{carbene}$-H bond in **X**-H^+ shows poor correlation with the proton affinity (R^2 = 0.24), illustrating that the studied compounds present very different values for the electrostatic interaction (Figure 4-11C).

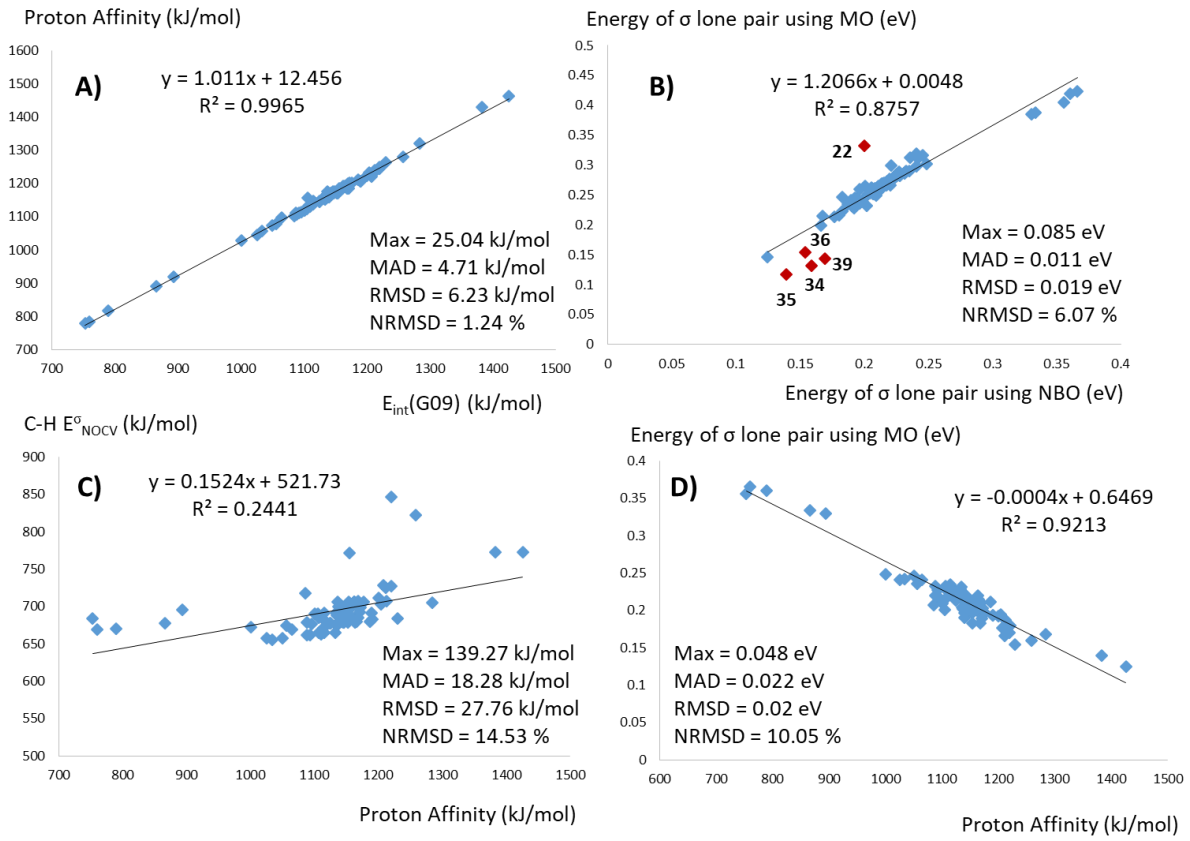

Figure 4-11: Correlations between different theoretical descriptors of σ-donation

- Another descriptor of the σ-donation ability is the energy of the σ-lone pair of **X**, which most often constitutes the largest component of the highest occupied molecular orbital (HOMO) or HOMO-1 orbital of **X**. Therefore, we used the HOMO/HOMO-1 energy (E_{HOMO}), as applicable, calculated at the B3LYP/TZVP level as a descriptor of the sigma donation capability. To consider the molecular (i.e. possibly delocalized) character of the HOMO, we also use the NBO approach to obtain the energy of the localized σ lone pair of the $C_{carbene}$ atom. These two methods are not equivalent as demonstrated by the less than perfect correlation (R^2 = 0.88, Figure 4-11 B) between these two methods. The greatest deviations are observed for **X** = **22**, **34**, **35**, **36**, **39** and deleting them, the R^2 value rises to 0.96. Of these **X** = **34**, **35**, **36** and **39** are carbones where the α-atom to $C_{carbene}$ is P or C, which are less electronegative than N/O found in the other cases. According to Bent's rule, the lower electronegativity of the α-atoms, increases the p-character of the carbene lone pair, thus increasing its energy and making it more reactive. Note that in the graphs the energy of the lone pair as calculated from MO and NBO have both been expressed as positive values for the sake of clarity – this means higher energy indicates greater stability. For **X** = **22**,

the $C_{carbene}$ is part of a highly strained 3-membered ring. Again, following Bent's rule, the smaller ring size forces the lone pair to have higher s-character this time, making it more stable. Although it is not clear why, these effects are possibly not similarly accounted for according to the two methods of calculating the energy of the σ lone pair, which leads to the deviation observed.

- Finally, we also measured with the NBO approach the hybridization of the C-H bond of **X**-H^+ as well as the hybridization of the sigma lone pair of **X**. The percentage of s character of the C-H bond ($\%s_{C-H}$) and those of the sigma lone-pair ($\%s_{LP}$) show the expected trend but the correlation is unsatisfactory (R^2 = 0.62, not shown).

Comparing these different parameters shows that they describe different characteristics of the divalent carbon compounds with respect to σ-bonding. This is illustrated by the comparison between the proton affinity and the energy of lone pair from MO analysis. The correlation is fairly good (R^2 = 0.92) in this case while no other significant correlation with E^{σ}_{NOCV} and these parameters are observed. From these correlations we can identify two different categories among the various theoretically calculated sigma bond descriptors studied – there is $E^{\sigma}_{NOCV,}$ which is the measure of σ-donation purely from an orbital point of view and there is the C-H bond strength which correlates with the energy of carbene lone pair and gives an idea of the total σ interaction, including the electrostatic component.

Can any of these parameters be linked to $^1J_{C-H}$?

The C-H coupling constant, $^1J_{C-H}$, has been compared with these various theoretical descriptors. The $^1J_{C-H}$ for the 81 molecules has been calculated in gas phase, as in the case of all the other quantities. In each case the correlations are quite poor (R^2 = 0.32 – 0.56). (Figure 4-12) This indicates that the C-H coupling constant does not correlate with any of the indicators of σ-donating ability of **X**.

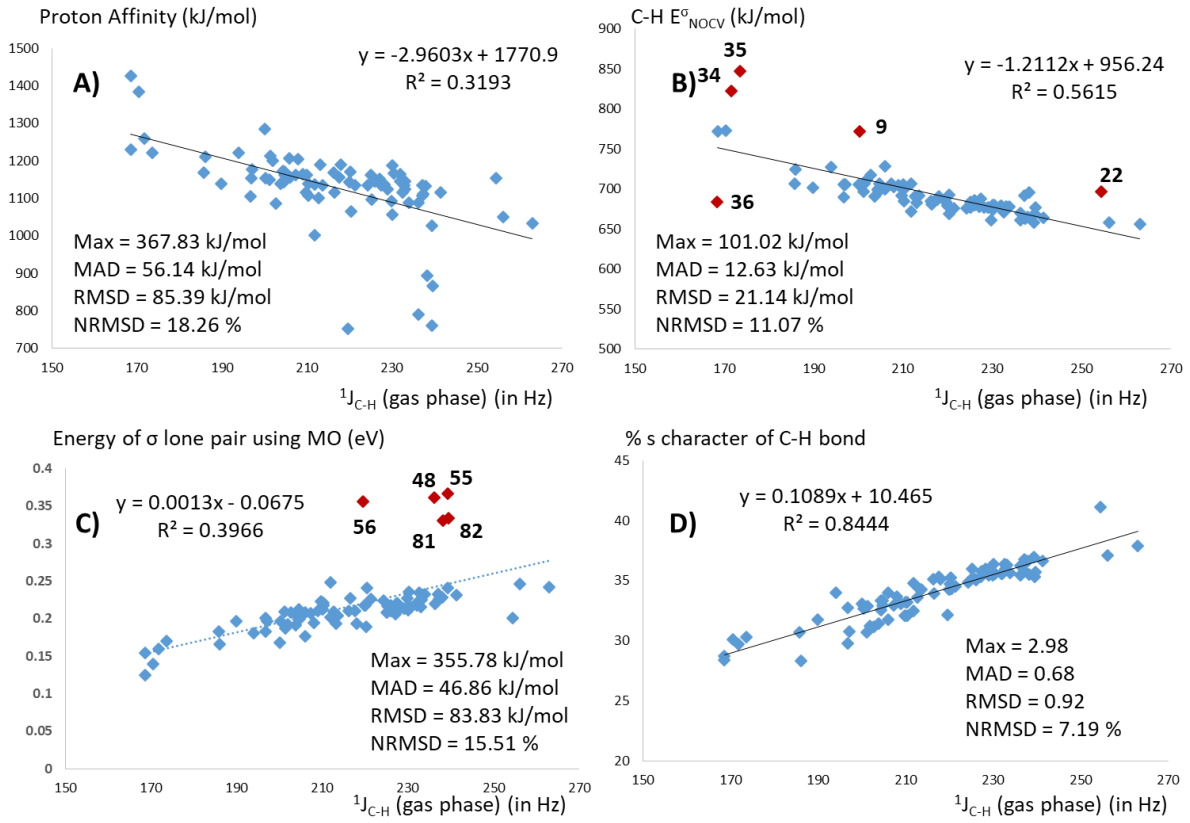

Figure 4-12: Correlation of $^{1}J_{C\text{-}H}$ with various other computed parameters

In Figure 4-12, graphs B and C, some clear deviants exist, which lie far away from the common trend. For graph B, deleting these deviating points (represented by red squares) which correspond to **X** = **9**, **22**, **34**, **35** and **36** improves correlation up to $R^2 = 0.74$, however a rational explanation for such deletion is yet to be offered. For graph C, the outliers are represented by **X** = **48**, **55**, **56**, **81** and **82**, which are all dipositive azolium cations. Deleting these points increases R^2 to 0.67. Such analysis was not done for Graph A which presents too many deviating points. In spite of significant improvement for graphs B and C, the final result is not good enough to conclude that either pair of parameters compared correspond to a common chemical entity. The coupling constant is known to be dependent on the s-character of the C-H bond due to high dependence on Fermi contact term on s-character.[6] The % s character of the C-H bond was computed from NBO analysis and indeed $^{1}J_{C\text{-}H}$ correlates with it ($R^2 = 0.84$). We proceed to take a closer look at the correlation between $^{1}J_{C\text{-}H}$ and %s character of the C-H bond. On identifying the individual carbenes, smaller groups of carbenes with related structures can again be identified. These groups show a stronger correlation (higher R^2 value) between $^{1}J_{C\text{-}H}$ and %s character of C-H bond. The identified groups, most of which have been

defined in Chapter I, are listed below along with the symbols used in Figure 4-13 to identify them:

i. Carbones (orange solid squares)
ii. cAACs (grey solid triangles)
iii. Saturated NHC with 5 member ring backbone (yellow cross)
iv. Saturated NHCs with 6-member ring backbone (blue asterix)
v. Arduengo carbenes (green solid dots)
vi. Abnormal/Mesoionic carbenes (red crosses)
vii. Remote carbenes (pink hollow squares)
viii. Dipositive **X**-H^{2+} (yellow solid squares)
ix. Unassigned (grey dots)

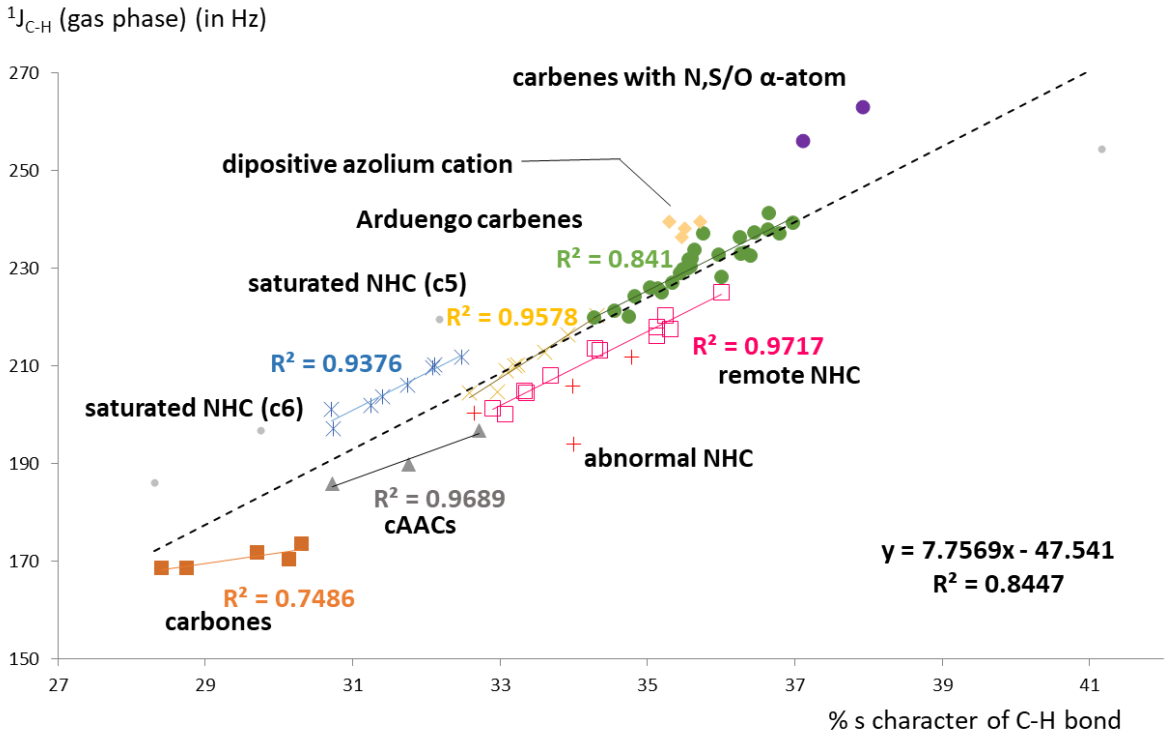

Figure 4-13: Correlation between $^1J_{C-H}$ and %s character

Some simple yet rewarding chemical observation can be made from this analysis about the factors that influence $^1J_{C-H}$ coupling constant which are congruous with our previous observations with a smaller subset of these molecules. We see that as the ring size decreases, the %s character of the C-H bond increases following Bent's rule. Again saturated NHCs, such as cAACs, saturated 5 and 6 member NHCs have lower s character of C-H bonds and smaller

$^1J_{C\text{-}H}$ coupling constants. The electronegativity of the α-atom also plays a role – when the α-atom pair is a less electronegative combination, e.g., in the case of cAACs as well as remote NHCs (combination of C and N in each), the $^1J_{C\text{-}H}$ coupling constant is lower due to lower s-character of the C-H bond compared to NHCs with a more electronegative combination of atoms (like N,O or N,S), indicated by purple dots. Finally, charge also plays a crucial role as we see higher charge makes the C-H bond stronger and the $^1J_{C\text{-}H}$ coupling constant automatically registers a higher value than the average. It must be noted, in each individual subgroup, the correlations are quite good with higher R^2 values (R^2 = 0.75 – 0.97) than the overall R^2 for the 81 molecules. The individual groups also form lines almost parallel to the overall correlation, showing that the nature of variation of $^1J_{C\text{-}H}$ and %s character in each of the cases are not drastically different. Due to the large variety of compounds chosen for the study, there are some molecule that cannot really be included in any of the subgroups and have been indicated as such by grey dots.

4.6. Conclusion

This chapter arises as a natural consequence of the previous one – if π-donation of carbenic compounds can be evaluated and compared using computational tools, can σ-donation be evaluated as well? And also, can we comment on the efficiency of computational tools in calculating experimentally recorded descriptors? A myriad of parameters are available to measure the stereo-electronic effects of ligands, however, it is not clear which of them indicate *only* the σ-donor strength and if all these methods are equivalent. Two such experimental descriptors include HEP and $^1J_{C\text{-}H}$ coupling constant. A handful of theoretical methods are also available to evaluate σ-donor strength, like, proton affinity, energy of σ-lone pair, energy of σ-transfer etc.

- The C-H coupling constant, $^1J_{C\text{-}H}$, as well as ^{13}C chemical shift have been calculated and found to correlate with experimentally recorded values. This proves the reliability of theoretically calculated NMR parameters.
- A comparison of $^1J_{C\text{-}H}$ and HEP reveals that although both these experimental parameters claim to measure the same chemical entity – σ-donation – they do not correlate with each other. $^1J_{C\text{-}H}$ shows variation with respect to the electronegativity of the atoms α to carbenes as well as the angle they form with $C_{carbene}$. The

dependence of HEP on structural parameters is more nuanced and correlates with the orbital component of the bond.

- Finally, $^{1}J_{C\text{-}H}$ is compared with the theoretical measures of σ-bond but it is found to have significant correlation only with the %s character of the C-H bond for the set of 81 molecules. The molecules of similar structural features form subsets where the correlation is stronger

The content of this chapter, which does not pertain directly to the carbene-borenium story successfully highlights the disparity between various experimental and theoretical σ-bond descriptors as each of them represent some different aspect of the bond and cannot be used interchangeably.

References

1. Lummiss, J. A. M.; Higman, C. S.; Fyson, D. L.; McDonald, R.; Fogg, D. E., The divergent effects of strong NHC donation in catalysis. *Chemical Science* **2015,** *6* (12), 6739-6746.
2. Antonova, N. S.; Carbó, J. J.; Poblet, J. M., Quantifying the Donor−Acceptor Properties of Phosphine and N-Heterocyclic Carbene Ligands in Grubbs' Catalysts Using a Modified EDA Procedure Based on Orbital Deletion. *Organometallics* **2009,** *28* (15), 4283-4287.
3. Gaggioli, C. A.; Bistoni, G.; Ciancaleoni, G.; Tarantelli, F.; Belpassi, L.; Belanzoni, P., Modulating the Bonding Properties of N-Heterocyclic Carbenes (NHCs): A Systematic Charge-Displacement Analysis. *Chemistry – A European Journal* **2017,** *23* (31), 7558-7569.
4. Hopkinson, M. N.; Richter, C.; Schedler, M.; Glorius, F., An overview of N-heterocyclic carbenes. *Nature* **2014,** *510* (7506), 485-496.
5. Vummaleti, S. V. C.; Nelson, D. J.; Poater, A.; Gómez-Suárez, A.; Cordes, D. B.; Slawin, A. M. Z.; Nolan, S. P.; Cavallo, L., What can NMR spectroscopy of selenoureas and phosphinidenes teach us about the π-accepting abilities of N-heterocyclic carbenes? *Chemical Science* **2015,** *6* (3), 1895-1904.
6. Liske, A.; Verlinden, K.; Buhl, H.; Schaper, K.; Ganter, C., Determining the π-Acceptor Properties of N-Heterocyclic Carbenes by Measuring the 77Se NMR Chemical Shifts of Their Selenium Adducts. *Organometallics* **2013,** *32* (19), 5269-5272.
7. Back, O.; Henry-Ellinger, M.; Martin, C. D.; Martin, D.; Bertrand, G., 31P NMR Chemical Shifts of Carbene–Phosphinidene Adducts as an Indicator of the π-Accepting Properties of Carbenes. *Angewandte Chemie International Edition* **2013,** *52* (10), 2939-2943.
8. Rodrigues, R. R.; Dorsey, C. L.; Arceneaux, C. A.; Hudnall, T. W., Phosphaalkene vs. phosphinidene: the nature of the P–C bond in carbonyl-decorated carbene → PPh adducts. *Chemical Communications* **2014,** *50* (2), 162-164.
9. Rezabal, E.; Frison, G., Estimating π binding energy of N-Heterocyclic carbenes: The role of polarization. *Journal of Computational Chemistry* **2015,** *36* (8), 564-572.
10. Gupta, R.; Rezabal, E.; Hasrack, G.; Frison, G., Comparison of Chemical and Interpretative Methods: the Carbon–Boron π-Bond as a Test Case**. *Chemistry – A European Journal* **2020,** *26* (71), 17230-17241.
11. Jones, W. D., Diverse Chemical Applications of N-Heterocyclic Carbenes. *Journal of the American Chemical Society* **2009,** *131* (42), 15075-15077.
12. Munz, D., Pushing Electrons—Which Carbene Ligand for Which Application? *Organometallics* **2018,** *37* (3), 275-289.
13. Clavier, H.; Nolan, S. P., Percent buried volume for phosphine and N-heterocyclic carbene ligands: steric properties in organometallic chemistry. *Chemical Communications* **2010,** *46* (6), 841-861.
14. Gómez-Suárez, A.; Nelson, D. J.; Nolan, S. P., Quantifying and understanding the steric properties of N-heterocyclic carbenes. *Chemical Communications* **2017,** *53* (18), 2650-2660.
15. Dorta, R.; Stevens, E. D.; Scott, N. M.; Costabile, C.; Cavallo, L.; Hoff, C. D.; Nolan, S. P., Steric and Electronic Properties of N-Heterocyclic Carbenes (NHC): A Detailed Study on

Their Interaction with Ni(CO)4. *Journal of the American Chemical Society* **2005,** *127* (8), 2485-2495.
16. Tolman, C. A., Steric effects of phosphorus ligands in organometallic chemistry and homogeneous catalysis. *Chemical Reviews* **1977,** *77* (3), 313-348.
17. Doyle, M. J.; Lappert, M. F.; Pye, P. L.; Terreros, P., Carbene complexes. Part 18. Synthetic routes to electron-rich olefin-derived monocarbenerhodium(I) neutral and cationic complexes and their chemical and physical properties. *Journal of the Chemical Society, Dalton Transactions* **1984,** (11), 2355-2364.
18. Herrmann, W. A.; Elison, M.; Fischer, J.; Köcher, C.; Artus, G. R. J., N-Heterocyclic Carbenes: Generation under Mild Conditions and Formation of Group 8–10 Transition Metal Complexes Relevant to Catalysis. *Chemistry – A European Journal* **1996,** *2* (7), 772-780.
19. Denk, K.; Sirsch, P.; Herrmann, W. A., The first metal complexes of bis(diisopropylamino)carbene: synthesis, structure and ligand properties. *Journal of Organometallic Chemistry* **2002,** *649* (2), 219-224.
20. Lavallo, V.; Canac, Y.; Präsang, C.; Donnadieu, B.; Bertrand, G., Stable Cyclic (Alkyl)(Amino)Carbenes as Rigid or Flexible, Bulky, Electron-Rich Ligands for Transition-Metal Catalysts: A Quaternary Carbon Atom Makes the Difference. *Angewandte Chemie International Edition* **2005,** *44* (35), 5705-5709.
21. Dröge, T.; Glorius, F., The Measure of All Rings—N-Heterocyclic Carbenes. *Angewandte Chemie International Edition* **2010,** *49* (39), 6940-6952.
22. Nelson, D. J.; Nolan, S. P., Quantifying and understanding the electronic properties of N-heterocyclic carbenes. *Chemical Society Reviews* **2013,** *42* (16), 6723-6753.
23. Huynh, H. V.; Han, Y.; Jothibasu, R.; Yang, J. A., 13C NMR Spectroscopic Determination of Ligand Donor Strengths Using N-Heterocyclic Carbene Complexes of Palladium(II). *Organometallics* **2009,** *28* (18), 5395-5404.
24. Huynh, H. V., Electronic Properties of N-Heterocyclic Carbenes and Their Experimental Determination. *Chemical Reviews* **2018,** *118* (19), 9457-9492.
25. Teng, Q.; Huynh, H. V., A unified ligand electronic parameter based on 13C NMR spectroscopy of N-heterocyclic carbene complexes. *Dalton Transactions* **2017,** *46* (3), 614-627.
26. Tapu, D.; Dixon, D. A.; Roe, C., 13C NMR Spectroscopy of "Arduengo-type" Carbenes and Their Derivatives. *Chemical Reviews* **2009,** *109* (8), 3385-3407.
27. Guo, S.; Sivaram, H.; Yuan, D.; Huynh, H. V., Gold and Palladium Hetero-Bis-NHC Complexes: Characterizations, Correlations, and Ligand Redistributions. *Organometallics* **2013,** *32* (13), 3685-3696.
28. Ratajczyk, T.; Pecul, M.; Sadlej, J.; Helgaker, T., Potential Energy and Spin−Spin Coupling Constants Surface of Glycolaldehyde. *The Journal of Physical Chemistry A* **2004,** *108* (14), 2758-2769.
29. Autschbach, J.; Le Guennic, B. J., Analyzing and Interpreting NMR Spin–Spin Coupling Constants Using Molecular Orbital Calculations. *Journal of Chemical Education*. **2007,** *84* (1), 156.

30. Thie, C.; Bruhn, C.; Leibold, M.; Siemeling, U. J. M., Coinage Metal Complexes of the Carbenic Tautomer of a Conjugated Mesomeric Betaine Akin to Nitron. **2017,** *22* (7), 1133.
31. Ruamps, M.; Lugan, N.; César, V., A Cationic N-Heterocyclic Carbene Containing an Ammonium Moiety. *Organometallics* **2017,** *36* (5), 1049-1055.
32. Thie, C.; Hitzel, S.; Wallbaum, L.; Bruhn, C.; Siemeling, U., Coinage metal complexes of the carbenic tautomer of Nitron. *Journal of Organometallic Chemistry* **2016,** *821*, 112-121.
33. Buck, D. M.; Kunz, D., Triazine Annelated NHC Featuring Unprecedented Coordination Versatility. *Organometallics* **2015,** *34* (21), 5335-5340.
34. Weiss, R.; Reichel, S.; Handke, M.; Hampel, F., Generation and Trapping Reactions of a Formal 1:1 Complex between Singlet Carbon and 2,2′-Bipyridine. *Angewandte Chemie International Edition* **1998,** *37* (3), 344-347.
35. Schwedtmann, K.; Schoemaker, R.; Hennersdorf, F.; Bauzá, A.; Frontera, A.; Weiss, R.; Weigand, J. J., Cationic 5-phosphonio-substituted N-heterocyclic carbenes. *Dalton Transactions* **2016,** *45* (28), 11384-11396.
36. Barfield, M.; Johnston, M. D., Solvent dependence of nuclear spin-spin coupling constants. *Chemical Reviews* **1973,** *73* (1), 53-73.
37. Lever, A. B. P., Electrochemical parametrization of metal complex redox potentials, using the ruthenium(III)/ruthenium(II) couple to generate a ligand electrochemical series. *Inorganic Chemistry* **1990,** *29* (6), 1271-1285.
38. Lever, A. B. P., Electrochemical parametrization of rhenium redox couples. *Inorganic Chemistry* **1991,** *30* (9), 1980-1985.
39. Fielder, S. S.; Osborne, M. C.; Lever, A. B. P.; Pietro, W. J., First-Principles Interpretation of Ligand Electrochemical (EL(L)) Parameters. Factorization of the .sigma. and .pi. Donor and .pi. Acceptor Capabilities of Ligands. *Journal of the American Chemical Society* **1995,** *117* (26), 6990-6993.
40. Savka, R. D.; Plenio, H., A hexahydro-s-indacene based NHC ligand for olefin metathesis catalysts. *Journal of Organometallic Chemistry* **2012,** *710*, 68-74.
41. Moerdyk, J. P.; Bielawski, C. W., Olefin Metathesis Catalysts Containing N,N′-Diamidocarbenes. *Organometallics* **2011,** *30* (8), 2278-2284.
42. Moerdyk, J. P.; Bielawski, C. W., Alkyne and Reversible Nitrile Activation: N,N′-Diamidocarbene-Facilitated Synthesis of Cyclopropenes, Cyclopropenones, and Azirines. *Journal of the American Chemical Society* **2012,** *134* (14), 6116-6119.
43. Furfari, S. K.; Gyton, M. R.; Twycross, D.; Cole, M. L., Air stable NHCs: a study of stereoelectronics and metallorganic catalytic activity. *Chemical Communications* **2015,** *51* (1), 74-76.
44. Meier, M.; Tan, T. T. Y.; Hahn, F. E.; Huynh, H. V., Donor Strength Determination of Benzoxazolin-2-ylidene, Benzobisoxazolin-2-ylidene, and Their Isocyanide Precursors by 13C NMR Spectroscopy of Their PdII and AuI Complexes. *Organometallics* **2017,** *36* (2), 275-284.
45. Wu, W.; Teng, Q.; Chua, Y.-Y.; Huynh, H. V.; Duong, H. A., Iron-Catalyzed Cross-Coupling Reactions of Arylmagnesium Reagents with Aryl Chlorides and Tosylates: Influence

of Ligand Structural Parameters and Identification of a General N-Heterocyclic Carbene Ligand. *Organometallics* **2017,** *36* (12), 2293-2297.

46. M.J. Frisch, G.W. Trucks, H.B. Schlegel, G.E. Scuseria, M.A. Robb, J.R. Cheeseman, G. Scalmani, V. Barone, B. Mennucci, G.A. Petersson, H. Nakatsuji, M. Caricato, X. Li, H.P. Hratchian, A.F. Izmaylov, J. Bloino, G. Zheng, J.L. Sonnenberg, M. Hada, M. Ehara, K. Toyota, R. Fukuda, J. Hasegawa, M. Ishida, T. Nakajima, Y. Honda, O. Kitao, H. Nakai, T. Vreven, J.A. Montgomery Jr, J.E. Peralta, F. Ogliaro, M. Bearpark, J.J. Heyd, E. Brothers, K.N. Kudin, V.N. Staroverov, R. Kobayashi, J. Normand, K. Raghavachari, A. Rendell, J.C. Burant, S.S. Iyengar, J. Tomasi, M. Cossi, N. Rega, J.M. Millam, M. Klene, J.E. Knox, J.B. Cross, V. Bakken, C. Adamo, J. Jaramillo, R. Gomperts, R.E. Stratmann, O. Yazyev, A.J. Austin, R. Cammi, C. Pomelli, J.W. Ochterski, R.L. Martin, K. Morokuma, V.G. Zakrzewski, G.A. Voth, P. Salvador, J.J. Dannenberg, S. Dapprich, A.D. Daniels, Ö. Farkas, J.B. Foresman, J.V. Ortiz, J. Cioslowski, D.J. Fox, Gaussian, Inc., Wallingford CT, Gaussian 09, Revision D.01, **2013**.

47. Glendening, E. D.; Landis, C. R.; Weinhold, F., Natural bond orbital methods. *Wiley Interdisciplinary Reviews-Computational Molecular Science* **2012,** *2* (1), 1-42.

48. Glendening, E. D.; Landis, C. R.; Weinhold, F., NBO 6.0: Natural bond orbital analysis program. *Journal of Computational Chemistry* **2013,** *34* (16), 1429-1437.

49. ADF2017, S., Theoretical Chemistry, Vrije Universiteit, Amsterdam, The Netherlands, http://www.scm.com.

50. te Velde, G.; Bickelhaupt, F. M.; Baerends, E. J.; Fonseca Guerra, C.; van Gisbergen, S. J. A.; Snijders, J. G.; Ziegler, T., Chemistry with ADF. *Journal of Computational Chemistry* **2001,** *22* (9), 931-967.

51. San Fabián, J.; García de la Vega, J. M.; Suardíaz, R.; Fernández-Oliva, M.; Pérez, C.; Crespo-Otero, R.; Contreras, R. H., Computational NMR coupling constants: Shifting and scaling factors for evaluating 1JCH. *Magnetic Resonance in Chemistry* **2013,** *51* (12), 775-787.

52. Chesnut, D. B.; Moore, K. D., Locally dense basis sets for chemical shift calculations. *Journal of Computational Chemistry* **1989,** *10* (5), 648-659.

53. DiLabio, G. A., Using Locally Dense Basis Sets for the Determination of Molecular Properties. *The Journal of Physical Chemistry A* **1999,** *103* (51), 11414-11424.

54. Sanchez, M.; Provasi, P. F.; Aucar, G. A.; Sauer, S. P. A., On the Usage of Locally Dense Basis Sets in the Calculation of NMR Indirect Nuclear Spin–Spin Coupling Constants: Vicinal Fluorine–Fluorine Couplings. In *Advances in Quantum Chemistry*, Academic Press: **2005**; Vol. 48, pp 161-183.

PART B – Interaction of NHC-derived Boreniums with External Bases

5. CHAPTER IV
Computational Investigation of Scales of Lewis Acidity

Abstract

The primary objective of this chapter is finding a satisfactory answer to the question: How to define and quantify Lewis acidity? Like the entities explored in the earlier chapters, i.e., σ and π-interaction, Lewis acidity, although well-known in the chemical community, is still a somewhat 'fuzzy' and flexible concept. Once again, there are several parameters that are commonly recognised as measures of Lewis acidity. In this thesis we focus on two of them – the hydride ion affinity (HIA) and the Gutmann-Beckett parameter. In each case the interaction of NHC-derived borenium adduct with external bases like hydride (H^-) and phosphine oxides like triethylphosphine oxide ($POEt_3$) has been investigated and their relationship with previously defined σ and π-donating ability has been analysed. This chapter aims to bridge the gap between structural features like σ and π bonds in boreniums with their interaction with external Lewis bases.

5.1. Introduction

Lewis acidity is the most chemically relevant property of the carbene/carbone borenium adducts. The vacant p orbital on the trivalent cationic boron is mainly credited for it. Sivaev mentions in his review that "Borane derivatives represent Lewis acids par excellence owing to the electron deficiency of the central boron atom with a vacant p-orbital".[1] Therefore it is tempting to draw parallel between the strength of π-donation in carbene/carbone borenium adducts, measure previously in chapter II and their Lewis acidity. To judge the validity of this hypothesis, first Lewis acidity needs to be defined and reliably quantified. There are several theoretical and experimental scales that are regularly used in chemical literature to quantify Lewis acidity. We choose to work with two of them – hydride ion affinity and the Gutmann-Becket parameter. Once again, the qualitative and quantitative significance of these scales needs some clarity and has been explored. In this chapter we try to correlate the chemical entities related to the carbene-borenium adduct quantified in the previous chapters (σ and π-donating ability of carbenes/carbones) with descriptors (Lewis acidity) relevant to the chemical reactivity of these molecules using computational tools.

5.1.1. Definition of Lewis Acidity

Like the π-bonds and σ-bonds mentioned in the first two chapters of this thesis, the concepts of acidity and basicity are also fundamental to the chemical sciences. Unsurprisingly, therefore, there coexist several different definitions of acids and bases, having emerged in the past century – including Arrhenius[i], Brønsted and Lowry[j] and G. N. Lewis' definitions.[2-6] In 1923, Lewis introduced a generalizable concept, in that it subsumes the definitions of an Arrhenius acid and a Brønsted acid, that defines Lewis acids as electron pair acceptors and Lewis bases as electron pair donors.[7] Lewis acidity is defined as the thermodynamic tendency of a substance to act as a Lewis acid.[8] Increased Lewis acidity shifts the equilibrium towards the formation of a Lewis adduct with a given Lewis base. (Scheme 5-1)

[i] The first molecular definition of acidity/basicity was provided by Arrhenius in 1884 where he defined an acid as a proton (H^+) donor (E.g. HCl, H_2SO_4, HNO_3, CH_3COOH etc) and a base as a hydroxide (OH^-) donor (E.g. NaOH, KOH). Clearly this definition was suitable only for the aqueous medium.

[j] In 1923, Brønsted and Lowry independently proposed that an acid can be defined as the proton donor while a base is defined as a proton acceptor.

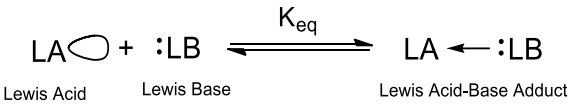

Scheme 5-1: A typical Lewis acid-base reaction leading to the formation of adduct

The Lewis acid-base theory has propelled to the forefront of chemistry particularly in the 21st century[k] with rapidly emerging applications[9] in material science,[10-13] anion recognition,[14, 15] organic synthesis[16] and organometallic pre-catalysts.[17-19] The recent development of frustrated Lewis pair (FLP) catalysis and other organo-main group catalyst-driven reactions have spiked the curiosity of chemists further in this field.[20-25]

With this in mind, the need for a reliable measure of the acceptor ability of a Lewis acid has certainly become exigent as this property provides the basis for the chemical utility of this species.[9, 26] Choosing the right Lewis acid to achieve the desired result is the key to success in most cases.[27, 28] And, frequently, the strength of the Lewis acid is correlated with its efficiency.[9, 29] Naturally, it *may* seem pertinent to test a reaction with the strongest Lewis acid first to get the best results (although this may not always be the case) hence, the need for a suitable scale for Lewis acidity.

5.1.2. Measurement of Lewis Acidity

For Brønsted acids an equilibrium very similar to the Lewis acid-base equilibrium shown above, can be quantified by the pH or pK_a of the system, although even minor environmental changes can shift this equilibrium and change the different orders of acidities because of the nature of the reference itself (H^+).[l] In fact, only recently, a unified description of Brønsted acidity in various media was also introduced[30, 31] where the chemical potential of a proton donor in a particular medium was referenced against the ideal proton gas. However, no such universal scaling is available for Lewis Acids even now. According to Drago's ECW scheme,[32, 33] (Figure 5-1B) the Lewis acidity can be measured in terms of the enthalpy (ΔH) of adduct formation. The enthalpy depends on three contributing terms – covalent (C), electrostatic (E) and steric effect (W). The Lewis acid is characterised by E_{LA} and C_{LA} values and the Lewis base is likewise characterised by E_{LB} and C_{LB} the combination of which give the electrostatic and covalent contribution to the bond strength. W represents a constant steric term (Figure 5-1).

[k] More than 10,000 papers have been published regarding Lewis acids in the past decade alone, figures obtained from Web of Science

[l] This is essentially the same as changing the reference in Lewis acid-base system.

In addition, in the absence of a standardised Lewis base and seeing that a particular Lewis acid behaves differently when allowed to interact with different Lewis bases, the electronic structure of the 'free' Lewis acid may not be sufficient to determine the Lewis acidity *a priori*. To illustrate this point, we take the example of a well-known family of Lewis acids, the boron trihalides (BX_3). For strong bases such as NH_3, BCl_3 is a stronger Lewis acid than BF_3 but for weak bases such as CO, BF_3 turns out to be the stronger acid.[34] BF_3 also forms more stable adduct with ethers than BH_3, but the opposite is true for thioethers.[35]

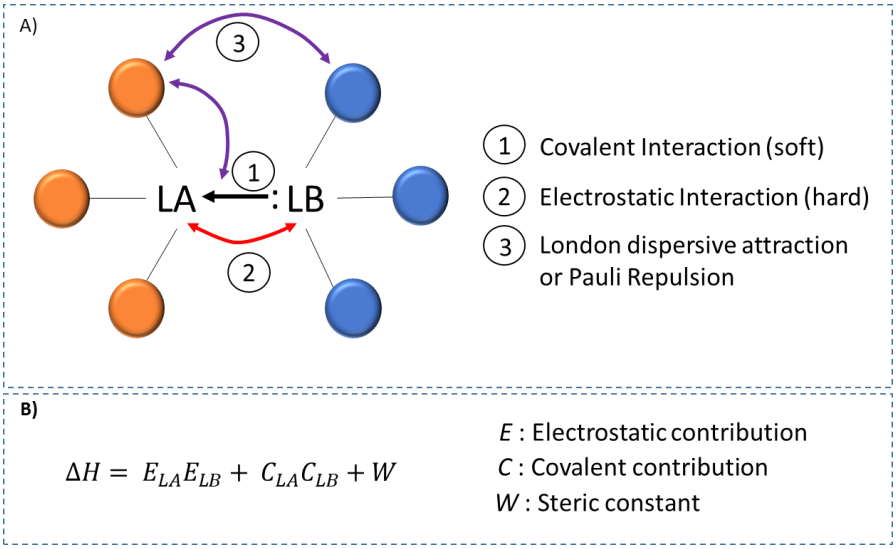

Figure 5-1: (A) Various attractive and repulsive forces within a Lewis acid – Lewis base adduct; (B) Drago's ECW scheme, diagram adapted from Lutz Greb's review[26]

These exceptional experimental trends have been explained using Pearson's concept of hard soft acids and bases (HSAB).[36] The HSAB principle classifies molecules as hard or soft acids or bases and states that soft acids form stronger and more stable bonds with soft bases and hard acids form stronger and more stable bonds with hard bases. To understand which term makes the most significant contribution to the enthalpy of formation of such acid-base adducts we go back to Drago's ECW scheme (Figure 5-1 B). To have a larger enthalpy, either the first term (E) has to be large, i.e., there must be a large electrostatic attraction between the Lewis acid and the Lewis base, or the second term, i.e., the covalent contribution (C) should be high enough. This falls in line with the HSAB principle as the first term corresponds to a hard-hard ionic interaction whereas the second corresponds to a soft-soft covalent interaction. For a mismatch hard-soft pair neither of the two terms in Drago's equation is large enough, making the adduct thermodynamically unstable. Mulliken and Klopman provided the theoretical basis for the electrostatic and covalent contributions through perturbational MO theory.[37-41] There

also are theoretical, statistical and empirical indications that Lewis acidity depends on a manageable number of factors and the compounds may indeed be classified as strong or weak within the limitations of these definition.[42]

5.1.3. Lewis Acidity Scales

Over the years several different scales of Lewis acidity have come to exist side by side in chemical literature.[43] Some of these scales are of experimentally determined parameters while others are predominantly theoretically defined. Among experimental scales, the Gutmann-Beckett method uses phosphine oxides (triethyl phosphine oxide, $Et_3P=O$, or triphenyl phosphine oxide, $Ph_3P=O$) as ^{31}P probes to coordinate with a given Lewis acid and the chemical shift of phosphorus measures the Lewis acidity of the compound.[44-46] There are several other methods that use NMR spectroscopy on a Lewis acid-probe complex to establish a relative scale of Lewis acidity. These include Child's method, which measures the chemical shift of the H3-proton in trans-crotonaldehyde upon binding to a Lewis acid,[47] Pier's method which uses ethyl benzoate[48] and Hilt's method that used deuterated pyridine as probes, to name a few.[49] Other spectroscopic methods include measurement of C-N stretching frequency in acetonitrile adducts.[50-52] Gaffen *et al*. have also proposed the use of fluorescent phosphole oxides that generate fluorescent Lewis acid-base adducts with distinctly different fluorescence and colouration properties as a naked-eye litmus test to determine relative Lewis acidity.[9]

Further methods of scaling Lewis acidity include thermochemistry[53-55] and chemical reactivity.[56-58] Many gas phase adduct dissociation enthalpies have also been obtained by tensimetry or mass spectrometry.[59, 60] The correlation of X-ray diffraction bond lengths with bond strengths does not do well as illustrated by several examples.[61-65]

Among computational methods, affinities towards several different kinds of bases, measured by their complexation enthalpies with the Lewis acid, have been studied. Fluoride ion affinity uses the enthalpy of complexation with the F^- ion as a measure of Lewis acidity.[66] Fluoride ions have high basicity, are small in size and coordinate with all Lewis acids. Moreover, early computational assessments of FIA revealed the reliability of these numbers.[67] Therefore, FIA has morphed into a popular theoretically calculated scale of Lewis acidity. However, FIA faces the criticism of being a measure of fluoridophilicity rather than Lewis acidity.[66] Similarly,

Ingleson and Krossing have attempted to measure Lewis acidity in terms of Hydride and Methyl ion affinity.[68, 69] Chloride ion affinity, ammonia and water affinities have also been studied to have multilateral scaling in order to achieve a less-biased picture of Lewis acidity.[70, 71] The Global Electrophilicity Index (GEI) has been recently proposed as an 'intrinsic' theoretical scale to measure Lewis acidity where Lewis acidity is determined in the absence of a Lewis base.[72] The computational measurement of the affinity of a compound towards an electron pair as Lewis base has been proposed but the theoretical description of an unbound dianionic state is complicated.[73]

With so many scales all measuring Lewis acidity at our disposal, we must again ask the question of whether they measure the same chemical entity and if not, what each scale represents. Thankfully, this question has already been partly answered by Lutz Greb in his recent review.[26] The following section classifying Lewis acidity scales is based on the same.

5.1.4. Classification of scaling methods

According to Lutz Greb,[26] the various Lewis acid scales discussed above can be put into three classes – global, effective and intrinsic – depending upon the nature of the observable that is used to quantify the Lewis acidity (Figure 5-2).

The first class of *global* scales considers the complete process of adduct formation and yields thermodynamic values (like ΔH or ΔG). These include FIA, HIA, calorimetric measurements, ICR-MS (ion cyclotron resonance mass spectrometry) etc. Here, the free, undisturbed Lewis acid is the reference state and enthalpy or free energy change with respect to the relaxed state of the adduct is measured. The descriptor includes factors like intramolecular coordination in the initial Lewis acid and deformation energies of the Lewis acid and base (geometry distortions, internal rotations etc.) which can all be bracketed under preorganisation energy (E_{prep}) in addition to the immediate interaction energy (E_{inter}). These global methods are ideally suited for the quantification of strength of a Lewis acid but are influenced by HSAB effects. They may even correlate quantitatively with experimentally obtained data like Mayr's electrophilicity.[74, 75] A point to note in this regard is that electrophilicity and Lewis acidity are not strictly equivalent, although they are frequently used interchangeably – while electrophilicity is related to the *rate* of formation of a new bond and

therefore indicates a kinetic behaviour, Lewis acidity is more concerned with the equilibrium of adduct formation and is a thermodynamic property.

The second class of descriptors, the *effective* descriptors, measures the interaction of a Lewis acid with a probe molecule by evaluating the change in some spectroscopic output of the probe due to coordination with the Lewis acid. Representative examples of this category include Gutmann-Beckett and Child's method (both measuring NMR outputs of the probe), coordination to acetonitrile (to measure IR peak shifts) or Gaffen's method of measuring change in fluorescence output. In this case, the geometry of the Lewis acid in the adduct is the reference state and the immediate interaction between the Lewis acid and base is expressed in the output of the probe molecule. These scales therefore necessarily characterise the adduct rather than the Lewis acid itself. Such scaling methods are useful for evaluating the effectiveness of a Lewis acid for a particular process (e.g. increase in polarisation of carbonyl group upon binding) but they too are influenced by HSAB effects.

The third category of *intrinsic* scales examines the free Lewis acids "non-invasively" through quantum mechanical calculations or spectroscopy. These include factors like energy of the LUMO (Lower LUMO energy generally indicates higher affinities, although quantitative predictions are not always successful[68]) and Global Electrophilicity Index.[72] Experimental estimates can be obtained [29] by Si-NMR chemical shifts or through electrochemical potentials.[76, 77] The intrinsic class of methods is rather promising as it does not depend on a reference Lewis base and is best suited for preliminary evaluations. However, these scales cannot evaluate the strength or effectiveness of the Lewis acid when it interacts with a base. Furthermore, these scales do not account for interactions arising from immediate interaction with a Lewis base (e.g. deformation energy, steric repulsion etc.)[78]

It is crucial to remember that there is no necessity for these three classes to correlate with each other, however, the deviations are often sufficiently small to allow for qualitative[58, 68, 72, 79] and sometimes even quantitative agreement.[80, 81]

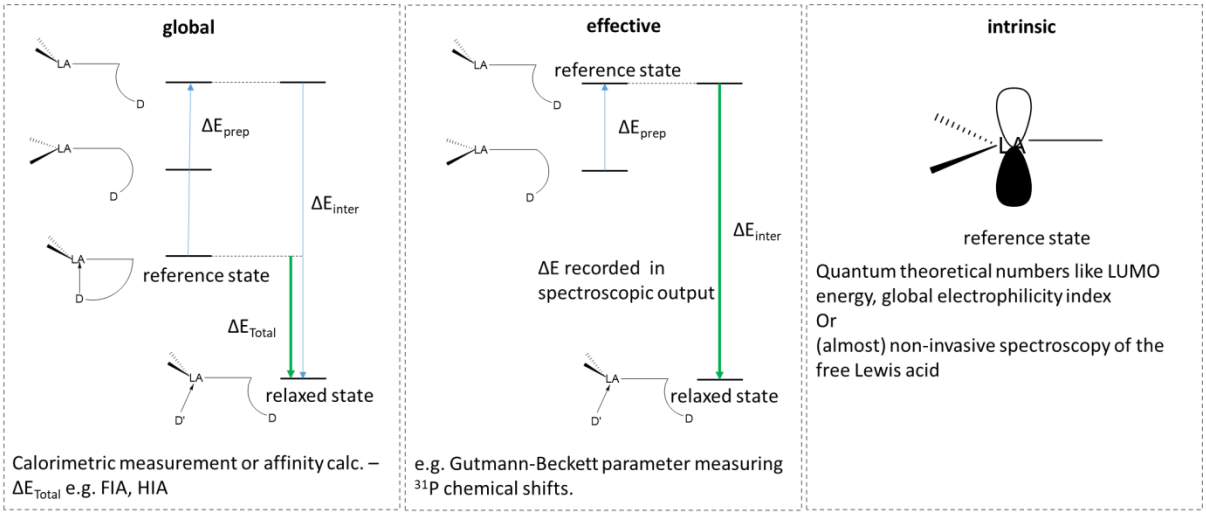

Figure 5-2: Classification of Lewis acidity scaling methods (ΔE_{prep} = preparation energy, ΔE_{inter} = intermolecular interaction energy, ΔE_{Total} = obtained output energy, D represents intramolecular donor and D' represents an external donor). Diagram adapted from Lutz Greb's review.[26]

In the next part we take a closer look at two of the most popular, experimentally determined Lewis acidity scales – the Gutmann-Beckett scale of acceptor numbers and hydride ion affinity.

5.1.4.1. Gutmann-Beckett Acceptor Number

In 1975, Viktor Gutmann published a paper that formulated a new parameter called the 'Acceptor Number' to be able to quantify the Lewis acidity of a solvent.[44] From the viewpoint of coordination chemistry, the solvation of a polar substrate in a solvent can be explained by the simultaneous electrophilic and nucleophilic attack of solvent molecules on the two poles of the solute molecule,[82] as illustrated in scheme 5-2.

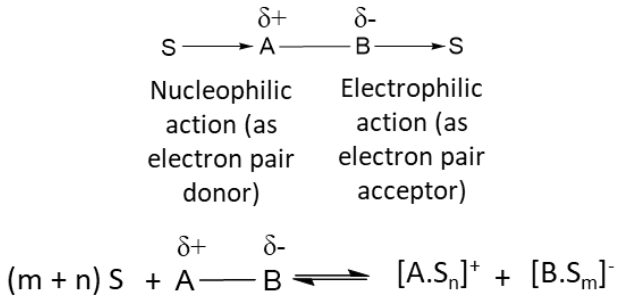

Scheme 5-2: Solvation of polar molecule A-B in a solvent S, scheme adapted from Gutmann's 1975 paper[44]

The extent of this reaction depends upon the nucleophilicity and electrophilicity of the solvent. The scale used to measure the nucleophilic character of a solvent molecule is given

by the enthalpy of complexation of the solvent with $SbCl_5$ in a dilute solution of 1,2 dichloroethane and it is called the donor number (DN).[83, 84] However a similar scale to measure the electrophilicity/Lewis acidity of the solvent had not been designed as this value varies largely even within the group of donor solvents.[85] Some investigators even showed the utility of NMR spectroscopy as an alternative method in measuring the nucleophilic properties of solvents.[86, 87]

Inspired by this line of thought, Gutmann and co-workers designed a scale of 'acceptor number' (AN) to measure the electrophilicity of the solvent. They chose triethylphosphine oxide as an NMR probe that forms a complex with the given solvent molecule. The chemical shift of the phosphorus center in the complex should then correlate with the Lewis acidity/ electrophilicity of the solvent. This is because the coordination of the solvent to the phosphine oxide weakens the P-O π-bond and simultaneously polarises the σ-bond as well. This leads to a reduction in electron density at the phosphorus atom, thus explaining the downfield shift compared to hexane, a non-coordinating solvent, as shown below (Scheme 5-3).

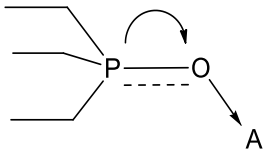

Scheme 5-3: Phosphine oxide forming adduct with Lewis acid, A

In view of the definition of donor number, the acceptor number for the $SbCl_5$.$POEt_3$ complex dissolved in dichloromethane (DCM) is arbitrarily set to 100 on the AN scale. The acceptor number, a dimensionless quantity, for a solvent can then be obtained from the chemical shift (δ_{corr}) according to formula (1).

$$AN = \frac{\delta_{corr}}{\delta_{corr}(SbCl_5\,.POEt_3\ in\ DCM)} \times\ 100 =\ \delta_{corr} \times 2{,}348 \qquad (1)$$

The choice of the probe to be triethyl phosphine oxide is justified by the following arguments:

- The ^{31}P nucleus is easily accessible for NMR measurements. ^{31}P nucleus is 100% naturally abundant, has good sensitivity and a very large chemical shift range.
- The probe nucleus (P) is away from the actual point of interaction, i.e., the oxygen atom. This eliminates theoretically ill-defined 'contact' contribution to the chemical shift values.

- Triethylphosphine oxide is a very strong base (DN = 40). This together with the P=O double bond makes P very sensitive to changes in the solvent.
- The donor-acceptor interaction always happens at a well-defined site – the oxygen atom. The remaining coordination sites of phosphorus are blocked by inert alkyl groups. The ethyl groups ensure electronic shielding without steric hindrance.
- Due to the ethyl groups, triethylphosphine oxide is also soluble in all kinds of solvents.
- Triethylphosphine oxide is also extraordinarily stable.

Beckett used the same AN scale to order boron-containing Lewis acids used in the polymerisation of epoxides according to their Lewis acidity.[46] Since then the Lewis acidity of many Lewis acids have been recorded by measuring their corresponding AN using the Gutmann-Beckett method. An extensive list of borane-based Lewis acids and other cationic boron species (like borenium and borinium) have been recorded in an excellent review by Sivaev *et al.*[1]

The Gutmann-Beckett method also has some shortcomings. The various data recorded over the years throughout chemical literature lacks uniformity. This is because the method is not explicit about the nature of solvents used or their concentrations or conditions of temperature and pressure during conducting the experiment, all of which could influence the chemical shift of the phosphorus nucleus. This results in multiple values corresponding to the same Lewis acid.[1] Therefore, it is advisable to compare values that have been recorded in the same environment. In spite of these problems, the Gutmann-Beckett method remains the most documented method to compare the Lewis acidity of compounds due to its ease and simplicity. However, no theoretical study regarding the Gutmann-Beckett parameter exists to the best of our knowledge.

5.1.4.2. Hydride Ion Affinity

Hydride Ion Affinity (HIA) is defined as the enthalpy change associated with the heterolytic dissociation of a complex between a hydride ion and a Lewis acid.[88] Drawing inspiration from the definition of Brønsted acidity, Bartlett *et al.* realised it is only possible to determine the absolute strength of a Lewis acid with respect to a well-defined Lewis base and introduced the concept of Fluoride ion affinity (FIA).[89] However, the fluoride is a hard base according to HSAB principles and therefore it may be misleading in the case of soft Lewis acids. Hence,

comparing scales by using different Lewis bases is generally advisable. Therefore, analogous to FIA, the affinities of Lewis acids towards many Lewis bases of varying hardness (H^-, Cl^-, Me^-, NH_3 etc.) have been analysed.[69, 90, 91]

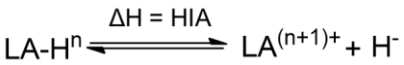

Scheme 5-4: Hydride Ion affinity

Of all of them, the H^- ion is the simplest Lewis base. HIA is an important thermodynamic quantity that can be used to characterise Lewis acids. The ease of calculating HIA makes it ubiquitous in both theoretical and experimental chemistry for comparing Lewis acidities.[68, 69, 88, 92-94] However compared to proton affinity, fewer research has been performed with respect to the trends of HIA in different Lewis acids. Parker and co-workers published the experimental HIA of a set of quinone, organic radicals and cations in 1993,[95-97] Maksić and co-workers calculated the acidity of boranes and alkenes in 2007 using the triadic formula,[m,93, 98, 99] Böhrer et al. augmented the HIA scale of group 13 acids based on isodesmic reactions.[88,99]

Up until this point in this chapter we have looked at various experimental and theoretical scales of Lewis acidity and classified them on the basis of what kind of information is available from each scale. Although there are several interesting parameters, we choose to focus on the theoretical investigation of two scales – the Hydride ion affinity (HIA) and the Gutmann-Beckett parameter. The choice of these two scales is dictated by their conceptual simplicity and a simultaneous and baffling lack of any computational investigation, particularly in the case of the Gutmann-Beckett scale. These two scales provide interesting contrast in two respects –

(i) These scales belong to two different categories according to Greb's classification. While HIA belongs to the first category of global descriptors, the Gutmann-Beckett parameter belongs to the second category of effective descriptors.

[m] The hydride ion affinity is expressed as a combination of three terms (hence, triadic) – the electron affinity calculated according to Koopmans' formulation, bond dissociation energy and reorganisation energy.

(ii) Since both these categories of descriptors are influenced by HSAB principles, it is important to note that $POEt_3$ is classically described as a 'hard' base due to the electronegative oxygen while hydride ion is categorised as a 'soft' base.

Therefore, noting these differences, we must first ask if these two scales correlate. If they do, then perhaps they represent what we call Lewis acidity, but if they do not, then what does each scale signify?

The Lewis acidity of boron compounds, as has been noted before, is attributed to the vacant p orbital of the boron centre. This π-population is related to the π-donating ability of the carbene/carbone. The π-population should be the main factor influencing Lewis acidity and the π-population represents an intrinsic scale of Lewis acidity according to Greb's classification. If this hypothesis is correct, then a linear correlation between the strength of π-donation from the carbene/carbone to the borenium adduct and the HIA and/or the Gutmann-Beckett parameter should exist. If it does not – then perhaps we need to take a critical look at this hypothesis as there may have been some oversimplification. Even without performing any calculation, if one were to imagine a hypothetical NHC-Borenium adduct where no π-donation exists – would changing the backbone of the carbene have no influence whatsoever on the borenium's strength of binding an external base such as hydride or $POEt_3$? Logically, this should not be the case, as although the π-acidity now no longer exists, the σ-donation of NHC→BH_2 should still influence the electronic demand of the boron centre. Then σ-donation should also influence the Lewis acidity scales. But what is the relative importance of σ and π-donation on the Lewis acidity scales then?

Finally, we also take a brief look at an example of intrinsic scale of Lewis acidity – ^{11}B NMR spectroscopic investigation of carbene/carbone-BH_2^+ adducts, trying to identify the difference of this scale compared to the others. However, the chemical shift of B in carbene-borenium compound has not been used as a measure of Lewis acidity.

Therefore, in this chapter we essentially take a step from structure (σ and π bonds) toward reactivity (Lewis acidity) for the NHC-borenium adducts. We would like to explore if any of their intrinsic characteristics correlate directly with the nature of their interaction with an external Lewis base.

In order to achieve these goals, the structures of the $POEt_3$ adducts and H^- adducts of **X**-BH_2^+ molecules have been investigated. Further, their energetic and structural features have been explored using the various computational tools encountered before. These include geometry optimisation, NBO analysis, ETS-NOCV analysis as well as NMR chemical shift calculation. The technical details of the computations have been discussed in the following section.

5.2. Computational Details

All geometries have been optimized at the B3LYP/TZVP level with G09 suit of programs.[100] For the transition states, the geometry has been characterized by the presence of a single imaginary vibrational frequency, connecting the two minima, at the same level of calculation. Wiberg bond index and atomic charges have been calculated using the natural bond orbital analysis with the NBO6 software.[101] Electron density at the bond critical point and Delocalisation Indices for P-O and B-O bonds have been calculated using multiwfn[102] from B3LYP/TZVP density. The interaction energy (ΔE_{inter}) due to the TEPO-adduct (TEPO = triethyl phosphine oxide) formation has been calculated at the B3LYP/TZ2P//B3LYP/TZVP level with ADF2018.[103-105] The theoretical basis of these methods have been discussed in Section 2B.9 of Chapter I.

The energy of interaction (ΔE_{inter}) is an important term calculated in this chapter. ΔE_{inter} is essentially the total energy of bond formation or complexation energy minus the energy for geometric distortion. Therefore, ΔE_{inter} is specific to particular conformation of the complex. ΔE_{inter} for a particular conformation of the adduct formed between **X**-BH_2^+ and $POEt_3$ has been calculated by two different approaches. This energy can be obtained directly from bond energy decomposition analysis or it can be calculated from the electronic energies of the two fragments (**X**$^{//}$-BH_2^+ and $POEt_3$) in their optimized geometry and their corresponding deformation energies. The deformation energies can in turn be calculated as the difference between the energy of the optimized geometry and that of the conformations that the fragments attain in the final complex. As expected, there is near perfect correlation between these two sets of numbers and the root mean square deviation is 1.75 kJ/mol, which could be attributed to the difference in the nature of basis sets used in gaussian and ADF.

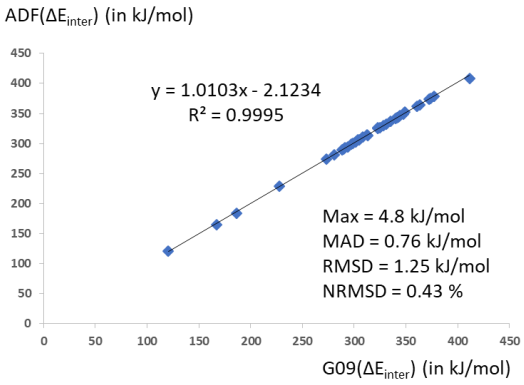

Figure 5-3: Correlation between energy of interaction calculated at the B3LYP/TZ2P (ADF) and B3LYP/TZVP (G09) levels, based on B3LYP/TZVP optimized geometries

The literature for computational calculation of isotropic shielding for phosphorus nucleus is quite extensive.[106-109] The recommendations made in most cases are system specific and generally advise the use of extensively large basis set, although even in such cases deviations and exceptions are found.[109, 110] However, Latypov *et al*. find that contrary to common belief, reasonably accurate results can be obtained, at least in some cases, by using relatively smaller basis sets in combination with the GIAO method.[109] They show that using PBE1PBE/6-31+G(d) level of calculation to determine the NMR chemical shifts for molecules optimized at PBE1PBE/6-311G(2d,2p) level provide reasonably satisfactory parity with chemical shifts recorded experimentally. They also show that using the B3LYP functional for optimizing the geometry only slightly affects the correlation. Therefore, we decided to test how well PBE1PBE/6-31+G(d) performs in combination with B3LYP/TZVP optimized structures in predicting the chemical shift of phosphorus. For this, we took a set of 7 Lewis acids (R**Y, Y** = **1**-**7,** Scheme 5-5), for which the experimental ^{31}P chemical shift of the TEPO adducts (R**Y**-POEt$_3$) have been determined experimentally.[69, 111-114] The molecules chosen are boronic Lewis acids and one silicon Lewis acid and are outside the set of molecules we study. This benchmark is limited to 7 structures because not too many instances of recorded experimental data for Lewis acidic molecules are available. Both cationic and neutral molecules were chosen.

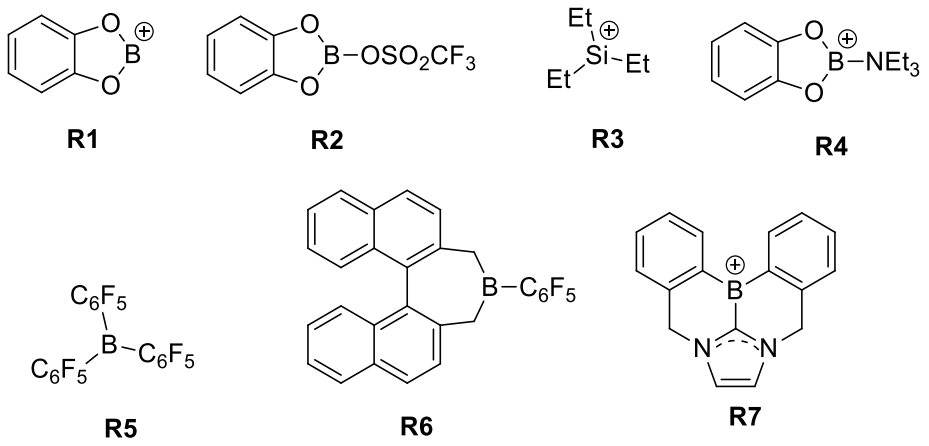

Scheme 5-5: The standardisation set of Lewis acids for phosphorus chemical shift calculations.

The calculated values, with and without using a solvent model, have been recorded in table 5-1.

Table 5-1: Chemical shifts and isotropic shielding of 31P nucleus for the standardization set of molecules

Molecules	Solvent	Experimental δ ^{31}P	Calculated Isotropic Shielding ^{31}P PBE1PBE/6-31G+(d)//B3LYP/TZVP	
			with solvent (pcm)	without solvent
		ppm	ppm	ppm
R1-POEt$_3$	C_6D_6	106.9	275.60	277.99
R2-POEt$_3$	C_6D_6	85.4	298.48	301.45
R3-POEt$_3$	C_6D_6	91.2	294.65	296.27
R4-POEt$_3$	DCM	88.3	289.90	291.94
R5-POEt$_3$	C_6D_6	76.6	300.26	303.04
R5-POEt$_3$	DCM	77	297.90	
R6-POEt$_3$	C_6D_6	71.2	309.33	312.11
R6-POEt$_3$	DCM	72.7	306.69	
R7-POEt$_3$	DCM	79.2	296.37	298.65

The correlation with experimentally recorded values is fairly satisfactory (R^2 = 0.89). The correlation is in fact slightly better without including solvent effect. Therefore, gas phase NMR calculations at the PBE1PBE/6-31+G(d) level have been used for (**X**-BH_2)-$POEt_3^+$ adducts.

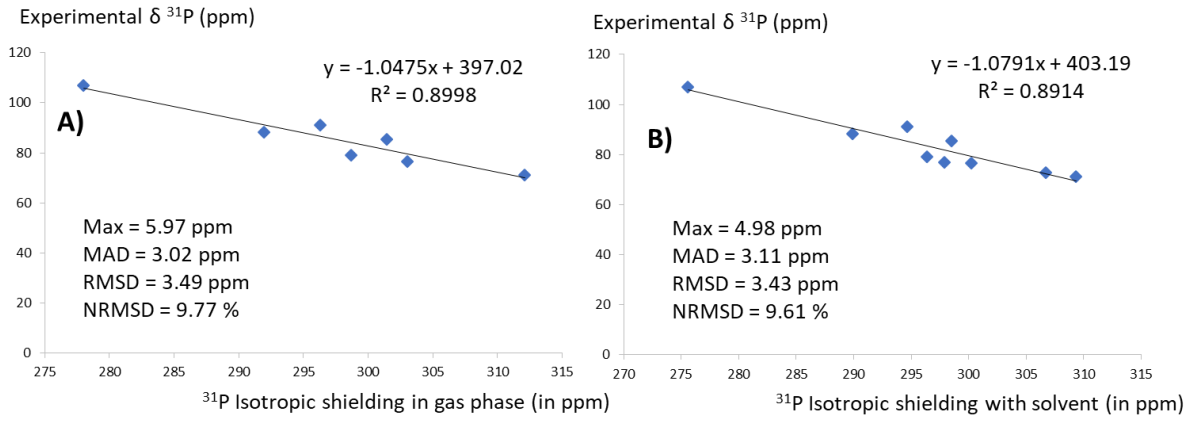

Figure 5-4: Correlation between theoretically calculated isotropic shielding values and experimental chemical shifts of ^{31}P nucleus for R**X**-POEt$_3$ molecules

The isotropic shielding for the boron nucleus in **X**$^{//}$-BH$_2^+$ was also calculated. These molecules being considerably smaller in size, it was possible to calculate the chemical shift at B3LYP/aug-cc-pVTZ level of theory. The computations were successfully carried out for all **X** except **23**, **36** and **38** which were too large for this level of theory. The LDBS approximation (see Chapter III, section 4.2) was employed for **23**, whereas **36** and **38** have been excluded from this specific part (section 5.3.6).

5.3. Results and Discussion

5.3.1. Geometric Structure

In Chapter II we have identified methods suitable to quantify π-donation of carbenic compounds in their dihydrido borenium adducts. Here, our objective is to relate this π-donation with the Gutmann-Beckett acceptor number (AN) and hydride ion affinity (HIA), both of which are descriptors of Lewis acidity. These two descriptors are normally measured experimentally, however, data is scarce and non-uniform. Furthermore, the exact chemical meaning, i.e., the relationship between structural features like σ and π bonds of the molecule with these parameters related to thermodynamic properties (Lewis acidity) are not clear. Therefore, the ^{31}P isotropic shielding (this is related to chemical shift inversely) of the POEt$_3$ adduct and the HIA have been calculated theoretically for **X**-BH$_2^+$ complexes. Parameters pertaining to 36 **X**-BH$_2^+$ complexes (**X** = all molecules on page 13 except **31**, **38** and **39** all of which were too large for reliable NMR calculations on POEt$_3$ adducts) were computed. As mentioned before (see Chapter II, 3.2), the **X**-BH$_3$, i.e., the borenium hydride complexes, show an average C-B bond length of 1.603 Å, which is significantly longer than the average **X**$^{//}$-BH$_2^+$

bond length (1.544 Å), indicating the (near-)absence of C-B π-interaction. (Figure 5-5 A) For the adducts with triethyl phosphine oxide ($POEt_3$), denoted by **X**-BH_2-$POEt_3^+$, geometry optimisation shows various behaviour depending on the **X** moiety. In most cases (**X** = **1**-**23**, **25**-**27** and **29**-**30**), **X**-BH_2-$POEt_3^+$ adopts in its ground state a geometry where the Y-C-B-O dihedral angle is close to 0 degrees, that is the P=O chemical group is located in the plane of **X** (Figure 5-5 C and D). Starting from the conformational arrangement observed for $\mathbf{X}^{//}$-BH_2^+, this conformation is obtained through rotation around the C-B bond due to the presence of the phosphine oxide. This conformation is noted as (**X**-BH_2)$^{//}$-$POEt_3^+$. Naturally this indicated that in unsymmetrical NHCs, there are two possible minima. The global minimum, where the Y-C-B-O dihedral angle is approximately 0°, is indicated by (**X**-BH_2)$^{//}$-$POEt_3^+$, whereas the second, local minimum, where the dihedral angle is approximately 180°, is indicated by (**X'**-BH_2)$^{//}$-$POEt_3^+$ (Figure 5-5 C and D). The energy difference between these two minima varies between 1-9 kJ/mol. In the other eight cases (**X** = **24**, **28** and **32**-**37**) the Y-C-B-O angle observed for the global minimum is close to 90°. This conformation is indicated by (**X**-BH_2)$^{\perp}$-$POEt_3^+$ (Figure 5-5 B). The (**X**-BH_2)$^{//}$-$POEt_3^+$ conformation for **X** = **24**, and **32**-**35**, **37**, as well as the (**X**-BH_2)$^{\perp}$-$POEt_3^+$ conformation for **X** = **1**-**23**, **25**-**27** and **29**-**30**, have also been calculated and correspond in all cases to a transition state. The (**X**-BH_2)$^{//}$-$POEt_3^+$ conformation for **X** = **32** and **36** could not be obtained as stationary point possibly due to steric bulk.

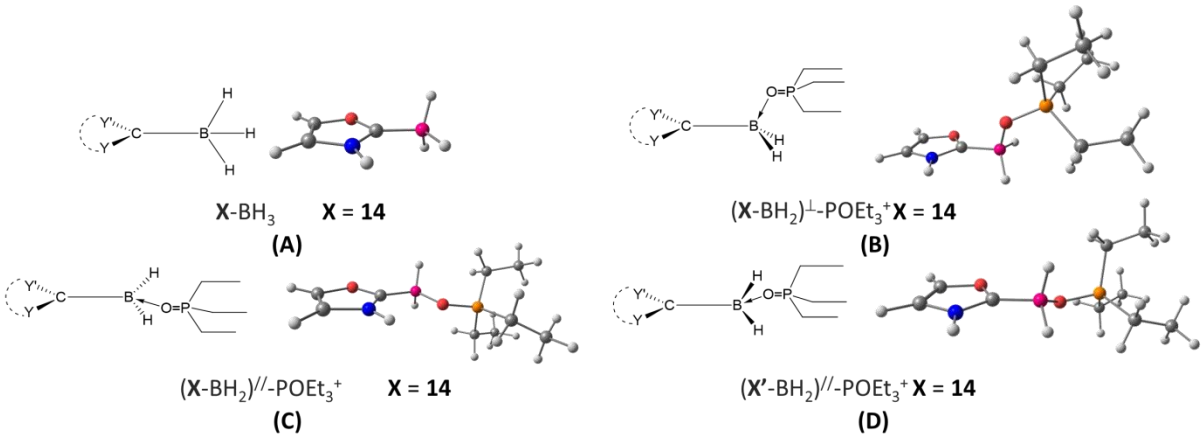

Figure 5-5: Geometric structure of **X**-BH_3 (A)and **X**-BH_2-$POEt_3^+$ (B), (C), (D) in its various conformations with specific example cited for **X** = **14**

The preference of the triethylphosphine oxide adduct to adopt one geometry over the other is possibly dictated by both steric and electronic effects. The energy difference between the

(**X**-BH_2)$^{\perp}$-$POEt_3^+$ and (**X**-BH_2)$^{//}$-$POEt_3^+$ conformations illustrate nicely the electronic effect (Figure 5-6).

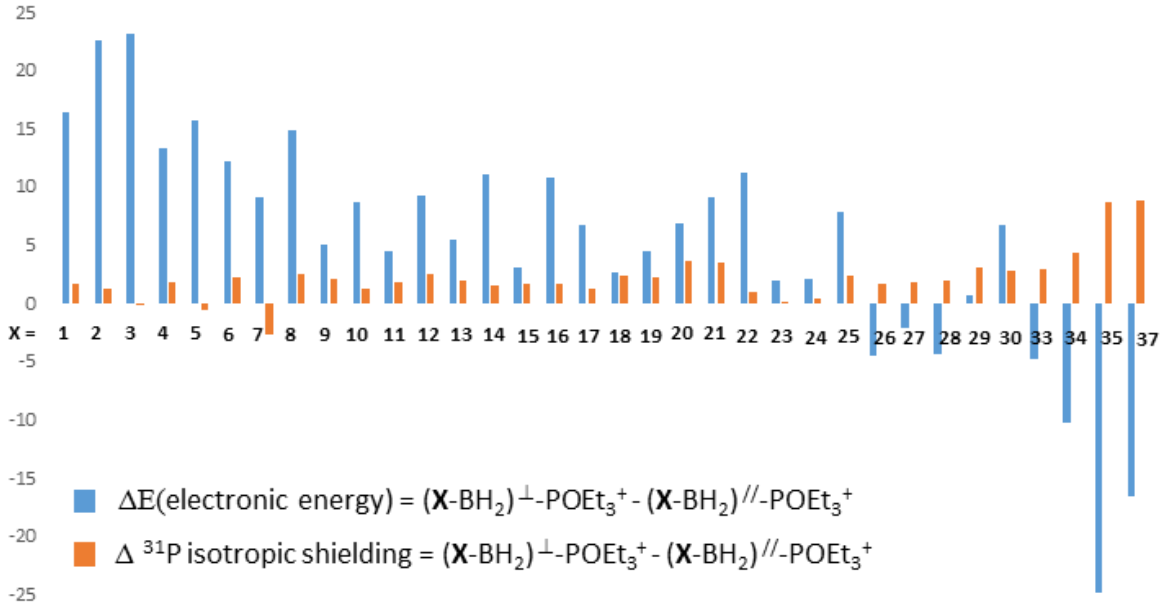

Figure 5-6: Bar graphs illustrating difference in energy and difference in ^{31}P isotropic shielding between two isomers - (**X**-BH_2)$^{\perp}$-$POEt_3^+$ and (**X**-BH_2)$^{//}$-$POEt_3^+$

(**X**-BH_2)$^{\perp}$-$POEt_3^+$ geometry is the preferable geometry for the stronger π-donors among **X** (i.e. the larger **X** values). In this conformation, the C to B π-electronic donation is indeed still possible, albeit weakened by the competitive coordination of $POEt_3$ which is associated by an electronic transfer from the phosphine oxide to the vacant p_z orbital of the boron centre (Figure 5-7). In (**X**-BH_2)$^{//}$-$POEt_3^+$ geometry, the loss of any possible C-B π-interaction is compensated by the possibility of stronger interaction between the B Lewis acid site and the $POEt_3$ Lewis base. Thus, the higher **X** has a donation capability (from **1** to **37**), the more stable (**X**-BH_2)$^{\perp}$-$POEt_3^+$ should be relative to structure (**X**-BH_2)$^{//}$-$POEt_3^+$. Small deviations from this trend are likely related to other electronic (hyperconjugative interactions between B-H and π-system of **X**) and steric effects (steric repulsion between N-substituents of NHC and $POEt_3$).

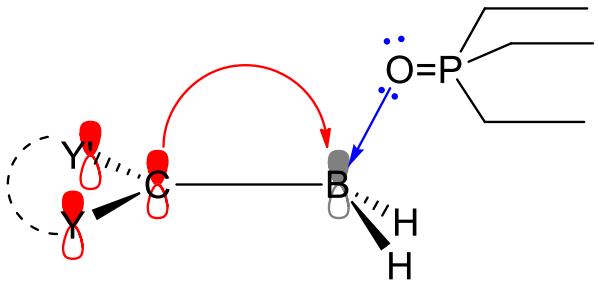

Figure 5-7: Competing electron-donating effects in (**X**-BH_2)$^{\perp}$-$POEt_3^+$

At this point, it is important to reiterate that methods of measuring Lewis acidity using probes, like the Gutmann-Beckett method, necessarily characterise the complex as a whole in a *particular* conformation. This is affirmed by the fact that in the various conformations obtained for each particular **X** case, the chemical shift at the phosphorus centre changes (Figure 5-6). The ^{31}P isotropic shielding of (**X**-BH_2)$^{\perp}$-$POEt_3^+$ is always larger than those for (**X**-BH_2)$^{//}$-$POEt_3^+$, except for **X** = **3**, **5** and **7**, in agreement with our previous results showing that the electronic population of the "vacant" p orbital at the boron center, is lower in **X**$^{\perp}$-BH_2^+than in **X**$^{//}$-BH_2^+conformation. The difference between the two chemical shift appears to be small (less than 10 ppm), but the calculated gas-phase isotropic shielding of phosphorus in (**X**-BH_2)$^{\perp}$-$POEt_3^+$ covers a range only slightly larger than 20 ppm (see below in Section 5.3.3), showing the strong influence of the conformation. These results confirm our previous statement about the influence of electronic effects between the 2 conformations of the Lewis acid – Lewis base (LA-LB) adducts. These results also clarify two aspect of the Gutmann-Beckett method:

- Experimentally, the conformation of the LA-LB adduct is never determined when measuring the ^{31}P chemical shift. Thus, if Lewis acids can change conformation upon coordination of the phosphine oxide, then the interpretation of the experimental data for several Lewis acids must consider this possible rearrangement.
- Conversely, if one wishes to obtain information on the intrinsic Lewis acidity of a family of compounds with this method, then the same conformation must be used.

In this chapter, we want in particular to know if the measured ^{31}P chemical shift in LA-$OPEt_3$ complexes is directly related to the electronic structure of Lewis acids. In other words, is there a strong link between the π donation capability of **X**, the Lewis acidity of B in **X**$^{//}$-BH_2^+, and the ^{31}P chemical shift in **X**$^{\perp}$-BH_2-$POEt_3^+$ adduct. Therefore, one necessarily deems **X**$^{\perp}$-BH_2-$POEt_3^+$

geometry as the interesting conformation to be studied. Therefore, unless mentioned otherwise, the investigations in this chapter have been done with respect to $\mathbf{X}^{\perp}$-BH_2-$POEt_3^+$.

5.3.2. P-O, B-O and C-B Bonds

In the simplest interpretation, the stronger the π-donation capability of **X** is, the shorter is the C-B bond, the weaker is the interaction between **X**-BH_2^+ and $POEt_3$, the longer is the B···O distance and the shorter is the P=O bond. Considering bond length to be an approximate measure of bond strength, the P-O bond length ($d_{P\text{-}O}$) increases with the decrease in ($d_{B\text{-}O}$) bond length. Indeed, such a trend is observed (Figure 5-8 A) although the correlation is far from perfect (R^2 = 0.81) for $\mathbf{X}^{\perp}$-BH_2-$POEt_3^+$. The correlation between $d_{P\text{-}O}$ and $d_{C\text{-}B}$ is quite poor (R^2 = 0.4) (Figure 5-8 B) but shows a slight increasing trend, in accordance with our expectations. But it also simultaneously indicates that C-B bond length is affected by other parameters (σ bond strength, electronic delocalisation between **X** and B-H bonds) and is not a reliable parameter to indicate the strength of the interaction with the Lewis acid. Further discussion about bond lengths and their correlations with other parameters and held in the following section.

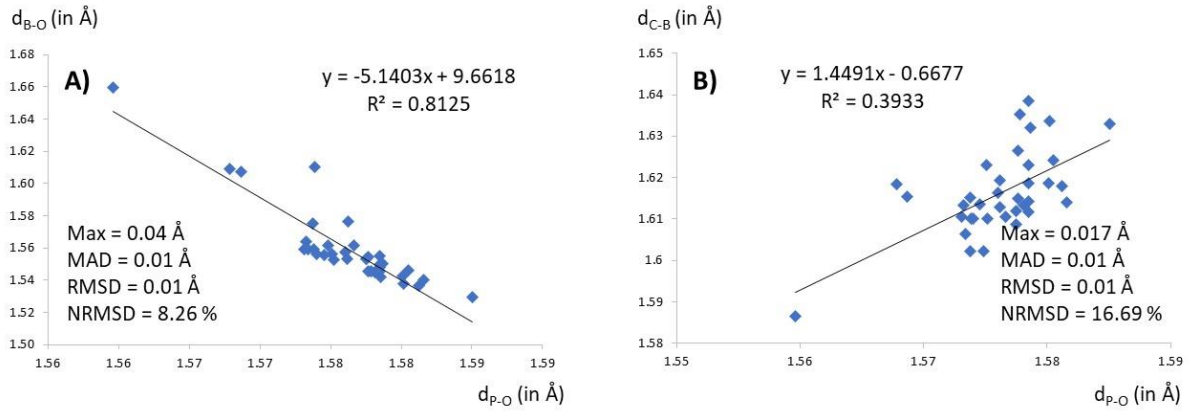

Figure 5-8: Correlation plots for the various bond lengths of (**X**-BH_2)$^{//}$-$POEt_3^+$ complexes

5.3.3. ^{31}P Isotropic Shielding, Interaction Energy and HIA

The calculated gas-phase isotropic shielding of phosphorus in (**X**-BH_2)$^{\perp}$-$POEt_3^+$ covers a range slightly larger than 20 ppm, which is quite a short range compared to the scale of phosphorus chemical shifts. This can be attributed to the fact that they all belong to a particular 'class' of Lewis acids. The greatest isotropic shielding is recorded for **X** = **37** where the isotropic shielding is 315.41 ppm which is due to the greater electron density on phosphorus atom,

leading to more shielding of the nucleus. The smallest isotropic shielding on the other hand is recorded for **X** = **2** at 294.48 ppm, due to a deshielded phosphorus nucleus. This sits well with our chemical intuition as **X** = **37** is a carbone and has one of the highest donating abilities according to the scale in Chapter II while **X** = **2** has poor π-donating ability due the electron withdrawing carbonyl (C=O) groups in its backbone.

ΔE_{inter}, calculated by two different methods as mentioned before, covers a range of around 290 kJ/mol with **X** = **2** showing the highest value at 409 kJ/mol and **X** = **37** is the minimum value of 120 kJ/mol, once again in conformity with our chemical understanding. ΔE_{inter} is higher for a stronger interaction and naturally corresponds to the weaker π-donor among **X** and therefore the strongest Lewis acid among $\mathbf{X}^{//}$-BH_2^+. There is a good correlation between the isotropic shielding of phosphorus and ΔE_{inter} (R^2 = 0.92). (Figure: 5-9 A)

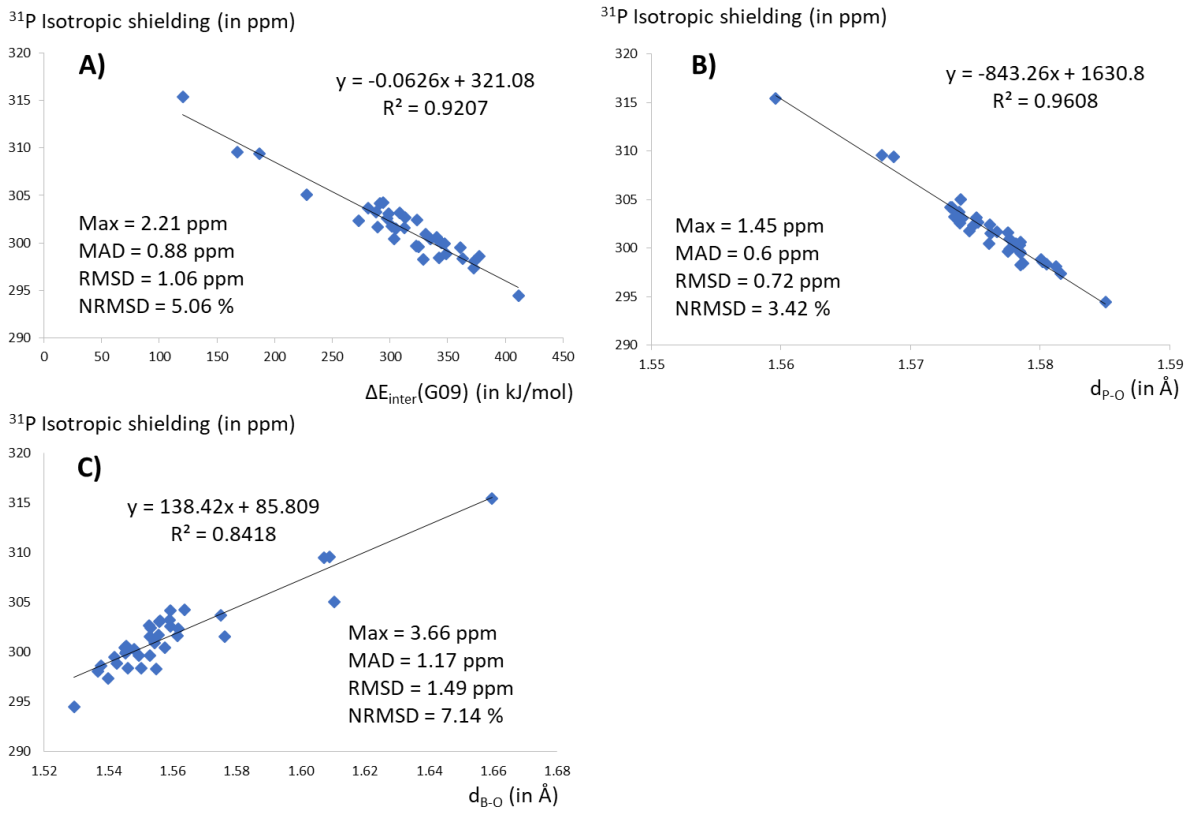

Figure 5-9: Correlation plots for (**X**-BH_2)$^{\perp}$-$POEt_3^+$ complexes optimised at B3LYP/TZVP: between calculated ^{31}P isotropic shielding and (A) ΔE_{inter}; (B) P-O bond length ($d_{P\text{-}O}$) and (C) B-O bond length ($d_{B\text{-}O}$).

The phosphorus centre is highly sensitive to any electronic changes to the P-O bond and this is nicely demonstrated by the fairly good correlation (R^2 = 0.96) between the P-O bond length and the isotropic shielding (Figure: 5-9 B). A reasonable correlation is also obtained for the B-

O bond (R^2 = 0.84), the obvious reduction in the quality of correlation being a consequence of the P centre being further away and being less sensitive to the B-O electronic environment (Figure: 5-9 C).

It is interesting to note that the correlations between P-O bond length, ΔE_{inter} and the isotropic shielding of P are 'global', in the sense that the correlation exists for all the conformations of the molecule - (**X**/**X'**)$^{//}$-BH_2-$POEt_3^+$ and **X**$^{\perp}$-BH_2-$POEt_3^+$ (Figure 5-10 A and B).

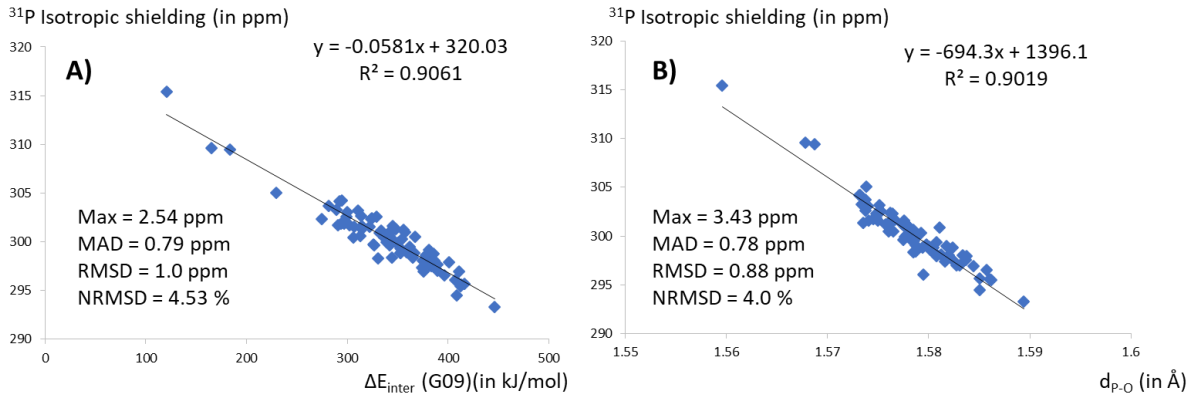

Figure 5-10: Correlation plots for (**X**-BH_2)$^{\perp}$-$POEt_3^+$ and (**X**-BH_2)$^{//}$-$POEt_3^+$ complexes between 31P isotropic shielding and (A) ΔE_{inter} and (B) P-O bond length ($d_{P\text{-}O}$).

The hydride ion affinity (HIA), which is essentially the measure of energy of complexation with another external Lewis base, the hydride (H^-) ion, has also been calculated from the electronic energy of the optimized geometries of **X**$^{//}$-BH_2^+, **X**-BH_3 and the H^- ion. The greatest HIA is demonstrated by **2**$^{//}$-BH_2^+, a strong Lewis acid, having a value of 983.5 kJ/mol and the least is for **37**$^{//}$-BH_2^+, a weak Lewis acid, with a value of 547.8 kJ/mol, with an average of 817 kJ/mol over the 37 compounds under study. It covers a range of 436 kJ/mol again showing the large range of Lewis acidities demonstrated by the examined set of molecules. HIA correlates well with ^{31}P isotropic shielding (R^2 = 0.95) (Figure 5-11 B) as well as the interaction energy of the TEPO complexes, ΔE_{inter} (R^2 = 0.98) (Figure 5-11 A). This is quite a pleasant surprise as we are now able to establish good correlations between the properties of two different adducts of **X**$^{//}$-BH_2^+ with two very different Lewis bases (H^- and $POEt_3$) and at least one of those properties (HIA) can be easily estimated experimentally (although the Gutmann-Beckett parameter can also be determined experimentally, it has ambiguity regarding the conformation).

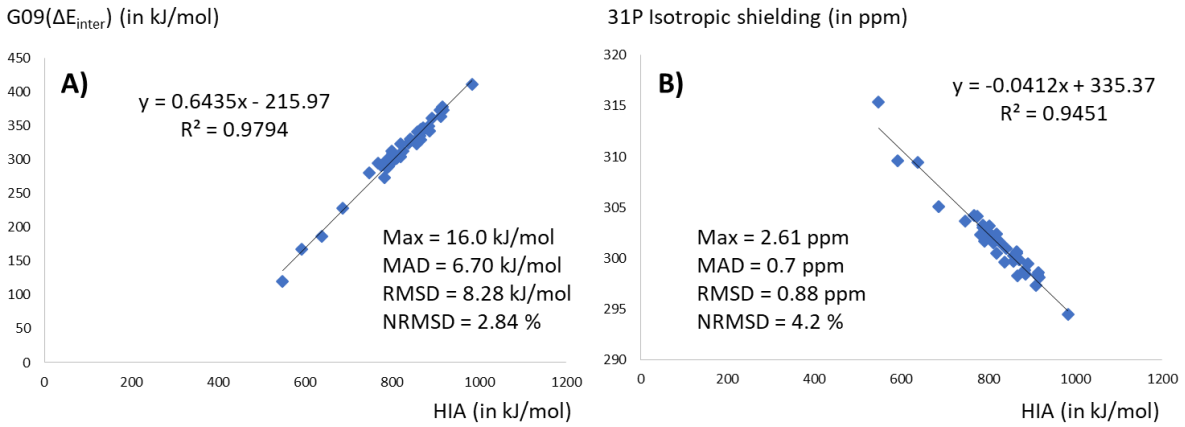

Figure 5-11: Correlation plots for (**X**-BH_2)$^{\perp}$-$POEt_3^+$ complexes between hydride ion affinity (HIA) and (A) ΔE_{inter} and (B) calculated 31P isotropic shielding

The B-O bond that is formed as a result of complexation with $POEt_3$, can be characterized by several descriptors. In this study, three of them have been used – the Wiberg Bond Index (WBI), electron density at bond critical point (ρ_{BCP}) and the delocalization index (DI). The energy of interaction for the formation of the complex (ΔE_{inter}) correlates well with these properties as they all measure the effectiveness of the Lewis Acid (**X**$^{//}$-BH_2^+) towards the Lewis base, $POEt_3$ (Figure 5-12 A, B and C). The HIA also correlates well with each of these properties ($R^2 \approx 0.92$) (Figure 5-12 D, E and F), and therefore can be used to measure the strength of Lewis acidity at the boron centre.

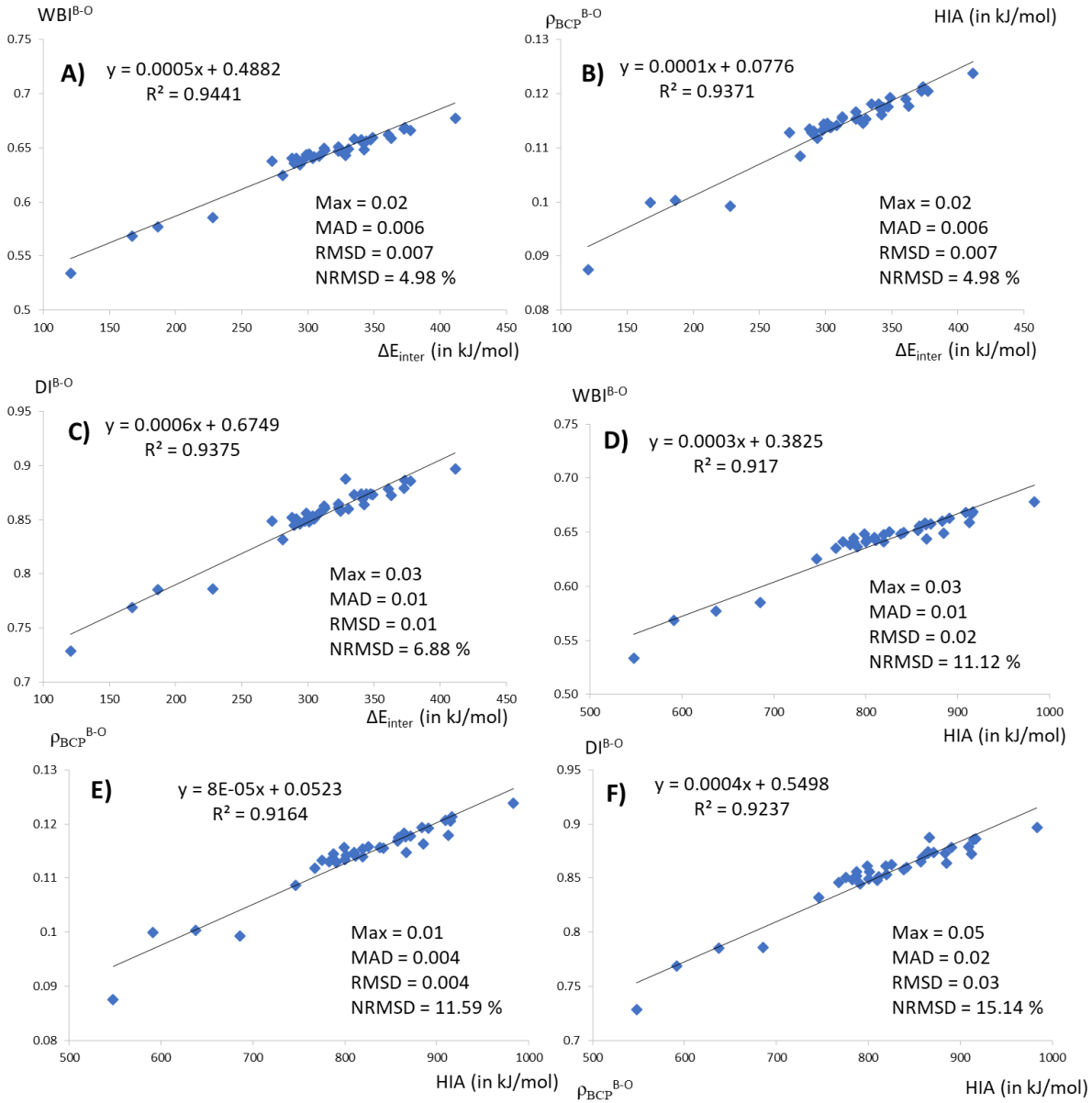

Figure 5-12: Correlation plots for (**X**-BH_2)$^{\perp}$-$POEt_3^+$ complexes between ΔE_{inter} and (A) WBI of B-O bond (WBI^{B-O}); (B) electron density at the bond critical point of the B-O bond (ρ_{BCP}^{B-O}) and (C) delocalization index of the B-O bond (DI^{B-O}) and also hydride ion affinity (HIA) and the same three quantities (D, E and F)

In the complex (**X**-BH_2)$^{\perp}$-$POEt_3^+$, the Lewis acidity of the boron centre is assuaged by electron donation from two sources – the **X** backbone that donates π-electrons and the lone pair on the oxygen atom of $POEt_3$ (Figure 5-7). It is expected that greater the strength of π-donation from **X**, weaker is the B-O bond. Therefore, the properties of the B-O bond or the energy of interaction during formation of such a complex should in principle measure the π-donating ability of **X**, and by extension, the intrinsic Lewis acidity of **X**$^{//}$-BH_2^+.

5.3.4. Correlation between HIA and σ and π donating ability

In Chapter II we encountered several methods of estimating this π-donation – one of the most reliable descriptors being the electronic occupancy of the vacant p orbital of B in $\mathbf{X}^{//}$-BH_2^+ - (pop(p_{vac}^B)). As HIA can be used as a measure of Lewis acidity, it is expected to correlate with pop(p_{vac}^B), and so should be the case for the ^{31}P isotropic shielding. However, this is not what we obtain. The quality of correlation between either HIA or 31P isotropic shielding against pop(p_{vac}^B)) is very poor (R^2 = 0.65 -0.67) although the trends observed are as expected – the greater the π-donating ability of **X**, smaller is the HIA and more shielded is the phosphorus nucleus. (Figure 5-13)

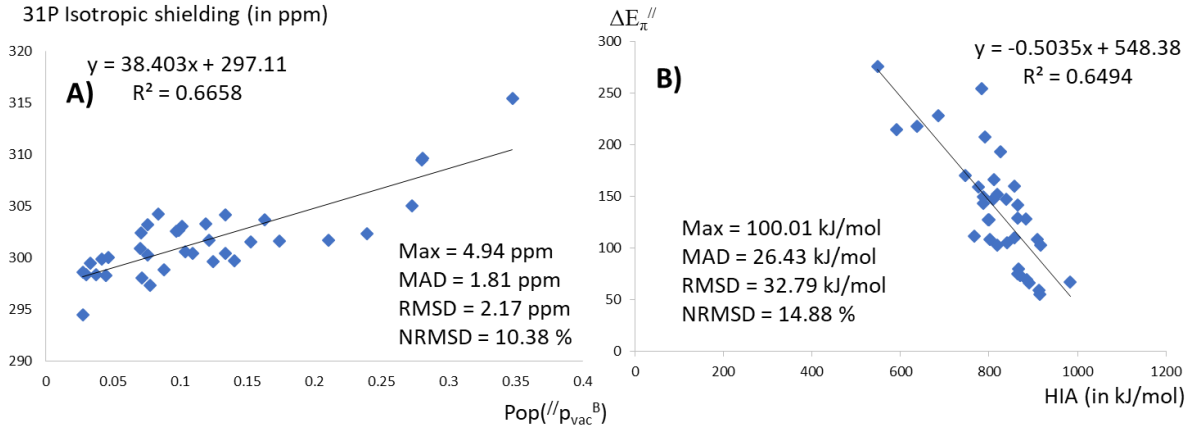

Figure 5-13: Correlation plots for (**X**-BH_2)$^{\perp}$-$POEt_3^+$ complexes between hydride ion affinity (HIA) and (A) occupancy of the vacant orbital of B in $X^{//}$-BH_2^+, (pop(p_{vac}^B)) and (B) energy of the C→B π-interaction as calculated by the EDA-NOCV analysis ($\Delta E_\pi^{//}$).

The lack of a correlation between HIA and occupancy of the vacant orbital on boron in the 'free' Lewis acid indicates a fundamental flaw in our formulation of Lewis acidity. The electron deficiency of the boron center in $\mathbf{X}^{//}$-BH_2^+ is compensated by donation from its three substituents. For our series of dihydrido borenium cations, the variation in Lewis acidity of the B centre is brought about by changing the electronic properties of the substituent **X**. **X** can donate to the boron centre via two channels - σ and π donation. Now, while we have accounted for the π-donation from **X**, the 'total' Lewis acidity of the boron, measured effectively by the HIA or the ^{31}P isotropic shielding, should actually be a combination of both σ and π-interactions at the boron centre, as this centre in **X**-BH_3 and (**X**-BH_2)$^{\perp}$-$POEt_3^+$ and **X**-BH_3 are not planar but pyramidal. If this assumption is correct HIA should be represented by a linear combination of σ-donation and π-donation. In graphs A and B $\Delta E^{//}_\pi$ is used in the

linear combination whereas in graph C $\Delta E^{//}{}_{\pi\ corr}$ has been used. Using $\Delta E^{//}{}_{\pi\ corr}$ lowers the R^2 value slightly.

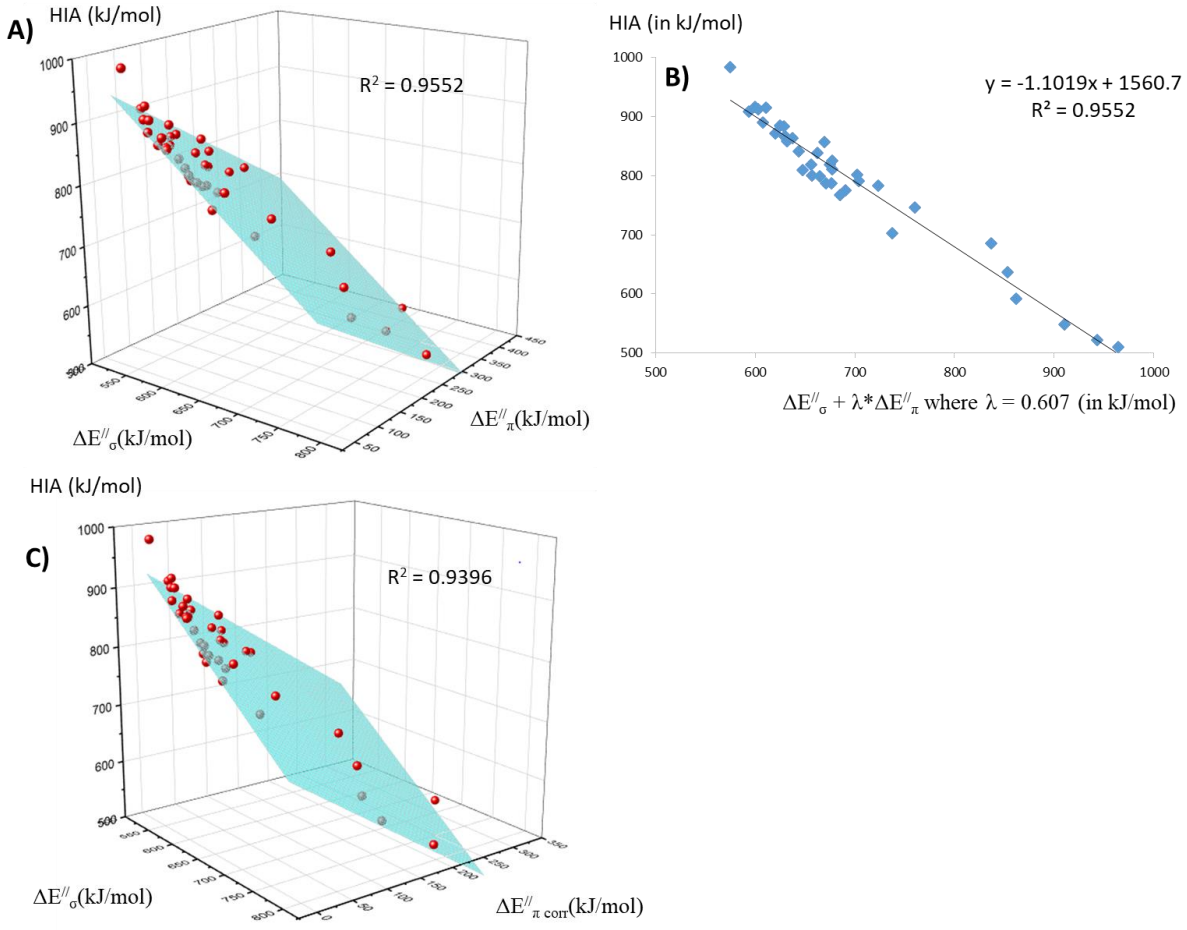

Figure 5-14: Correlation plot for (**X**-BH_2)$^{\perp}$-$POEt_3^+$ complexes between HIA and $\Delta E^{//}{}_{\sigma}$ and $\Delta E^{//}{}_{\pi}$ energy computed using ETS-NOCV analysis (**A** and **B**); Correlation plot for (**X**-BH_2)$^{\perp}$-$POEt_3^+$ complexes between HIA and $\Delta E^{//}{}_{\sigma}$ and $\Delta E^{//}{}_{\pi\ corr}$ (**C**)

Our hypothesis is proved correct by the excellent correlation between the energy of σ-donation and the energy of the π-donation of **X** to -BH_2^+ calculated by ETS-NOCV and HIA (R^2 = 0.94). HIA can be expressed as $a*E^{//}{}_{\sigma} + b*E^{//}{}_{\pi} + c$ where |a| = 1.10185 ± 0.08399 and |b| = 0.66546 ± 0.07152 which makes |a| : |b| range between 1.38 and 2. This means that the σ-effect plays a more dominant role in formulating the HIA than the π-effect, constituting between 58 - 66 % of the total (σ+π) effect. However, the influence of π-interaction is in no way insignificant.

One can arrive at the exact same conclusion by modifying the equation, appropriating it for a 2D graph as well.

As HIA = $a*E_{\sigma}^{//} + b*E_{\pi}^{//} + c$,

HIA = $a*(E_{\sigma}^{//} + \lambda*E_{\pi}^{//}) + c$ where $\lambda = b/a$

Now, when λ is varied to obtain a coefficient of determination as close to 1 as possible, we end up with $R^2 = 0.955189$, a = 1.1019 and λ = 0.61 – i.e., the exact same equation as the one obtained from the 3-D graph.

5.3.5. Charge Analysis

The charge associated with each atom in (**X**-BH_2)$^{\perp}$-$POEt_3^+$ and **X**$^{//}$-BH_2^+ can be obtained from NBO analysis (Table 2). In **X**$^{//}$-BH_2^+ the BH_2 unit has an average positive charge of 0.3 and the **X** unit has an average positive charge of 0.7. In (**X**-BH_2)$^{\perp}$-$POEt_3^+$ molecule, there is a small negative charge on the BH_2 unit, **X** has a smaller average positive charge of 0.6 and $POEt_3$ has an average positive charge of 0.4. This indicates that there is a flow of electrons from $POEt_3$ to the **X**$^{//}$-BH_2^+ unit as a result of the adduct formation with the Lewis base $POEt_3$.

The net electron flow can be measured by the charge that appears on $POEt_3$ in the adduct as compared to its 'free' state, where it is neutral. This outflow of charge is found to be quite well correlated to the total hydride ion affinity ($R^2 = 0.94$, Figure 5-15 A). This is again expected as both parameters represent overall effectiveness of **X**$^{//}$-BH_2^+ as a Lewis acid by measuring properties of its adducts.

Table 2: Charge distribution analysis in $\mathbf{X}^{//}$-BH_2^+ and $(\mathbf{X}\text{-}BH_2)^{\perp}$-$POEt_3^+$. Geometry optimization carried out at B3LYP/TZVP level.

	$(\mathbf{X}\text{-}BH_2)^{\perp}$-$POEt_3^+$			$\mathbf{X}^{//}$-BH_2^+		Charge Flow		
X	X	BH_2	$POEt_3$	BH_2	X	Δ Charge BH_2	Δ Charge X	Δ Charge $POEt_3$
1	0.60773	-0.03697	0.42923	0.37992	0.62006	0.41689	0.01233	-0.42923
2	0.57464	-0.01691	0.44226	0.39995	0.60005	0.41686	0.02541	-0.44226
3	0.60064	-0.02720	0.42655	0.38331	0.61670	0.41051	0.01606	-0.42655
4	0.60020	-0.02715	0.42693	0.38650	0.61350	0.41365	0.01330	-0.42693
5	0.61273	-0.03276	0.41999	0.36397	0.63603	0.39673	0.02330	-0.41999
6	0.60807	-0.03014	0.42205	0.36989	0.63011	0.40003	0.02204	-0.42205
7	0.61634	-0.03330	0.41700	0.35267	0.64732	0.38597	0.03098	-0.41700
8	0.61341	-0.03352	0.42012	0.35920	0.64078	0.39272	0.02737	-0.42012
9	0.59112	-0.00101	0.40987	0.36529	0.63470	0.36630	0.04358	-0.40987
10	0.60055	-0.01632	0.41578	0.36071	0.63930	0.37703	0.03875	-0.41578
11	0.59057	-0.00429	0.41369	0.37321	0.62679	0.37750	0.03622	-0.41369
12	0.58975	-0.02254	0.43279	0.36643	0.63357	0.38897	0.04382	-0.43279
13	0.59419	-0.01525	0.42104	0.36558	0.63443	0.38083	0.04024	-0.42104
14	0.58868	-0.02119	0.43253	0.35511	0.64490	0.37630	0.05622	-0.43253
15	0.60757	-0.01086	0.40328	0.35109	0.64892	0.36195	0.04135	-0.40328
16	0.57988	-0.00758	0.42768	0.35830	0.64170	0.36588	0.06182	-0.42768
17	0.60487	-0.01514	0.41027	0.33361	0.66638	0.34875	0.06151	-0.41027
18	0.61089	-0.02459	0.41370	0.33444	0.66556	0.35903	0.05467	-0.41370
19	0.61415	-0.02529	0.41116	0.32543	0.67455	0.35072	0.06040	-0.41116
20	0.60798	-0.03132	0.42336	0.32620	0.67379	0.35752	0.06581	-0.42338
21	0.60700	-0.03094	0.42393	0.31591	0.68408	0.34685	0.07708	-0.42393
22	0.63327	-0.04234	0.40906	0.28845	0.71154	0.33079	0.07827	-0.40906
23	0.61121	-0.02518	0.41401	0.30122	0.69878	0.32640	0.08757	-0.41401
24	0.61603	-0.03140	0.41538	0.29281	0.70722	0.32421	0.09119	-0.41538
25	0.61738	-0.02500	0.40759	0.29372	0.70627	0.31872	0.08889	-0.40759
26	0.62770	-0.03832	0.41063	0.28004	0.71994	0.31836	0.09224	-0.41063
27	0.61299	-0.03203	0.41904	0.28258	0.71742	0.31461	0.10443	-0.41904
28	0.62687	-0.03762	0.41075	0.26180	0.73820	0.29942	0.11133	-0.41075
29	0.63566	-0.02970	0.39404	0.25339	0.74661	0.28309	0.11095	-0.39404
30	0.61508	-0.03157	0.41651	0.25063	0.74936	0.28220	0.13428	-0.41651
32	0.62738	-0.03320	0.40581	0.20756	0.79240	0.24076	0.16502	-0.40581
33	0.63186	-0.04040	0.40851	0.18172	0.81829	0.22212	0.18643	-0.40851
34	0.65273	-0.02028	0.36754	0.14970	0.85031	0.16998	0.19758	-0.36754
35	0.64258	-0.00204	0.35946	0.15734	0.84270	0.15938	0.20012	-0.35946
36	0.62385	0.01739	0.35874	0.16110	0.83888	0.14371	0.21503	-0.35874
37	0.70818	-0.03479	0.32669	0.06198	0.93802	0.09677	0.22984	-0.32669

The electron density lost from $POEt_3$ is redistributed in the $(\mathbf{X}\text{-}BH_2)^{\delta+}$ unit. The charge gained at the BH_2 unit and the **X** unit can be calculated by a simple subtraction of the charges possessed by these units in $\mathbf{X}^{//}\text{-}BH_2^+$ and $(\mathbf{X}\text{-}BH_2)^{\perp}\text{-}POEt_3^+$.

Δ Charge POEt3 = Charge ($POEt_3$ in $(\mathbf{X}\text{-}BH_2)^{\perp}\text{-}POEt_3^+$) – Charge (free $POEt_3$)

Δ Charge BH2 = Charge (BH_2 in $(\mathbf{X}\text{-}BH_2)^{\perp}\text{-}POEt_3^+$) – Charge ($BH_2$ in $\mathbf{X}^{//}\text{-}BH_2^+$)

Δ Charge X = Charge (**X** in $(\mathbf{X}\text{-}BH_2)^{\perp}\text{-}POEt_3^+$) – Charge (**X** in $\mathbf{X}^{//}\text{-}BH_2^+$)

This goes to show an average gain of 0.32 electrons on the BH_2 unit and that of 0.08 electrons on the **X** fragment. It is interesting to note that there is a very strong correlation between the charge gained at BH_2 and the original occupancy of the vacant B orbital in the free Lewis acid, $\mathbf{X}^{//}\text{-}BH_2^+$(Figure 5-15 B). This goes to indicate that the charge distribution within $(\mathbf{X}\text{-}BH_2)^{\perp}\text{-}POEt_3^+$ adduct is dictated by the Lewis acidity of the free acid ($\mathbf{X}^{//}\text{-}BH_2^+$). Another interesting consequence of such a correlation is that the B vacant orbital seems to have an upper limit to the total number of electrons that can occupy it in the $(\mathbf{X}\text{-}BH_2)^{\perp}\text{-}POEt_3^+$ complex.

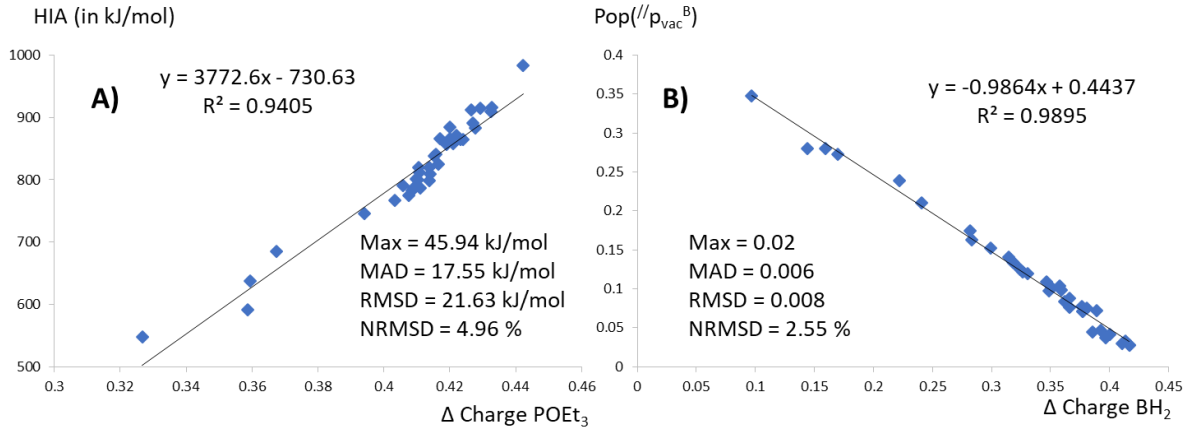

Figure 5-15: Correlation plots for $(\mathbf{X}\text{-}BH_2)^{\perp}\text{-}POEt_3^+$ complexes between (A) HIA and Δ Charge $POEt_3$ and (B) pop($^{//}p_{vac}^{B}$) and Δ Charge BH_2

5.3.6. ^{11}B NMR Analysis

In principle, measuring the Lewis acidity of the free $\mathbf{X}^{//}$-BH_2^+ using NMR spectroscopy can probably be done by measuring the chemical shift of the B centre in $\mathbf{X}^{//}$-BH_2^+. This method is non-intrusive – i.e. no probe molecule is required and it should measure the electron donation from **X** to BH_2^+ unit. This was indeed the logic behind measuring the chemical shift of phosphorus in carbene-phospinidene adducts as a measure of π-accepting ability of carbenes.[115] ^{11}B chemical shifts have been recently calculated using DFT in combination with GIAO and compared with experimental values for a range of boron containing compound.[116] The correlation with experimental value has been found to be reasonably good. However, there are no experimental accounts that use the chemical shift of ^{11}B nucleus as a scale for measuring Lewis acidity.

The isotropic shielding of the boron centre in $\mathbf{X}^{//}$-BH_2^+ was measured and it was found to correlate quite well with the π-donating ability of **X**, represented by $E^{//}_{\pi\ corr}$. The calculations were performed for all $\mathbf{X}^{//}$-BH_2^+ on page 13 except **36** and **38**. The correlation clearly shows that the carbones (**34**, **35**, **37** and **39**) stand apart from the other carbenes as a separate class. It is difficult to say why the carbones show such a distinctive feature consistent with the *weaker* shielding of the boron nucleus and demands further investigation.

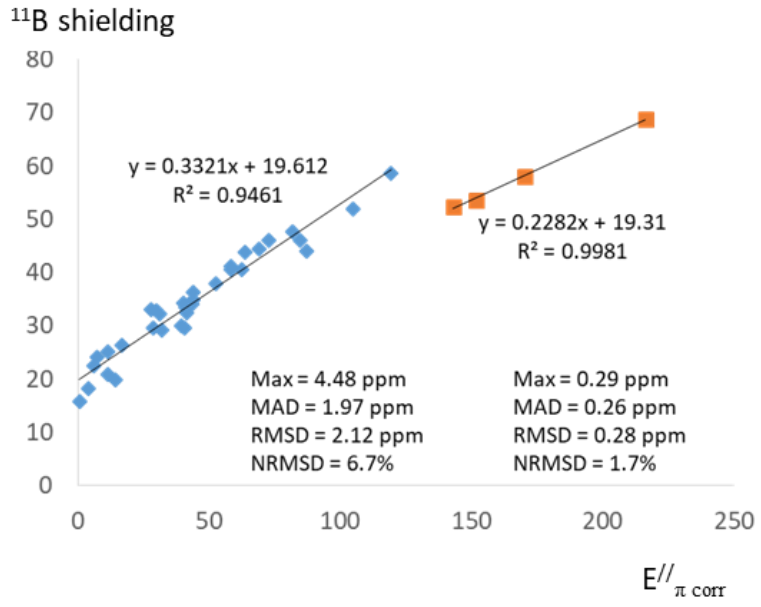

Figure 5-16: Correlation between ^{11}B isotropic shielding and $E^{//}_{\pi\ corr}$

5.4. Conclusion

In this chapter our primary objective was to bring clarity to Lewis acidity descriptors like hydride ion affinity and Gutmann-Beckett parameter and also establish a quantitative relationship between structural feature like the σ and π-bonds with Lewis acidity descriptors.

- With this in mind, at first the method for calculating ^{31}P isotropic shielding has been standardised. After that the HIA, chemical shift of P (related to the AN) and interaction energy associated with the formation of $POEt_3$ adduct (ΔE_{inter}) were evaluated. It was found that these three quantities correlate surprisingly well with each other in spite of being in different categories with respect to Greb's classification. These three parameters were therefore believed to quantify the same chemical entity – Lewis acidity of **X**-BH_2^+. HIA was then adopted as the main Lewis acidity descriptor, as it does not suffer any limitation compared to the chemical shift of P which required the adapted conformation to be selected.
- The correlation between descriptor of $C_{carbene}\rightarrow B$ π-bond and HIA is found to be unexpectedly low, casting doubt on the hypothesis that the vacant p-orbital on B is the main source of Lewis acidity in these molecules. In fact, a combination of σ and π C→B bond correlates very well with HIA, indicating that both these factors play an important role.
- Finally, a third intrinsic measure of Lewis acidity has been investigated – the isotropic shielding of ^{11}B boron. This parameter correlates exclusively with the C→B π-donation.

Therefore, at the end of this chapter we are equipped with a measure for Lewis acidity and we also know how the structural features of **X**-BH_2^+ molecules quantitatively influence the Lewis acidity. In the next chapter we will explore how this Lewis acidity scale can be used in predicting the reactivity of these molecules in activating H_2.

References

1. Sivaev, I. B.; Bregadze, V. I., Lewis acidity of boron compounds. *Coordination Chemistry Reviews* **2014,** *270-271*, 75-88.
2. Arrhenius, S., On the dissociation of substances dissolved in water.*Zeitschrift für physikalische Chemie.* **1887,** *1*, 631.
3. Miessler, G. L.; Tarr, D. A., Inorganic Chemistry J. Pearson Education International. **2000**, 380-388.
4. Brönsted, J. N., Einige Bemerkungen über den Begriff der Säuren und Basen. *Recueil des Travaux Chimiques des Pays-Bas* **1923,** *42* (8), 718-728.
5. Lowry, T. M., The uniqueness of hydrogen. *Journal of the Society of Chemical Industry* **1923,** *42* (3), 43-47.
6. Lewis, G. N., The atomand themolecule. *Journal of the American Chemical Society* **1916,** *38* (4), 762-785.
7. Lewis, G. N., Valence and the Structure of Atoms and Molecules. *Chemical Catalog Company, Incorporated*: **1923**, 172.
8. Muller, P., Glossary of terms used in physical organic chemistry (IUPAC Recommendations 1994). *Pure and Applied Chemistry* **1994,** *66* (5), 1077-1184.
9. Gaffen, J. R.; Bentley, J. N.; Torres, L. C.; Chu, C.; Baumgartner, T.; Caputo, C. B., A Simple and Effective Method of Determining Lewis Acidity by Using Fluorescence. *Chem* **2019,** *5* (6), 1567-1583.
10. Baumgartner, T.; Jäkle, F., *Main group strategies towards functional hybrid materials*. John Wiley & Sons: **2018.**
11. Yurash, B.; Cao, D. X.; Brus, V. V.; Leifert, D.; Wang, M.; Dixon, A.; Seifrid, M.; Mansour, A. E.; Lungwitz, D.; Liu, T.; Santiago, P. J.; Graham, K. R.; Koch, N.; Bazan, G. C.; Nguyen, T. Q., Towards understanding the doping mechanism of organic semiconductors by Lewis acids. *Nature Materials* **2019,** *18* (12), 1327-1334.
12. Reddy, S. S.; Arivunithi, V. M.; Sree, V. G.; Kwon, H.; Park, J.; Kang, Y. C.; Zhu, H.; Noh, Y. Y.; Jin, S. H., Lewis acid-base adduct-type organic hole transport material for high performance and air-stable perovskite solar cells. *Nano Energy* **2019,** *58*, 284-292.
13. Fang, H.; Oestreich, M., Defunctionalisation catalysed by boron Lewis acids. *Chemical Science* **2020,** *11* (47), 12604-12615.
14. Wade, C. R.; Broomsgrove, A. E. J.; Aldridge, S.; Gabbaï, F. P., Fluoride Ion Complexation and Sensing Using Organoboron Compounds. *Chemical Reviews* **2010,** *110* (7), 3958-3984.
15. Jäkle, F., Advances in the Synthesis of Organoborane Polymers for Optical, Electronic, and Sensory Applications. *Chemical Reviews* **2010,** *110* (7), 3985-4022.
16. Davies A. G., Lewis acids in organic synthesis. H. Yamamoto (ed.), Wiley–VCH, Weinheim, **2000**.
17. Chen, E. Y. X.; Marks, T., Cocatalysts for metal-catalyzed olefin polymerization: activators, activation processes, and structure− activity relationships. *Chemical Reviews.* **2000,** *100* (4), 1391-1434.

18. Erker, G., The (butadiene)metal complex/B(C6F5)3 pathway to homogeneous single component Ziegler–Natta catalyst systems. *Chemical Communications.* **2003,** (13), 1469-1476.
19. Simocko, C.; Wagener, K. B., Effects of Boron-Containing Lewis Acids on Olefin Metathesis. *Organometallics* **2013,** *32* (9), 2513-2516.
20. Stephan, D. W.; Erker, G., Frustrated Lewis Pair Chemistry: Development and Perspectives. *Angewandte Chemie International Edition* **2015,** *54* (22), 6400-6441.
21. Stephan, D. W. , The broadening reach of frustrated Lewis pair chemistry. *Science* **2016,** 354 (6317), aaf7229.
22. Fasano, V.; Ingleson, M. J., Recent advances in water-tolerance in frustrated Lewis pair chemistry. *Synthesis.* **2018,** *50* (09), 1783-1795.
23. Ishihara, K. Chiral B(III) Lewis Acids. *In Lewis Acids in Organic Synthesis*, H. Yamamoto (Ed.) **2000**.
24. Ishihara, K.; Yamamoto, H., Arylboron Compounds as Acid Catalysts in Organic Synthetic Transformations. *European Journal of Organic Chemistry* **1999,** *1999* (3), 527-538.
25. Hosmane, N. S., *Boron science: new technologies and applications*. CRC press: 2011.
26. Greb, L., Lewis Superacids: Classifications, Candidates, and Applications. *Chemistry – A European Journal* **2018,** *24* (68), 17881-17896.
27. Woodward, S., HSAB matching and mismatching in selective catalysis and synthesis. *Tetrahedron* **2002,** *58* (6), 1017-1050.
28. Olah, G. A.; Prakash, G. S.; Sommer, J.; Molnar, A., *Superacid chemistry (2nd Edition).* United States of America. Wiley-Interscience. **2009**.
29. Olah, G. A.; Klumpp, D. A., *Superelectrophiles and their chemistry*. United States of America. Wiley-Interscience. **2008**.
30. Himmel, D.; Goll, S. K.; Leito, I.; Krossing, I., A Unified pH Scale for All Phases. *Angewandte Chemie International Edition* **2010,** *49* (38), 6885-6888.
31. Himmel, D.; Radtke, V.; Butschke, B.; Krossing, I., Basic Remarks on Acidity. *Angewandte Chemie International Edition* **2018,** *57* (16), 4386-4411.
32. Drago, R. S., The coordination model for non-aqueous solvents. *Pure and Applied Chemistry* **1980,** *52* (10), 2261-2274.
33. Drago, R. S., The interpretation of reactivity in chemical and biological systems with the E and C model. *Coordination Chemistry Reviews* **1980,** *33* (3), 251-277.
34. Rowsell, B. D.; Gillespie, R. J.; Heard, G. L., Ligand Close-Packing and the Lewis Acidity of BF3 and BCl3. *Inorganic Chemistry* **1999,** *38* (21), 4659-4662.
35. Coyle, T. D.; Kaesz, H. D.; Stone, F. G. A., Molecular Addition Compounds of Boron. II. Thiophane-Borane and Related Adducts1,2. *Journal of the American Chemical Society* **1959,** *81* (12), 2989-2994.
36. Pearson, R. G., Hard and Soft Acids and Bases. *Journal of the American Chemical Society* **1963,** *85* (22), 3533-3539.
37. Klopman, G., Chemical reactivity and the concept of charge- and frontier-controlled reactions. *Journal of the American Chemical Society* **1968,** *90* (2), 223-234.

38. Mulliken, R. S., Molecular Compounds and their Spectra. II. *Journal of the American Chemical Society* **1952,** *74* (3), 811-824.
39. Hayes, I. C.; Stone, A. J., An intermolecular perturbation theory for the region of moderate overlap. *Molecular Physics* **1984,** *53* (1), 83-105.
40. Jeziorski, B.; Moszynski, R.; Szalewicz, K., perturbation-theory approach to intermolecular potential-energy surfaces of van-der-waals complexes. *Chemical Reviews* **1994,** *94* (7), 1887-1930.
41. Frenking, G.; Wichmann, K.; Fröhlich, N.; Loschen, C.; Lein, M.; Frunzke, J.; Rayón, V. c. M., Towards a rigorously defined quantum chemical analysis of the chemical bond in donor–acceptor complexes. *Coordination Chemistry Reviews* **2003,** *238-239*, 55-82.
42. Maria, P. C.; Gal, J. F.; De Franceschi, J.; Fargin, E., Chemometrics of solvent basicity: multivariate analysis of the basicity scales relevant to nonprotogenic solvents. *Journal of the American Chemical Society* **1987,** *109* (2), 483-492.
43. Laurence, C.; Graton, J.; Gal, J.-F., An Overview of Lewis Basicity and Affinity Scales. *Journal of Chemical Education* **2011,** *88* (12), 1651-1657.
44. Mayer, U.; Gutmann, V.; Gerger, W., The acceptor number — A quantitative empirical parameter for the electrophilic properties of solvents. *Monatshefte für Chemie / Chemical Monthly* **1975,** *106* (6), 1235-1257.
45. Gutmann, V., Solvent effects on the reactivities of organometallic compounds. *Coordination Chemistry Reviews* **1976,** *18* (2), 225-255.
46. Beckett, M. A.; Strickland, G. C.; Holland, J. R.; Sukumar Varma, K., A convenient n.m.r. method for the measurement of Lewis acidity at boron centres: correlation of reaction rates of Lewis acid initiated epoxide polymerizations with Lewis acidity. *Polymer* **1996,** *37* (20), 4629-4631.
47. Childs, R. F.; Mulholland, D. L.; Nixon, A., The Lewis acid complexes of α,β-unsaturated carbonyl and nitrile compounds. A nuclear magnetic resonance study. *Canadian Journal of Chemistry* **1982,** *60* (6), 801-808.
48. Morgan, M. M.; Marwitz, A. J. V.; Piers, W. E.; Parvez, M., Comparative Lewis Acidity in Fluoroarylboranes: B(o-HC6F4)3, B(p-HC6F4)3, and B(C6F5)3. *Organometallics* **2013,** *32* (1), 317-322.
49. Hilt, G.; Nödling, A., The Correlation of Lewis Acidities of Silyl Triflates with Reaction Rates of Catalyzed Diels–Alder Reactions. *European Journal of Organic Chemistry* **2011,** *2011* (35), 7071-7075.
50. Beattie, I. R.; Gilson, T., 430. A normal co-ordinate analysis of MeCN, BX3, and its relevance to the thermodynamic stability of co-ordination compounds. *Journal of the Chemical Society (Resumed)* **1964,** (0), 2292-2295.
51. Purcell, K. F.; Drago, R. S., Studies of the Bonding in Acetonitrile Adducts1. *Journal of the American Chemical Society* **1966,** *88* (5), 919-924.
52. Swanson, B.; Shriver, D. F., Vibrational spectra, vibrational analysis and bonding in acetonitrile-boron trifluoride. *Inorganic Chemistry* **1970,** *9* (6), 1406-1416.

53. Fenwick, J. T. F.; Wilson, J. W., Thermochemical investigation into the Lewis acidity of the boron atom in some triaryloxyboranes. *Inorganic Chemistry* **1975,** *14* (7), 1602-1604.
54. Luo, L.; Marks, T. J., Ziegler–Natta catalyst activation. Thermodynamic and kinetic aspects of metallocenium ion-pair formation, dissociation, and structural reorganization. *Topics in Catalysis* **1999,** *7* (1), 97-106.
55. Metz, M. V.; Schwartz, D. J.; Stern, C. L.; Marks, T. J.; Nickias, P. N., New Perfluoroarylborane Activators for Single-Site Olefin Polymerization. Acidity and Cocatalytic Properties of a "Superacidic" Perfluorodiboraanthracene. *Organometallics* **2002,** *21* (20), 4159-4168.
56. Olah, G. A.; Kobayashi, S.; Tashiro, M., Aromatic substitution. XXX. Friedel-Crafts benzylation of benzene and toluene with benzyl and substituted benzyl halides. *Journal of the American Chemical Society* **1972,** *94* (21), 7448-7461.
57. Kobayashi, S.; Busujima, T.; Nagayama, S., A Novel Classification of Lewis Acids on the Basis of Activity and Selectivity. *Chemistry – A European Journal* **2000,** *6* (19), 3491-3494.
58. Lappert, M. F., 103. Co-ordination compounds having carboxylic esters as ligands. Part II. Relative acceptor strengths of some Group III and IV halides. *Journal of the Chemical Society (Resumed)* **1962,** (0), 542-548.
59. Davydova, E. I.; Sevastianova, T. N.; Suvorov, A. V.; Timoshkin, A. Y., Molecular complexes formed by halides of group 4,5,13–15 elements and the thermodynamic characteristics of their vaporization and dissociation found by the static tensimetric method. *Coordination Chemistry Reviews* **2010,** *254* (17), 2031-2077.
60. Gal, J.-F.; Iacobucci, C.; Monfardini, I.; Massi, L.; Duñach, E.; Olivero, S., A Quantitative Approach of the Interaction between Metal Triflates and Organic Ligands Using Electrospray Mass Spectrometry. *Journal of the American Society for Mass Spectrometry* **2012,** *23* (12), 2059-2062.
61. Leopold, K. R.; Canagaratna, M.; Phillips, J. A., Partially Bonded Molecules from the Solid State to the Stratosphere. *Accounts of Chemical Research* **1997,** *30* (2), 57-64.
62. Kaupp, M.; Metz, B.; Stoll, H., Breakdown of Bond Length-Bond Strength Correlation: A Case Study. *Angewandte Chemie International Edition* **2000,** *39* (24), 4607-4609.
63. Timoshkin, A. Y.; Bodensteiner, M.; Sevastianova, T. N.; Lisovenko, A. S.; Davydova, E. I.; Scheer, M.; Graßl, C.; Butlak, A. V., Do Solid-State Structures Reflect Lewis Acidity Trends of Heavier Group 13 Trihalides? Experimental and Theoretical Case Study. *Inorganic Chemistry* **2012,** *51* (21), 11602-11611.
64. Phillips, J. A.; Cramer, C. J., B−N Distance Potential of CH3CN−BF3 Revisited: Resolving the Experiment−Theory Structure Discrepancy and Modeling the Effects of Low-Dielectric Environments. *The Journal of Physical Chemistry B* **2007,** *111* (6), 1408-1415.
65. Smith, E. L.; Sadowsky, D.; Cramer, C. J.; Phillips, J. A., Structure, Bonding, and Energetic Properties of Nitrile−Borane Complexes: RCN−BH3. *The Journal of Physical Chemistry A* **2011,** *115* (10), 1955-1963.

66. Müller, L. O.; Himmel, D.; Stauffer, J.; Steinfeld, G.; Slattery, J.; Santiso-Quiñones, G.; Brecht, V.; Krossing, I., Simple Access to the Non-Oxidizing Lewis Superacid PhF→Al(ORF)3 (RF=C(CF3)3). *Angewandte Chemie International Edition* **2008,** *47* (40), 7659-7663.
67. O'Keeffe, M., Calculated structures and fluoride affinities for fluorides. *Journal of the American Chemical Society* **1986,** *108* (15), 4341-4343.
68. Böhrer, H.; Trapp, N.; Himmel, D.; Schleep, M.; Krossing, I., From unsuccessful H2-activation with FLPs containing B(Ohfip)3 to a systematic evaluation of the Lewis acidity of 33 Lewis acids based on fluoride, chloride, hydride and methyl ion affinities. *Dalton Transactions* **2015,** *44* (16), 7489-7499.
69. Clark, E. R.; Del Grosso, A.; Ingleson, M. J., The Hydride-Ion Affinity of Borenium Cations and Their Propensity to Activate H2 in Frustrated Lewis Pairs. *Chemistry – A European Journal* **2013,** *19* (7), 2462-2466.
70. Erdmann, P.; Greb, L., Multidimensional Lewis Acidity: A Consistent Data Set of Chloride, Hydride, Methide, Water and Ammonia Affinities for 183 p-Block Element Lewis Acids. *ChemPhysChem* **2021,** *22* (10), 935-943.
71. De Vries, T. S.; Prokofjevs, A.; Vedejs, E., Cationic Tricoordinate Boron Intermediates: Borenium Chemistry from the Organic Perspective. *Chemical Reviews* **2012,** *112* (7), 4246-4282.
72. Jupp, A. R.; Johnstone, T. C.; Stephan, D. W., The global electrophilicity index as a metric for Lewis acidity. *Dalton Transactions* **2018,** *47* (20), 7029-7035.
73. Mercier, H. P. A.; Moran, M. D.; Schrobilgen, G. J.; Suontamo, R. J., Energetics of hydride and electron pair attachment to EX30/+ (E=B, C, Al, Si and X=F, Cl, Br, I) and the study of bonding trends among EX30/+, EX32−/−, and EX3H−/0 by use of ELF and NBO analyses. *Journal of Fluorine Chemistry* **2004,** *125* (11), 1563-1578.
74. Horn, M.; Mayr, H., Electrophilicity versus Electrofugality of Tritylium Ions in Aqueous Acetonitrile. *Chemistry – A European Journal* **2010,** *16* (25), 7478-7487.
75. Horn, M.; Mayr, H., Electrophilicities of Acceptor-Substituted Tritylium Ions. *European Journal of Organic Chemistry* **2011,** (32), 6470-6475.
76. Ashley, A. E.; Herrington, T. J.; Wildgoose, G. G.; Zaher, H.; Thompson, A. L.; Rees, N. H.; Krämer, T.; O'Hare, D., Separating Electrophilicity and Lewis Acidity: The Synthesis, Characterization, and Electrochemistry of the Electron Deficient Tris(aryl)boranes B(C6F5)3–n(C6Cl5)n (n = 1–3). *Journal of the American Chemical Society* **2011,** *133* (37), 14727-14740.
77. Müther, K.; Hrobárik, P.; Hrobáriková, V.; Kaupp, M.; Oestreich, M., The Family of Ferrocene-Stabilized Silylium Ions: Synthesis, 29Si NMR Characterization, Lewis Acidity, Substituent Scrambling, and Quantum-Chemical Analyses. *Chemistry – A European Journal* **2013,** *19* (49), 16579-16594.
78. Gonzalez, M. M., Cardenas, C., Rodríguez, J. I., Liu, S.; Heidar-Zadeh, F., Miranda-Quintana, R. A.; Ayers, P. W. Quantitative electrophilicity measures. *Acta-Phys -Chim. Sin*. **2018,** *34* (6), 662-674.

79. Childs, R. F.; Mulholland, D. L.; Nixon, A., Lewis acid addticts of α,β-unsaturated carbonyl and nitrile compounds. A calorimetric study. *Canadian Journal of Chemistry* **1982,** *60* (6), 809-812.
80. Brown, D. G.; Drago, R. S.; Bolles, T. F., The linear .DELTA.H-.DELTA.nu(sub C:O) relation for ethyl acetate adducts and its significance for donor-acceptor interactions. *Journal of the American Chemical Society* **1968,** *90* (21), 5706-5712.
81. Bolles, T. F.; Drago, R. S., The Enthalpy of Formation of Coordination Compounds of Trimethyltin Chloride. *Journal of the American Chemical Society* **1966,** *88* (17), 3921-3925.
82. Gutmann, V., *Chemische Funktionslehre*. New York. Springer-Verlag Wien. **2013**.
83. Gutmann, V.; Wychera, E. J. I.; Letters, N. C., Coordination reactions in non aqueous solutions-The role of the donor strength. **1966,** *2* (9), 257-260.
84. Gutmann, V., *Coordination chemistry in non-aqueous solutions*. Wien, New York. Springer-Verlag. **2012.**
85. Mayer, U.; Gutmann, V., The functional approach to ionization phenomena in solutions. In *Advances in Inorganic Chemistry and Radiochemistry (1st Edition)*, Vol. 17. Academic Press. **1975.** pp 189-230.
86. Erlich, R. H.; Popov, A. I. , Spectroscopic studies of ionic solvation. X. Study of the solvation of sodium ions in nonaqueous solvents by sodium-23 nuclear magnetic resonance. *Journal of American Chemical Society.* **1971,** *93* (22), 5620-5623.
87. Spaziante, P.; Gutmann, V. , The interaction of trifluoroiodomethane with donor molecules.*Inorganica Chimica Acta.* **1971,** *5*, 273-275.
88. Blokker, E.; Groen, C. G. T.; van der Schuur, J. M.; Talma, A. G.; Bickelhaupt, F. M., Hydride affinities of cationic maingroup-element hydrides across the periodic table. *Results in Chemistry* **2019,** *1*, 100007.
89. Mallouk, T. E.; Rosenthal, G. L.; Mueller, G.; Brusasco, R.; Bartlett, N., Fluoride ion affinities of germanium tetrafluoride and boron trifluoride from thermodynamic and structural data for (SF3)2GeF6, ClO2GeF5, and ClO2BF4. *Inorganic Chemistry* **1984,** *23* (20), 3167-3173.
90. Timoshkin, A. Y.; Frenking, G., Gas-Phase Lewis Acidity of Perfluoroaryl Derivatives of Group 13 Elements. *Organometallics* **2008,** *27* (3), 371-380.
91. Mock, M. T.; Potter, R. G.; Camaioni, D. M.; Li, J.; Dougherty, W. G.; Kassel, W. S.; Twamley, B.; DuBois, D. L., Thermodynamic Studies and Hydride Transfer Reactions from a Rhodium Complex to BX3 Compounds. *Journal of the American Chemical Society* **2009,** *131* (40), 14454-14465.
92. Grant, D. J.; Dixon, D. A.; Camaioni, D.; Potter, R. G.; Christe, K. O., Lewis Acidities and Hydride, Fluoride, and X− Affinities of the BH3−nXn Compounds for (X = F, Cl, Br, I, NH2, OH, and SH) from Coupled Cluster Theory. *Inorganic Chemistry* **2009,** *48* (18), 8811-8821.
93. Vianello, R.; Maksić, Z. B., Hydride Affinities of Borane Derivatives: Novel Approach in Determining the Origin of Lewis Acidity Based on Triadic Formula. *Inorganic Chemistry* **2005,** *44* (4), 1095-1102.

94. Kim, C.-K.; Lee, K.-A.; Bae, S.-Y.; Han, I.-S.; Kim, C.-K. J. B. o. t. K. C. S., Theoretical studies on the hydride ion affinities of carbocations. **2004,** *25* (2), 311-313.
95. Cheng, J.; Handoo, K. L.; Parker, V. D., Hydride affinities of carbenium ions in acetonitrile and dimethyl sulfoxide solution. *Journal of the American Chemical Society* **1993,** *115* (7), 2655-2660.
96. Handoo, K. L.; Cheng, J. P.; Parker, V. D., Hydride affinities of organic radicals in solution. A comparison of free radicals and carbenium ions as hydride ion acceptors. *Journal of the American Chemical Society* **1993,** *115* (12), 5067-5072.
97. Cheng, J.; Handoo, K. L.; Xue, J.; Parker, V. D., Free energy hydride affinities of quinones in dimethyl sulfoxide solution. *The Journal of Organic Chemistry* **1993,** *58* (19), 5050-5054.
98. Maksić, Z. B.; Vianello, R., Physical origin of chemical phenomena: Interpretation of acidity, basicity, and hydride affinity by trichotomy paradigm. *Pure and Applied Chemistry* **2007,** *79* (6), 1003-1021.
99. Vianello, R.; Peran, N.; Maksić, Z. B., Hydride Affinities of Substituted Alkenes: Their Prediction by Density Functional Calculations and Rationalisation by Triadic Formula. *European Journal of Organic Chemistry* **2007,**(3), 526-539.
100. M.J. Frisch, G.W. Trucks, H.B. Schlegel, G.E. Scuseria, M.A. Robb, J.R. Cheeseman, G. Scalmani, V. Barone, B. Mennucci, G.A. Petersson, H. Nakatsuji, M. Caricato, X. Li, H.P. Hratchian, A.F. Izmaylov, J. Bloino, G. Zheng, J.L. Sonnenberg, M. Hada, M. Ehara, K. Toyota, R. Fukuda, J. Hasegawa, M. Ishida, T. Nakajima, Y. Honda, O. Kitao, H. Nakai, T. Vreven, J.A. Montgomery Jr, J.E. Peralta, F. Ogliaro, M. Bearpark, J.J. Heyd, E. Brothers, K.N. Kudin, V.N. Staroverov, R. Kobayashi, J. Normand, K. Raghavachari, A. Rendell, J.C. Burant, S.S. Iyengar, J. Tomasi, M. Cossi, N. Rega, J.M. Millam, M. Klene, J.E. Knox, J.B. Cross, V. Bakken, C. Adamo, J. Jaramillo, R. Gomperts, R.E. Stratmann, O. Yazyev, A.J. Austin, R. Cammi, C. Pomelli, J.W. Ochterski, R.L. Martin, K. Morokuma, V.G. Zakrzewski, G.A. Voth, P. Salvador, J.J. Dannenberg, S. Dapprich, A.D. Daniels, Ö. Farkas, J.B. Foresman, J.V. Ortiz, J. Cioslowski, D.J. Fox, Gaussian, Inc., Wallingford CT, Gaussian 09, Revision D.01, **2013**.
101. Glendening, E. D.; Landis, C. R.; Weinhold, F., Natural bond orbital methods. *Wiley Interdisciplinary Reviews-Computational Molecular Science* **2012,** *2* (1), 1-42.
102. Lu, T.; Chen, F., Multiwfn: A multifunctional wavefunction analyzer. *Journal of Computational Chemistry* **2012,** *33* (5), 580-592.
103. te Velde, G.; Bickelhaupt, F. M.; Baerends, E. J.; Fonseca Guerra, C.; van Gisbergen, S. J. A.; Snijders, J. G.; Ziegler, T., Chemistry with ADF. *Journal of Computational Chemistry* **2001,** *22* (9), 931-967.
104. Fonseca Guerra, C.; Snijders, J. G.; te Velde, G.; Baerends, E. J., Towards an order-N DFT method. *Theoretical Chemistry Accounts* **1998,** *99* (6), 391-403.
105. ADF2017, S., Theoretical Chemistry, Vrije Universiteit, Amsterdam, The Netherlands, http://www.scm.com.
106. Krivdin, L. B., Recent advances in computational 31P NMR: Part 1. Chemical shifts. *Magnetic Resonance in Chemistry* **2020,** *58* (6), 478-499.

107. Dutta, S.; Maity, B.; Thirumalai, D.; Koley, D., Computational Investigation of Carbene–Phosphinidenes: Correlation between 31P Chemical Shifts and Bonding Features to Estimate the π-Backdonation of Carbenes. *Inorganic Chemistry* **2018,** *57* (7), 3993-4008.
108. Rusakov, Y. Y.; Rusakova, I. L.; Semenov, V. A.; Samultsev, D. O.; Fedorov, S. V.; Krivdin, L. B., Calculation of 15N and 31P NMR Chemical Shifts of Azoles, Phospholes, and Phosphazoles: A Gateway to Higher Accuracy at Less Computational Cost. *The Journal of Physical Chemistry A* **2018,** *122* (33), 6746-6759.
109. Latypov, S. K.; Polyancev, F. M.; Yakhvarov, D. G.; Sinyashin, O. G., Quantum chemical calculations of 31P NMR chemical shifts: scopes and limitations. *Physical Chemistry Chemical Physics* **2015,** *17* (10), 6976-6987.
110. Jensen, P.; Bunker, P., The potential surface and stretching frequencies of X˜ 3 B 1 methylene (CH2) determined from experiment using the Morse oscillator-rigid bender internal dynamics Hamiltonian. *The Journal of Chemical Physics.* **1988,** *89* (3), 1327-1332.
111. Del Grosso, A.; Pritchard, R. G.; Muryn, C. A.; Ingleson, M. J., Chelate Restrained Boron Cations for Intermolecular Electrophilic Arene Borylation. *Organometallics* **2010,** *29* (1), 241-249.
112. Beckett, M. A.; Brassington, D. S.; Coles, S. J.; Hursthouse, M. B., Lewis acidity of tris(pentafluorophenyl)borane: crystal and molecular structure of B(C6F5)3·OPEt3. *Inorganic Chemistry Communications* **2000,** *3* (10), 530-533.
113. Farrell, J. M.; Stephan, D. W., Planar N-Heterocyclic Carbene Diarylborenium Ions: Synthesis by Cationic Borylation and Reactivity with Lewis Bases. *Angewandte Chemie International Edition* **2015,** *54* (17), 5214-5217.
114. Mewald, M.; Fröhlich, R.; Oestreich, M., An Axially Chiral, Electron-Deficient Borane: Synthesis, Coordination Chemistry, Lewis Acidity, and Reactivity. *Chemistry – A European Journal* **2011,** *17* (34), 9406-9414.
115. Dutta, S.; Maity, B.; Thirumalai, D.; Koley, D., Computational Investigation of Carbene-Phosphinidenes: Correlation between P-31 Chemical Shifts and Bonding Features to Estimate the pi-Backdonation of Carbenes. *Inorganic Chemistry* **2018,** *57* (7), 3993-4008.
116. Gao, P.; Wang, X.; Huang, Z.; Yu, H., 11B NMR Chemical Shift Predictions via Density Functional Theory and Gauge-Including Atomic Orbital Approach: Applications to Structural Elucidations of Boron-Containing Molecules. *ACS Omega* **2019,** *4* (7), 12385-12392.

PART C – Application in the Activation of H_2

6. CHAPTER V
Interaction of Borenium Catalysts with H_2 and its Activation

Abstract

In this final part of the thesis, our main objective is to quantify the interaction of the **X**-BH_2^+ with molecular H_2. This chapter has two main parts – the first deals with the interaction between **X**-BH_2^+ and H_2 while the second deals with the heterolytic cleavage of H_2 by the FLP pair – **X**-BPh_2^+ and $P(^tBu)_3$. The theoretical indicator of structure (C-B σ and π bond strength) and Lewis acidity (HIA) have been compared with activation barrier for the reaction as well as experimental yield to demonstrate the utility of computational tools in building a bridge between structure and reactivity.

6.1. Introduction

In the previous chapters, we first looked at the electronic structure of divalent carbon borenium adducts (**X**-BH_2^+). We have thus identified features that reliably describe the electronic interactions between the divalent carbon part and the BH_2^+ borenium part, as described in chapters II and III. The next step of our work, described in chapter IV, was to study if these same features, specific to **X**-BH_2^+ adducts, can explain their interactions with external Lewis bases like H^- and $POEt_3$. In other words, can the characterization of a divalent carbon ligand **X** or its complex with the BH_2^+ moiety determine the Lewis acidity of the boron atom in the **X**-BH_2^+ adducts. We were thus able to show that the *thermodynamic* properties of these adducts, such as the strength of their interaction with H^-, is well correlated with a linear combination of σ- and π-donating abilities of **X**. The objective of this chapter is to go one step further by studying the reactivity of the borenium adducts. Can the above-mentioned properties established for ligand **X** explain the *kinetic* properties of the **X**-BH_2^+ adducts? The example chosen to answer this question is the activation of dihydrogen. We will proceed in 2 steps. We will first examine the interaction between **X**-BH_2^+ and molecular H_2. Then we will model the activation of hydrogen by Frustrated Lewis Pair (FLP) catalysts combining borenium ion Lewis acid and phosphine as Lewis base.

6.1.1. Hydrogen Activation

Hydrogen (H_2) is the simplest known molecule. Despite this, H_2 sits poised at the very centre of today's economy and promises to become even more significant in the future. The addition of hydrogen across unsaturated bonds is undoubtedly the most used transformation in the chemical industry.[1-6] The catalytic activation of hydrogen is used in hydrogenation,[7] dehydrogenation,[8] hydrodesulfurization,[9] hydrodenitrogenation[10] and many other processes. Hydrogen also has the potential to be a clean, renewable source of energy.[11] It has high energy content per mass compared to petroleum (120 MJ/kg for hydrogen vs. 44 MJ/kg for petroleum), although it has poor energy content per volume (0.01 kJ/L at standard temperature and pressure and 8.4 MJ/L for liquid hydrogen vs. 32 MJ/L for petroleum).[12] Catalytic hydrogen activation is a significant application in the field of energy storage as well.[13]

The activation of hydrogen is a challenging problem because of the very strong H-H σ-bond.[14-18] The energy of the H-H bond is 436 kJ/mol. However, it is possible to cleave this linkage in

more ways than one. The best known of these are of course solids – metals (mostly transition metals, some oxides (Al_2O_3, Cr_2O_3, ZnO etc.) and certain salts.[19] This explains that the hydrogenation of ethylene has an activation barrier of 50 kJ/mol in the gas phase whereas it is only 10 kJ/mol on the surface of a transition metal such as nickel or palladium. Furthermore, such hydrogenation reactions are occurring in nature around us all the time, at standard temperature and pressure (298 K, 1 atm). This is due to biological catalysts, better known as enzymes. This particular class of enzymes are called hydrogenases.[20] More recently, the role of metal ions and complexes have been recognised in catalysing hydrogenations homogenously.[21, 22]

In considering the function of the hydrogenation catalyst, three types of reactions may be noted:

(i) Exchange with deuterium or protolytic substances:

$H_2 + D_2 \longrightarrow 2HD$

(ii) Reduction of substances which are also reduced readily by reversible electron donors or at electrodes:

$2Ag^+ + H_2 \longrightarrow 2Ag\ (s) + 2H^+$

(iii) Reduction of 'inert' molecules, particularly reactions that lead to the formation of new carbon-hydrogen bonds:

$R_2C{=}CR_2 + H_2 \longrightarrow R_2CH\text{-}CHR_2$

By a general rule of thumb, the cataysts that are effective in the reaction of the last type are also effective in the reactions of the first two types, but the reverse is not necessarily true as the successive reactions impose more stringent requirement from the catalyst.[19] There are however instances of all three types of hydrogenation catalysts – homogeneous, heterogeneous and enzymatic – being useful in all three types of reactions. The fact that a catalyst is often handy in a wide variety of reactions suggests that the catalyst operates by activating the hydrogen molecule, in the sense of forming a reactive complex with it, which then participates in reactions with a variety of substrates.[23] This hypothesis holds true at least for the first two types of reactions described, the third one usually involves the need for activating the 'inert' substrate as well and naturally exhibits a more complicated pattern of catalytic effect.

In our present exploration, we are concerned only with homogenous activation of hydrogen by borenium ions. Therefore, we present only a brief overview of the other modes of activation of hydrogen before proceeding with our objective. For a detailed insight into these, the reader is directed to the excellent review by Halpern.[19]

6.1.2. Enzymatic Activation of Hydrogen

Hydrogenase enzymes constitute a special family of organometallic biomolecules that are capable of both producing hydrogen from water as well as the reverse reaction. The hydrogenases were first discovered in the 1930s and have captured the attention of the chemical audience since, with their high turnover numbers (1500 to 20000 molecules of H_2 per second at pH 7 and 37 °C in water), almost no overpotential and cheap raw materials.[24, 25] The success of hydrogenases is, of course, to be attributed to the metal centre present in the enzyme that weakens the H-H σ-bond by donating electrons to the σ* orbital from its filled d-orbitals. This is the common theme of H_2 activation by the involvement of any metal centre.

While hydrogen is often referred to as the post-oil fuel, most technological advancements made so far, such as petrochemical cells or proton-exchange-membrane fuel cells and electrolysers, all depend heavily on the catalytic abilities of the expensive platinum metal. Hydrogenase enzymes on the other hand have shown catalytic efficiency as high as the Pt-based catalysts, whilst only employing earth-abundant 3d-transition-metals (iron or nickel) based structures.[26] This remarkable ability motivated chemists to study the active site (the metal centre) and its ligand environment in an effort to mimic their coveted efficiency in cleaving the H-H bond.[27-32] The mimics have then been improved by methodically controlling their immediate environment by supramolecular chemistry.[33-35] Then, of course are the bio-hybrid systems arising from biosynthetic approaches which consist of synthetic mimics of the hydrogenase active site enclosed within peptides or protein cavities.[36-38]

Extensive theoretical and experimental studies have been performed in the last decades to understand the catalytic ability of the hydrogenases.[39-46] These enzymes can be put in three classes – Fe-Fe hydrogenase, Ni-Fe hydrogenase and Fe-only hydrogenases (Scheme 6-1). Established understanding of hydrogenases include the following points:[25]

(i) [NiFe] and [FeFe] bimetallic hydrogenases are able to decompose dihydrogen molecule into proton and electron whereas [Fe]-hydrogenases merely activate H_2 in the presence of a substrate;

(ii) [FeFe] hydrogenases show greater turnover frequency than the [NiFe] ones;

(iii) [NiFe] hydrogenases show better oxygen tolerance.

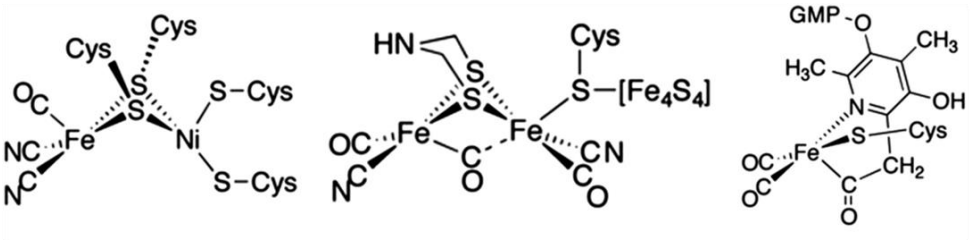

[NiFe] Hydrogenase [FeFe] Hydrogenase Fe Hydrogenase

Scheme 6-1: Three kinds of hydrogenase enzymes

Experimentally a large number of biomimetic enzymes have been designed but so far none surpass the original model. This makes the detailed study of the metal centre and their ligand environment indispensable. Another shortcoming of these enzymes is their oxygen-sensitivity, i.e., the enzymes are deactivated in an oxygen-rich environment.[47, 48] A lot of research is presently being dedicated to understanding the mechanism of oxygen mediated deactivation of the enzymes and to the characterisation of the few oxygen tolerant hydrogenases.[39, 40, 46, 49]

6.1.3. Heterogeneous Hydrogenation Catalysts

Heterogeneous catalysis is catalysis where the phase of the catalyst differs from the phase of the reactant and/or the product.[50-52] Usually, the metal catalyst is present as a finely divided solid (eg. Raney Ni) in the liquid solution to be reduced and H_2 gas is bubbled through it. Alternatively, the metal can be deposited on an inert solid support such as carbon, barium sulphate, alumina or calcium carbonate. The reaction takes place at the surface of the metal catalyst (Pt or Pd supported on charcoal).

For maximum catalytic activity, the surface area of the catalyst has to be maximised, and therefore the metal is usually in a finely divided state. For Pt or Pd this is achieved by reducing their respective oxides prior to hydrogenation. A particularly active form of Nickel ('Raney Nickel') is prepared by dissolving Ni-Al alloy with sodium hydroxide:

$2Ni\text{-}Al + 2OH^- + 2H_2O \rightarrow 2Ni + 2AlO_2^- + 3H_2$

It is difficult to determine the exact mechanisms of heterogeneous hydrogenation. It is at least known that the reaction takes place on the metal surface, at the interface of solid and solution phases. Most of the metals used in heterogeneous catalysis are packed in face centered cubic (FCC) fashion, with each member having 12 nearest neighbouring atoms, except the ones at the surface. These atoms present vacancies where the substrate can bind.

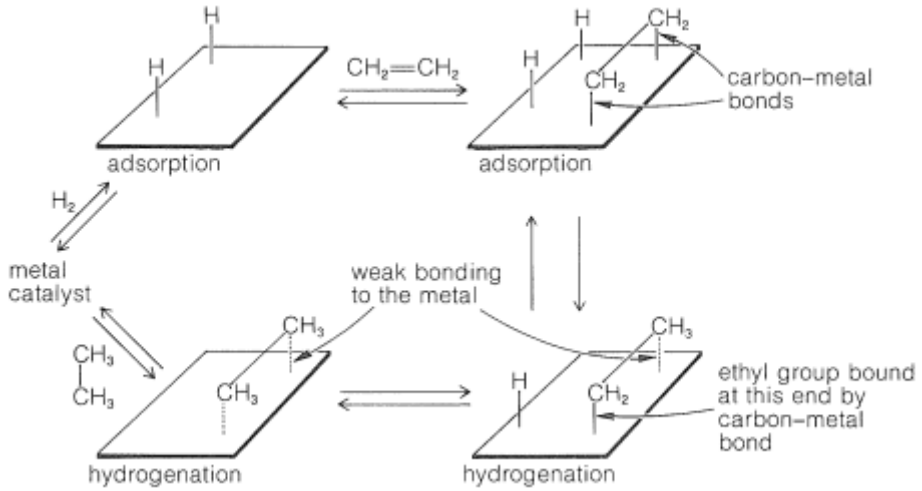

Scheme 6-2: Heterolytic activation of hydrogen for the hydrogenation of ethylene, scheme adapted from article by John D Roberts and Marjorie Caserio[50]

It has been shown that ethylene combines with the metal surface exothermically and reversibly. The process of adsorption occurs in two stages – *physisorption*, characterised by weak (van der Waals') interactions followed by *chemisorption* characterised by the formation of strong chemical bonds. The hydrogenation is believed to proceed in several, reversible steps. At first, the H_2 molecules as well as the alkene (say ethylene) are adsorbed onto the surface of the metal catalyst (say Ni). The energies of the metal-C and metal-H bonds are such that in the next step, one hydrogen is transferred to the carbon to give an ethyl physisorbed to the nickel. This is followed by the breaking of the other Ni-C bond and formation of another C-H bond. Ethane (in general, alkanes) are much more weakly adsorbed to the metal surface, therefore readily vacates the spot for more H_2 and alkenes. The reaction continues until one of the reagents is consumed or, until the catalyst is 'poisoned', rendering it incapable of further catalysis.

As is evident from the proposed mechanism, the spacing of the metal atoms on the crystal lattice is a crucial factor in determining the rate of the reaction. Also, H_2 is added in a

suprafacial manner, i.e. both the H atoms are added to the same face of the alkene. It must also be pointed out that not all alkenes are hydrogenated with equal ease and therefore some amount of selectivity can be exercised in the hydrogenation process.

6.1.4. Homogenous Hydrogenation Catalysis

The earliest example of homogenous catalysis involved the activation of H_2 by metal ions such as Ag^+, Cu^{2+}, Hg^{2+} ions in aqueous solution.[19, 53, 54] The coordination of H_2 to metals was not well understood until the metal hydrides were first characterised in 1955[55] while the exact mechanism by which H_2 binds to these metal centres was not discovered until even later. Before this date, there were only a handful of reports regarding homogenous hydrogenation – the first one being in 1938 from Calvin[56] who reported that Cu(I) salts catalyse the reduction of quinone in the presence of H_2 acting as the reducing agent. As is often the case, the reactivity of H_2 with the metal centres was established far ahead of any structural characterisation or mechanistic studies. Both homogenous and heterogeneous activation of hydrogen were in fact established long before the simplest metal hydride complexes were even characterised.

Since the late 1950s, considerable debate existed as to how H_2 bonded to the metal centres. While some researchers claimed that H_2 acted as a Lewis base and interacted with the metal by donating the electron pair from its σ-bond to the vacant d-orbitals in the metal, others believed it to be a Lewis acid that accepted electrons from filled metal d-orbitals into the vacant σ*. It was eventually proved that the interaction is actually a combination of both σ-donation and π-backdonation. The following scheme (Scheme 6-3) demonstrates the two bonding modes of H_2 with a transition metal (M), discussed above.

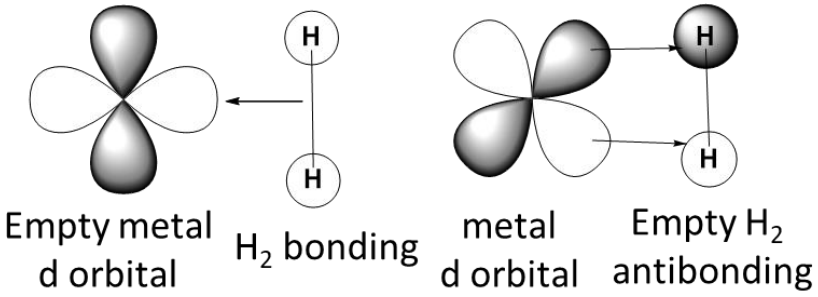

Scheme 6-3: H_2 acting as a Lewis acid and Lewis base in transition metal-H_2 complexes

Regardless of structure, the M-H_2 were considered a transient species rather than intermediates and were considered far too unstable to be isolated. This assumption was proven to be entirely faulty with the isolation of the first H_2-metal complex, $W(CO)_3(P^iPr_3)_2(H_2)$, where the dihydrogen molecule was almost intact (Scheme 6-4).[57]

There are two primary mechanisms for homogenous hydrogen activation which involve homolytic cleavage or heterolytic cleavage of the H_2 molecule (Scheme 6-5). In homolytic cleavage both the H atoms are incorporated into the complex as hydride ligands while the metal centre undergoes an oxidation. The intermediate, which was initially unknown, has now been characterised as a 'σ-complex'. This is most commonly observed for nucleophilic metal centre in their lower oxidation states, which after the addition of H_2, is raised by +2. Hence the name oxidative addition. Vaska's Ir(I) complex ($Ir(CO)Cl(PPh_3)_2$) that binds H_2 reversibly,[58] Wilkinson's catalyst $RhCl(PPh_3)_2$[59] and hydroformylation catalyst $Co_2(CO)_8$[60, 61] are all noteworthy examples of this category (Scheme 6-4).

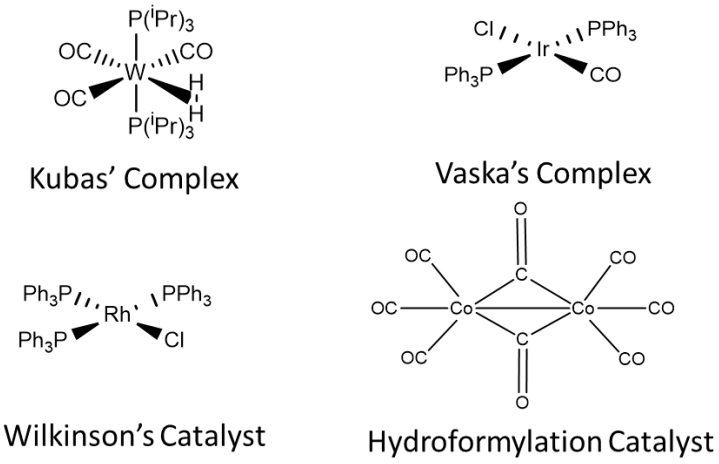

Scheme 6-4: Some important compounds in the history of organometallic hydrogenation catalysts

The second activation process is the heterolytic cleavage of H_2. It involves the polarisation of the H-H bond until a H^- is produced which binds to the metal centre and the H^+ is coordinated either to an external base, an ancillary ligand or an anion. This process is generally more facile than homolytic cleavage and also more prevalent.

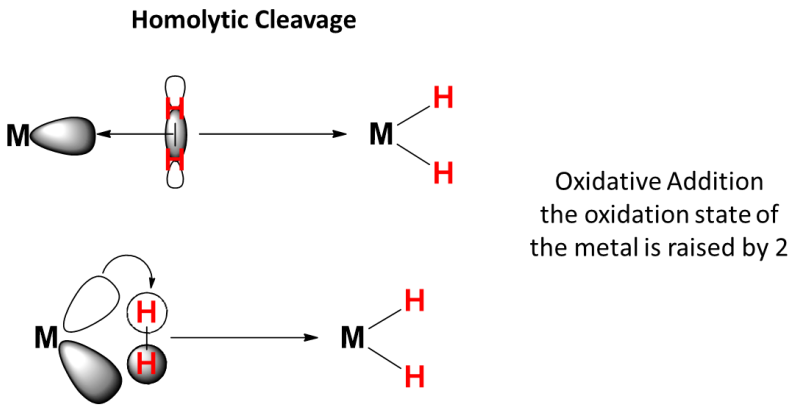

Scheme 6-5: Homolytic cleavage of dihydrogen

The presence of these two pathways actually shows the amphoteric nature of H_2 as a ligand. It can act as a Lewis base by donating electron from its σ-bond during homolytic cleavage also accepts electrons, acting as Lewis acid, in its σ* orbital at the same time. During heterocylic cleavage H_2 primarily as an electron donor and binds to the metal as hydride. Virtually any coordinatively unsaturated transition metal can bind H_2.

While organometallic complexes are the most popular choice for activation of hydrogen, the metals are often expensive, toxic and difficult to dispose. Therefore, the chemical community is increasingly gravitating towards metal-free, 'green' alternatives like using frustrated Lewis pair chemistry. This is elaborated in the next section.

6.1.5. H_2 Activation by Frustrated Lewis Pair[62]

Under ordinary circumstances, a Lewis acid and a Lewis base react with each other to form a classical Lewis acid-base complex. This, of course, takes place by an overlap between the lowest unoccupied molecular orbital (LUMO) of the Lewis acid and the highest occupied molecular orbital (HOMO) of the Lewis base. The first example of an exception to this general axiom was noted by Brown and co-workers while studying the reactions between pyridines and various boranes.[63] They found that a mixture of α,α'-lutidine with trimethylboron resulted in no reaction at all[64] (Scheme 6-6). The lack of a reaction was attributed to the ortho methyl groups which caused a steric hindrance to the formation of the adduct. Similar exceptions were reported by Wittig and Benz[65] and then again by Tochtermann, who called this phenomenon "antagonistisches Paar".[66]

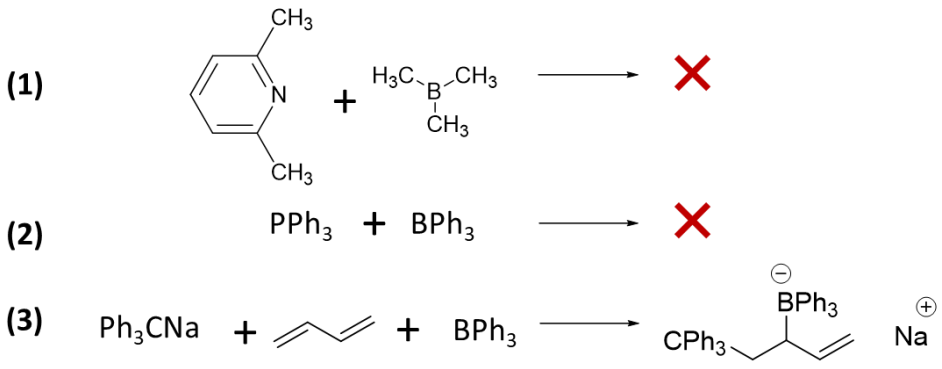

Scheme 6-6: Examples of frustrated Lewis pair chemistry – reaction 1 reported by Brown,[63] reaction 2 reported by Wittig and Benz[65] and reaction 3 reported by Tochtermann[66]

The term "frustrated Lewis pair" was first proposed by Stephan *et al*. in 2006.[67] In this seminal paper they studied a phosphino-borane $Mes_2PH(C_6F_4)BH(C_6F_5)_2$ (Mes = Mesityl = $Me_3C_6H_2$) which can reversibly activate H_2 molecule (see also Section 2A.6).The aryl group between P and B atoms prevents any B···P intramolecular interaction. Furthermore, this molecule exits as a monomer as the dimerization is prevented by the large substituents on B and P (Scheme 6-7). At the same time, this phosphino-borane compound contains both a Lewis acid (LA; B centre) and a Lewis base (LB; P centre). Each centre not only retains their typical reactivity, but also exhibits a cooperative action of Lewis acidic and Lewis basic sites. Therefore, these systems present themselves as 'metal-free' catalytic agents with applications in reactions typically catalysed by transition metal-based catalysts e.g. activation of H_2,[67, 68] capture of greenhouse gases like CO_2,[69, 70] N_2O,[71] SO_2,[72] reduction of CO_2,[73, 74] imines[75-77] and other unsaturated compounds.

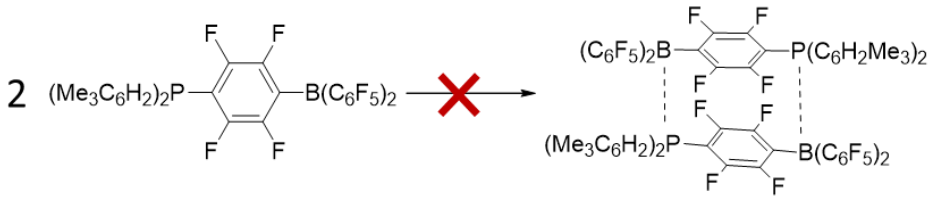

Scheme 6-7: Stephan's phosphine-borane frustrated Lewis acid

Based on the structure of the resulting Lewis acid-base complex, there are two types of FLPs – one where the LA and LB centre are in the same molecule called intramolecular FLP and the other where LA and LB centres are on different molecules, called intermolecular FLP. For intermolecular FLP it is assumed that when the LA and LB containing molecules are brought into contact in solution, they form a loosely bound complex, referred to as an 'encounter complex', through secondary interactions, consisting mainly of London dispersion forces.[78, 79]

In spite of several investigations using various techniques[80-82] there were no experimental proofs expounding the existence of such a complex and the molecular level details of the association remain foggy. The electronic structure of these loosely bound FLPs could only be probed using DFT calculations.[78, 79, 83-86] It was found that the loosely bound complexes are slightly energetically stable although the process not being entropically favourable, renders ΔG slightly endergonic or 0.[78] Molecular dynamics (MD) simulations show that the association happens spontaneously, although the probability of finding such an FLP complex is excruciatingly low (2%).[87]

Thankfully, H_2 can be activated by FLPs even at micromolar (10^{-6} moles/L) concentrations. A constrained potential energy surface (PES) scan also goes to show that an optimum distance between the LA (B) and LB (P) of 3 – 5 Å is favourable for an 'active' FLP that successfully cleaves H_2.[85] Excessively bulky groups makes this distance too large whereas small substituents favour the formation of the classical Lewis acid-base adduct – making the combination of LA and LB inimical for activation of H_2 in either case. For intramolecular FLPs the LA and LB centres are covalently linked by C-C linkage. To make this molecule useful for H_2 activation, the closed ring structure must be opened (Scheme 6-8). Although this makes the process slightly more entropically favourable, there is also an additional energy requirement for the ring opening (ΔE_1).

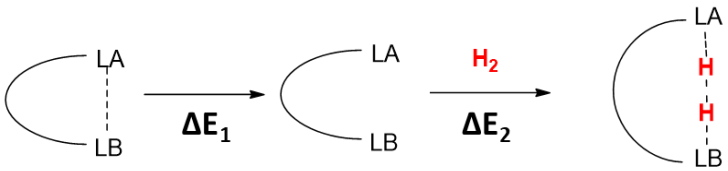

Scheme 6-8: Steps involve in H_2 activation by an intramolecular FLP

Once the encounter complex is formed, the FLP can interact with small molecules like H_2, CO_2, SO_2 etc. There are two DFT based models that can be used to describe the polarisation of H_2 (Scheme 6-8). The first one, proposed by Pápai et al.,[83] called the electron transfer (ET) model, says that the encounter complex interacts with H_2 and polarises it in a concerted manner. Molecular orbital analysis reveals a simultaneous electron transfer from the lone pair on P to the $\sigma^*_{H\text{-}H}$ orbital and from the $\sigma_{H\text{-}H}$ orbital to the vacant p orbital on the Lewis acidic B during the activation of H_2 by $P(^tBu)_3$ and $B(C_6F_5)_3$.[88] This leads to weakening and subsequent cleavage of the bond. The transition state (TS) is characterised by slightly lengthened H-H

bond length with P-H-H-B arranged in an almost linear fashion and the imaginary stretching frequency corresponds to stretching of the H-H bond and formation of the P-H and B-H bonds.

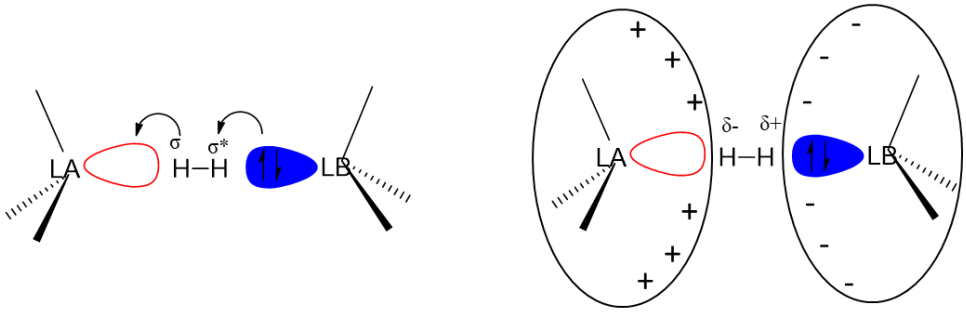

Electron Transfer (ET) Model Electric Field (EF) Model

Scheme 6-9: Schematic representation of DFT based H_2 activation models – electron transfer (ET) model proposed by Pápai et al[88] and Electric field (EF) model proposed by Grimme *et al.*[84]

The other, simpler mechanistic picture was provided by Grimme and co-workers who proposed the so-called electric field (EF) model.[84] This alternative model was proposed in view of gross oversimplification in the treatment of non-covalent interactions between large substituents for each specific FLP pair in Pápai's model. Here also an encounter complex is formed. The incoming H_2 molecule is polarised by the electric field created by the FLP. In that case, the computed imaginary frequency corresponds to the entrance of the H_2 molecule into the FLP pocket. According to this model, the most uphill step is the entrance of the H_2 molecule into the FLP pocket and afterwards the reaction is practically barrier-less.

There is some debate over these two models.[89] Several DFT and full CI based methods show that the activation barrier is strongly dependent on the electric field created by the FLP.[89] However, Camaioni et al. also indicated in their study that the polarisation of H_2 by Lewis pairs NH_3 and BX_3 (X = H, F, Cl) is too weak to cleave the H_2 molecule.[18] A further investigation of a set of H_2 activation reaction showed that EF model had more short-comings while ET model provides more insight into the specific features of H_2 activation.[90] Interestingly, a recent MD study reveals that the two models may be complementary to each other.[90] A further study by Liu and co-workers shows that the EF model is effective at larger distances, where the elongation of the H-H bond is mainly due to polarisation, whereas at shorter distance the ET model can be applied because clear indications of charge transfer from P to H^+ and from H^- to B can be identified.[91]

There can be several factors affecting the reactivity of these FLPs. It has been shown that intramolecular FLPs show greater reactivity than intermolecular FLPs[92] as they have an entropic advantage. In either case, the reaction thermodynamics is strongly dependent on the cumulative strength of the LA and LB which can be measured from their hydride affinity and proton affinity, respectively.[93] The cumulative strength not only affects the thermodynamics of the H_2 activation reaction but has systematic effect on kinetics as well. According to DFT calculations, increase of strength of LA/LB pair decreases the activation barrier.[94] Also, the individual roles of the LA and LB in the activation process have been explored using DFT based metadynamic simulations.[91] The authors find that the rate limiting kinetics is determined by the Lewis acid while the exergonic thermodynamics is determined by the Lewis base.

From the various aspects of activation reactions discussed above, it is evident that the kinetics of such a reaction depends on several different factors, one of which is presumably the effective Lewis acidity of the LA partner towards the molecule being activated. Such hypotheses have been made after various experimental studies that claim that higher the Lewis acidity of the catalyst, greater is its efficiency. However, no quantitative proof of this statement exists yet. As mentioned in the introduction, hydride ion affinity has been found to be an effective measure of Lewis acidity, and this has indeed been found to be true in the case of our **X**-BH_2^+ boreniums as well, as seen from the results of Chapter IV. The utility of this HIA scale in predicting the activation energy for the activation of H_2 has been examined in the following sections. The beginning of this study deals with the interaction of **X**-BH_2^+ with H_2, in the absence of an external base.[n] In the latter part, the activation of H_2 in the presence of a related Lewis acid (**X**-BPh_2^+) and a Lewis base (phosphine) has been investigated.

6.2. Computational Details

All the molecules in Section 6.3 and 6.4 were optimised and characterised through frequency calculation at M06/6-311G(d,p) level of theory using Gaussian09 program.[95] The WBI and population analysis was done using NBO6 program at the same level of theory. The ETS-NOCV analysis has been carried out using ADF2017 at B3LYP/TZ2P level.[96, 97] All single point

[n] Part of the calculations described in this chapter have been performed by Jacob S Hirschi, a master student from UC San Diego (USA) who performed an internship in the LCM lab from mid-June to mid-September 2019 under the supervision of Gilles Frison. I have participated in his supervision.

calculations to determine electronic energy and Gibbs free energy in the gas phase were also carried out at M06/6-311G(d,p) level. For energy calculation in the solvent phase the PCM model was used with toluene as solvent. The choice of solvent was inspired by a study by Fernández.[98]

The molecules in section 6.5 were optimised and characterised at B3LYP/ TZVP level.

6.3. Interaction of X-BH_2^+ with H_2

In this section, the interaction between **X**-BH_2^+ and H_2 has been examined, where **X**-BH_2^+ acts as a Lewis acid and H_2 acts as the Lewis base. This is the preliminary study to see to what extent our range of **X**-BH_2^+ molecules can activate H_2. There are two possible pathways for hydrogen cleavage – homolytic and heterolytic. Heterolytic cleavage is preferred in the presence of an external base which proceeds via the polarisation of the H-H bond. Homolytic cleavage is the preferred pathway in the absence of an external base.[99, 100] This computational study of the interaction between a Lewis acid, **X**-BH_2^+ and molecular hydrogen gives insight into the variance in chemical behaviour due to change in Lewis acidity by changing the electronic environment. Many of the adducts in our study display a double-minima in their 1D potential energy surface. This feature has been previously noted in some studies for Lewis acid-base adducts[101, 102] but has not been discussed in the context of the interaction between H_2 and Lewis acid before.

6.3.1. Geometry Optimisation and Electronic Structure

The structure of the global minimum of the H_2 adduct with **X**-BH_2^+ (**X** = **1** – **38**) were optimised at M06/6-311G(d,p) level of theory. An examination of the optimised geometries clearly reveals two different kinds of structures. In most cases (26 out of 38 corresponding to **X** = **1** – **24**, **27**, **28**) the H_2 molecule approaches the **X**-BH_2^+ unit in a side on fashion, indicative of its role as a Lewis base in these complexes,[103] the BH_2 unit undergoes some distortion, with the B-H bonds bending out of plane to accommodate the incoming H_2, accompanied by a simultaneous B-C bond rotation in some cases (Figure 6-1 A). Furthermore, the H-H bond length is slightly higher than 0.8 Å. For 12 molecules (**X** = **25**-**26**, **29**, **31**, **33**-**38**) the global minima show no significant distortions of the BH_2 unit is noted and the H_2 molecule is stationed significantly further away from the **X**-BH_2^+ moiety, conserving a short H-H bond

length around 0.75 Å. The structure of an example from each of these categories of complexes has been provided in the figure 6-1.

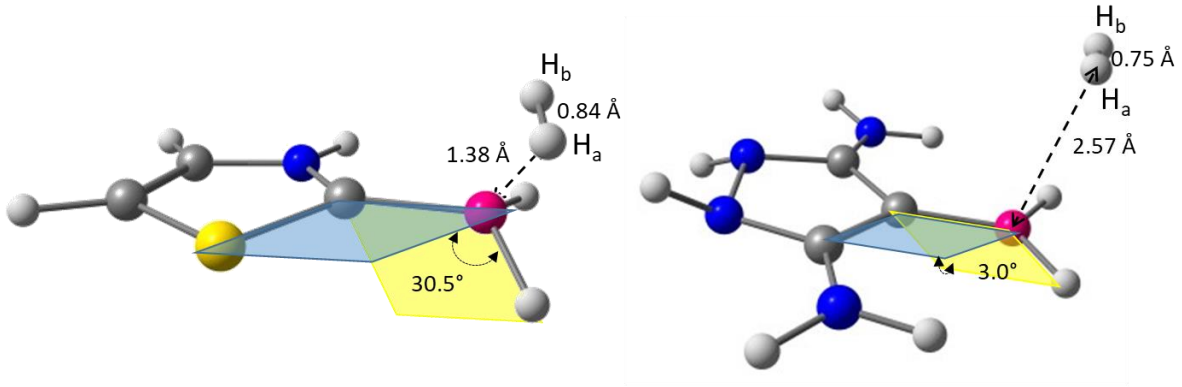

(η^2-H_2)**16**-BH_2^+ η^2 adduct **(A)**

29-BH_2–H_2^+ van der Waals' complex **(B)**

Figure 6-1: Optimised geometry of (A) η^2-adduct of **16**-BH_2^+ and H_2 and (B) van der Waals' complex formed between **29**-BH_2^+ and $H_{2Dihydrogen}$ complex

It is interesting to note here that we specifically speak in terms of the 'global minima' in these cases because in the case of 11 of the adducts (**18**-**19**, **22**-**27**, **30**, **32**) considered, there are two minima on the potential energy surface. This has been discussed in further detail in section 6.3.2.

The η^2 adducts and van der waals' complexes were further analysed using several computational tools. Using NBO analysis the η^2 complexes can be described using two Lewis structures (scheme 6-10) -

(i) 3c-2e bond - The weakening of the H-H σ-bond in this adduct can be attributed to two simultaneous interactions – the donation of electrons from the H-H σ-orbital to the vacant p-orbital on B and the backbonding interaction via electron donation from the B-H σ-bonds to the 3c antibonding orbital. This is represented as Lewis structure 1 in the scheme below (Scheme 6-10).

(ii) 2c-2e H^a-H^b bond and a vacant orbital on B while the bonding and backbonding interactions are described by H^a-H^b (σ) → B (p) and B-$H^{1/2}$→ H^a-H^b (σ*) respectively.

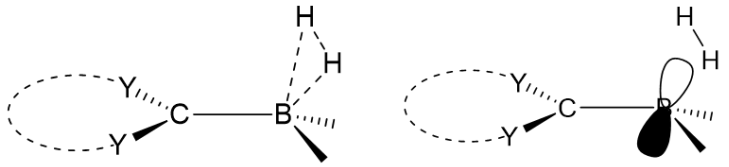

Lewis Structure 1 Lewis Structure 2

Scheme 6-10: The possible Lewis structures for $(\eta^2\text{-}H_2)$**X**-BH_2^+

These two Lewis structures can be considered equivalent both donation and backdonation are similar. Indeed, a very strong correlations exist between the percentage contribution of B to the 3c-2e bond computed from the first Lewis structure and $\Delta E^{\sigma\rightarrow p(B)}$ calculated from 2nd order perturbative analysis of the second Lewis structure, which both evaluate σ-donation interaction (Figure 6-2 A). Furthermore, similar correlation is obtained between the strength of back-donation, calculated by 2nd order perturbation energy analysis in either case, between the two Lewis structures (Figure 6-2 B). The second structure, of course, offers the advantage of making a direct energetic correlation between donation and back-donation hence we find that the magnitude of $H^a\text{-}H^b$ (σ) → B (p) donation is significantly much larger than $B\text{-}H^{1or2}$ → $H^a\text{-}H^b$ (σ*) back-donation and can be considered the primary interaction of interest.

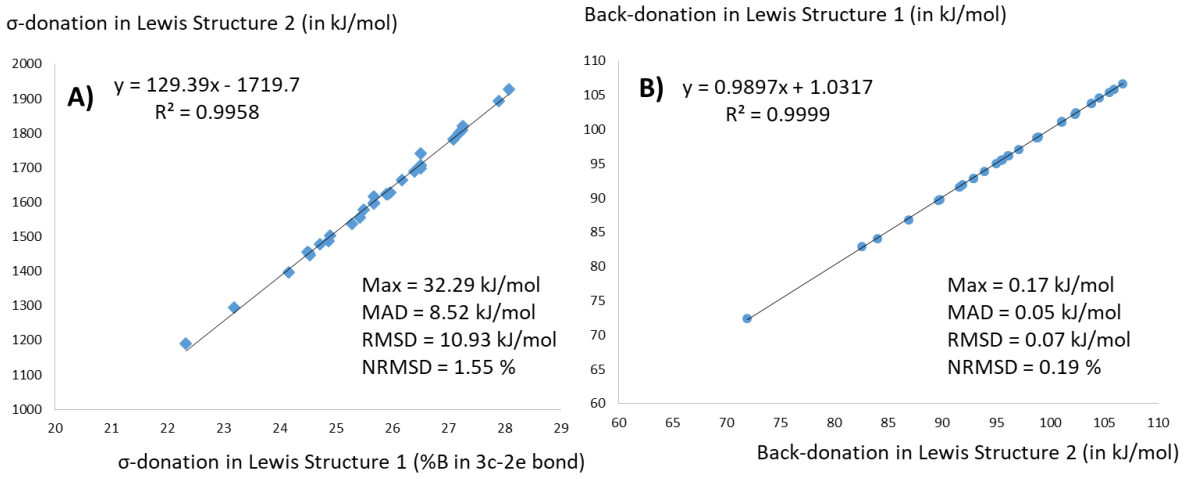

Figure 6-2: Correlations between the measures of σ-donation and back-donation belonging to the two Lewis structures of $(\eta^2\text{-}H_2)$**X**-BH_2^+

The η^2 complexes have been further analysed using the ETS-NOCV analysis. The first NOCV indicates the donation of electrons from H-H σ-bond and the second NOCV indicates a π-type accumulation of electron density. This indicates the π-backdonation from the B-H bond to the σ* H-H bond. This has been represented in Figure 6-3 A and B for $(\eta^2\text{-}H_2)$**14**-BH_2^+. There is a

reasonably good correlation between σ-donation measured by NBO analysis and NOCV analysis and the same is true of π-backdonation. (Figures 6-3 C and D)

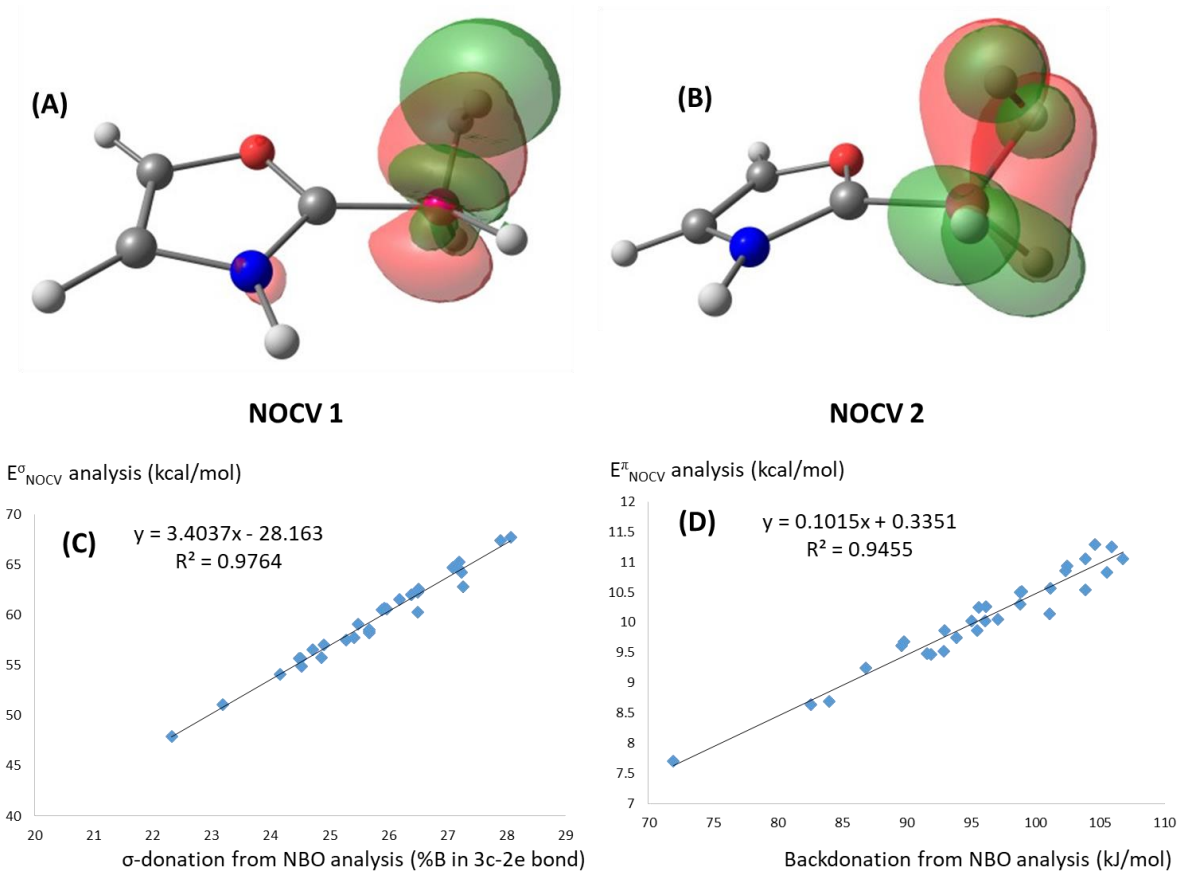

Figure 6-3: NOCV1 and NOCV2 of (η^2-H_2) **X**-BH_2^+ where **X** = **14** Isosurface value = 0.003; correlation between different donation and back-donation components measured by NBO and ETS-NOCV analysis. The charge flow of the electronic density is green → red. Isosurface value: 0.003 a.u.

6.3.2. Results and Discussion

As we have seen before two different categories of complexes exist – in the first set, H_2 binds **X**-BH_2^+ coordinatively, forming a much stronger η^2 adduct (Figure 6-1 A); the second set clearly indicates the formation of a weaker van der Waals' complexes (Figure 6-1B). Dihydrogen complexes with the substantial retention of H-H σ-bond are no longer a rarity and there are 3 structural types that are currently recognised[104] – Kubas dihydrogen, stretched dihydrogen and compressed dihydride, each category representing progressively longer H-H bonds and diminishing H-H σ-bond character.

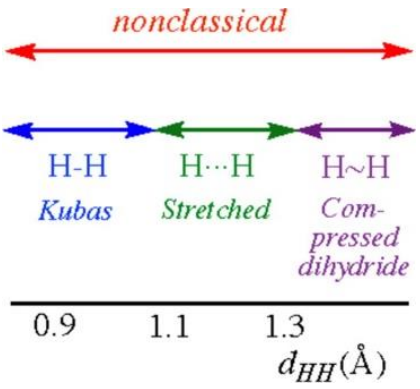

Figure 6-4: Various dihydrogen complexes, image taken from Crabtree's review.[104]

In our case, for the η^2 adducts, the average H-H bond length of 0.836 Å places the complexes squarely in Kubas region (0.8 – 1.0 Å).[104] Unlike the stretched dihydrogen (1.0 – 1.25 Å) and the compressed dihydride (1.25 – 1.6 Å), complexes in Kubas region are still characterised by substantial retention of the H-H σ-bond. However, the bond is much weaker than in the van der Waals' complex, where the H_a-H_b bond length is slightly longer (the average bond length being 0.752 Å) than that of free molecular H_2 (0.747 Å).

The H-H bond length can be considered as a marker of the strength of the interaction between **X**-BH_2^+ and H_2 molecule – the greater the length of the H-H bond, the stronger is the σ-donation from H_2 to **X**-BH_2^+, indicating its higher Lewis acidity. Measuring H-H bond length against our known scale of Lewis acidity reaffirms the previously obtained results, which can now be expressed in the form of an intuitive graph. There are two distinct categories of complexes formed by the different **X**-BH_2^+ boreniums with H_2 molecule – the η^2 adducts and the van der Waals' complexes, identified clearly in Figure: 6-5.

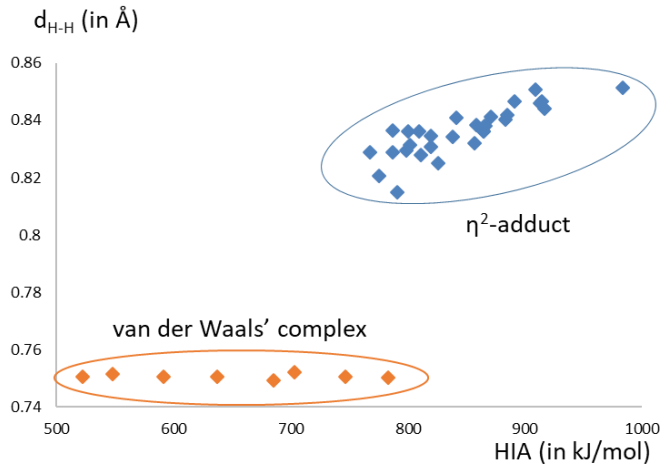

Figure 6-5: Correlation between H-H bond length (d_{H-H}) in $H_2\cdots$**X**-BH_2^+ complexes and HIA of **X**-BH_2^+ showing the formation of van der Waals' complexes (orange) and η^2-adducts (blue).

It was interesting to consider the possibility if the ability of **X**-BH_2^+ to form an η^2 adduct or a van der Waals' complex was mutually exclusive, that is to say, could the molecules that form η^2 adducts also form van der Waals' complexes and vice versa? To answer this, the relaxed 1D potential energy surface (PES) with respect to the B-$H^{a/b}$ bond length was scanned (M06/6-311G(d,p) level). The PES scans revealed that 8 **X**-BH_2^+ molecules of low HIA and therefore, low Lewis acidity form exclusively van der Waals' complexes (**X** = **29**, **31**, **33**-**38**) (red points in the graph in Figure 6-6); 19 **X**-BH_2^+ molecules of very high HIA and consequently high Lewis acidity form exclusively η^2 adducts (**X** = **1**-**10**, **12**-**17**, **20**-**21**, **28**) (blue points) and 11 **X**-BH_2^+ molecules of intermediate Lewis acidity and, naturally, intermediate values of HIA can form both η^2 adduct and van der Waals' complex(**X** = **11**, **18**-**19**, **22**-**27**, **30**, **32**) (green points).

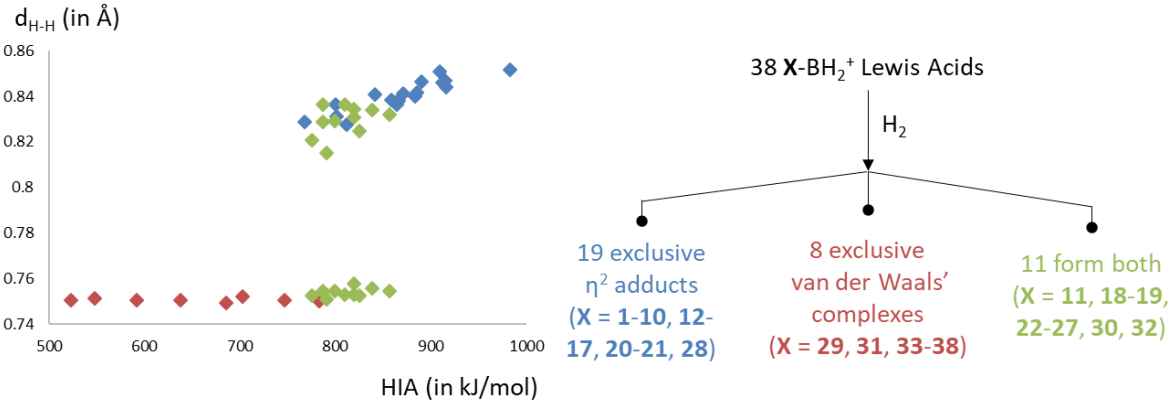

Figure 6-6: The classification of complexes formed by **X**-BH_2^+ (**X** = **1** – **38**) with H_2

These 11 **X**-BH_2^+ molecules exhibit two distinct minima on their PES, the one at smaller B-$H^{a/b}$ distance signifying the formation of an η^2 adduct and another minima at a longer B-$H^{a/b}$

distance corresponding to the van der Waals complex. This is illustrated with the example of **11**-BH_2^+, in Figure 6-7. The PES shows these two minima, one where $d_{B\text{-}Ha}$ is 1.4 Å and the corresponding $d_{Ha\text{-}Hb}$ is 0.83Å (η^2 adduct) and the other where $d_{B\text{-}Ha}$ is 2.07Å and the corresponding $d_{Ha\text{-}Hb}$ is 0.76 Å (van der Waals' complex) (Figure 6-6). The relative depth of each minima depends upon the relative stability of the η^2 adduct vs. the van der Waals complex. Among the 11 molecules that show the dual minima the van der Waals' complex is the global minima for 4 cases (**X** = **25**, **26**, **30**, **32**) and the η^2 complex is the minima for 7 cases (**X** = **11**, **18**-**19**, **22**-**24**, **27**).

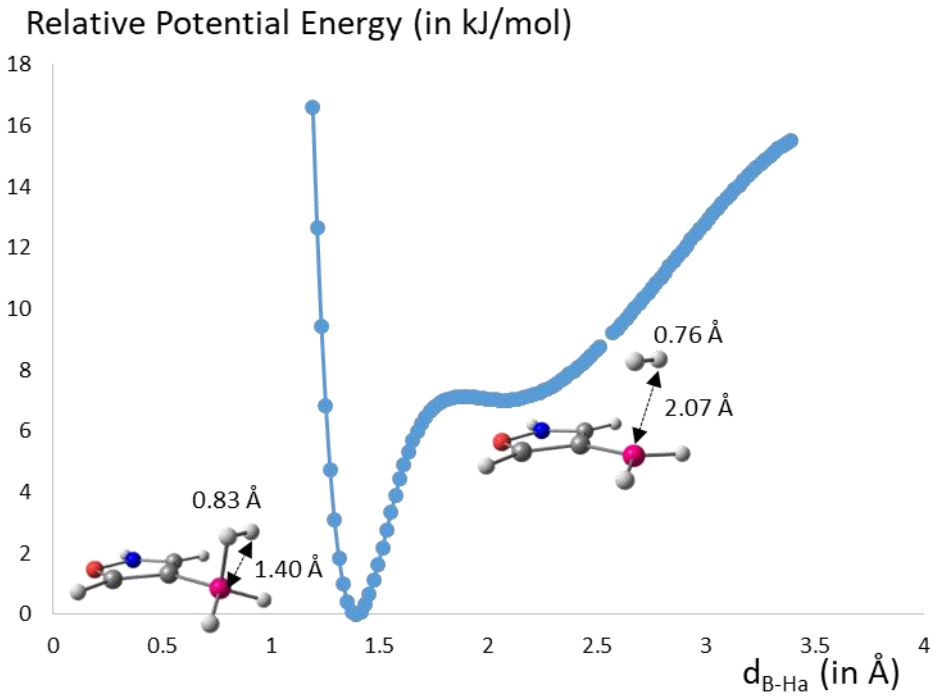

Figure 6-7: The 1D potential energy surface for interaction between **11**-BH_2^+ and H_2

The interaction of molecular H_2 with **X**-BH_2^+ clearly indicates the difference in the cumulative Lewis acid strengths of **X**-BH_2^+ which gives rise to different chemical behaviour. The behaviour also turns out to be consistent with HIA calculated for the **X**-BH_2^+ molecules to a reasonable extent. However, in none of the cases, not even the strongest Lewis acid examined in our set of molecules, molecular hydrogen can be homolytically cleaved by **X**-BH_2^+ alone although there is a weakening of the H-H σ-bond. The absence of external base also prevents any heterolytic cleavage to form **X**-BH_3 and H^+. Such heterolytic cleavage, as mentioned before, can be achieved in the presence of a base (like phosphine).

6.4. Activation of H_2 with FLP pair - X-BR_2^+ and P^tBu_3

Up until this point, the behaviour of the dihydrido borenium **X**-BH_2^+ with molecular H_2 has been explored and we find that in none of the cases does H_2 molecule undergo a complete cleavage. Naturally, the next logical step would be to introduce a Lewis base into the system, thus completing the Lewis acid-base pair to rip the H_2 into H^+ and H^-. The choice of a base can in itself become the subject of another thesis. To speak about it briefly, in most cases the base is not just responsible for the cleavage of H_2 but is the compound that undergoes reduction by accepting H^- in a following step. A large variety of 'Lewis bases' can undergo such reductions – imines,[1, 92] amides,[105] nitriles,[106] aziridines[75] and alkynes.[76] That said, however, the most popular FLP pair is that formed by a boron Lewis acid and a phosphine Lewis base. We have chosen this kind of a pair with a borenium Lewis acid and phosphine Lewis base constituting an FLP pair to heterolytically cleave H_2. The theoretical studies conducted in this chapter is inspired in part by the investigations conducted in the paper by Cabrera-Trujillo and Fernandez where the influence of Lewis bases on the reactivity of various FLP have been explored.[98]

6.4.1. Moving from X-BH_2^+ to X-BPh_2^+

We start our study by modelling the activity of the **X**-BH_2^+ and P(^{t}Bu)$_3$ FLP with respect to hydrogen splitting. Quickly, we faced two problems: undesirable interactions between the fragments where obtained in many cases and, when the expected orientation and interaction of the partners were obtained, the excessively high acidity of **X**-BH_2^+ makes the reaction proceed without an energy barrier. Therefore, we decided to replace the H atoms on dihydrido boreniums by phenyl groups (Ph). Such substituents, which are used experimentally, solve the above problems when carrying on theoretical investigations. Compared to **X**-BH_2^+ Lewis acid, **X**-BPh_2^+ includes phenyl groups, which have electron withdrawing inductive effect (-I) and electron donating mesomeric (+M) effect with respect to H. However, this change should be uniform and the electronic properties of **X** in these complexes could be expected to still bear some parallelism to their **X**-BH_2^+ counterparts.

6.4.2. Geometry Optimisation and Electronic Structure

The geometry of 33 **X**-BPh_2^+ (**X** = **1**-**26**, **28**-**30**, **32**-**34**, **37**, see the list provided on page 13) have been optimised at M06/6-311G(d,p) level to study their activity as the Lewis acid counterpart

of a frustrated Lewis pair with $P(^tBu)_3$ in the activation of H_2. For the other molecules of the initial set (**X** = **27**, **31**, **35**-**36**, **38**-**39**) the transition state for this activation could not be obtained and therefore had to be left out of the discussion. The chosen set of 33 molecules still present a diverse range of molecules including normal NHC (**1**-**2**, **4**, **6**, **8**, **10**, **12**, **14**, **16**, **20**-**24**, **26**, **28**, **30**, **32**, **33**), mesoionic NHC (**9**, **11**, **13**, **15**, **17**-**19**, **25**, **29**), cyclic alkyl amino carbenes (cAAC **3**, **5**, **7**), and carbodicarbenes (**34**, **37**).

The optimised geometry of **X**-BPh_2^+ shows certain key differences with respect to the optimised geometry of **X**-BH_2^+. One of the **X**-BPh_2^+ molecules has been shown in Figure 6-8. **X** and BPh_2 units are not coplanar, i.e., Y-C-B-C_{Ph} dihedral angle is non-zero in all cases as opposed to the Y-C-B-H bond angle which is zero in most cases. The phenyl groups are also not coplanar. This could be attributed to a combination of steric and electronic factors. As mentioned before, the boron in **X**-BPh_2^+ experienced vastly different σ and π electronic environments compared to **X**-BH_2^+. Here, the vacant boron p orbital receives π-electrons from both the phenyl groups and the **X** moiety, and the σ- electrons in the sp^2 hybridised orbital of B experience an electron withdrawing effect due to the higher electronegativity of the sp^2 hybridised C of the Ph groups. It is also important to appreciate that due to the non-coplanarity of the **X**-BPh_2^+ molecule, it becomes considerably difficult to segregate the various σ and π interactions from each other, rendering it impossible to evaluate each interaction individually. Herein lies the value of a scale such as HIA, which can assign a number to the total Lewis acidity of the molecule, even if its individual σ-acidity and π-acidity cannot be determined.

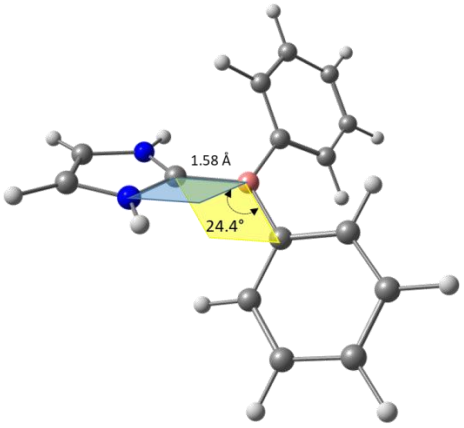

Figure 6-8: Optimised geometry of **20**-BPh_2^+

In figure 6-9, a comparison of two chemical characteristics of the B-C bond in **X**-BH_2^+ and **X**-BPh_2^+ – bond length ($d_{B\text{-}C}$) and Wiberg bond index ($WBI_{B\text{-}C}$) have been presented. We see that the correlation between bond lengths are quite poor, but it is better with bond indices although still far from perfect. The correlation between the occupancies of the p_z orbital on B in **X**-BH_2^+ and **X**-BPh_2^+ is also very poor, due to smaller variation of this population in **X**-BPh_2^+ compared to **X**-BH_2^+. This indicates that the π-donation in the two cases is not similar, a low π-donation of **X** can be compensated by π-donation of the Ph substituents. However, the hydride ion affinity of **X**-BH_2^+ and **X**-BPh_2^+ show very good correlation (Figure 6-9 D). This shows that the overall Lewis acidity that arises as a combination of σ and π effects at the boron centre are actually quite similar for **X**-BH_2^+ and **X**-BPh_2^+.

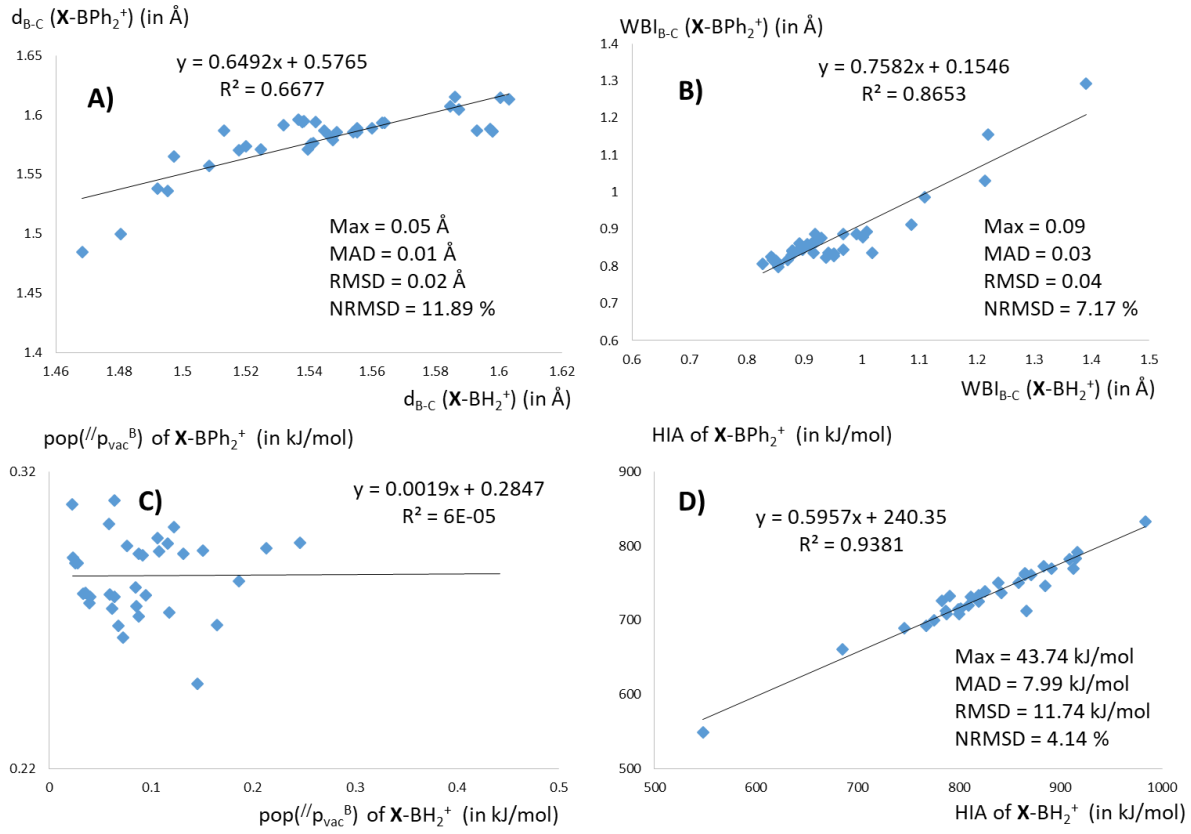

Figure 6-9: Correlation between different parameters of **X**-BH_2^+ and **X**-BPh_2^+

6.4.3. Calculating Energy of Activation

The activation of H_2 by the Lewis acid-base FLP proceeds via the formation of a reactant complex (RC) followed by a transition state (TS) and finally, the product complex (PC) which then dissociates into products. The structures of each of these stages has been illustrated with the example of **20**-BPh_2^+ and $P(^tBu)_3$ acting on H_2 in Figure 6-10. The RC is characterised

by the H_2 molecule poised between the **X**-BPh_2^+ and $P(^tBu)_3$ in a roughly triangular fashion. The molecular axis of H_2 runs parallel to the B-C_X bond and lies relatively far away from the $P(^tBu)_3$ unit. This conformation is similar to the one obtained by Fernández for reactant complex formed between $B(C_6F_5)_3$ and $P(^tBu)_3$ with H_2 positioned between them.[98] As the two hydrogen atoms of H_2 are no longer equivalent in the complex, for the sake of clarity, they have been indicated as H_a and H_b in figure 6-10. In each case (RC, TS, PC), the hydrogen atom closer to $P(^tBu)_3$ unit is indicated as H_a and the other one, closer to the borenium **X**-BPh_2^+ is indicated by H_b. In the case of the RC formed for **X** = **20**, the distance between H_a and B / P atoms is 2.80 / 3.11 Å, respectively. The P-H_a-B bond angle is 111.2°. The overlap is side-on with B and end-on with P. The H_a-H_b bond is 0.77 Å, which is slightly longer than free H_2 (0.74 Å). The RC proceeds along the intrinsic reaction coordinate (IRC), reaching the top of the hill, which is the transition state (TS). The TS has a single imaginary frequency which, for all **X** except the two carbones, i.e. **X** = **34** and **37**, is a combination of the H_2 molecule entering into the FLP pocket and a tetragonal distortion of B. For **X** = **34** and **37**, the imaginary frequency corresponds to the stretching of the H-H bond, in agreement with a later transition state due to a lower reactivity induced by a lower Lewis acidity. In the TS, the H_2 molecule is shared more equally between the Lewis acidic B and Lewis basic P, each interacting with one end of the molecule. For the TS of **X** = **20**, the P-H_a distance is 2.16 Å and B-H_b distance is 1.77 Å. The B-H_b-H_a bond angle is 125.5° while the H_a-H_b bond is considerably elongated to 0.82 Å. The TS is converted into the product complex (PC), where the H_2 molecule has been heterolytically split into H^+ and H^- to form neutral **X**-$BHPh_2$ and cationic $P(^tBu)_3H^+$.

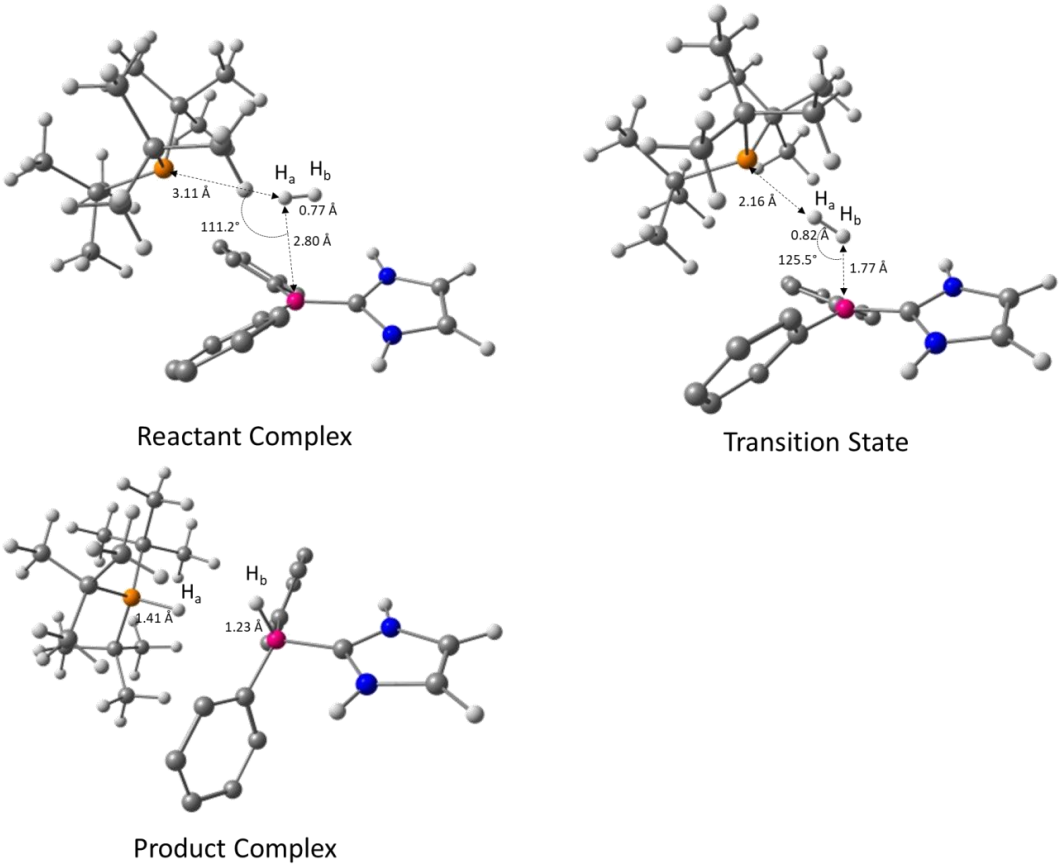

Figure 6-10: Optimised geometry of reactant complex (RC), transition state (TS) and product complex (PC) of the activation of H_2 by **20**-BPh_2^+ and $P(^tBu)_3$.

The computed reaction profiles for the activation of H_2 with respect to the electronic energy, E and the sum of electronic and thermal free energy i.e. Gibbs free energy, denoted by G, for **X** = **20** has been presented in Figure 6-11. The energies associated with the RC, TS and PC for all the 33 cases of **X**-BPh_2^+ have been calculated in gas phase as well as with the PCM model using toluene as solvent. The difference of electronic energy between RC and TS denoted by ΔE_2 is highest for **X** = **37** and least for **X** = **2** in either case. This is in line with our expectations as **X** = **37** is a carbodicarbone and **X**-BPh_2^+ consequently has low Lewis acidity, and so, the activation barrier for **37**-BPh_2^+ should be high. At the same time for **X** = **2**, the NHC has electron withdrawing carbonyl substituents in its backbone, making **2**-BH_2^+ strongly Lewis acidic. This makes the activation barrier low.

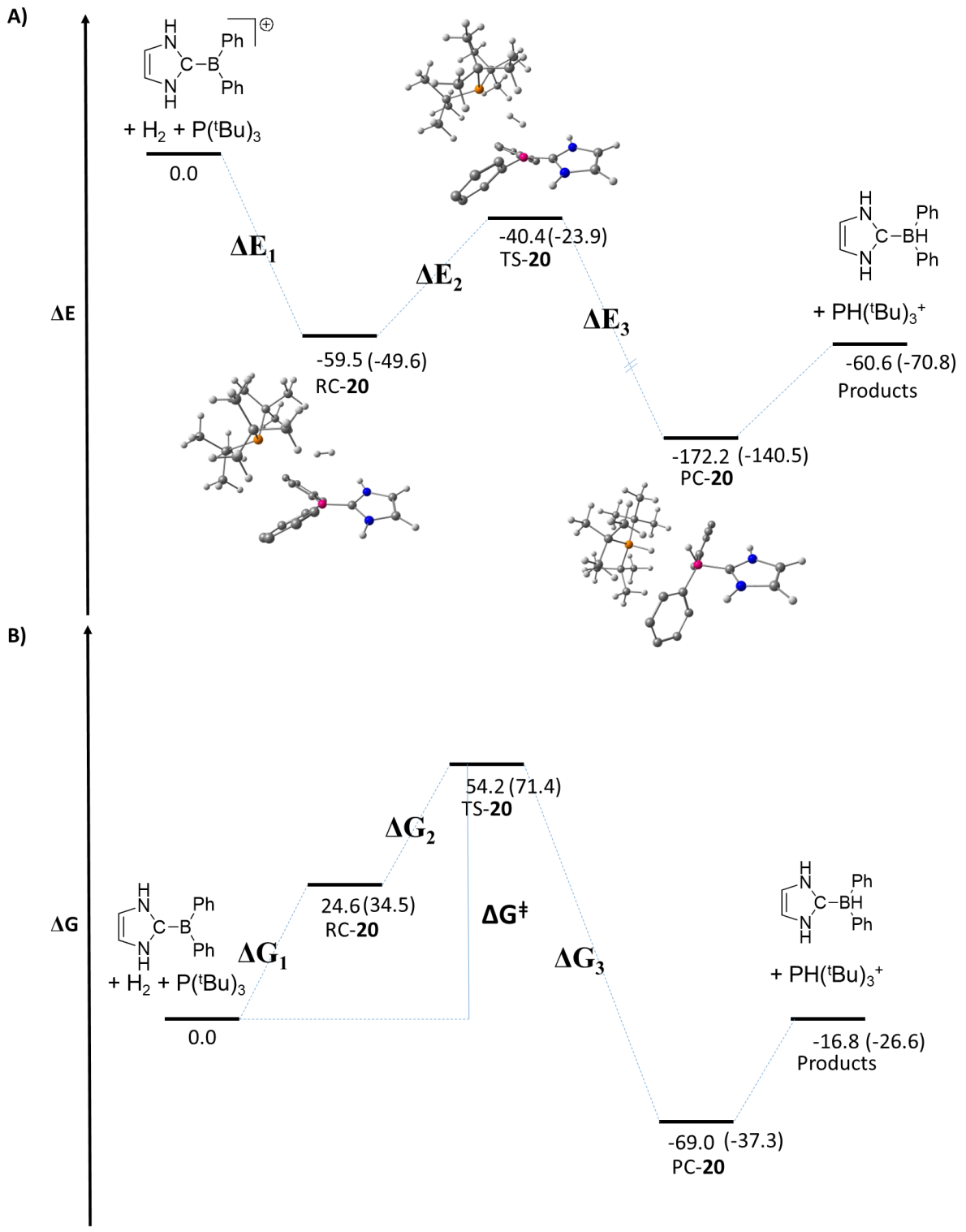

Figure 6-11: Computed reaction profiles for the H_2 activation reaction by **20**-BPh_2^+ and $P(tBu)_3$: (A) relative energies (B) free energies at 298 K given in kJ/mol. All data was calculated at M06/6-311G(d,p) level in the gas phase with energy for solvated systems provided in parenthesis

Despite this qualitative agreement for **X** = **2** and **37**, ΔE_2 shows only a modest correlation with the HIA as calculated for **X**-BH_2^+ molecules in the previous chapter (Figure 6-12). The greatest

deviation is observed in the cases of **X** = **3**, **5** and **7**. This could possibly be attributed to the fact that in each of these cases, in the optimised geometry of **X**-BPh_2^+ the Y-C-B-C dihedral angle is close to 90°, whereas the HIA has been calculated for **X**$^{//}$-BH_2^+. Removing these three points improves the correlations significantly. Notwithstanding this problem, clearly the trend of the correlation denotes that this HIA is roughly inversely proportional to ΔE_2.

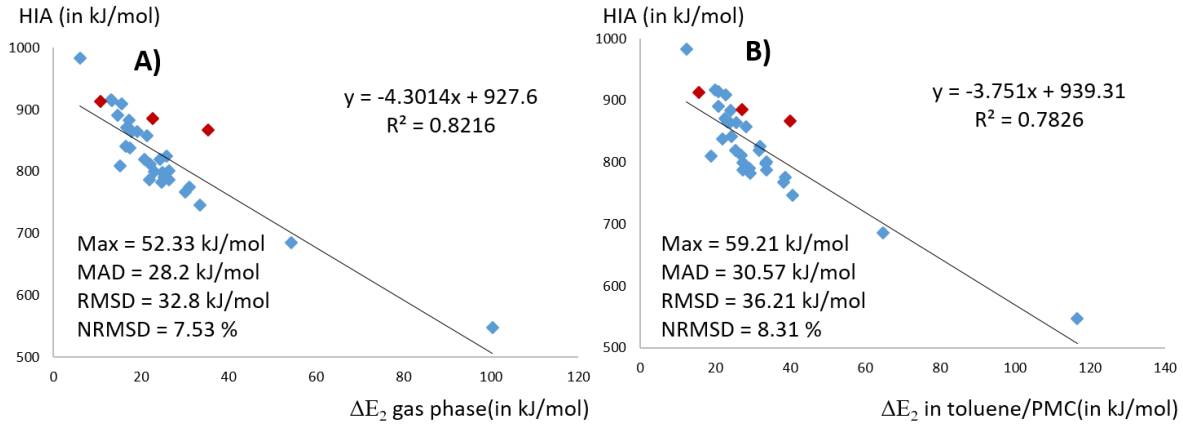

Figure 6-12: Correlations between HIA and Δ_2^{elec} calculated in (A) gas phase and (B) with toluene (PCM), the red squares represent **X** = **3**, **5**, **7** which have not been included in the correlation.

Including entropic effect induces the RC complexes to be located above the separated reactants **X**-BPh_2^+, H_2 and $P(^tBu)_3$, in free energy. The activation free energy ($\Delta G^{\ddagger}$) therefore correspond to $\Delta G_1 + \Delta G_2$ (Figure 6-11). HIA, which reflect the cumulative σ and π acidities of **X**-BH_2^+, as well as of **X**-BPh_2^+, has been shown previously (chapter III) to be lower for poor Lewis acids and such Lewis acids have been shown (6.2) to be weak activators of H_2, owing to the higher activation energy. $\Delta G^{\ddagger}$ does as such correlate quite well with HIA (Figures 6-13 A and B). This demonstrates the utility of HIA as a predictive tool in measuring the relative efficiency of the borenium catalysts.

$\Delta G^{\ddagger}$ has also been compared to a linear combination of the σ and π donation energies (noted as σ + λ*π, where λ is a linear coefficient to be optimised) of **X**-BH_2^+ as noted in chapter III. Once again discluding the cAACs (which have already been excluded), the correlation is optimised to the maximum possible value of R^2 (0.87) for λ = 0.32 (Figure 6-13 C). This shows that properties of **X** can be connected to reactivity of the **X**-BPh_2^+ molecules in a tangible way.

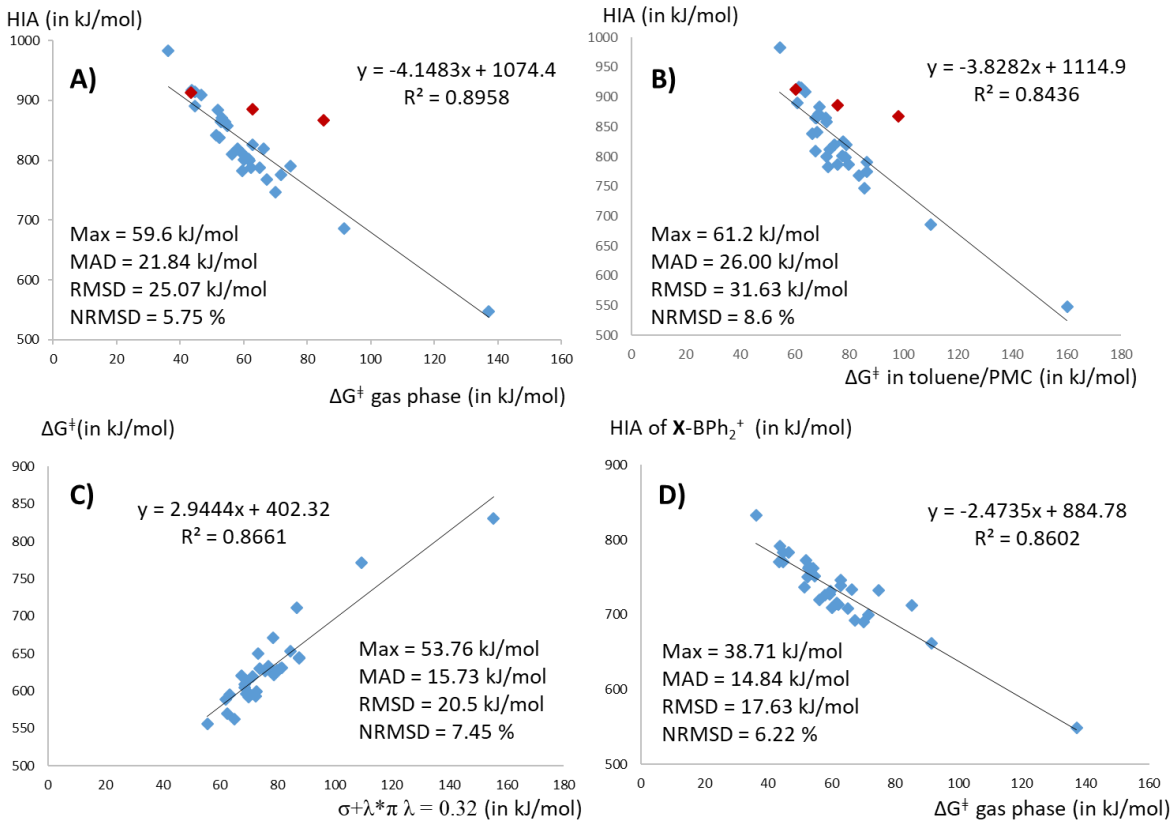

Figure 6-13: Correlations between HIA of **X**-BH_2^+ and $\Delta G^{\ddagger}$ calculated in (A) gas phase and (B) in toluene (PCM); correlations between HIA of **X**-BPH_2^+ and (A) **X**-BH_2^+ and (D) $\Delta G^{\ddagger}$ calculated in gas phase. The red dots represent cAACs which have not been included in the correlation.

6.5. Calculating HIA for some Experimental Cases

As the catalysts chosen in our study have been selected from a theoretical perspective, keeping in mind the limitations of size, most of the **X**-BH_2^+ and **X**-BPh_2^+ cations have not been tested for their catalytic efficiency through experimental work. For this reason, we chose some molecules from a seminal publication in this field from Stephan's group,[107] whose catalytic efficiency has been thoroughly studied. For these molecules, we calculate their HIA and compare it with the yields of the catalytic reactions obtained experimentally with these molecules.

Stephan's catalysts catalyse the hydrogenation of an imine (Figure 6-14). From this experimental study, we have selected 7 catalysts, noted **Cat.X** (**X** = **1**-**7**), for which the yields of the final product have been reported for similar experimental condition, that is a given mol% of the catalyst. The details of the catalyst with their yields and mol% concentration are reported in Table 6-1. The HIA of **Cat.X**-9BBN (9BBN = 9-borabicyclononane) have been calculated at B3LYP/TZVP level of theory.

Table 6-1: catalyst loading, HIA and yield for **Cat.X X**= **1** - **7**

Cat.X **X**	mol%	HIA kJ/mol	yield
1	5	704.2	0
2	1	705.4	0
3	1	712.7	0
4	0.5	732.1	35
5	0.5	747.1	67
6	0.5	727.2	21
7	0.5	763.6	100

As the comparison between experiment and theoretical results can only be made for the same catalyst loading, this means that, strictly speaking, only 4 cases can be used ((**Cat.X** for **X** = **4**-**7**), those for which the catalyst loading is 0.5%. For **X** = **1**-**3**, as the yield of the reaction is 0 for a higher catalyst loading (1 to 5%), therefore it is expected that with a smaller catalyst loading their yield would have remained at 0. Hence, they have been included in the comparison between experiment and calculation. Our results are depicted in Figure 6-14 and can be rationalized as follow:

(1) We obtain near perfect correlation for **Cat.X** where **X** = **4**-**7** between HIA and yield (blue points). This significant result confirms our previous result about the reliability of HIA as a confident parameter to estimate the reactivity of Lewis acid. In that case, the correlation has been established between a theoretically calculated HIA and an experimentally reported yield, strengthened our conclusion.

(2) According to this correlation, there is a cut-off value of HIA (given by the x-intercept) below which the yield is always 0. This is true for **X** = **1**-**3** (orange points). This limiting value of HIA, HIA_0, turns out to be 1534.3 / 2.1415 = 716 kJ/mol. Below this value of HIA, catalytic ability of the NHC-borenium catalyst is expected to be too poor to catalyse any reaction at all.

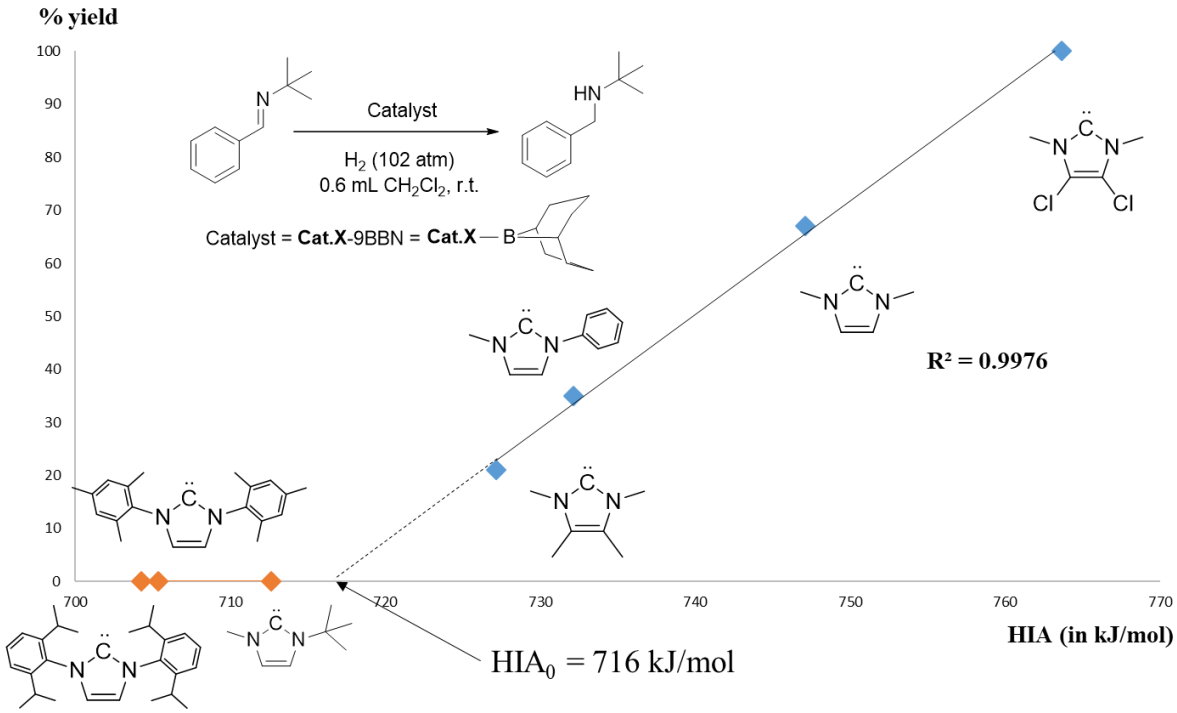

Figure 6-14: Correlation between HIA and % yield associated with the catalysts from Stephan's publication

6.6 Conclusion

Through Chapters II-IV, we have discussed theoretical methods to evaluate the Lewis acidity of divalent carbon compound-borenium adducts, **X**-BH_2^+. Due to the simplicity of the system chosen, it is possible to unentangle the σ and π-interactions and characterise them individually. The total Lewis acidity at the boron centre is clearly a combination of the two effects. An efficient method to evaluate this combined effect is through the use of hydride ion affinity (HIA).

- In this chapter we present one example of how evaluating the HIA of **X**-BH_2^+ may be beneficial in designing efficient Lewis acids for the activation of H_2, one of the most interesting areas of FLP-catalysis. At the same time, it also demonstrates the ability of theoretical approaches to relate structure and reactivity. Of course, the design of ideal catalysts for the activation of dihydrogen and/or other small molecules involves the optimisation of several different criteria, like, modification of the strength of Lewis acid and base, effect of solvents, steric interactions etc. In this thesis, we deal with Lewis acid strengths and therefore we address only one of the several factors that may contribute to make this activation reaction more efficient.

- We started by taking a look at the interaction of molecular H_2 with **X**-BH_2^+ alone. Although we find that H_2 cannot be cleaved (either homolytically or heterolytically) even with the strongest Lewis acid, we gained indispensable insight regarding the varying nature of the adducts formed with gradual change of the strength of the Lewis acid, measured using HIA. The strongest Lewis acids form exclusively η^2-adducts, the weakest on the other hand form exclusively van der Waals' complexes which those of intermediate Lewis acidity form both.
- Next, we study the efficiency of the **X**-BPh_2^+ molecules (the more 'realistic counterparts of **X**-BH_2^+), as a part of a frustrated Lewis pair with $P(^tBu)_3$, in heterolytically cleaving H_2 molecule. It was shown that the activation energy for the dissociation of H_2 by the **X**-BPh_2^+ and $P(^tBu)_3$ FLP is nicely correlated to the HIA of **X**-BH_2^+ molecules or in other words the Lewis acidity of **X**-BH_2^+ (or **X**-BPh_2^+), which in turn, is controlled by the nature of the divalent carbon compound, **X**. Indeed, the activation energy could also be correlated to the individual structural components of the **X**-BH_2^+ molecule – the C-B σ and π bonds.
- We have further been able to establish that HIA has a good correlation with the experimentally determined yields, based on catalysts selected from Stephan's paper. Stephan and Crudden have hypothesised a correlation between strength of Lewis acidity and yield.[2, 108] Our correlation clearly establishes that increased Lewis acidity, measured in terms of HIA increases the yield of the catalyst for a given catalyst load.

References

1. Farrell, J. M.; Hatnean, J. A.; Stephan, D. W., Activation of Hydrogen and Hydrogenation Catalysis by a Borenium Cation. *Journal of the American Chemical Society* **2012,** *134* (38), 15728-15731.
2. Farrell, J. M.; Stephan, D. W., Planar N-Heterocyclic Carbene Diarylborenium Ions: Synthesis by Cationic Borylation and Reactivity with Lewis Bases. *Angewandte Chemie International Edition* **2015,** *54* (17), 5214-5217.
3. J. G. de Vries, L. Lefort. Development of Asymmetric Hydrogenation Catalysts via High Throughput Experimentation. Oil & Gas Science and Technology - Revue d'IFP Energies nouvelles, Institut Français du Pétrole, **2013**, 68 (3), pp.519-528.
4. Herrmann, W. A.; Cornils, B. J. , Organometallic Homogeneous Catalysis—Quo vadis? *Angewandte Chemie International Edition* **1997,** *36* (10), 1048-1067.
5. Blaser, H. U.; Malan, C.; Pugin, B.; Spindler, F.; Steiner, H.; Studer, M. J. A. S.; Selective hydrogenation for fine chemicals: Recent trends and new developments *Catalysis*, **2003,** *345* (1-2), 103-151.
6. Shimizu, H.; Nagasaki, I.; Matsumura, K.; Sayo, N.; Saito, T. J. , Developments in asymmetric hydrogenation from an industrial perspective. *Accounts of Chemical Research* **2007,** *40* (12), 1385-1393.
7. Clapham, S. E.; Hadzovic, A.; Morris, R. H., Mechanisms of the H2-hydrogenation and transfer hydrogenation of polar bonds catalyzed by ruthenium hydride complexes. *Coordination Chemistry Reviews* **2004,** *248* (21), 2201-2237.
8. Keaton, R. J.; Blacquiere, J. M.; Baker, R. T., Base Metal Catalyzed Dehydrogenation of Ammonia−Borane for Chemical Hydrogen Storage. *Journal of the American Chemical Society* **2007,** *129* (7), 1844-1845.
9. Sattler, A.; Parkin, G., Carbon−Sulfur Bond Cleavage and Hydrodesulfurization of Thiophenes by Tungsten. *Journal of the American Chemical Society* **2011,** *133* (11), 3748-3751.
10. Suresh, C.; Santhanaraj, D.; Gurulakshmi, M.; Deepa, G.; Selvaraj, M.; Sasi Rekha, N. R.; Shanthi, K., Mo–Ni/Al-SBA-15 (Sulfide) Catalysts for Hydrodenitrogenation: Effect of Si/Al Ratio on Catalytic Activity. *ACS Catalysis* **2012,** *2* (1), 127-134.
11. Satyapal, S.; Petrovic, J.; Read, C.; Thomas, G.; Ordaz, G., The U.S. Department of Energy's National Hydrogen Storage Project: Progress towards meeting hydrogen-powered vehicle requirements. *Catalysis Today* **2007,***120* (3), 246-256.
12. Hamilton, C. W.; Baker, R. T.; Staubitz, A.; Manners, I., B–N compounds for chemical hydrogen storage. *Chemical Society Reviews* **2009,** *38* (1), 279-293.
13. Li, Y.; Hou, C.; Jiang, J.; Zhang, Z.; Zhao, C.; Page, A. J.; Ke, Z., General H2 Activation Modes for Lewis Acid–Transition Metal Bifunctional Catalysts. *ACS Catalysis* **2016,** *6* (3), 1655-1662.
14. Torrent, M.; Solà, M.; Frenking, G., Theoretical Studies of Some Transition-Metal-Mediated Reactions of Industrial and Synthetic Importance. *Chemical Reviews* **2000,** *100* (2), 439-494.

15. Niu, S.; Hall, M. B., Theoretical Studies on Reactions of Transition-Metal Complexes. *Chemical Reviews* **2000,** *100* (2), 353-406.
16. He, T.; Tsvetkov, N. P.; Andino, J. G.; Gao, X.; Fullmer, B. C.; Caulton, K. G., Mechanism of Heterolysis of H2 by an Unsaturated d8 Nickel Center: via Tetravalent Nickel? *Journal of the American Chemical Society* **2010,** *132* (3), 910-911.
17. Kimura, T.; Koiso, N.; Ishiwata, K.; Kuwata, S.; Ikariya, T., H–H and N–H Bond Cleavage of Dihydrogen and Ammonia with a Bifunctional Parent Imido (NH)-Bridged Diiridium Complex. *Journal of the American Chemical Society* **2011,** *133* (23), 8880-8883.
18. Camaioni, D. M.; Ginovska-Pangovska, B.; Schenter, G. K.; Kathmann, S. M.; Autrey, T., Analysis of the Activation and Heterolytic Dissociation of H2 by Frustrated Lewis Pairs: NH3/BX3 (X = H, F, and Cl). *The Journal of Physical Chemistry A* **2012,** *116* (26), 7228-7237.
19. Halpern, J., The Catalytic Activation of Hydrogen in Homogeneous, Heterogeneous, and Biological Systems. In *Advances in Catalysis (Eley, D. D.; Selwood, P. W.; Weisz, P. B.)*, Vol. 11, Academic Press. **1959**; pp 301-370.
20. Stephenson, M.; Stickland, L. H., Hydrogenase: The bacterial formation of methane by the reduction of one-carbon compounds by molecular hydrogen. *Biochem J.* **1933,** *27* (5), 1517-1527.
21. Jiménez, M. V.; Pérez-Torrente, J. J.; Bartolomé, M. I.; Gierz, V.; Lahoz, F. J.; Oro, L. A., Rhodium (I) complexes with hemilabile N-heterocyclic carbenes: Efficient alkyne hydrosilylation catalysts. *Organometallics* **2008,** *27* (2), 224-234.
22. Crabtree, R., Iridium compounds in catalysis. *Accounts of Chemical Research.* **1979,** *12* (9), 331-337.
23. Polanyi, M., *The Scientific Journal of the Royal College of Science.* **1937**, 7, 21.
24. T. R. Simmons, Gustav Berggren, Marine Bacchi, Marc Fontecave, Vincent Artero. Mimicking hydrogenases: From biomimetics to artificial enzymes. *Coordination Chemistry Reviews*, Elsevier, **2014**, 270-271, pp.127-150.
25. Qiu, S.; Li, Q.; Xu, Y.; Shen, S.; Sun, C., Learning from nature: Understanding hydrogenase enzyme using computational approach. *WIREs Computational Molecular Science.* **2020,** *10* (1), e1422.
26. Jones, A. K.; Sillery, E.; Albracht, S. P. J.; Armstrong, F. A., Direct comparison of the electrocatalytic oxidation of hydrogen by an enzyme and a platinum catalyst. *Chemical Communications.* **2002,** (8), 866-867.
27. Reihlen, H.; Gruhl, A.; v. Hessling, G., Über den photochemischen und oxydativen Abbau von Carbonylen. *Justus Liebigs Annalen der Chemie.* **1929,** *472* (1), 268-287.
28. Le Cloirec, A.; C. Davies, S.; J. Evans, D.; L. Hughes, D.; J. Pickett, C.; P. Best, S.; Borg, S., A di-iron dithiolate possessing structural elements of the carbonyl/cyanide sub-site of the H-centre of Fe-only hydrogenase. *Chemical Communications.* **1999,** (22), 2285-2286.
29. Schmidt, M.; Contakes, S. M.; Rauchfuss, T. B., First Generation Analogues of the Binuclear Site in the Fe-Only Hydrogenases: Fe2(μ-SR)2(CO)4(CN)22. *Journal of the American Chemical Society.* **1999,** *121* (41), 9736-9737.

30. Lyon, E. J.; Georgakaki, I. P.; Reibenspies, J. H.; Darensbourg, M. Y., Carbon Monoxide and Cyanide Ligands in a Classical Organometallic Complex Model for Fe-Only Hydrogenase. *Angewandte Chemie International Edition* **1999,** *38* (21), 3178-3180.
31. Tard, C.; Pickett, C. J., Structural and Functional Analogues of the Active Sites of the [Fe]-, [NiFe]-, and [FeFe]-Hydrogenases. *Chemical Reviews* **2009,** *109* (6), 2245-2274.
32. Capon, J.-F.; Gloaguen, F.; Pétillon, F. Y.; Schollhammer, P.; Talarmin, J., Electron and proton transfers at diiron dithiolate sites relevant to the catalysis of proton reduction by the [FeFe]-hydrogenases. *Coordination Chemistry Reviews* **2009,** *253* (9), 1476-1494.
33. Knörzer, P.; Silakov, A.; Foster, C. E.; Armstrong, F. A.; Lubitz, W.; Happe, T., Importance of the Protein Framework for Catalytic Activity of [FeFe]-Hydrogenases. *Journal of Biological Chemistry* **2012,** *287* (2), 1489-1499.
34. Esselborn, J.; Lambertz, C.; Adamska-Venkatesh, A.; Simmons, T.; Berggren, G.; Noth, J.; Siebel, J.; Hemschemeier, A.; Artero, V.; Reijerse, E.; Fontecave, M.; Lubitz, W.; Happe, T., Spontaneous activation of [FeFe]-hydrogenases by an inorganic [2Fe] active site mimic. *Nature Chemical Biology* **2013,** *9* (10), 607-609.
35. Berggren, G.; Adamska, A.; Lambertz, C.; Simmons, T. R.; Esselborn, J.; Atta, M.; Gambarelli, S.; Mouesca, J. M.; Reijerse, E.; Lubitz, W.; Happe, T.; Artero, V.; Fontecave, M., Biomimetic assembly and activation of [FeFe]-hydrogenases. *Nature* **2013,** *499* (7456), 66-69.
36. Sano, Y.; Onoda, A.; Hayashi, T., A hydrogenase model system based on the sequence of cytochrome c: photochemical hydrogen evolution in aqueous media. *Chemical Communications* **2011,** *47* (29), 8229-8231.
37. Jones, A. K.; Lichtenstein, B. R.; Dutta, A.; Gordon, G.; Dutton, P. L., Synthetic Hydrogenases: Incorporation of an Iron Carbonyl Thiolate into a Designed Peptide. *Journal of the American Chemical Society* **2007,** *129* (48), 14844-14845.
38. Roy, S.; Shinde, S.; Hamilton, G. A.; Hartnett, H. E.; Jones, A. K., Artificial [FeFe]-Hydrogenase: On Resin Modification of an Amino Acid to Anchor a Hexacarbonyldiiron Cluster in a Peptide Framework. *European Journal of Inorganic Chemistry* **2011,** (7), 1050-1055.
39. Bruschi, M.; Zampella, G.; Fantucci, P.; De Gioia, L., DFT investigations of models related to the active site of [NiFe] and [Fe] hydrogenases. *Coordination Chemistry Reviews* **2005,** *249* (15), 1620-1640.
40. Siegbahn, P. E. M.; Tye, J. W.; Hall, M. B., Computational Studies of [NiFe] and [FeFe] Hydrogenases. *Chemical Reviews* **2007,** *107* (10), 4414-4435.
41. Vignais, P. M.; Billoud, B., Occurrence, Classification, and Biological Function of Hydrogenases: An Overview. *Chemical Reviews.* **2007,** *107* (10), 4206-4272.
42. Lubitz, W.; Reijerse, E.; van Gastel, M., [NiFe] and [FeFe] Hydrogenases Studied by Advanced Magnetic Resonance Techniques. *Chemical Reviews* **2007,** *107* (10), 4331-4365.
43. Fontecilla-Camps, J. C.; Volbeda, A.; Cavazza, C.; Nicolet, Y., Structure/Function Relationships of [NiFe]- and [FeFe]-Hydrogenases. *Chemical Reviews* **2007,** *107* (10), 4273-4303.

44. De Lacey, A. L.; Fernández, V. M.; Rousset, M.; Cammack, R., Activation and Inactivation of Hydrogenase Function and the Catalytic Cycle: Spectroelectrochemical Studies. *Chemical Reviews* **2007,** *107* (10), 4304-4330.
45. Volbeda, A.; Fontecilla-Camps, J. C., Structure–function relationships of nickel–iron sites in hydrogenase and a comparison with the active sites of other nickel–iron enzymes. *Coordination Chemistry Reviews* **2005,** *249* (15), 1609-1619.
46. Lubitz, W.; Ogata, H.; Rüdiger, O.; Reijerse, E., Hydrogenases, *Chemical Reviews* **2014**, 114, 8, 4081–4148.
47. Stripp, S. T.; Goldet, G.; Brandmayr, C.; Sanganas, O.; Vincent, K. A.; Haumann, M.; Armstrong, F. A.; Happe, T., How oxygen attacks [FeFe] hydrogenases from photosynthetic organisms. *Proceedings of the National Academy of Sciences* **2009,** *106* (41), 17331.
48. Abou Hamdan, A.; Burlat, B.; Gutiérrez-Sanz, O.; Liebgott, P.-P.; Baffert, C.; De Lacey, A. L.; Rousset, M.; Guigliarelli, B.; Léger, C.; Dementin, S., O2-independent formation of the inactive states of NiFe hydrogenase. *Nature Chemical Biology* **2013,** *9* (1), 15-17.
49. Fritsch, J.; Lenz, O.; Friedrich, B., Structure, function and biosynthesis of O2-tolerant hydrogenases. *Nature Reviews Microbiology* **2013,** *11* (2), 106-114.
50. Roberts, J. D., & Caserio, M. C. (2021, July 31). Hydrogenation with Heterogeneous Catalysts. Retrieved September 14, 2021, from https://chem.libretexts.org/@go/page/22252
51. Nerozzi, F., Heterogeneous catalytic hydrogenation. *Platinum Metals Review* **2012,** *56* (4), 236-241.
52. Hutchings, G. J.; Wells, R. P. K.; Bailie, J. E., Heterogeneous catalytic hydrogenation. *Science Progress* **1999,** *82* (3), 233-250.
53. Halpern, J., Homogeneous catalytic hydrogenation: A retrospective account. *Journal of Organometallic Chemistry* **1980,** *200* (1), 133-144.
54. Halpern, J., Homogeneous Catalytic Activation of Molecular Hydrogen by Metal Ions and Complexes. *The Journal of Physical Chemistry* **1959,** *63* (3), 398-403.
55. Wilkinson, G.; Birmingham, J. M., biscyclopentadienylrhenium hydride—a new type of hydride. *Journal of the American Chemical Society* **1955,** *77* (12), 3421-3422.
56. Calvin, M., Homogeneous Catalytic Hydrogenation. *Journal of the American Chemical Society* **1939,** *61* (8), 2230-2234.
57. Kubas, G. J.; Ryan, R. R.; Swanson, B. I.; Vergamini, P. J.; Wasserman, H. J., Characterization of the first examples of isolable molecular hydrogen complexes, M(CO)3(PR3)2(H2) (M = molybdenum or tungsten; R = Cy or isopropyl). Evidence for a side-on bonded dihydrogen ligand. *Journal of the American Chemical Society* **1984,** *106* (2), 451-452.
58. Vaska, L.; DiLuzio, J. W., Activation of hydrogen by a transition metal complex at normal conditions leading to a stable molecular dihydride. *Journal of the Americal Chemical Society* **1962,** *84* (4), 679-680.
59. Osborn, J. A.; Jardine, F. H.; Young, J. F.; Wilkinson, G., The preparation and properties of tris(triphenylphosphine)halogenorhodium(I) and some reactions thereof including catalytic

homogeneous hydrogenation of olefins and acetylenes and their derivatives. *Journal of the Chemical Society A: Inorganic, Physical, Theoretical* **1966,** (0), 1711-1732.
60. Roelen, O., German patent DE 849,548, 1938/1952. **1943,** *2*, 066.
61. Roelen, O., DRP 849548 (1938). *Angewandte Chimie* **1948,** *60*, 62.
62. Skara, G.; De Vleeschouwer, F.; Geerlings, P.; De Proft, F.; Pinter, B., Heterolytic Splitting of Molecular Hydrogen by Frustrated and Classical Lewis Pairs: A Unified Reactivity Concept. *Scientific Reports* **2017,** *7* (1), 16024.
63. Brown, H. C.; Kanner, B., Preparation and Reactions of 2,6-Di-t-butylpyridine and Related Hindered Bases. A Case of Steric Hindrance toward the Proton1,2. *Journal of the American Chemical Society* **1966,** *88* (5), 986-992.
64. Brown, H. C.; Schlesinger, H. I.; Cardon, S. Z., Studies in Stereochemistry. I. Steric Strains as a Factor in the Relative Stability of Some Coördination Compounds of Boron. *Journal of the American Chemical Society* **1942,** *64* (2), 325-329.
65. Wittig, G.; Benz, E., Über das Verhalten von Dehydrobenzol gegenüber nucleophilen und elektrophilen Reagenzien. *Chemische Berichte* **1959,** *92* (9), 1999-2013.
66. Tochtermann, W., Structures and Reactions of Organic ate-Complexes. *Angewandte Chemie International Edition in English* **1966,** *5* (4), 351-371.
67. Welch, G. C.; San Juan, R. R.; Masuda, J. D.; Stephan, D. W., Reversible, metal-free hydrogen activation. *Science* **2006,** *314* (5802), 1124-1126.
68. Welch, G. C.; Stephan, D. W., Facile Heterolytic Cleavage of Dihydrogen by Phosphines and Boranes. *Journal of the American Chemical Society* **2007,** *129* (7), 1880-1881.
69. Mömming, C. M.; Otten, E.; Kehr, G.; Fröhlich, R.; Grimme, S.; Stephan, D. W.; Erker, G., Reversible Metal-Free Carbon Dioxide Binding by Frustrated Lewis Pairs. *Angewandte Chemie International Edition* **2009,** *48* (36), 6643-6646.
70. Peuser, I.; Neu, R. C.; Zhao, X.; Ulrich, M.; Schirmer, B.; Tannert, J. A.; Kehr, G.; Fröhlich, R.; Grimme, S.; Erker, G.; Stephan, D. W., CO2 and Formate Complexes of Phosphine/Borane Frustrated Lewis Pairs. *Chemistry – A European Journal* **2011,** *17* (35), 9640-9650.
71. Otten, E.; Neu, R. C.; Stephan, D. W., Complexation of Nitrous Oxide by Frustrated Lewis Pairs. *Journal of the American Chemical Society* **2009,** *131* (29), 9918-9919.
72. Sajid, M.; Klose, A.; Birkmann, B.; Liang, L.; Schirmer, B.; Wiegand, T.; Eckert, H.; Lough, A. J.; Fröhlich, R.; Daniliuc, C. G.; Grimme, S.; Stephan, D. W.; Kehr, G.; Erker, G., Reactions of phosphorus/boron frustrated Lewis pairs with SO2. *Chemical Science* **2013,** *4* (1), 213-219.
73. Ashley, A. E.; Thompson, A. L.; O'Hare, D., Non-Metal-Mediated Homogeneous Hydrogenation of CO2 to CH3OH. *Angewandte Chemie International Edition* **2009,** *48* (52), 9839-9843.
74. Tran, S. D.; Tronic, T. A.; Kaminsky, W.; Michael Heinekey, D.; Mayer, J. M., Metal-free carbon dioxide reduction and acidic C–H activations using a frustrated Lewis pair. *Inorganica Chimica Acta* **2011,** *369* (1), 126-132.

75. Chase, P. A.; Welch, G. C.; Jurca, T.; Stephan, D. W., Metal-Free Catalytic Hydrogenation. *Angewandte Chemie International Edition* **2007,** *46* (42), 8050-8053.
76. Spies, P.; Schwendemann, S.; Lange, S.; Kehr, G.; Fröhlich, R.; Erker, G., Metal-Free Catalytic Hydrogenation of Enamines, Imines, and Conjugated Phosphinoalkenylboranes. *Angewandte Chemie International Edition.* **2008,** *47* (39), 7543-7546.
77. Schwendemann, S.; Tumay, T. A.; Axenov, K. V.; Peuser, I.; Kehr, G.; Fröhlich, R.; Erker, G., Metal-Free Frustrated Lewis Pair Catalyzed 1,4-Hydrogenation of Conjugated Metallocene Dienamines. *Organometallics.* **2010,** *29* (5), 1067-1069.
78. Bannwarth, C.; Hansen, A.; Grimme, S., The Association of Two "Frustrated" Lewis Pairs by State-of-the-Art Quantum Chemical Methods. *Israel Journal of Chemistry.* **2015,** *55* (2), 235-242.
79. Bistoni, G.; Auer, A. A.; Neese, F., Understanding the Role of Dispersion in Frustrated Lewis Pairs and Classical Lewis Adducts: A Domain-Based Local Pair Natural Orbital Coupled Cluster Study. *Chemistry – A European Journal.* **2017,** *23* (4), 865-873.
80. Marwitz, A. J. V.; Dutton, J. L.; Mercier, L. G.; Piers, W. E., Dihydrogen Activation with tBu3P/B(C6F5)3: A Chemically Competent Indirect Mechanism via in Situ-Generated p-tBu2P–C6F4–B(C6F5)2. *Journal of the American Chemical Society* **2011,** *133* (26), 10026-10029.
81. Wiegand, T.; Siedow, M.; Ekkert, O.; Möbus, J.; Daniliuc, C. G.; Kehr, G.; Erker, G.; Eckert, H., Solid-state NMR studies for the determination of 11B electric field-gradient tensor orientations in P/B Frustrated Lewis Pairs and related systems. *Solid State Nuclear Magnetic Resonance* **2014,** *61-62*, 8-14.
82. Rocchigiani, L.; Ciancaleoni, G.; Zuccaccia, C.; Macchioni, A., Probing the Association of Frustrated Phosphine–Borane Lewis Pairs in Solution by NMR Spectroscopy. *Journal of the American Chemical Society* **2014,** *136* (1), 112-115.
83. Rokob, T. A.; Hamza, A.; Stirling, A.; Soós, T.; Pápai, I., Turning Frustration into Bond Activation: A Theoretical Mechanistic Study on Heterolytic Hydrogen Splitting by Frustrated Lewis Pairs. *Angewandte Chemie International Edition* **2008,** *47* (13), 2435-2438.
84. Grimme, S.; Kruse, H.; Goerigk, L.; Erker, G., The Mechanism of Dihydrogen Activation by Frustrated Lewis Pairs Revisited. *Angewandte Chemie International Edition* **2010,** *49* (8), 1402-1405.
85. Zeonjuk, L. L.; Vankova, N.; Mavrandonakis, A.; Heine, T.; Röschenthaler, G.-V.; Eicher, J., On the Mechanism of Hydrogen Activation by Frustrated Lewis Pairs. *Chemistry – A European Journal* **2013,** *19* (51), 17413-17424.
86. Becerra, M.; Real-Enriquez, M.; Espinosa-Gavilanes, C.; Zambrano, C. H.; Almeida, R.; Torres, F. J.; Rincón, L., On the thermodynamic stability of the intermolecular association between Lewis acids and Lewis bases: a DFT study. *Theoretical Chemistry Accounts* **2016,** *135* (3), 77.
87. Bakó, I.; Stirling, A.; Bálint, S.; Pápai, I., Association of frustrated phosphine–borane pairs in toluene: molecular dynamics simulations. *Dalton Transactions* **2012,** *41* (30), 9023-9025.

88. Hamza, A.; Stirling, A.; András Rokob, T.; Pápai, I., Mechanism of hydrogen activation by frustrated Lewis pairs: A molecular orbital approach. *International Journal of Quantum Chemistry* **2009,** *109* (11), 2416-2425.
89. Schirmer, B.; Grimme, S., Electric field induced activation of H2—Can DFT do the job? *Chemical Communications* **2010,** *46* (42), 7942-7944.
90. Rokob, T. A.; Bakó, I.; Stirling, A.; Hamza, A.; Pápai, I., Reactivity Models of Hydrogen Activation by Frustrated Lewis Pairs: Synergistic Electron Transfers or Polarization by Electric Field? *Journal of the American Chemical Society* **2013,** *135* (11), 4425-4437.
91. Liu, L.; Lukose, B.; Ensing, B., Hydrogen Activation by Frustrated Lewis Pairs Revisited by Metadynamics Simulations. *The Journal of Physical Chemistry C* **2017,** *121* (4), 2046-2051.
92. Stephan, D. W.; Greenberg, S.; Graham, T. W.; Chase, P.; Hastie, J. J.; Geier, S. J.; Farrell, J. M.; Brown, C. C.; Heiden, Z. M.; Welch, G. C.; Ullrich, M., Metal-Free Catalytic Hydrogenation of Polar Substrates by Frustrated Lewis Pairs. *Inorganic Chemistry* **2011,** *50* (24), 12338-12348.
93. Rokob, T. A.; Hamza, A.; Pápai, I., Rationalizing the Reactivity of Frustrated Lewis Pairs: Thermodynamics of H2 Activation and the Role of Acid−Base Properties. *Journal of the American Chemical Society* **2009,** *131* (30), 10701-10710.
94. Liu, L.; Vankova, N.; Heine, T., A kinetic study on the reduction of CO2 by frustrated Lewis pairs: from understanding to rational design. *Physical Chemistry Chemical Physics* **2016,** *18* (5), 3567-3574.
95. M.J. Frisch, G.W. Trucks, H.B. Schlegel, G.E. Scuseria, M.A. Robb, J.R. Cheeseman, G. Scalmani, V. Barone, B. Mennucci, G.A. Petersson, H. Nakatsuji, M. Caricato, X. Li, H.P. Hratchian, A.F. Izmaylov, J. Bloino, G. Zheng, J.L. Sonnenberg, M. Hada, M. Ehara, K. Toyota, R. Fukuda, J. Hasegawa, M. Ishida, T. Nakajima, Y. Honda, O. Kitao, H. Nakai, T. Vreven, J.A. Montgomery Jr, J.E. Peralta, F. Ogliaro, M. Bearpark, J.J. Heyd, E. Brothers, K.N. Kudin, V.N. Staroverov, R. Kobayashi, J. Normand, K. Raghavachari, A. Rendell, J.C. Burant, S.S. Iyengar, J. Tomasi, M. Cossi, N. Rega, J.M. Millam, M. Klene, J.E. Knox, J.B. Cross, V. Bakken, C. Adamo, J. Jaramillo, R. Gomperts, R.E. Stratmann, O. Yazyev, A.J. Austin, R. Cammi, C. Pomelli, J.W. Ochterski, R.L. Martin, K. Morokuma, V.G. Zakrzewski, G.A. Voth, P. Salvador, J.J. Dannenberg, S. Dapprich, A.D. Daniels, Ö. Farkas, J.B. Foresman, J.V. Ortiz, J. Cioslowski, D.J. Fox, Gaussian, Inc., Wallingford CT, Gaussian 09, Revision D.01, **2013**.
96. te Velde, G.; Bickelhaupt, F. M.; Baerends, E. J.; Fonseca Guerra, C.; van Gisbergen, S. J. A.; Snijders, J. G.; Ziegler, T., Chemistry with ADF. *Journal of Computational Chemistry* **2001,** *22* (9), 931-967.
97. ADF2017, S., Theoretical Chemistry, Vrije Universiteit, Amsterdam, The Netherlands, http://www.scm.com.
98. Cabrera-Trujillo, J. J.; Fernández, I., Carbones and Heavier Ylidones (EL2) in Frustrated Lewis Pair Chemistry: Influence of the Nature of EL2 on Dihydrogen Activation. *Inorganic Chemistry* **2019,** *58* (12), 7828-7836.

99. Könczöl, L.; Makkos, E.; Bourissou, D.; Szieberth, D., Computational Evidence for a New Type of η2-H2 Complex: When Main-Group Elements Act in Concert To Emulate Transition Metals. *Angewandte Chemie International Edition* **2012,** *51* (38), 9521-9524.
100. Könczöl, L.; Turczel, G.; Szpisjak, T.; Szieberth, D., The stability of η2-H2 borane complexes – a theoretical investigation. *Dalton Transactions* **2014,** *43* (36), 13571-13577.
101. Almas, Q. L.; Pearson, J. K., Novel Bonding Mode in Phosphine Haloboranes. *ACS Omega* **2018,** *3* (1), 608-614.
102. Wu, D.; Jia, D.; Liu, L.; Zhang, L.; Guo, J., Reactivity of 2,6-Lutidine/BR3 and Pyridine/BR3 Lewis Pairs (R = F, Me, C6F5): A Density Functional Study. *The Journal of Physical Chemistry A* **2010,** *114* (43), 11738-11745.
103. Kubas, G. J., Activation of dihydrogen and coordination of molecular H2 on transition metals. *Journal of Organometallic Chemistry* **2014,** *751*, 33-49.
104. Crabtree, R. H., Dihydrogen Complexation. *Chemical Reviews* **2016,** *116* (15), 8750-8769.
105. Sitte, N. A.; Bursch, M.; Grimme, S.; Paradies, J., Frustrated Lewis Pair Catalyzed Hydrogenation of Amides: Halides as Active Lewis Base in the Metal-Free Hydrogen Activation. *Journal of the American Chemical Society* **2019,** *141* (1), 159-162.
106. Chase, P. A.; Jurca, T.; Stephan, D. W., Lewis acid-catalyzed hydrogenation: B(C6F5)3-mediated reduction of imines and nitriles with H2. *Chemical Communications* **2008,** (14), 1701-1703.
107. Farrell, J. M.; Posaratnanathan, R. T.; Stephan, D. W., A family of N-heterocyclic carbene-stabilized borenium ions for metal-free imine hydrogenation catalysis. *Chemical Science* **2015,** *6* (3), 2010-2015.
108. Eisenberger, P.; Bestvater, B. P.; Keske, E. C.; Crudden, C. M., Hydrogenations at Room Temperature and Atmospheric Pressure with Mesoionic Carbene-Stabilized Borenium Catalysts. *Angewandte Chemie International Edition* **2015,** *54* (8), 2467-2471.

General Conclusion and Perspectives

From the study conducted in this thesis, we can derive the following conclusions:

- Density functional theory can be successfully used in modelling NHC-derived borenium compounds and measure σ and π interactions within these molecules. We find that while some descriptors of σ and π donation correlate with each other, a lot of them do not. To establish a correlation some modifications may be necessary (like for ETS-NOCV analysis). Sometimes the lack of correlation also indicates a conceptual difference in the descriptors. Nevertheless, unambiguous descriptors of σ and π donations have been identified.
- A linear combination of σ and π donation energy, which are properties of the NHC-derived compound-borenium adduct, can be correlated to their Hydride ion affinities (HIA), a well-recognised parameter of measuring Lewis acidity.
- The HIA can in turn be correlated with the activation energy associated with the activation of H_2 by **X**-BPh_2^+ and $P(^tBu)_3$. A linear combination of σ and π interaction also correlates with the energy of activation.

We set out with the objective of building a bridge between structure and activity in the particular case of borenium adducts of carbenic compounds using computational tools. This goal has been fulfilled to a large extent. And yet, as has been pointed out at different stages of the investigation – there are several aspects that demand further investigation.

Looking to the future, the results obtained from this thesis can stimulate research in several new directions. One could pursue the investigation with the parameters for σ-donation whose theoretical origin is still not completely understood. More investigation needs to be conducted to understand how NMR based parameters could become useful in obtaining structural information. Finally, it could be interesting to see if the same techniques used here can be extended to quantify other bonds, with particular emphasis on the NBO approach. Systems under investigation could include adducts of borenium with other divalent donors (N, O, S etc.) and perhaps some transition metal-based catalysts as well.

Appendix

Statistical Parameters for the Estimation of Errors

In the course of our investigation we often correlate similar or related quantities in order to understand the relationship between them. How closely these quantities are related can be understood by some statistical parameters, which will then help us to conclude if the correlation between them is good, moderate or poor. Below we discuss five such parameters that have been calculated for most correlations presented in this thesis.

i. Coefficient of Determination(R^2)[1]

The coefficient of determination, R^2, is used to analyse how differences in one variable can be explained by the difference in a second variable. R^2 gives the percentage of variation in y explained by the variation in x. R^2 ranges between 0 to 1. This means that 0% to 100% variation in y can be explained by the variation in x respectively.

The utility of R^2 lies in its ability to find the likelihood of future events falling within the predicted outcome. That is, if more samples were added to the set, the coefficient would show the probability of the new point falling on the line. For a set of n (x_n, y_n) points, R^2 is defined as -

$$R^2 = \left[\frac{n\,(\sum xy - (\sum x)(\sum y))}{\sqrt{[n(\sum x^2 - (\sum x)^2]\,[n(\sum y^2 - (\sum y)^2]}} \right]^2$$

ii. Maximum Error (Max)

The absolute deviation of a given point (x_i,y_i) from a line y = Ax +B is given by abs(y_{calc} – y) where y_{calc} is the expected value of the variable y for x = x_i, i.e. Ax_i + B. The maximum deviation calculated in this way calculated for a set of point (x_n, y_n) is defined as the maximum error.

$$Max = max|y_{calc} - y_i| = max|Ax_i + B - y_i|$$

iii. Mean Absolute Deviation (MAD)

The mean of the deviations calculated as explained above is called the mean average deviation (MAD). It is given by:

$$MAD = \frac{\sum_i |Ax_i + B - y_i|}{n}$$

iv. Root Mean Square Deviation (RMSD)[2]

The root mean square deviation is frequently used to measure the difference between values predicted by a model (represented by a line y = Ax +B) and the values observed. The RMSD serves to aggregate the magnitudes of the errors in prediction of various data points into a single measure of predictive power. The RMSD is a means of measuring errors for different models for a particular dataset and not between different datasets, as RMSD is scale dependent. It is given, for a set of n points by:

$$RMSD = \sqrt{\frac{\sum_i (Ax_i + B - y_i)^2}{n}}$$

v. Normalised Root Mean Square Deviation (NRMSD)[3]

The Normalised RMSD facilitates the comparison between models with different scales. NRMSD relates the RMSD to the observed range of the variable.

$$NRMSD = \frac{RMSD}{[\max(y_i) - \min(y_i)]}$$

References

1. https://www.statisticshowto.com/probability-and-statistics/coefficient-of-determination-r-squared/.

2. Wikipedia https://en.wikipedia.org/w/index.php?title=Root-mean-square_deviation&oldid=1018370414 (accessed July 1, 2021).

3. AgriMetSoft (2019). Online Calculators. Available on: https://agrimetsoft.com/calculators/Normalized%20Root%20Mean%20Square%20Error

ECOLE DOCTORALE

Titre : Un cheminement computationnel entre structure électronique et réactivité : Les catalyseurs de type NHC-borénium comme exemple

Mots clés : DFT, catalyse, carbène N-hétérocyclique

Résumé : La chimie computationnelle est omniprésente dans l'évaluation numérique des propriétés physiques et chimiques des molécules. Il s'agit d'un outil de prédiction pour les chimistes théoriciens et d'un outil complémentaire en chimie organique et inorganique pour éviter de réaliser des expériences et des synthèses ardues en laboratoire. La chimie computationnelle s'intéresse à la fois à la mesure des propriétés physiques et à l'évaluation de l'efficacité des méthodes théoriques à prédire ces valeurs.
Au cours de cette these, nous explorons ces deux facettes dans le contexte des adduits borénium-dérivés de carbènes N-hétérocycliques (NHC). Ces adduits sont des acides de Lewis reconnus en chimie, comme illustré par leur rôle de catalyseurs pour l'activation de petites molécules comme H_2. De plus, ces composés présentent des caractéristiques chimiques qui permettent de décomposer finement les transferts électroniques entre ses constituants borénium et carbone divalent (ligands NHC ou carbone(0)). L'objectif de cette these a donc été l'établissement d'une relation structure-activité pour ces composés, ouvrant la voie vers la conception rationnelle in silico de nouveaux catalyseurs plus performants.
La déficience en électrons de l'atome de bore est atténuée par la donation d'électrons du ligand carbone divalent. La force de ces interactions σ et π a été évaluée par calculs en utilisant de nombreuses approches théoriques, permettant d'identifier les descripteurs les plus efficaces pour ces interactions. La pertinence de nos résultats théoriques a été renforcée par la comparaison avec les valeurs expérimentales disponibles. Dans l'étape suivante, une relation quantitative entre les interactions σ et π et l'acidité de Lewis, évaluée par l'affinité aux ions hydrures, a été établie. Enfin, il a été démontré que cette acidité de Lewis est corrélée avec l'énergie d'activation de H_2, établissant ainsi une relation directe entre les caractéristiques structurelles de ces catalyseurs au borénium et leur réactivité.

Title : A computational journey from electronic structure to reactivity: NHC-derived borenium catalysts as test case

Keywords : DFT, catalysis, N-heterocyclic carbene

Computational chemistry is ubiquitous in the numerical evaluation of physical and chemical properties of molecules. It is a predictive tool for theoretical chemists and a complementary tool in organic and inorganic chemistry to avoid arduous laboratory experiments and syntheses. Computational chemistry is concerned with both measuring physical properties and evaluating how efficiently theoretical methods can predict these values.
In this work we explore both these facets in the context of N-Heterocyclic carbene (NHC) derived borenium adducts. These compounds are recognised for their role as Lewis acids in chemistry, as illustrated for their catalytic role for activating small molecules like H_2. Moreover, these compounds present chemical characteristics that allow to finely decompose the electronic transfers between its borenium and divalent carbon (NHC or carbone ligands) constituents. The objective of this research was to computationally establish a structure-activity relationship for these adducts, paving the way to the rational in silico design of new and better catalysts.The electron deficiency of the boron atom is mitigated by electron donation from the divalent carbon ligand. The strength of these σ and π interactions have been evaluated computationally through numerous theoretical approaches, allowing to identify the most efficient descriptors for these interactions. The reliability of our computational results has been strengthened by comparison with available experimentally recorded values. In the next stage a quantitative relationship between the σ and π interaction and the overall Lewis acidity, evaluated through hydride ion affinity, has been established. Finally, this overall Lewis acidity is shown to correlate with the energy of H_2 activation, thereby establishing a direct relationship between the structural features of these borenium catalysts and their reactivity.